

Keep

M.T. Charles
RU-1

RU-1
22

REPORT NO. AE62-0413

212p

CASE FILE COPY

N 68 16028

code 1

STUDY OF PRINCIPLES OF METEOROID PROTECTION

by

R. F. ROLSTEN, H. H. HUNT, AND J. N. WELLNITZ

APRIL 1962

CONTRACT NAS-8-875

FINAL REPORT

*George C. Marshall Space Flight Center
National Aeronautics and Space Administration
Huntsville, Alabama*

GD

GENERAL DYNAMICS | ASTRONAUTICS

OTS PRICE

XEROX

\$

14.50 ph.

MICROFILM

\$

6.56 mf.

STUDY OF PRINCIPLES
OF
METEOROID PROTECTION

BY

R. F. Rolsten, H. H. Hunt, and J. N. Wellnitz

April 1962

Contract NAS-8-875

Final Report

GEORGE C. MARSHALL SPACE FLIGHT CENTER
NATIONAL AERONAUTICS AND SPACE ADMINISTRATION
Huntsville, Alabama

RDF62-034

ABSTRACT

/6028

The hypervelocity impact data related to meteoroid bumper protection systems for aerospace vehicles that were produced during the program can be summarized as follows:

1. One hundred and forty-two impact experiments were made with the explosive driver accelerator and eight with the light gas gun (see Sections 2, 3, 4, 5, 6, 7, and 8).
2. Impact data were obtained with 0.1875-, 0.125-, 0.090-, 0.063-, and 0.032-inch aluminum (6061-T6) bumpers (see Section 3.1).
3. Bumpers other than aluminum were: a) plate glass; b) wire screen; c) magnesium-lithium alloy; and d) 301 stainless steel (see Sections 3.1, 3.2, and 3.3).
4. Structures pressurized with water, air, liquid, and gaseous oxygen are discussed in Section 4.
5. The preliminary results of the protection efficiency of energy-absorbing core materials are given in Section 5.
6. Projectile mass was 0.57, 0.34, 0.21, 0.12, and 0.097 gram for steel; 0.67 gram for copper; 0.08 gram for glass; and 0.299 gram for nylon (see Section 6).
7. Projectiles were accelerated in air and vacuum with and without premature fragmentation, to velocities in the range from 10,000 to 28,600 ft/sec (see Section 6).
8. Preliminary data relating the shear-plug diameter to plate thickness of several materials are given in Section 7.
9. Photographic coverage of the impact phenomena was obtained (see Section 8).
10. A summary and discussion of the results observed in this program are given in Section 9.
11. The principles of meteoroid protection are delineated in Section 10.
12. Literature data pertinent to the phenomena associated with hypervelocity impact of relatively thin plates are summarized in the Appendix. This survey is not intended to be exhaustive.

FOREWORD

This report contains the results of a 12-month study conducted by the Materials Research Group of General Dynamics/Astronautics in compliance with the National Aeronautics and Space Administration Contract NAS-8-875, "Study of Principles of Meteoroid Protection". The program was conducted under the direction of Mr. Henry L. Martin of the Research Projects Division of the Marshall Space Flight Center.

Drs. R. F. Rolsten and W. H. Steurer of General Dynamics/Astronautics were responsible for the study organization and technical direction of the work performed. In addition to the forementioned, the principal contributors to the program were Messrs. H. H. Hunt, J. N. Wellnitz, and H. Anderson.

In the three previous progress reports, primary emphasis was placed on the interaction between the projectile and bumper, and to the establishment of numerical data to delineate the significance of total mass and spacing. These reports were prepared to record and reflect the progress of the work during each phase of the program experiments. Conclusions drawn and concepts developed were tentative only, and based on the data available at the time of reporting.

The purpose of this final report was to refine all the experimental data evolved during the program, and to develop the tentative concepts into a synthesis of the individual relationships in order to evolve the principles of meteoroid protection. This required the establishment of experimental data on the projectile behavior, projectile mass, bumper material and structure, energy-absorbing core materials, and on pressurized vessel behavior during impact from a high velocity particle. High speed photographic equipment was utilized in order to study the impact phenomena.

TABLE OF CONTENTS

<u>Section</u>		<u>Page</u>
1	INTRODUCTION	1-1
2	EXPERIMENTAL	2-1
2.1	Explosive Projection	2-1
2.1.1	Projectiles	2-1
2.1.2	Projectile Integrity	2-4
2.1.3	Velocity Measurement	2-9
2.2	Ballistic Range	2-9
2.3	Test Program	2-15
2.3.1	The Bumper	2-15
2.3.2	Pressurized Test Cylinder	2-16
3	INVESTIGATION OF BUMPER EFFECTIVENESS	3-1
3.1	Solid Metal Bumper	3-1
3.1.1	Aluminum Bumper, Type 6061-T6, 0.125 Inch Thick . .	3-1
3.1.2	Aluminum Bumper, Type 6061-T6, 0.090 Inch Thick . .	3-6
3.1.3	Aluminum Bumper, Type 6061-T6, 0.063 Inch Thick . .	3-19
3.1.4	Aluminum Bumper, Type 6061-T6, 0.032 Inch Thick . .	3-19
3.1.4.1	Steel Projectile: 0.57 Gram	3-19
3.1.4.2	Steel Projectile: 0.21 Gram	3-28
3.1.5	Aluminum Bumper, Type 6061-T6, 0.1875 Inch Thick . .	3-28
3.1.6	Aluminum Bumper, Type 6061-T6, 0.090 Inch Thick; Copper Projectile	3-28
3.1.7	Magnesium-Lithium Alloy (LA-141)	3-30
3.1.8	Stainless Steel, Type 301, 0.063 Inch Thick	3-30
3.2	Glass Bumpers	3-30
3.3	Wire Screen Bumpers	3-36
4	PRESSURIZED STRUCTURES	4-1
4.1	Test Panel No. 1: 5Al-2.5Sn-Ti; 20-psi Gaseous Oxygen .	4-1
4.2	Test Panel No. 2: 301 Full-Hard Stainless Steel; 60-psi Gaseous Oxygen	4-2

TABLE OF CONTENTS, Contd

<u>Section</u>	<u>Page</u>
4.3 Test Panel No. 3: 6Al-4V-Ti; 60-psi Liquid Oxygen . .	4-2
4.4 Test Panel No. 4: Aluminum (2024-T3); 60-psi Liquid Oxygen	4-2
5 ENERGY-ABSORBING CORE MATERIALS	5-1
6 PROJECTILES	6-1
6.1 Damage Related to Physical State: Mass, Composition, and Geometry	6-1
6.1.1 Physical State	6-1
6.1.2 Cylinders: Explosively Accelerated	6-1
6.1.2.1 Steel: 0.57 Gram	6-1
6.1.2.2 Steel: 0.21 Gram	6-1
6.1.2.3 Steel: 0.097 Gram	6-1
6.1.2.4 Copper: 0.67 Gram	6-1
6.1.3 Glass Spheres: 0.08 Gram	6-1
6.1.4 Nylon Spheres: 0.299 Gram	6-3
6.1.5 Accelerated Steel Spheres	6-3
6.1.5.1 Light Gas Gun: 0.12 Gram	6-3
6.1.5.2 Explosive Driver: 0.34 Gram	6-3
6.2 Orientation and Fragmentation	6-3
6.3 Recovery After Acceleration	6-7
7 HOLE DIAMETER IN METAL PLATES	7-1
8 PHOTOGRAPHIC ANALYSIS OF IMPACT PHENOMENA	8-1
8.1 Low Speed Photographs	8-1
8.2 Moderate Speed Photographs	8-1
8.3 High Speed Photographs	8-5
9 SUMMARY AND DISCUSSION	9-1
9.1 Prediction of Damage From Hypervelocity Crater Data: The 1.5 Times Rule	9-1

TABLE OF CONTENTS, Contd

<u>Section</u>		<u>Page</u>
9.2	Meteoroid Bumpers	9-3
9.2.1	Material or Composition	9-4
9.2.2	Thickness	9-7
9.2.3	Separation Distance from the Vehicle Hull	9-14
9.2.4	Dependence on Projectile Mass	9-17
9.2.5	Dependence on Impact Velocity	9-17
9.3	Pressurized Structures	9-17
9.4	Energy-Absorbing Core Materials	9-20
9.5	Projectiles	9-26
9.6	Application of Scaling to Data in this Report	9-30
10	PRINCIPLES OF METEOROID PROTECTION	10-1
10.1	Case I: The Relatively Thin Single Plate	10-2
10.2	Case II: The Single Meteoroid Bumper	10-2
11	BIBLIOGRAPHY	11-1
<u>Appendix</u>		
A	HYPERVELOCITY IMPACT: LITERATURE SUMMARY	A-1
A-1	Introduction	A-1
A-2	Theories of Penetration and/or Cratering	A-2
A-2.1	Rigid Projectile	A-2
A-2.2	Thermal Penetration	A-2
A-2.3	Explosive Impact	A-3
A-2.4	Hydrodynamic	A-3
A-3	Impact Phenomena Relative to Velocity	A-4
A-4	Penetration Dependence on Bumper Thickness	A-13
A-5	Penetration Dependence on Bumper Spacing	A-16
A-6	Angle of Fragment Dispersion	A-16
A-7	Hole Diameter	A-16
A-8	Dependence on Incidence	A-16

TABLE OF CONTENTS, Contd

<u>Appendix</u>		<u>Page</u>
A-9	Dependence on Temperature	A-23
A-10	Target Strength	A-27
A-11	Density	A-31
A-11.1	Projectile	A-31
A-11.2	Target	A-33
A-12	Kinetic Energy	A-33
A-13	Momentum	A-42
A-14	Penetration Related to the Volume and Area of the Crater .	A-42
A-15	Single Bumpers	A-46
A-16	Multiple Bumpers	A-46

LIST OF ILLUSTRATIONS

<u>Figure</u>		<u>Page</u>
1	Velocity and Mass Regimes	2-2
2	Explosive Driver and Projectile	2-3
3	Test Arrangement	2-4
4	Velocities Obtained in Air With Various Steel Projectiles	2-5
5	Titanium Plate Impacted With a 0.57-Gram Projectile at 18,000 Ft/Sec	2-6
6	Magnesium Plate Impacted With a 0.215-Gram Projectile at 13,600 Ft/Sec	2-7
7	Flash X-Ray Photograph of a Projectile in Flight	2-8
8	Break Circuit for Measurement of Projectile Velocity	2-10
9	Velocity Measuring Equipment	2-11
10	Oscilloscope Traces for Measurement of Projectile Velocity	2-12
11	Ballistic Range [Ref 1]	2-13
12	Mylar Gate [Ref 1]	2-14
13	Pressurized Test Cylinder and Fixture [Ref 2]	2-18
14	Construction Details of the Test Cylinder [Ref 2].	2-19
15	Thick Aluminum Plate (Panel J-2)	3-2
16	Test Panel Mass Versus Spacing (0.125-Inch Bumper)	3-5
17	Test Panel Mass Versus Spacing (0.090-Inch Bumper)	3-7
18	Aluminum Bumper With Zero Spacing (Panel J-19)	3-8
19	Reverse Side of Hull Plate (Panel J-19)	3-9
20	Aluminum Bumper With 0.25-Inch Spacing (Panel A-49)	3-10
21	Reverse Side of Bumper (Panel A-49)	3-11
22	Aluminum Bumper With Zero Spacing (Panel J-5)	3-12
23	Aluminum Bumper With 0.25-Inch Spacing (Panel A-43)	3-13

LIST OF ILLUSTRATIONS, Contd

<u>Figure</u>		<u>Page</u>
24	Aluminum Bumper With 0.5-Inch Spacing (Panel J-6)	3-14
25	Reverse Side of Test Panel A-43	3-15
26	Reverse Side of Bumper (Panel J-6)	3-16
27	Aluminum Bumper With 2.56-Inch Spacing (Panel A-40)	3-17
28	Reverse Side of Bumper (Panel A-40)	3-18
29	Aluminum Bumper With 4.06-Inch Spacing (Panel A-42)	3-20
30	Test Panel Mass Versus Spacing (0.063-Inch Bumper)	3-21
31	Aluminum Bumper With 0.5-Inch Spacing (Panel A-48)	3-22
32	Reverse Side of Hull (Panel A-48)	3-23
33	Aluminum Bumper With 0.75-Inch Spacing (Panel A-37)	3-24
34	Aluminum Bumper With 3.0-Inch Spacing (Panel J-23)	3-25
35	Test Panel Mass Versus Spacing (0.032-Inch Bumper)	3-26
36	Test Panel Mass Versus Spacing (Aluminum and Plate Glass Bumpers)	3-31
37	Craters Produced in Aluminum With Copper and Steel Projectiles	3-32
38	Comparison of Mass Versus Spacing for Magnesium-Lithium and 0.090-Inch Aluminum Bumpers	3-34
39	Comparison of Mass Versus Spacing for Magnesium-Lithium and 0.063-Inch Aluminum Bumpers	3-35
40	Vehicle Hull Protected With a Plate Glass Bumper	3-37
41	Liquid-Pressurized Tank During Impact [Ref 3]	4-3
42	Liquid-Pressurized Tank After Impact [Ref 3].	4-4
43	Gas-Pressurized Tank During Impact [Ref 3]	4-5
44	Oxygen-Pressurized Tank; Test Panel No. 1 [Ref 2]	4-6
45	Oxygen-Pressurized Tank; Test Panel No. 2 [Ref 2]	4-7
46	Test Panel No. 3: 6Al-4V-Ti; 0.097-Gram Projectile; 60-psi Liquid Oxygen [Ref 2]	4-8

LIST OF ILLUSTRATIONS, Contd

<u>Figure</u>		<u>Page</u>
47	Test Panel No. 4: 2024-T3 Aluminum; 0.097-Gram Projectile; 60-psi Liquid Oxygen [Ref 2]	4-9
48	Mass Versus Spacing for Fiberglas Energy Absorber	5-2
49	Mass Versus Spacing for MIN K-1300 Energy Absorber	5-3
50	Mass Versus Spacing for Fibrous Potassium Titanate Energy Absorber	5-4
51	Energy Absorber Test Panel Configurations (See Table 9)	5-5
52	Honeycomb Panel No. 1	5-6
53	Honeycomb Panel No. 2	5-9
54	Penetration Dependence on Impact Velocity of Solid and Liquid Projectiles [Ref 5 and 13]	6-2
55	Glass Projectile Damage to Aluminum Panels	6-5
56	Crater Formed in Aluminum With a Nylon Sphere	6-6
57	Crater Formed in Aluminum With a Steel Sphere	6-7
58	Fragmentation Behavior on Flat-Face Impact	6-8
59	Fragmentation Behavior on Edge Impact	6-9
60	Shooting Arrangement, Projectile Data, and Projectile Photos	6-11
61	Shear Plug Diameter Dependence on Impact Velocity (0.57-Gram Steel Projectile and Aluminum Plate)	7-2
62	Shear Plug Diameter Dependence on Impact Velocity (0.57-Gram Steel Projectile and Titanium Plate)	7-3
63	Shear Plug Diameter Dependence on Impact Velocity (0.57-Gram Steel Projectile and Magnesium HK-31A Plate)	7-4
64	Shear Plug Diameter Dependence on Impact Velocity (0.57-Gram Steel Projectile and 301 Full-Hard Stainless Steel Plate	7-5
65	Shear Plug Diameter Dependence on Density (0.57-Gram Projectile)	7-6
66	Shear Plug Diameter Dependence on Density (0.21-Gram Projectile)	7-7

LIST OF ILLUSTRATIONS, Contd

<u>Figure</u>		<u>Page</u>
67	Shear Plug Diameter Dependence on Density (0.097-Gram Projectile)	7-7
68	Damage to Aluminum Plates by a Calibre .30-06 Bullet	8-2
69	Slow Speed Impact Photographs	8-3
70	Impact Flash.	8-4
71	Dynafax Photographs of Impact Phenomena Associated With Intermediate Speed Projectile	8-6
72	Aluminum Plates Used in Experiment D-155	8-7
73	Dynafax Photograph of the Impact Phenomena Associated With a High Speed Projectile	8-8
74	Aluminum Plates Used in Experiment D-157	8-10
75	Test Panel Mass and Spacing: Bumpers of Aluminum, Plate Glass, Mg-Li Alloy, and Stainless Steel	9-5
76	Total Weight Dependence on Aluminum Bumper Thickness (0.57-Gram Steel Projectile)	9-8
77	Effect of Bumper Thickness on Damage	9-9
78	Predicted Total Weight Dependence on Thickness of Aluminum Bumper With Zero Spacing (0.57-Gram Projectile)	9-12
79	Summary of Total Mass and Bumper Spacing	9-15
80	Curve for Those Experiments With Velocities From 16,000 to 21,700 Ft/Sec	9-18
81	Summary of Energy-Absorbing Material	9-21
82	An Experiment Which Shows the Advantage of Energy-Absorbing Core Material in Certain Configurations	9-22
83	Cross Sections of Bumpered Systems Showing Locations of Spray Cone of Fragments	9-24
84	Impact Regions [Ref 52]	10-3

LIST OF ILLUSTRATIONS, Contd

<u>Figure</u>		<u>Page</u>
A-1	Impact Flash	A-5
A-2	The Effect of Velocity on Penetration [Ref 52]	A-7
A-3	Penetration into Thick Targets Divided by Projectile Diameter as Function of Velocity [Ref 53]	A-8
A-4	Ratio of Crater Depth/Projectile Diameter Versus Velocity for Two Types of Aluminum [Ref 53]	A-9
A-5	Aluminum Impact on Aluminum [Ref 4]	A-12
A-6	Total Penetration Versus Impact Velocity [Ref 56]	A-14
A-7	Total Penetration Versus Bumper Thickness [Ref 56 and 59]	A-15
A-8	Dependence of Total Penetration on Bumper Spacing [Ref 56 and 59]	A-17
A-9	Half Angle of Spray Dependence on Target Thickness [Ref 59]	A-18
A-10	Bumper Hole Diameter Versus Bumper Thickness [Ref 59]	A-19
A-11	Diameter Ratio to Thickness Ratio [Ref 59]	A-20
A-12	Crater Diameter Dependence on Velocity [Ref 61]	A-21
A-13	Crater Volume Plotted Against the Cosine Square of the Angle-of-Incidence [Ref 63]	A-22
A-14	Normal and Oblique Impact in Lead Targets [Ref 67]	A-24
A-15	Normal and Oblique Impact in Hard Copper Targets [Ref 54]	A-25
A-16	Normal and Oblique Impact in Soft Copper Targets [Ref 54]	A-26
A-17	Effect of Temperature on Crater Volume [Ref 68]	A-28
A-18	Comparison of Crater Volume With Temperature and Tensile Strength With Annealing Temperature [Ref 68]	A-29
A-19	Comparison Between Crater Volume Temperature and the Elongation of Zinc Before Fracture [Ref 68]	A-30
A-20	Crater Volume Per-Unit-Projectile Energy Versus Projectile Density for Impact into Lead [Ref 69]	A-32
A-21	Projectile Fracture Velocity Versus Target Density for Impact of Hardened Steel Spheres into Various Targets [Ref 69]	A-34

LIST OF ILLUSTRATIONS, Contd

<u>Figure</u>		<u>Page</u>
A-22	Crater Volume Versus Impact Energy for Aluminum Spheres and Cylinders into 1100F Aluminum [Ref 53]	A-36
A-23	Crater Volume Versus Projectile Energy for Several Projectile-Target Systems [Ref 53]	A-37
A-24	Volume-Energy for Al into Pb and WC into Cu [Ref 53]	A-38
A-25	Striking Energy/Cavity Volume as a Function of Velocity [Ref 53]	A-39
A-26	Penetration Dependence on Momentum [Ref 61]	A-43
A-27	Penetration Dependence on Momentum Per-Unit-Area [Ref 61]	A-44
A-28	Crater Depth Versus Crater Volume/Crater Area for Nylon, Copper, and Tungsten Impacted into Lead [Ref 71]	A-45
A-29	Variation of Total Penetration With Impact Velocity in a Bumper Protected Target [Ref 72]	A-47
A-30	Penetration of Varying Number of Plates With Increasing Velocity [Ref 64]	A-48

LIST OF TABLES

<u>Table</u>		<u>Page</u>
1	Typical Velocity Results in Air for Steel Projectiles of Known Mass and Size	2-1
2	Definition of Symbols Used in the Figures to Describe the Projectile Impact Conditions	2-17
3	Materials for Pressurized Test Cylinder	2-20
4	Summary of Bumper Impact Data: 0.57-Gram Steel Projectile	3-3
5	Summary of Bumper Impact Data: 0.21-Gram Cylindrical Steel and 0.34-Gram Spherical Steel Projectiles	3-27
6	Summary of Massive Bumper Impact Data: 0.57-Gram Steel Projectile	3-29
7	Summary of Impact Data: Copper Projectile; 0.090-Inch Al Bumper	3-29
8	Comparison of Craters in Aluminum Produced With a Copper and Steel Projectile	3-33
9	Summary of Bumper Impact Data: Energy-Absorbing Core Materials and 0.57-Gram Steel Projectile (See Figure 51)	5-7
10	Steel, Glass, and Nylon Projectiles (Light Gas Gun)	6-3
11	Effect of Bumper Thickness on Damage	9-10
A-1	Summary of Penetration Data	A-40
A-2	Projectile Materials and the Constants for the Equations, $V = i_1 + k_1 E$, and $A = i_2 + k_2 M$	A-41

SECTION 1

INTRODUCTION

Vehicles operating in space will be exposed to the natural environment of vacuum; thermal, solar, corpuscular, and cosmic radiation; force fields; and meteoric particles. Space debris of artificial (Earth) origin will contribute to the entire environment. Unfortunately, the space environment is inadequately defined due to the paucity of experimental data. This can be attributed to the infancy of rocket and satellite programs for environmental testing, to the uncertainty in the data telemetered from space vehicles to Earth, and to the variable environment resulting from solar flare and meteoric particle shower activity.

The solid meteoric material in space presents a probable hazard to manned and unmanned vehicles that must operate for long periods of time in space, and particularly in the asteroid belt between Mars and Jupiter. Meteoric material with a mass as low as 10^{-14} gram may erode and damage radomes, optical windows, solar cells, and surfaces designed for temperature control and heat balance systems. Particles of this low mass and at meteoric velocities probably will not possess sufficient energy (or momentum) to form a significant crater in either a metal or other hard surface. In addition to this relatively slow destructive action from minute particles, there exists the possibility of catastrophic destruction via total demolition, puncture, and fluid* loss from larger particle impacts. The probability of puncture of a pressurized manned vehicle is of monumental importance, since it can result in mission failure through death or disablement of the crew from explosion, fire, or rapid decompression, as well as severe damage to the vehicle from the loss of fuel, radiator working fluid, etc. Fragment as well as shock damage to the crew, delicate instruments, and electronic components are also important possibilities.

Meteoroid technology has grown in importance and in urgency with the programming of missions involving greater exposure to meteoroid fluxes. In view of the obvious significance of meteoric particle damage to space vehicles, numerous investigations have been carried out during the past several years. These investigations have been concerned, however, primarily with the theory of hypervelocity impact and the experimental assessment of the related phenomena. On the other hand, designers have proposed several schemes and configurations for protecting vehicles from meteoric particles, but these configurations are partly supported by very isolated and inconsistent experimental data. The paucity of pertinent design information has resulted from the concentration of most laboratory research programs on the impact phenomena occurring with targets of semi-infinite thickness, rather than on thin sheet configurations. The need for obtaining useful design data was the primary reason for the awarding of this contract.

*Fluid designates both the gaseous and liquid states.

The lack of useful test data is also caused, in part, by the experimental difficulties, particularly in attempting to accurately simulate the actual environmental conditions. Accurate particle mass and velocity measurements are also difficult, since present laboratory instrumentation techniques do not appear to be either precise or reliable. To further complicate the problem, aerospace vehicles have numerous areas of variable vulnerability which necessitate different levels of shielding requirements. In addition, the damage inflicted by the particle, material behavior, and an acceptable risk-level must be balanced against the probability of impact with a given meteoric particle. Based on this risk-level, vehicle structures must be designed which will:

- a. Completely defeat all meteoric particles of a selected mass and velocity range.
- b. Completely defeat some particles of a limited mass and velocity range, but permit more energetic particles to completely penetrate the hull, followed by repair of the puncture via self-sealing action or by action of the crew.

The greatest certainty about the hazard to aerospace vehicles from meteoric particles is the great uncertainty in the predictions. The predictability of micrometeoroid impact damage to aerospace vehicles is limited by large uncertainties. Neither the number, mass, velocity, nor composition of the natural meteoric particles that constitute our local space environment is precisely known. Of the parameters which describe the meteoroid environment, only the number density is being accurately determined. Detectors that are used in the current series of satellites are accumulating data on the number of impact events over increasing periods of time. These impact events can be scaled in magnitude according to the response of the particular detector used. Existing impact detectors cannot be calibrated in the laboratory with particles of known mass at meteoroid velocities, and it is uncertain whether the various detectors respond linearly to momentum, kinetic energy, or some other function of mass and velocity at these extreme velocities. Signal output, therefore, cannot be uniquely correlated with the properties of the particles.

Thus, it can be seen that large areas of ignorance exist, and this ignorance can be attributed not only to the paucity of knowledge of the meteoroid environment of space, but to the response of materials and structures to this environment. A considerable amount of the current experimental and theoretical data are subject to uncertainty. Moreover, most of the research programs have dealt with cratering in semi-infinite plates which are limited in usefulness in the design of a space vehicle. Comparisons of penetration data (thick plates and low velocity particles) from the various laboratories, and of experimental data with theory have shown important discrepancies. Confusion exists because the data from the various laboratories cannot be compared directly, since identical projectile and target plate materials, environmental conditions, projectile sizes, shapes, masses, and velocity ranges were not used. Consequently, the host of empirical equations for penetration reported by the various

laboratories were derived to fit their own data, and therefore, are of limited use for other test conditions.

Only the lower end of the meteoric velocity range has been explored experimentally in any great detail. Extrapolations of the various empirical data-fits to higher velocities also leads to great discrepancies. Experimental-theoretical comparisons have been unsatisfactory due to the: a) laxity in reporting the material properties used as projectiles and/or target plates; and b) simplification so the proposed theories fit particular sets of data, resulting in applicability only to a very limited range of impact velocities and materials properties. The range of applicability of these theories is not clearly known. Consequently, the quantitative predictions necessary for sensible and adequate protection designs derived from these crude estimates are only indicative of the orders of magnitude involved. When these estimates are properly interpreted they can serve as useful but not exact design guides.

Thus, it can be seen that theory and design have generally followed separate paths, and presently, there are only a few attempts to integrate theoretical concepts and recognized phenomena in the development of structural systems. The prime prerequisite for the establishment of realistic design criteria is a systematic experimental investigation, carried out on materials and structural configurations useful in actual vehicle construction. Such a systematic approach would also permit an expeditious revision when new environmental or other parametric data become available.

There is a dearth of empirical data concerning the impact behavior of materials and configurations suitable for space vehicles. Experimental programs on composite structures, self-sealants, and meteoroid bumpers for manned and unmanned space vehicles are in their infancy. These protection systems, based on data from experimental programs limited in both impact velocity and mass, appear far more attractive than the massive resistance approach (semi-infinite plates), and therefore, merit extensive investigation. In addition, these systems may be designed so they can function in more than one capacity. For example, a configuration with energy-absorbing core material may provide meteoroid and thermal protection, etc; that is, a multipurpose vehicle hull.

It was attempted in this program to evolve and experimentally establish the fundamental principles of meteoroid protection, as well as to evaluate various meteoroid protection concepts which may be considered feasible for use on aerospace vehicles.

SECTION 2

EXPERIMENTAL

Velocity and mass ranges of importance in meteoric particle impact would fall in Zone A of Figure 1. The velocity range obtained by explosive charges, light gas guns, and similar techniques fall in Zone B, while Zone C indicates the possible attainment by exploding liners and staged explosive charges. It seems unlikely that laboratory experiments will be devised within the next several years to cover very much of Zone A.

The explosive charge (end projection) and light gas gun facilities were used in this investigation to propel projectiles of known mass and velocity at selected materials and test panel configurations.

2.1 EXPLOSIVE PROJECTION. The explosive charge (end projection) technique was used to propel projectiles of known geometry, mass, and velocity at selected targets. The explosive charge (Figure 2) consisted of a plastic explosive (composition C-4) molded into a 2-inch diameter by 5-inch long cylinder with an air cavity at one end. A conical lead collet, ultimately mated to the charge cavity, was used to mount the cylindrical steel projectiles. A Number 10 blasting cap initiated the explosion. Projectile velocities between 5,000 and 25,000 ft/sec were measured by breaking three equally spaced printed circuits. The resulting signals were detected on two Tektronix Model 360 Oscilloscopes and recorded on polaroid film. Debris and fragments from the explosive and lead collet were prevented from contacting the test panel through the use of three steel baffle plates (Figure 3), each provided with a small diameter hole.

2.1.1 Projectiles. The projectile mass versus velocity for various T/D ratios* that have been attained consistently in this program are shown in Figure 4. These data pertain to those masses that can be accelerated without premature projectile fragmentation. It should be noted that the accelerated and impact masses (see Section 6.3) are not identical. The average velocity for four different projectiles is summarized in Table 1.

Table 1. Typical Velocity Results in Air for Steel
Projectiles of Known Mass and Size

ACCELERATED MASS (GM)	THICKNESS (IN.)	DIAMETER (IN.)	TYPICAL VELOCITY (FT/SEC)	T/D*
0.097	0.063	0.125	11,400	0.504
0.196	0.125	0.125	10,400	1.000
0.215	0.063	0.189	13,300	0.333
0.570	0.094	0.250	15,000	0.375

* Ratio of Thickness to Diameter

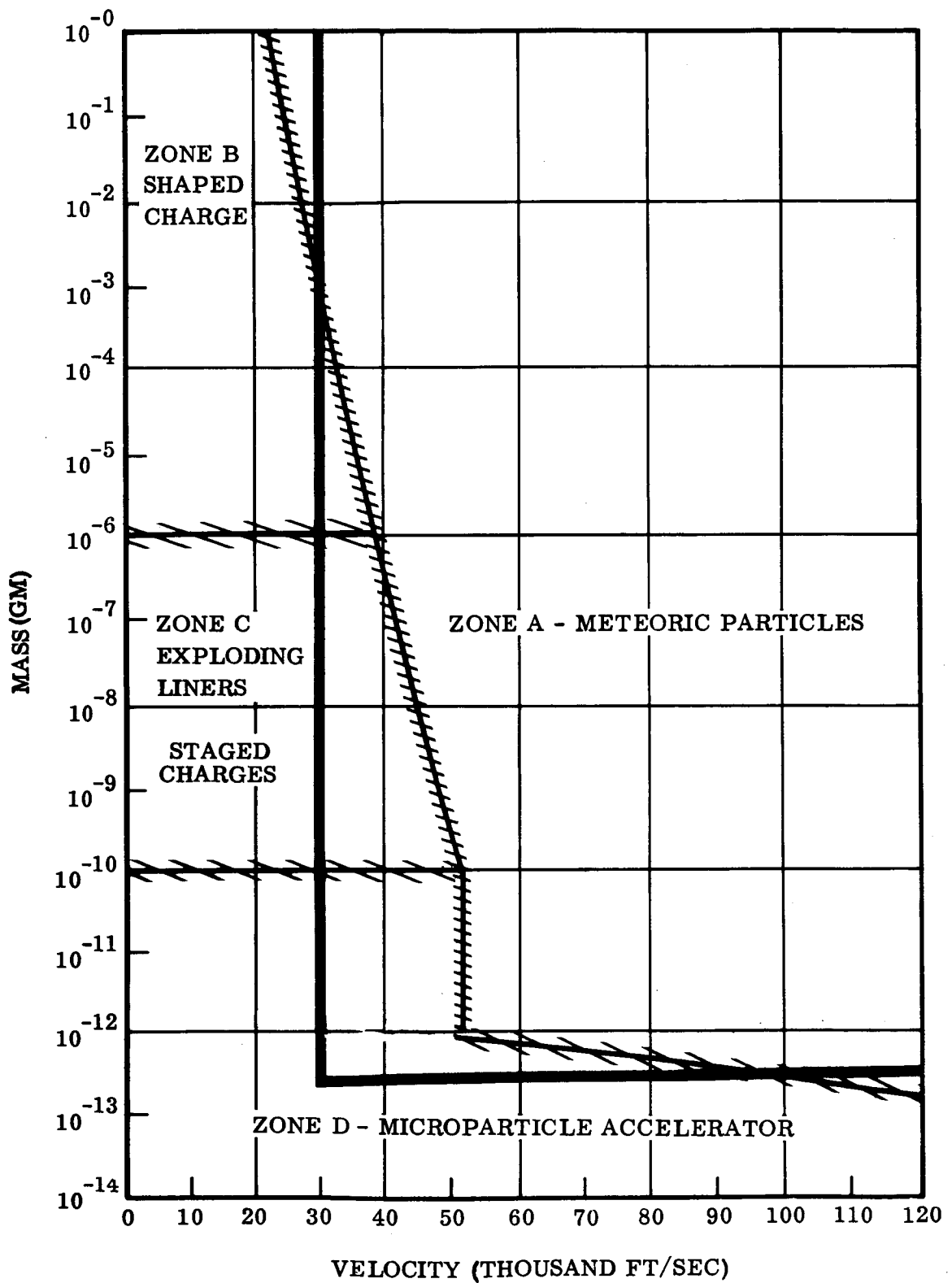


Figure 1. Velocity and Mass Regimes

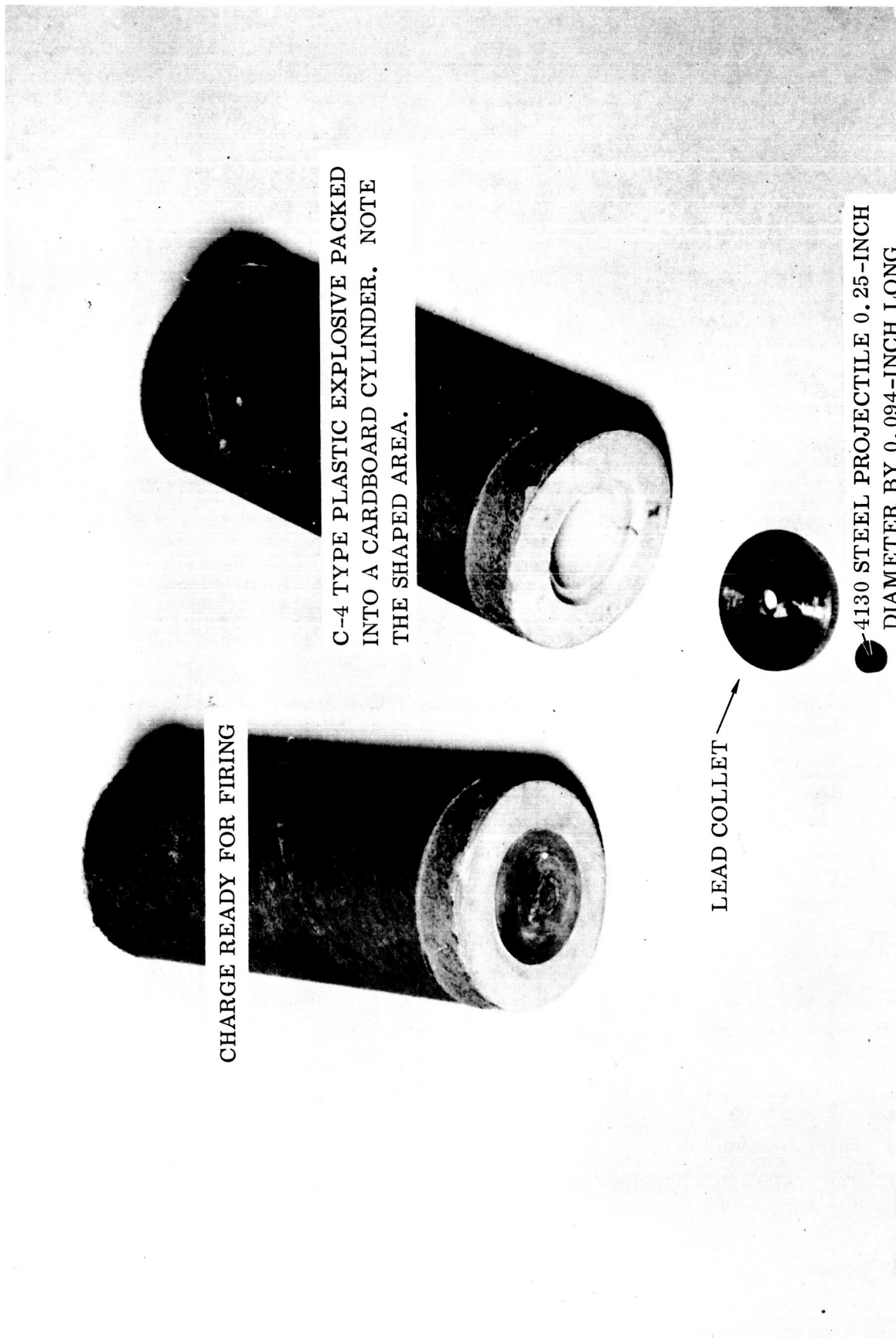


Figure 2. Explosive Driver and Projectile

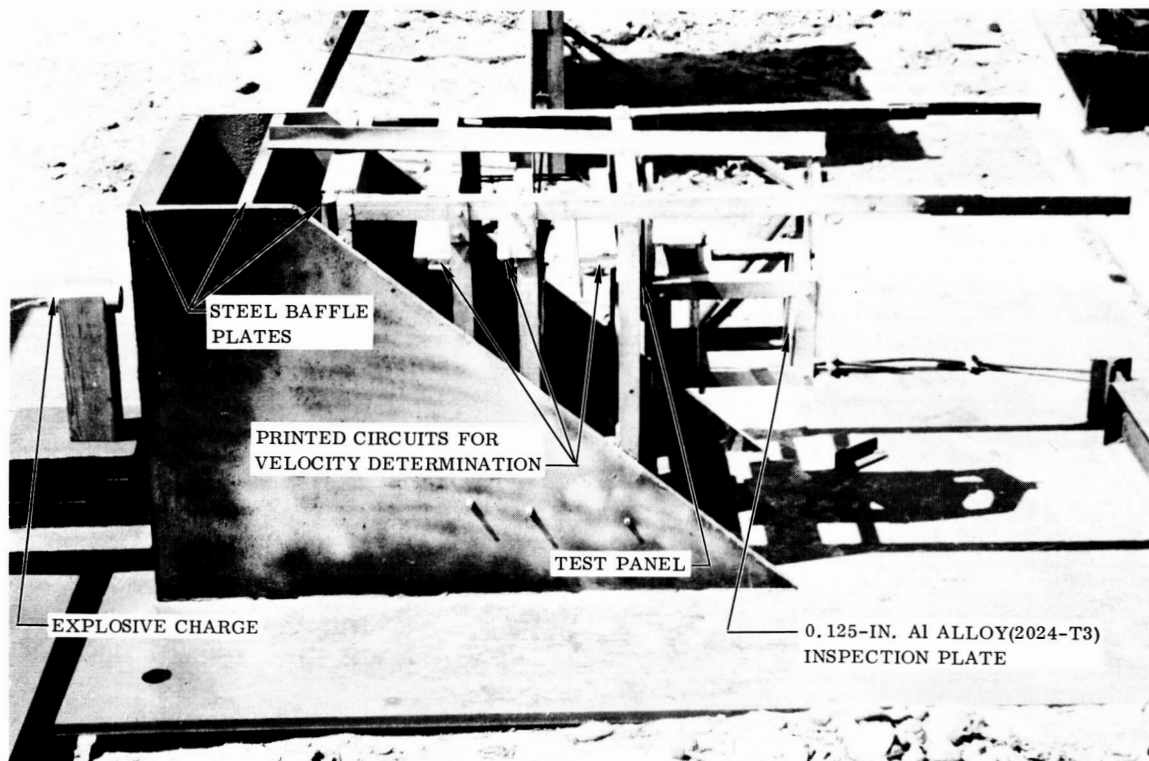


Figure 3. Test Arrangement

2.1.2 Projectile Integrity. The projectile maintained its integrity during acceleration and prior to impact with the target plate. This can be deduced from the projectiles recovered after acceleration (see Section 6.3), as well as from inspection of test panels (photographs of commercially pure titanium, Figure 5; and magnesium alloy AZ-31A-H24, Figure 6, since there was a single large hole in each plate). The 0.45-inch diameter tapered hole in the 0.375-inch titanium plate was produced by a 0.57 gram, 0.094-inch thick by 0.25-inch in diameter projectile with a velocity of 18,000 ft/sec. At this velocity, the steel projectile was fragmented on impact with the titanium target and neither the fragments nor the shear plug penetrated the 0.125-inch aluminum (2024-T3) inspection plate, positioned 4 inches behind the titanium plate. The 0.53- by 0.56-inch hole in the magnesium target was produced by a 0.215 gram, 0.063- by 0.188-inch steel projectile with a velocity of 13,600 ft/sec. This velocity was not sufficient to completely* fragment the projectile.

Further indication of projectile integrity has been demonstrated with a flash X-ray system, and a photograph of the projectile in flight can be seen in Figure 7. The projectile has tipped, decreased in thickness (14.9 percent), increased in diameter (36 percent), but apparently has not fragmented under the high acceleration loads.

*The projectile was fragmented, but not to the degree which was desired.

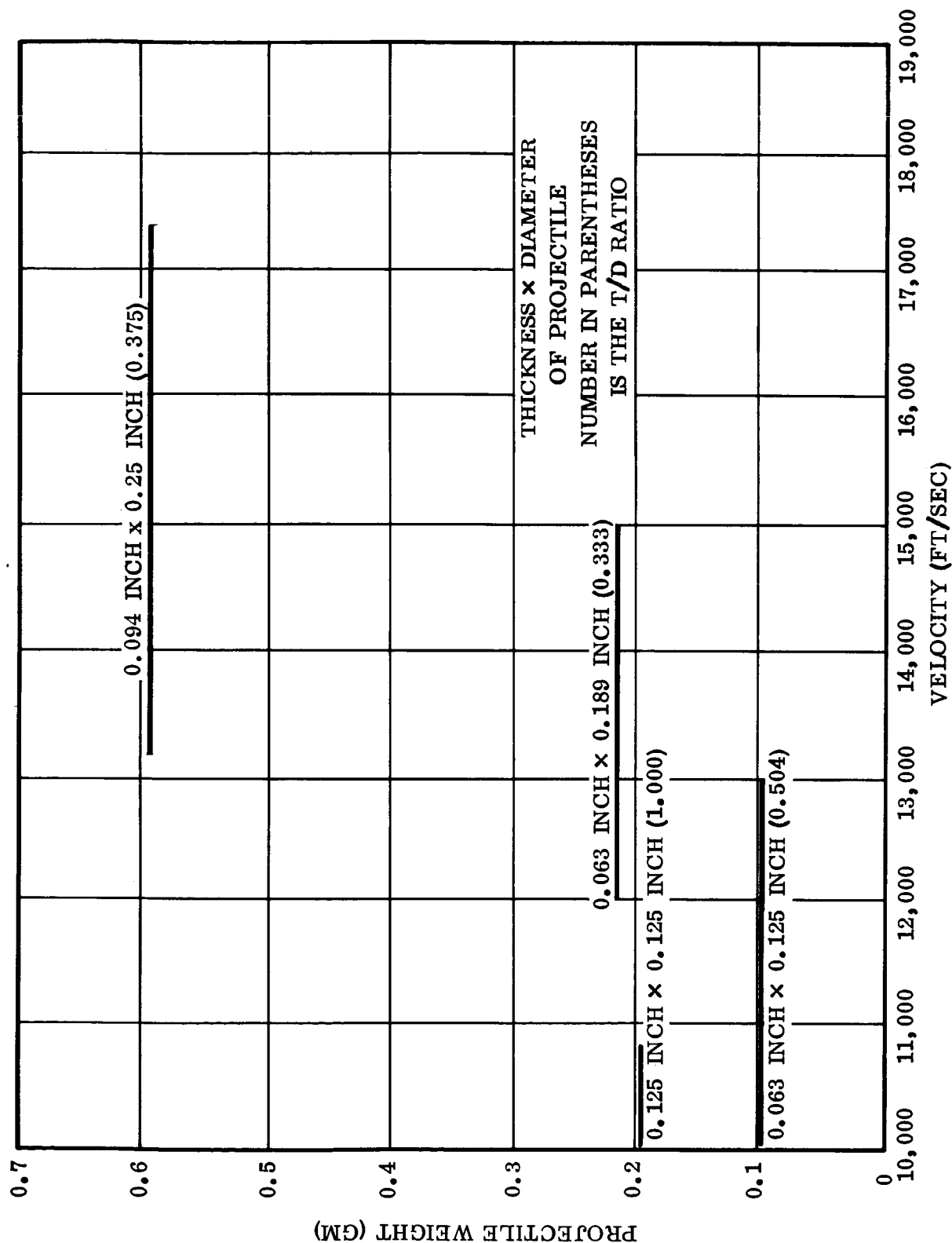
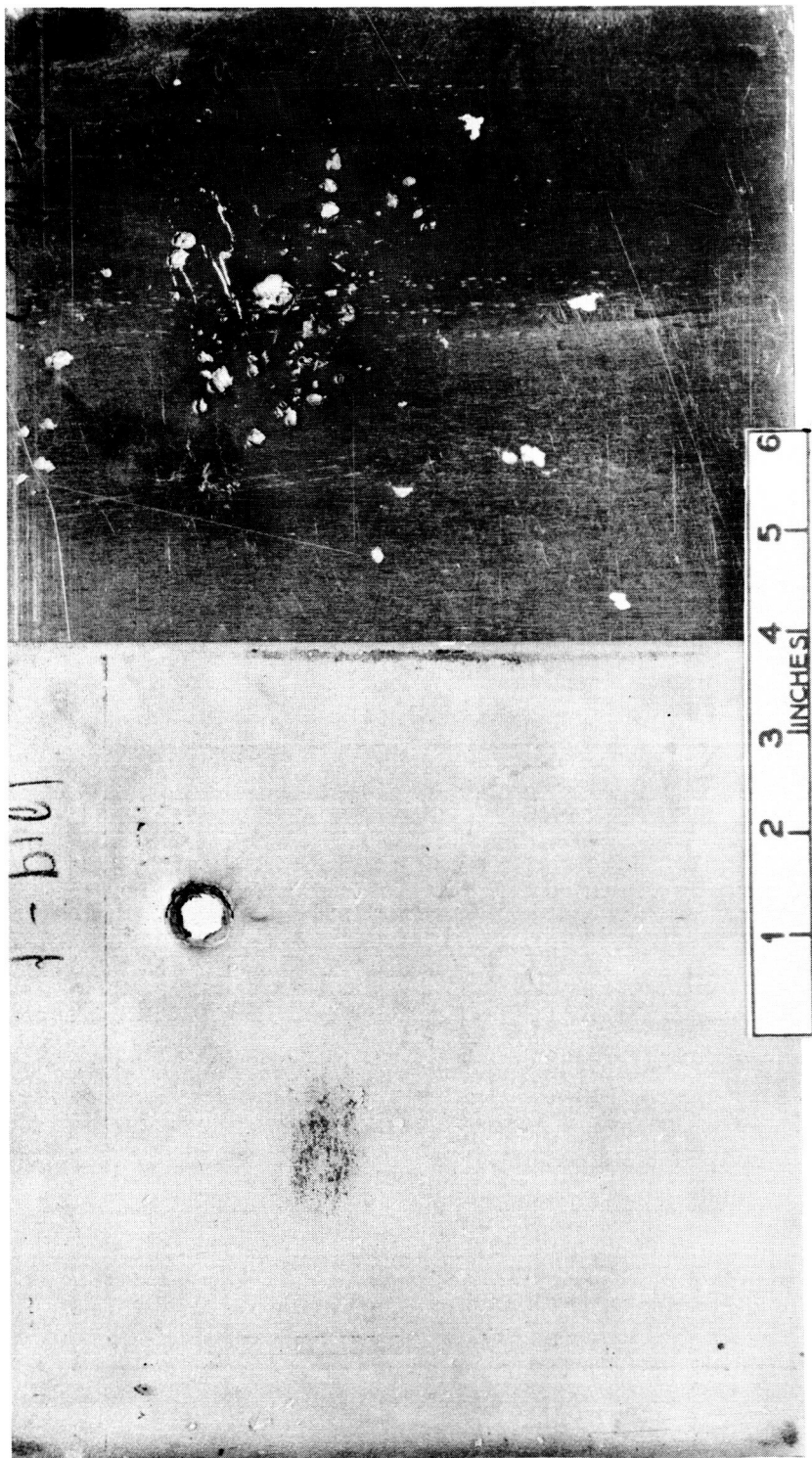


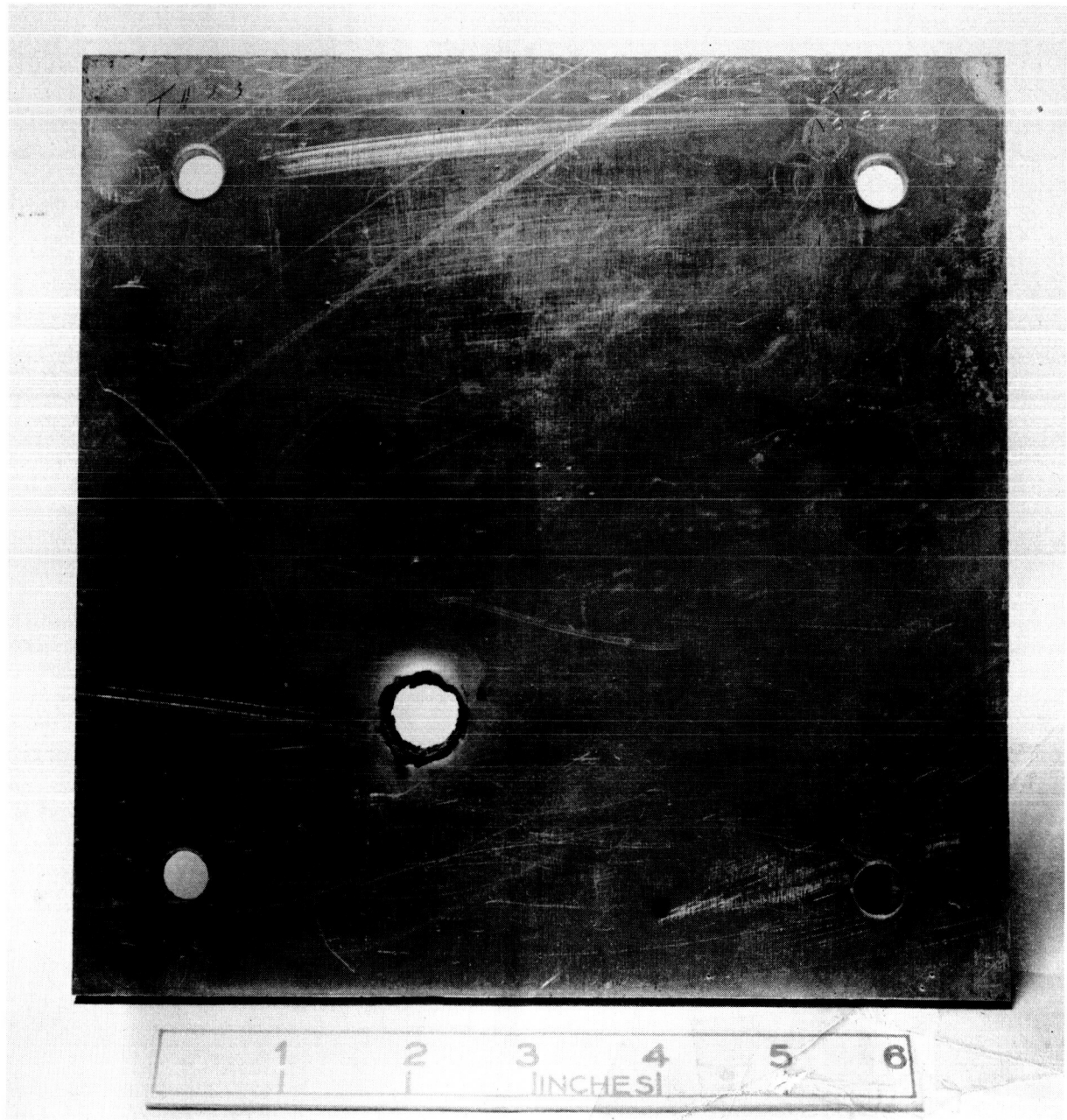
Figure 4. Velocities Obtained in Air With Various Steel Projectiles



0.375-IN. TITANIUM (75A)

0.125-IN. ALUMINUM (2024-T3) PLACED
4 IN. BEHIND TITANIUM BUMPER

Figure 5. Titanium Plate Impacted With a 0.57-Gram Projectile at 18,000 Ft/Sec



0.250-IN. MAGNESIUM (AZ-31A-H24)

Figure 6. Magnesium Plate Impacted With a 0.215-Gram
Projectile at 13,600 Ft/Sec

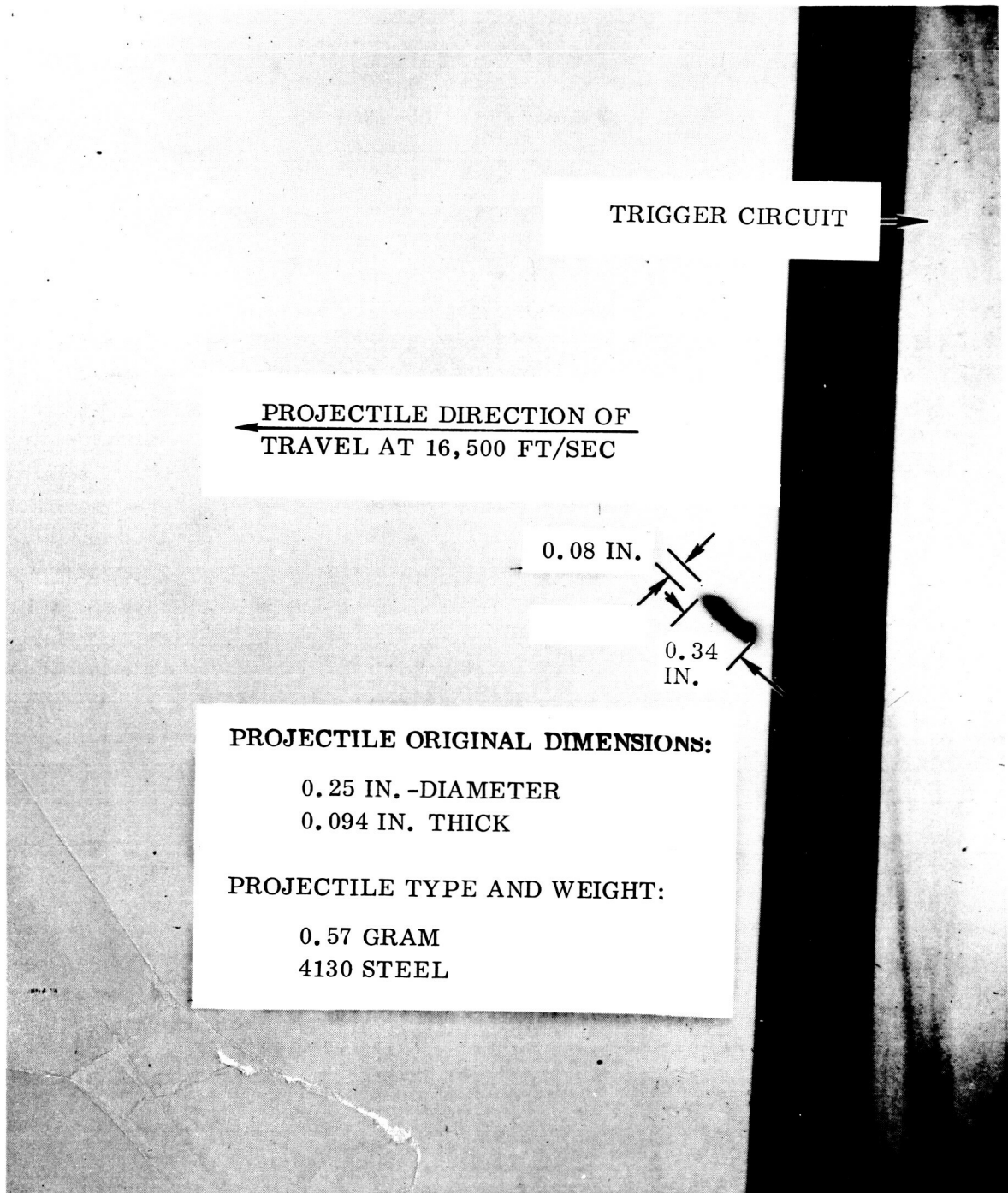


Figure 7. Flash X-Ray Photograph of a Projectile in Flight

2.1.3 Velocity Measurement. A break circuit system was used to determine projectile velocities, and the circuit diagram is given in Figure 8. Conductive grid circuit paper was placed at 2, 2-1/2, and 3 feet from the initial position of the projectile. The test panel was positioned 3-1/3 feet from the initial position of the projectile. Signals were recorded with the cameras mounted on the oscilloscopes that are shown in Figure 9, and typical oscilloscope traces are shown in Figure 10.

When the projectile passed through the first grid paper, a trace was started on both oscilloscopes. The trace continued until the projectile passed through the second grid paper, at which time a change in slope was observed on the first oscilloscope, and as the projectile broke the third grid paper, a change in slope was observed on the second oscilloscope. Full scale on the oscilloscope corresponds to 1.0×10^{-4} second, and since the distance between the grid papers was known precisely, the average velocity of the projectile was determined. The smoothness of the observed traces indicated essentially no "jitter" as the projectile passed through the grid papers. The flash X-ray is considered to be the most precise method of checking the velocity of a projectile. This method was used to confirm the grid measurements; accuracy was within 6 percent. A typical X-ray photograph of a projectile in flight is shown in Figure 7.

2.2 BALLISTIC RANGE. The controlled atmosphere range, light-gas and powder guns, shadow-graph system, and velocity measuring instrumentation have been discussed in the General Dynamics/Convair Report by Dana [1]*. The range facility used (Figure 11) is approximately 100 feet long and 5 inches in diameter. The 4-foot long by 2-foot diameter blast chamber was constructed of 0.50-inch steel plate. At the centerline of the tank are located four 0.50-inch thick steel baffles. These baffles retard the gun gases from entering the test section of the range. The gun muzzle enters the blast tank through a vacuum sealed adapter plate.

Two Mylar gates separate sections of the range for which additives to the atmosphere or different pressures can be used on the same experiment. Figure 12 illustrates the 5-inch diameter Mylar gate. This gate uses 5-mil Mylar sandwiched between components 3 and 4. These two pieces are sealed by O-rings against the Mylar, and slide into components 1 and 2, which are held together in the range by five 0.75-inch bolts. Five-mil Mylar will hold one-atmosphere pressure differential and does not damage high velocity aluminum projectiles. However, nylon and ethocel projectiles usually shatter when striking the Mylar under a one-atmosphere pressure differential. The gates provide a quick and easy means of putting new Mylar diaphragms in the test sections without disassembling the range.

The launching device used in the hypervelocity range facility was a piston-compressor-type, helium, light gas gun. The gun has a 3-foot long by 0.3125-inch diameter launch

*Figures contained in brackets refer to reference data listed in Section 11, Bibliography.

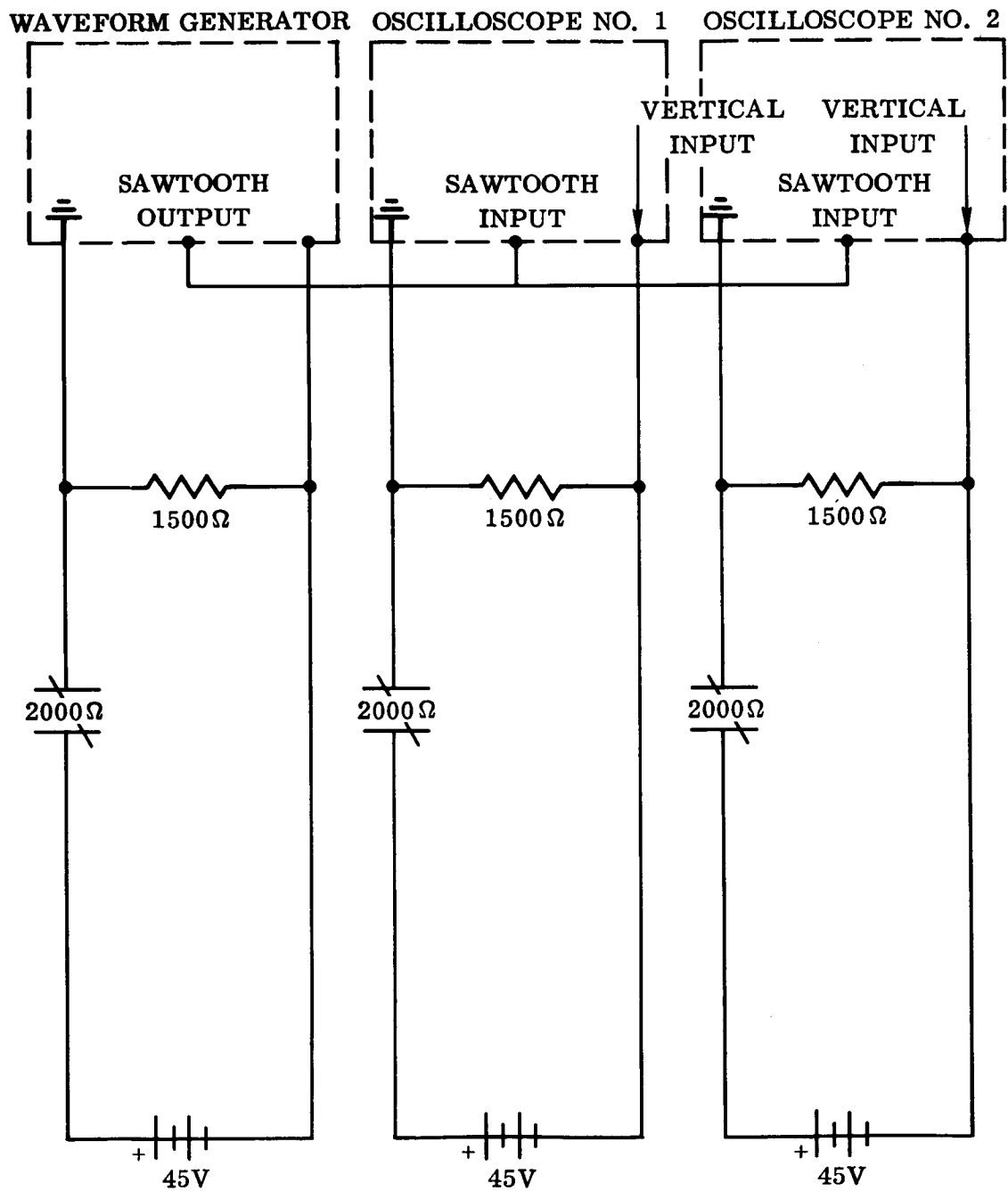


Figure 8. Break Circuit for Measurement of Projectile Velocity

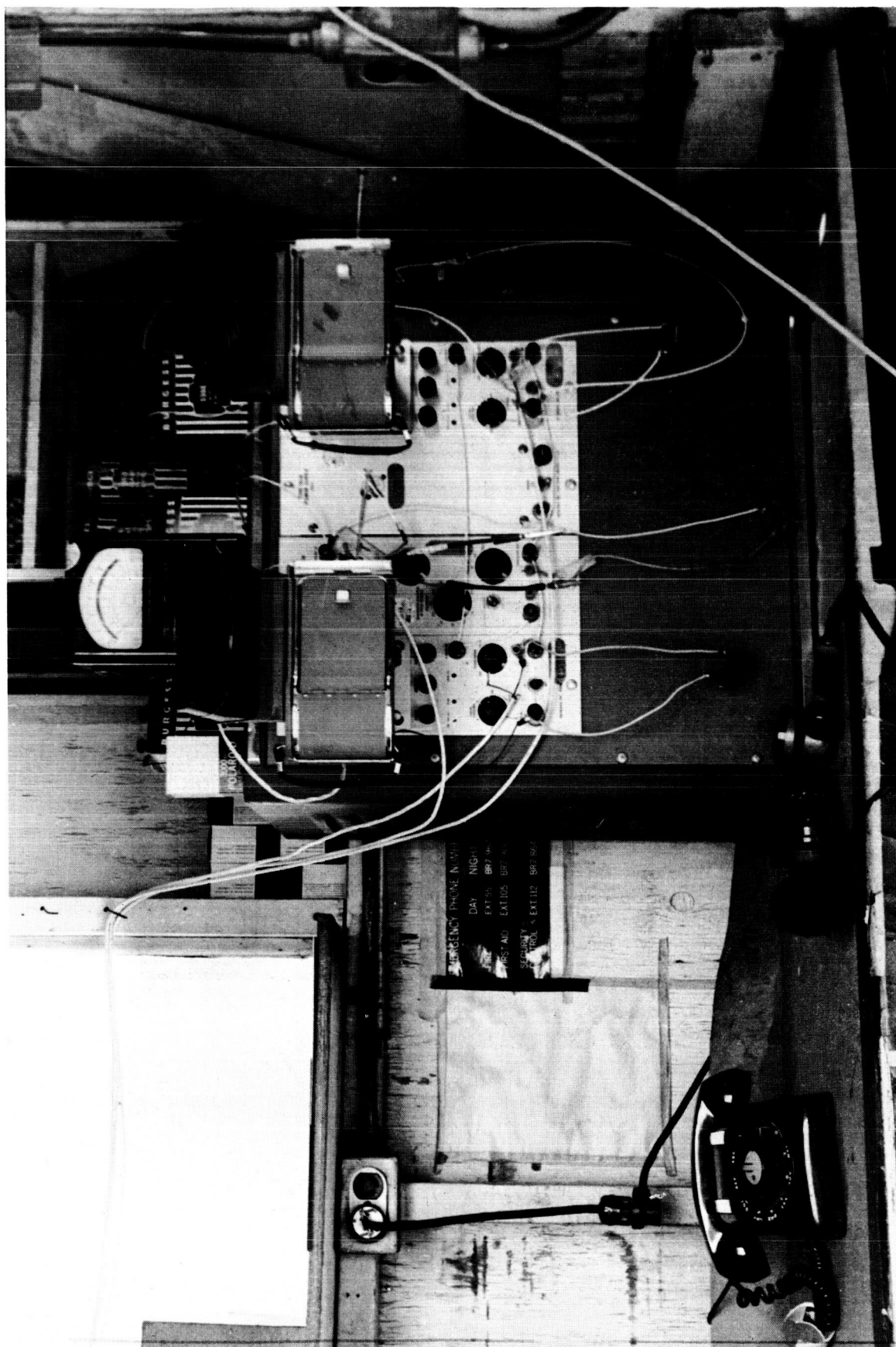
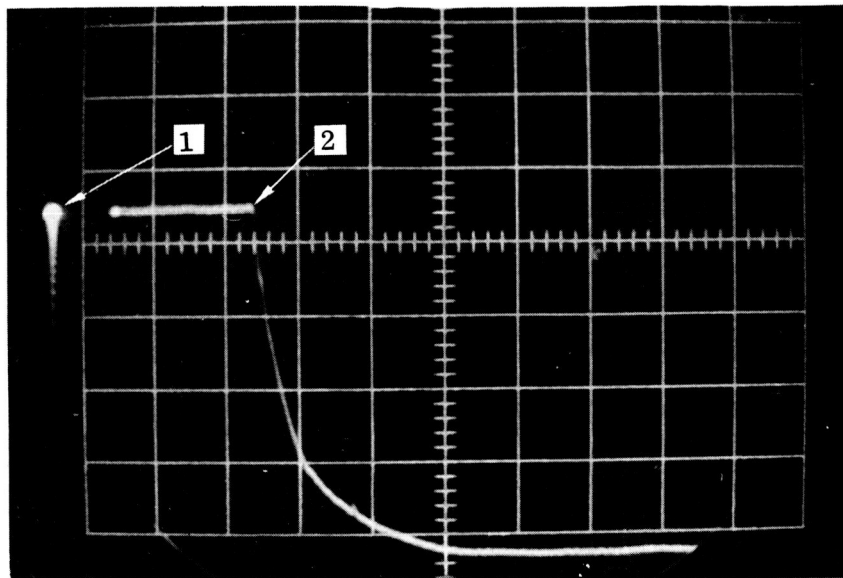
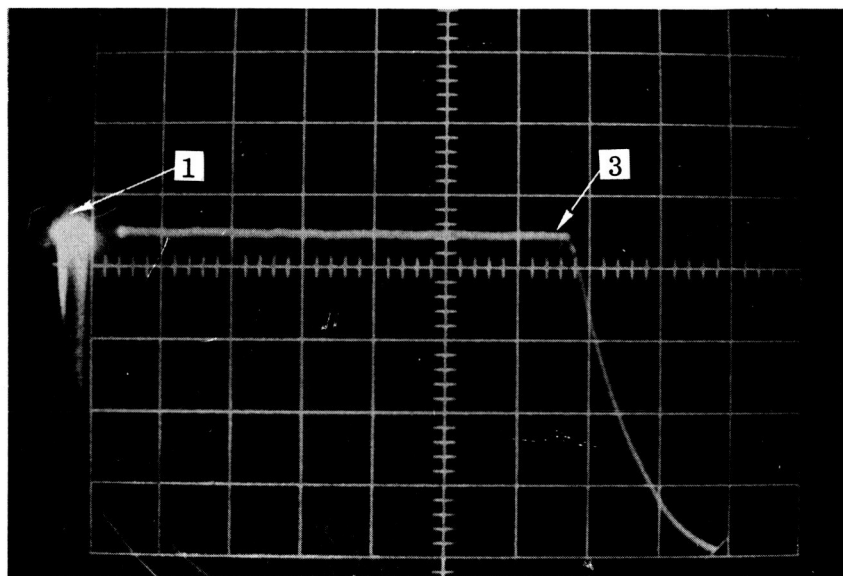


Figure 9. Velocity Measuring Equipment



OSCILLOSCOPE NO. 1



OSCILLOSCOPE NO. 2

1. First grid paper starts traces on both oscilloscopes
2. Second grid paper is broken
3. Third grid paper is broken

Figure 10. Oscilloscope Traces for Measurement of Projectile Velocity



Figure 11. Ballistic Range [Ref 1]

April 1962

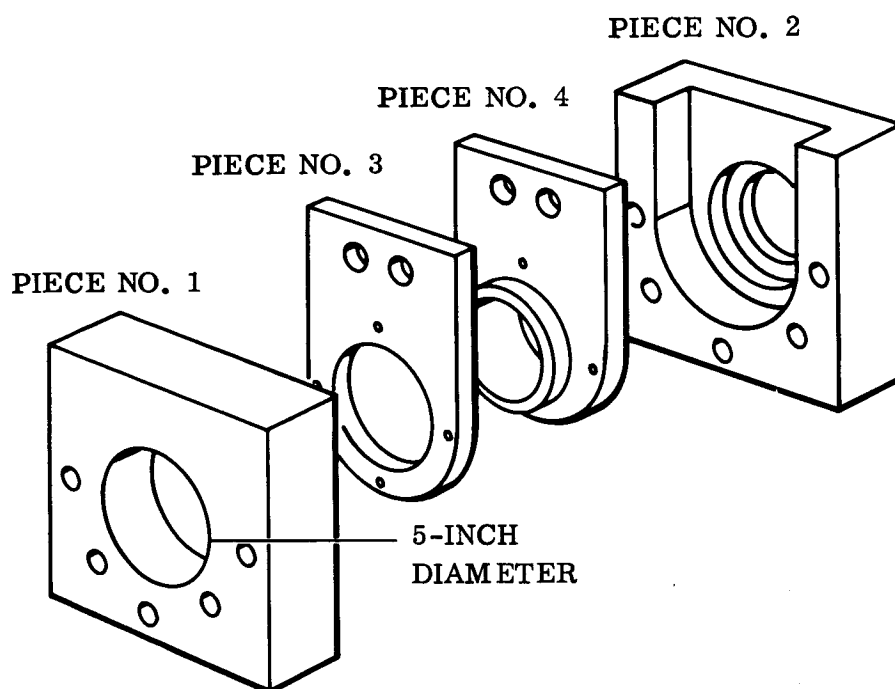


Figure 12. Mylar Gate [Ref 1]

tube, and a 6-foot long by 0.552-inch diameter pump tube, with a standard calibre 0.50 primed cartridge case to contain and ignite the powder loaded into the powder chamber. A variety of loading conditions have been used in obtaining the maximum velocity of the gun. The most effective loading conditions are 125 grains of Hercules unique powder (50,000 psi), a 15-gram aluminum pump piston, a 0.30-gram nylon projectile, and a helium charging pressure of 300 to 400 psi. A mild steel piston weighing about 40 grams produces slightly higher velocities but causes considerable damage to the piston stop, diaphragm holder, and launch tube. Nylon (0.299 gram), steel (0.12 gram) and glass (0.08 gram) projectiles have been accelerated in vacuum to 17,800, 14,000 and 15,700 ft/sec, respectively.

2.3 TEST PROGRAM. The explosive driver was one technique used to propel the cylindrical steel projectiles during this experimental program. Experience has demonstrated that a 450-gram shaped charge of composition C-4 explosive will consistently accelerate these projectiles, without fragmentation, to velocities in the range of 15,000 to 20,000 ft/sec. With these velocities, the hypervelocity (fluid impact) regime can be achieved, and the projectile will fragment on impact with the target. The attainment of the fluid impact regime is, of course, a prerequisite for hypervelocity studies directed toward the establishment of meteoroid bumper protection concepts.

2.3.1 The Bumper. The bumper is defined as a shield set up at some distance from the main vehicle hull to destroy the structure of the projectile. In order to attain the greatest projectile destruction, maximum violence between the bumper and projectile must be achieved during the initial impact. No series of tests* were made in which the bumper was divided into a number of thin plates, since this arrangement would increase the number of variables in an already complex system.

Aluminum alloy, 6061-T6, comprised both the bumper and the vehicle hull plates** that were subjected to normal impact. The 6061 alloy is a readily available and weldable structural material. Bumper plates with a thickness of 0.032, 0.063, 0.090, 0.125, and 0.1875 inch were used in the experiments. This range of bumper thickness was expected to provide the requisite information for establishing the relationship between the projectile, bumper, and vehicle hull, as well as to include the most effective bumper mass per-unit-area to oppose the steel projectiles. Bumpers of plate glass, magnesium-lithium alloy, stainless steel, and wire screen were also used with the 6061 aluminum vehicle hull. These bumper materials include a wide range in physical properties; i.e., density, strength, ductility, etc.

* Several multiple bumper tests were made in which impact phenomena were studied photographically (see Section 8).

** The test panel was comprised of a bumper and the vehicle hull plate.

April 1962

A series of tests were conducted with each thickness of bumper plate in order to investigate the importance of bumper mass and the distance of separation from the main vehicle hull. With a fixed bumper mass, the distance of separation for any given total mass* per-unit-area was varied from zero to a distance where the main vehicle hull just stopped the projectile and shear plug fragments. Belling** was not considered as complete penetration or piercing of the test panel, if cracks were not produced in the rear surface. The total weight per-unit-area which would prevent the formation of a hole or crack in the vehicle hull, distance between the bumper and vehicle hull, thickness of the bumper, and mass of the bumper, were the parameters considered so that the total weight for a protected and unprotected vehicle hull could be compared.

Pertinent data are summarized in the appropriate tables. Definition of the symbols used in the figures are summarized in Table 2. For example, Experiment J-20 with a reliability code ABB, indicates that the projectile A, struck the target nearly flat; B, fragmented to a slight extent before contacting the bumper; and B, had an impact velocity in the range of 12,000 to 16,000 ft/sec. Although the desired impact conditions are AAC or AAD, it should be observed that impact conditions corresponding to BAC or BAD are more severe.

2.3.2 Pressurized Test Cylinder. The five-inch diameter test cylinder was fabricated [2] from 0.50-inch thick stainless steel and the details of construction are given in Figures 13 and 14 and Table 3. A 0.375-inch thick flange, provided with a Toruseal groove (0.25 inch by 0.075 inch) for sealing, was welded on each end of the cylinder. The two 7-inch diameter test diaphragms were placed between the cylinder and mating flanges held in place with twelve 0.25-inch bolts. The cylinder was purged for 3 to 5 minutes with gaseous nitrogen, and 5 minutes with gaseous oxygen before the tank was pressurized for impact testing. Purging and overflow was accomplished by opening the 1-inch line located on the top of the cylinder, while the 0.5-inch line located on the side of the cylinder was used to fill the tank.

* The mass of both the bumper and the vehicle hull constitutes the total mass of the test panel.

**Belling designates the formation of a bulge on the rear surface of the vehicle hull.

Table 2. Definition of Symbols Used in the Figures to
Describe the Projectile Impact Conditions

ORIENTATION	INTEGRITY	IMPACT VELOCITY
A. Projectile struck bumper nearly flat.	A. No projectile fragmentation prior to impact on bumper.	A. Velocity less than 12,000 ft/sec
B. Projectile struck bumper on edge.	B. Very little premature fragmentation.	B. Velocity between 12,000 and 16,000 ft/sec
C. Impact angle not indicated.	C. Moderate premature fragmentation.	C. Velocity between 16,000 and 20,000 ft/sec
		D. Velocity between 20,000 and 25,000 ft/sec
		E. Velocity between 25,000 and 30,000 ft/sec

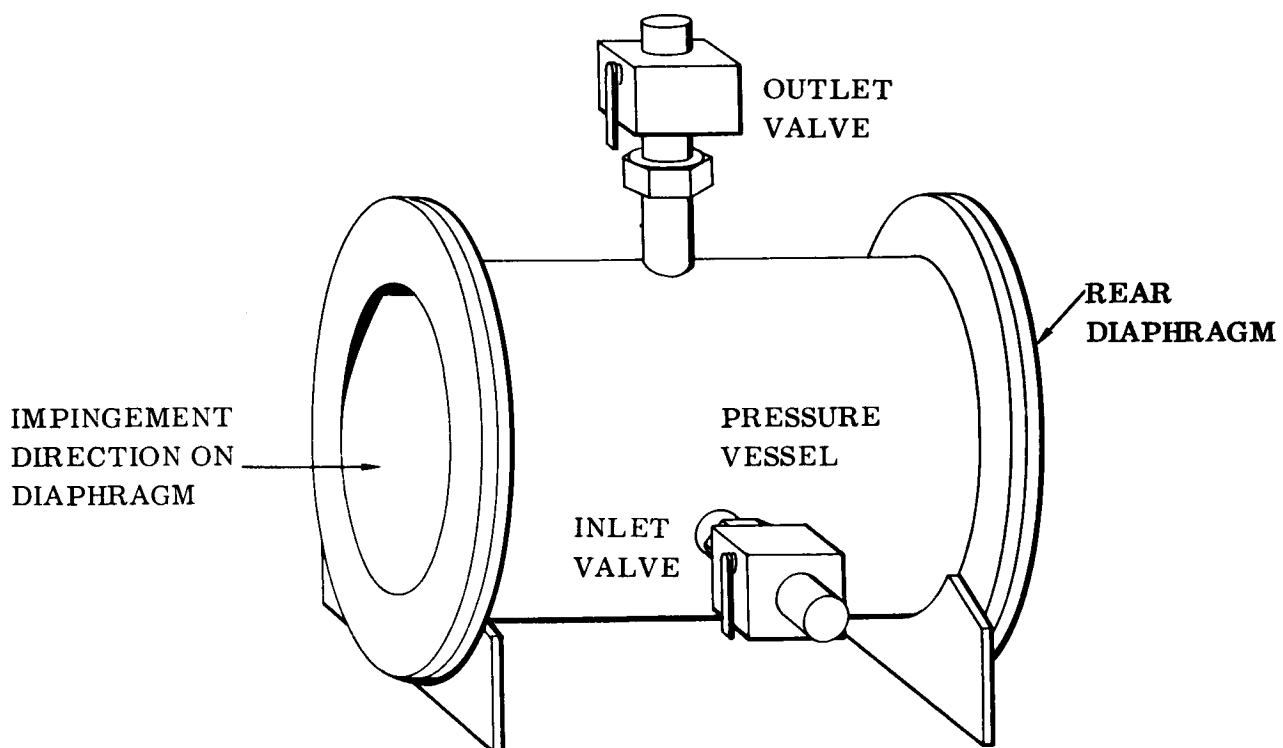


Figure 13. Pressurized Test Cylinder and Fixture [Ref 2]

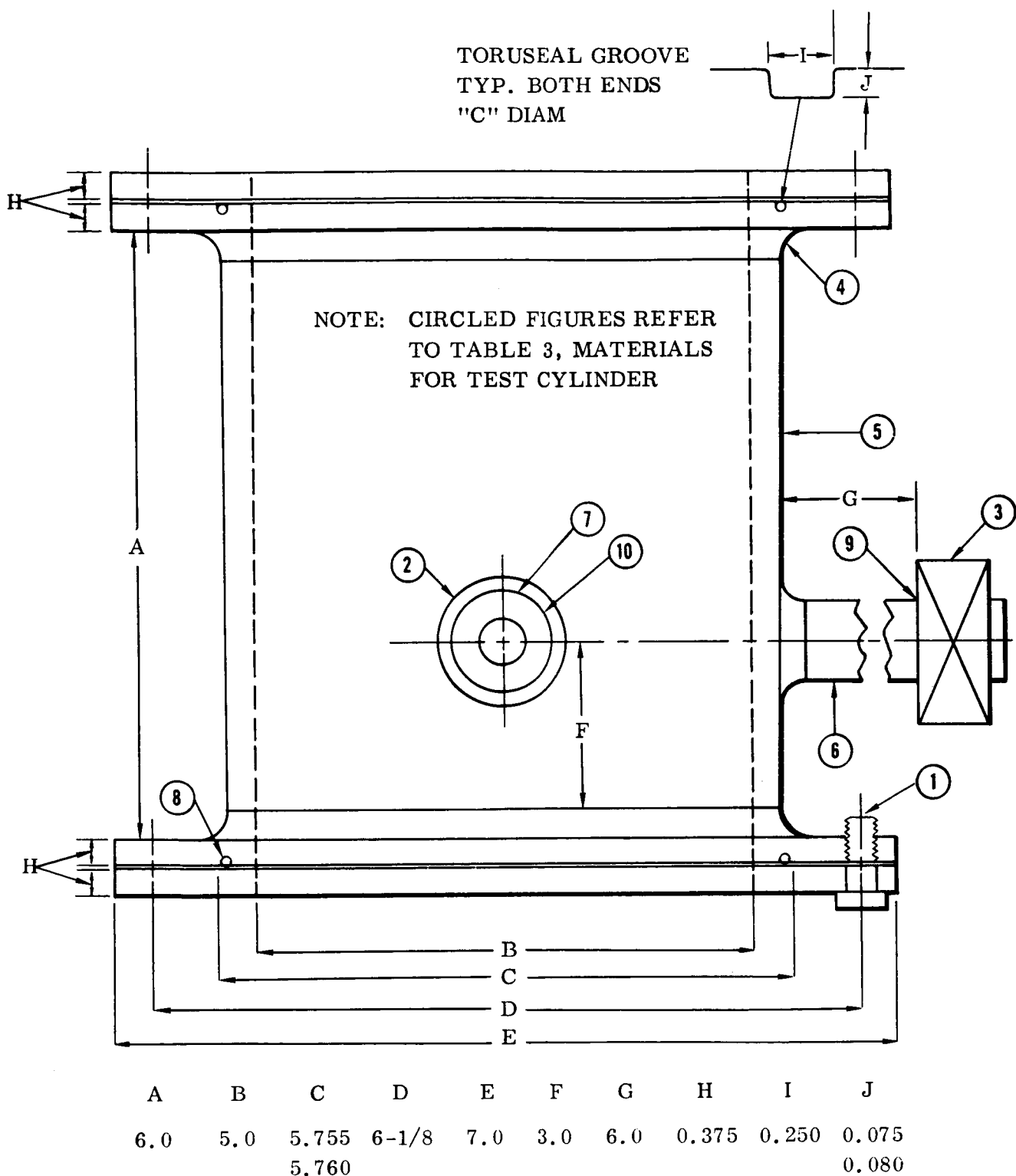


Figure 14. Construction Details of the Test Cylinder [Ref 2]

Table 3. Materials for Pressurized Test Cylinder

ITEM	MATERIAL DETAILS AND INSTRUCTIONS
① *	Twelve hex head cap screws, 0.25-inch and 0.75-inch long. Typical for both ends of test cylinder.
②	Manually operated Flo-Ball valve, Hydromatics Inc., Model 115C stainless steel for liquid-oxygen service, 0.50-inch nominal size. Valves 2 and 3 are positioned 90 degrees apart, 8 inches from tank.
③	Manually operated Flo-Ball valve, Hydromatics Inc., Model 115F stainless steel for liquid-oxygen service, 1-inch nominal size.
④	Weld flange rings to pipe. Machine flange surface after welding.
⑤	Stainless steel pipe, 5-inch nominal size.
⑥	Stainless steel fitting (1 inch) and 10056-16. Weld to Tank. Use stainless steel flare nuts and 8 inches of Type 304 tubing.
⑦	Stainless steel fitting (0.50 inch) and 10056-8. Weld to Tank. Use stainless steel flare nuts and 8 inches of Type 304 tubing.
⑧	Stainless steel Toruseal, Size No. C5750A. Typical for both ends of test cylinder.
⑨	Stainless steel flare nut (1 inch) on 8-inch length of Type 304 tubing to fit, and 10056-16 on valve.
⑩	Stainless steel flare nut (0.50 inch) on 8-inch length of Type 304 tubing to fit and 10056-8 on valve.

* Circled figures refer to construction details of Figure 14.

SECTION 3

INVESTIGATION OF BUMPER EFFECTIVENESS

3.1 SOLID METAL BUMPER. The aluminum (6061-T6) bumper and vehicle hull were subjected to normal impact from an explosively accelerated 0.57-gram cylindrical steel projectile. Criteria for a satisfactory bumper-hull and mass-distance arrangement was based on the vehicle hull plate not being penetrated or cracked. If the bumper has the proper mass and distance from the main hull, the projectile particles and shear plug fragments moving from the bumper toward the vehicle hull will be dispersed in time, direction, and space, and material strength in the vehicle hull becomes the important factor. Pertinent data are summarized in Table 4.

Initial impact experiments were made with relatively thick aluminum (6061-T6) slabs. The 0.57-gram projectile*, traveling at 13,500 ft/sec, did not completely penetrate or crack an 0.875-inch plate, but produced (Figure 15) an 0.625-inch diameter non-hemispherical crater, with a 0.08-inch lip around the crater and a 0.1-inch high bulge on the rear surface. This panel weighed 12.43 lb/ft² and was used as the fiducial point (Experiment J-2 of Figures 16, 17, 30, and 35), for all subsequent experiments in which the 0.57-gram projectile was used to study the effect of total mass (bumper plus target) of the test panel, and the distance of separation on total penetration.

Note that in a number of instances, for example, with copper projectiles or with glass bumpers, that experiments which did not result in the complete penetration or cracking of the vehicle hull plates were not repeated with a reduced spacing. Experience has shown that whenever a pronounced bulge appears on the rear surface of the vehicle hull plate, a small reduction in spacing will result in complete penetration and/or cracking.

3.1.1 Aluminum Bumper, Type 6061-T6, 0.125 Inch Thick. Nine 0.125-inch aluminum bumpers with a spacing from 0.5 to 6 inches have been subjected to impact from the 0.57-gram steel projectile. The curve in Figure 16 (data are summarized in Table 4) represents the change in total weight (fixed bumper thickness plus variable vehicle hull) per area with distance of separation between the bumper and vehicle hull. All experimental points are coded for easy reference. A description of the impact conditions are given in Table 2 for the experiment (or Round Number) designated O-80(CAB), etc., in Figure 16.

* The projectile maintained its integrity during acceleration and produced one large and one very small crater. The small crater may have been formed by a fragment of lead from the collet used to position the steel projectile.

AE62-0413

April 1962

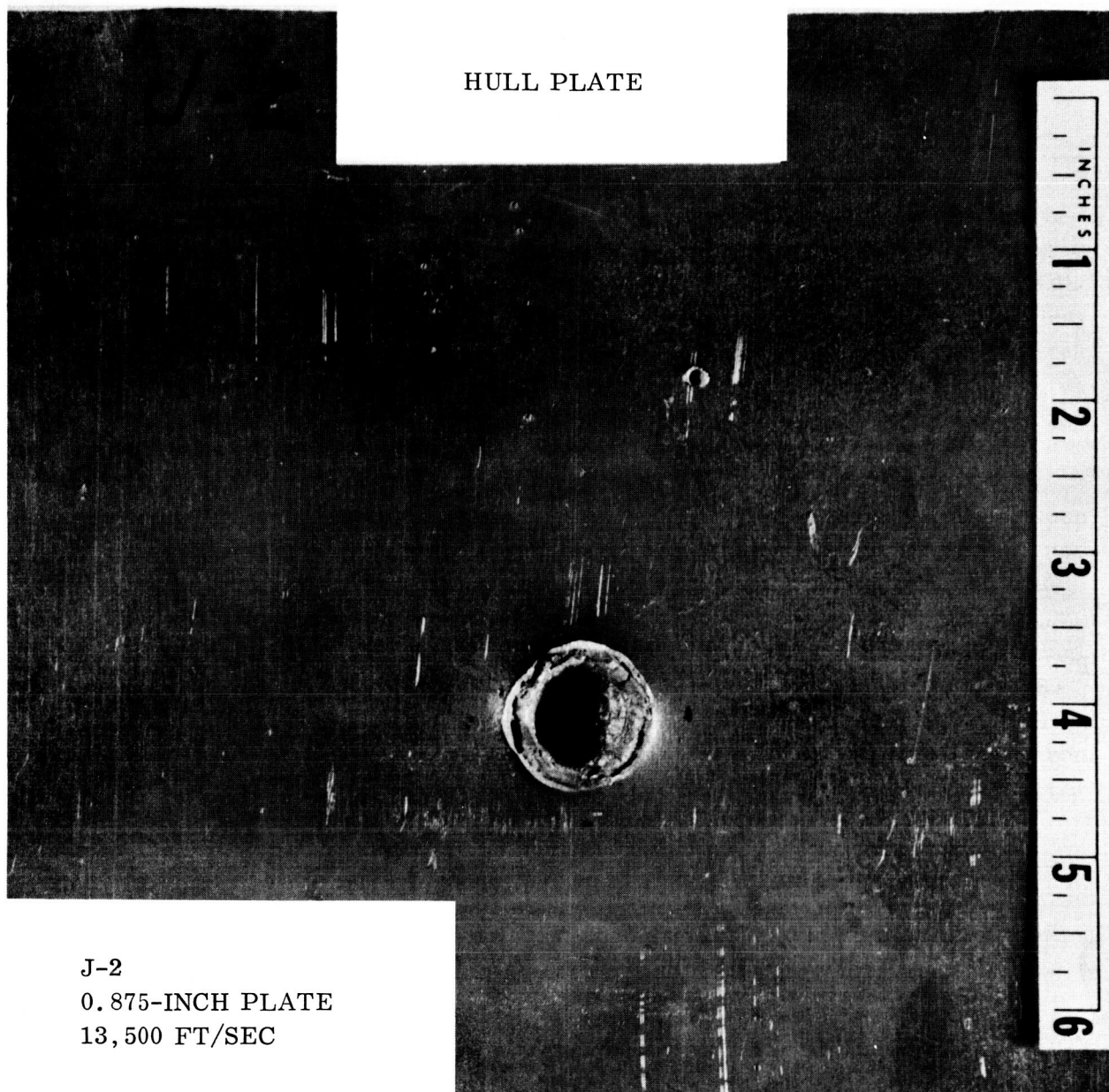


Figure 15. Thick Aluminum Plate (Panel J-2)

Table 4. Summary of Bumper Impact Data: 0.57-Gram Steel Projectile

ROUND NO.	REL * CODE	ACCEL-** ERATED PROJEC- TILE WEIGHT (GM)	VELOCITY (FT/SEC)	BUMPER THICKNESS (IN.)	SPACING (IN.)	VEHICLE HULL PLATE THICKNESS (IN.)	TOTAL WEIGHT OF TEST PANEL *** (LB/FT ²)	HOLE DIA. BUMPER (IN.)	SPRAY CONE DIA. (IN.)	PRINCIPAL CONE DIA. (IN.)	VEHICLE HULL PLATE		REMARKS
											PENETRATION (IN.)	CRACKED	
J-1	-CC	0.57	16,400	None	-	1.5	21.17	-	-	-	0.625	No	Dia of crater 0.61", Lip 0.25"
J-2	-AB	0.5742	13,500	None	-	0.875	12.43	-	-	-	0.72	No	Dia of crater 0.625", Lip 0.08", Bulge on back 0.75" dia.
O-78	CCB	0.5835	14,300	0.125	0.5	0.625	10.63	0.4 x 0.48	0.9	≤ 0.5	0.2	No	Crater 0.5" dia.
O-79	CBB	0.5835	15,800	0.125	0.5	0.625	10.63	0.35 x 0.52	1.0	≤ 0.4	0.37	No	Crater 0.4" dia.
O-80	CAB	0.5850	15,600	0.125	1.0	0.50	8.87	0.4 x 0.48	1.4 x 1.6	-	Punctured	-	0.35" dia perforation - Spall 0.8" dia x 0.1" thick
F-204	ABB	0.5655	14,300	0.125	1.75	0.50	8.87	0.61 x 0.65	3.0	1.5	No	No	0.25" x 0.31" puncture
S-51	CBC	0.5745	16,400	0.125	2.25	0.375	7.05	0.56 x 0.62	3.0	1.5	Punctured	-	
A-50	AB-	0.5700	Est. 15,000±1,000	0.125	4.0	0.375	7.05	0.62 x 0.65	4.5	2.25	0.28	-	None
F-191	BAA	0.5755	11,700	0.125	4.0	0.375	7.05	0.3 x 0.4	3 x 5	0.5 x 0.7	Punctured	-	0.4" x 0.5" dia puncture
F-206	ABB	0.578	13,000	0.125	4.0	0.375	7.05	0.65	4.0	1.0	Punctured	-	0.15" x 0.2" dia puncture 0.25" dia spall
F-205	ABB	0.578	14,700	0.125	6.0	0.375	7.05	0.65	6	1.5	No	No	0.06
J-19	-BB	0.5750	14,750	0.090	0	0.75	11.86	1.0*	-	-	0.09 + 0.75	Yes	Dia of crater 0.57", Lip 0.094", Bulge on back 1" dia.
J-5	-AA	0.5725	9,400	0.090	0	0.625	10.15	1.65*	-	-	Punctured	-	Dia of hole in plate 0.6"
A-49	ABB	0.5782	15,200	0.090	0.25	0.75	11.86	0.45 x 0.5	0.9	0.9	0.42	No	Dia of crater, 0.85" x 0.9", Lip 0.07", Bulge 0.8" dia x 0.05" Backsplash on bumper 1.7" dia, cratered ring 1.1", 0.05" deep
A-43	ACB	0.5711	13,300	0.090	0.25	0.625	10.15	0.437	0.87	0.87	0.55	Yes	Dia of crater 0.5", 0.06" Lip, Bulge 1" dia x 0.15", cracked. Backsplash on Bumper 2" dia, Pitted semicircle 1" dia.
J-6	AAB	0.5741	15,600	0.090	0.5	0.625	10.15	0.5	1.0	1.0	0.45	No	Dia of crater 1.0", Lip 0.094", Bulge 0.75" dia x 0.1". Backsplash on bumper
J-21	CCB	0.5707	15,400	0.090	1.0	0.5	8.36	0.4	1.8	0.9	Punctured	-	Dia of hole in plate 0.4", Spall 0.7" dia x 0.15" thick
J-20	ABB	0.5719	15,400	0.090	1.5	0.5	8.36	0.5	2.75	1.25	0.36	No	Dia of crater 0.9", Bulge on back 1.1" dia.
J-10	AAB	0.5752	15,900	0.090	2.0	0.375	6.57	0.55 x 0.6	3.5	1.3	0.3	Yes	Dia of crater 1.3", Bulge 1.5" dia.
A-38	CBB	0.5718	14,700	0.090	2.31	0.438	7.48	0.44 x 0.5	4.0	-	Punctured	-	Dia of hole 0.62", Spall 0.81" dia, x 0.09"
A-40	AAD	0.5807	21,700	0.090	2.57	0.438	7.48	0.37 x 0.4	3.0	1.2	Punctured	-	Dia of hole 0.37" x 0.5", Spall 0.87" x 0.94" dia x 0.08". Reverse face of bumper pitted in semicircle dia 3" to 5"
J-18	CBB	0.5704	14,100	0.090	3.0	0.375	6.57	0.37	4.0	0.9 x 1.2	Punctured	-	Dia of hole 0.6", Spall 0.95" x 1.0" dia x 0.15"
O-65	AAB	0.5702	12,500	0.090	3.0	0.375	6.57	0.38	5.0	1.0	Punctured	-	0.7" dia puncture; 0.15" thick x 1.1" dia spall
A-41	BAB	0.5708	15,200	0.090	3.06	0.438	7.48	0.31 x 0.44	2.5	-	Punctured	-	Dia of hole 0.56", Spall 0.87" x 0.94" dia x 0.12"
O-90	BBB	0.5718	15,200	0.090	3.25	0.438	7.48	0.27 x 0.42	4.0	0.5 x 0.3	Punctured	-	0.3" dia puncture
O-91	-C-	0.5780	-	0.090	3.25	0.438	7.48	0.4	4.0	0.8 x 1.4	Punctured	-	0.5" dia puncture
A-33	CCA	0.5726	10,200	0.090	4.0	0.375	6.57	0.45	6.0	1.1	0.37	Yes	Dia of crater 1.1", Bulge 0.6" dia.
A-42	ABB	0.5785	15,000	0.090	4.06	0.438	7.48	0.5 x 0.63	6.0	3.5	0.31	No	0.031
A-32	ABB	0.5765	14,000	0.090	5.0	0.375	6.57	0.5	6.0	3.0	0.18	No	None
O-64	ABC	0.5682	18,900	0.090	5.0	0.25	4.81	0.48	8.0	1 x 1.4	Punctured	-	--
O-88	CCB	0.5850	13,500	0.090	6.06	0.313	5.71	0.3 x 0.44	6.0	0.6 x 1.0	Punctured	-	2 - 0.375" and 1 - 0.25" dia perforations
O-66	ABB	0.5845	14,800	0.063	0.25	0.75	11.48	0.56	-	-	0.42	No	0.5" x 0.75" puncture, Spall 0.75" dia 0.05" thick
O-81	CCC	0.5748	17,200	0.063	0.25	0.75	11.48	-	-	-	No	No	0.82" x 0.94" dia crater
O-82	BCC	0.5778	16,200	0.063	0.25	0.75	11.48	0.28 x 0.37	0.5	-	0.56	No	Pellet broke into 5 parts
A-48	AAB	0.5765	14,700	0.063	0.5	0.625	9.77	0.5	0.75	0.75	0.5	Yes	Crater 0.5" dia, Lip 0.08"
A-37	AAB	0.5775	14,300	0.063	0.75	0.625	9.77	0.5	1.7	1.1	0.34	No	Dia. of crater 0.75", Bulge 1" dia, Spall 0.62" dia x 0.06". Backsplash on bumper 2.1" dia. Slight bell, Backsplash on bumper 3.2" dia.

* Impact conditions are described in Table 2. ** Accelerated Weight. *** The Test Panel includes the weight of the Bumper and Vehicle Hull.

Table 4. Summary of Bumper Impact Data: 0.57-Gram Steel Projectile, Contd

ROUND NO.	REL * CODE	ACCEL-** ERATED PROJEC- TILE WEIGHT (GM)	VELOCITY (FT/SEC)	BUMPER THICKNESS (IN.)	SPACING (IN.)	VEHICLE HULL PLATE THICKNESS (IN.)	TOTAL WEIGHT OF TEST PANEL *** (LB/FT ²)	HOLE DIA. BUMPER (IN.)	SPRAY CONE DIA. (IN.)	PRINCIPAL CONE DIA. (IN.)	VEHICLE HULL PLATE			REMARKS
											PENETRATION (IN.)	CRACKED	BULGE HEIGHT ON REAR SURFACE (IN.)	
O-86	AAB	0.5832	14,300	0.063	1.0	0.562	8.918	0.44	1.9	1.2	0.25	No	0.08	Crater 1.15" dia.
O-87	CAB	0.5846	14,700	0.063	1.0	0.562	8.918	0.53 x 0.58	3.0	1.6 x 1.1	No	No	-	---
J-29	CCB	0.5733	14,300	0.063	1.5	0.5	8.014	0.34 x 0.37	2.25 x 4	-	Punctured	-	-	Dia of hole 0.6", Spall 0.93" dia x 0.13"
A-36	BCB	0.5804	14,700	0.063	1.75	0.5	8.014	0.25 x 0.4	3.1	-	Punctured	-	-	Dia of hole 0.6" x 0.7"
A-34	CCB	0.5664	14,100	0.063	2.0	0.5	8.014	0.38	3.5	1.35	0.25	No	-	---
J-22	BCB	0.5637	13,200	0.063	2.0	0.375	6.17	0.33 x 0.45	3.0	0.9 x 1.25	Punctured	-	-	Dia of hole 0.4" x 1.0"
A-45	CCB	0.579	13,500	0.063	2.5	0.375	6.17	0.095 x 0.37	2.25	-	Punctured	-	-	Dia of hole 0.37" x 0.62", Spall 0.75" dia x 0.09"
J-23	AAC	0.5736	16,000	0.063	3.0	0.375	6.17	0.48	4.5	3.5	0.25	No	0.03	0.37" dia bulge
A-44	ABB	0.5773	14,000	0.063	5.06	0.3125	5.338	0.5	2.5	1.6	0.25	Yes	0.15	0.5" x 0.65" diameter puncture
O-89	BCB	0.5730	15,200	0.063	6.06	0.3125	5.338	0.3 x 0.37	0.6	0.5 x 1.9	Punctured	-	-	0.55" dia puncture - Spall 0.85" dia x 0.15" thick
O-70	BAB	0.5835	14,800	0.032	0.25	0.75	11.032	0.12 x 0.4	0.9	-	Punctured	-	-	Crater 0.85" dia , Lip 0.08"
O-71	ABC	0.5838	16,100	0.032	0.25	0.75	11.032	0.47	0.9	-	0.52	No	0.05	Tapered 0.6" to 0.35" dia puncture
O-69	BBC	0.5837	18,100	0.032	1.0	0.625	9.322	0.3 x 0.4	-	-	Punctured	-	-	Tapered 0.75" to 0.04" x 0.7", Spall 0.4" x 0.85" x 0.15" thick
O-72	BBB	0.5838	14,300	0.032	1.0	0.625	9.322	0.2 x 0.35	-	-	Punctured	-	-	Crater 0.4" x 0.65", Bulge 0.08" high
O-73	AAB	0.5848	14,800	0.032	1.0	0.625	9.322	0.4 x 0.48	1.1 x 1.3	≤0.4 x 0.65	0.38	No	0.08	0.32" dia crater
F-193	BBA	0.5836	11,000	0.032	1.5	0.563	8.46	0.18 x 0.27	1.0	0.32	0.4	No	0.05	0.6" dia puncture, Spall 0.8" dia x 0.1" thick
S-55	BBB	0.5845	14,000	0.032	2.0	0.500	7.562	0.14 x 0.38	0.8	≤0.7	Punctured	-	-	Spall 0.7" dia x 0.1 thick
S-57	ABB	0.5855	14,300	0.032	2.0	0.500	7.562	0.4 x 0.5	2.0	≤0.55 x 1.3	0.35	No	0.05	0.6" x 0.7" dia puncture
S-54	ABC	0.5880	16,100	0.032	3.0	0.375	5.742	0.5	1.6	≤0.5	Punctured	-	-	4 holes in bumper
O-74	BAB	0.5853	15,100	0.032	4.0	0.375	5.742	0.25 x 0.42	-	-	Punctured	-	-	Moderate pellet breakup
O-83	CC~	0.5790	-	0.032	4.0	0.375	5.742	0.33	-	-	No	No	-	0.44" dia hole - Spall 0.8" dia x 0.1 thick
O-84	CCD	0.5750	20,000	0.032	4.0	0.375	5.742	0.32 x 0.4	-	-	No	No	-	Main Crater 0.5" dia.
O-85	CCB	0.5845	15,200	0.032	4.0	0.375	5.742	0.32 x 0.4	4	0.8	Punctured	-	-	0.3" dia hole
O-61	C-D	0.5845	20,000	0.094 window glass	0.5	0.625	10.03	-	1.1	≤0.7	No	No	0.03	0.25 dia puncture
O-60	C-C	0.5837	17,500	0.094 window glass	1.5	0.5	8.25	-	2	0.5	0.4	No	0.094	0.4" dia Spall. Crater 0.75" dia NOT punctured
O-58	C-B	0.5835	14,700	0.094 window glass	2.5	0.375	6.43	-	3	0.5 x 1.4	Punctured	-	0.5	Hole tapered 0.8" to 0.4" dia.
O-59	C-B	0.5840	13,500	0.094 window glass	3.0	0.375	6.43	-	2.5 x 4	-	Punctured	-	-	0.6" dia crater
O-94	ABB	0.5780	15,200	2 layers Al screen 0.028 16 mesh	1.0	0.625	9.436	1st Scr 0.48 2nd Scr 0.7	1.75	0.75	0.47	Yes	-	---
O-95	CBB	0.5795	14,300	1 layer Al screen 0.028 16 mesh	1.0	0.625	9.173	0.48 x 0.5	-	-	Punctured	No	-	0.54" dia puncture
F-195	ABB	0.5625	14,700	0.062 MgLi	0.5	0.75	11.078	0.5 x 0.57	-	-	No	No	0.05	0.4" dia puncture
F-196	ABB	0.5795	14,700	0.098 MgLi	1.0	0.625	9.655	0.6 x 0.65	1.25	0.7	0.1	No	0.05	---
F-197	BBB	0.5770	12,200	0.063 MgLi	2.0	0.475	7.253	0.24 x 0.34	2.0	0.54	Punctured	-	-	0.4" dia puncture
F-198	ACB	0.5800	14,300	0.095 MgLi	4.0	0.375	5.98	0.62 x 0.66	4	0.5	Punctured	-	-	

* Impact conditions are described in Table 2. ** Accelerated Weight. *** The Test Panel includes the weight of the Bumper and Vehicle Hull.

April 1962

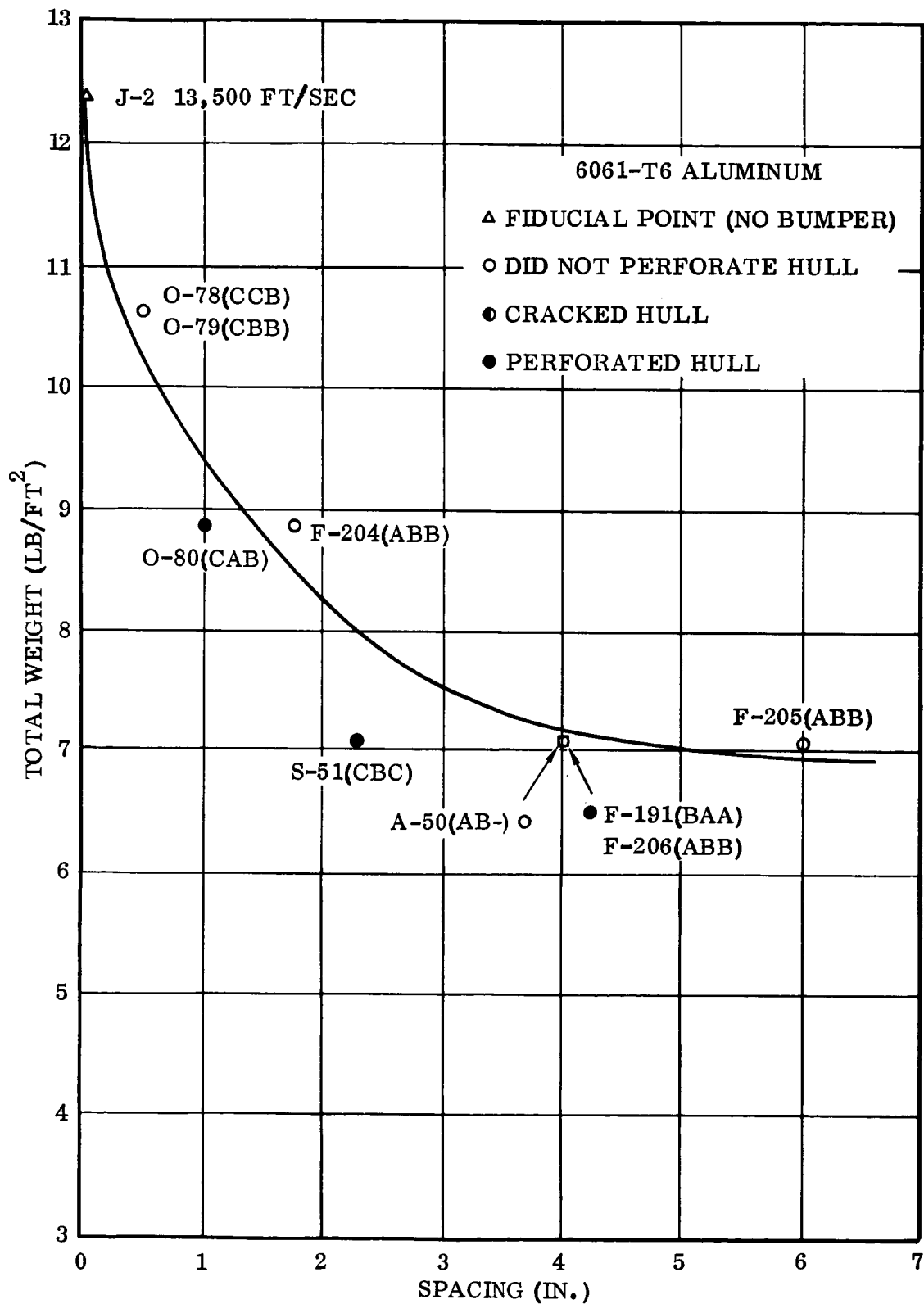


Figure 16. Test Panel Mass Versus Spacing (0.125-Inch Bumper)

April 1962

3.1.2 Aluminum Bumper, Type 6061-T6, 0.090 Inch Thick. Twenty 0.090-inch aluminum bumpers*, with a spacing from zero to 6 inches, have been subjected to impact from the 0.57-gram steel projectile. The data are summarized in Table 4 and Figure 17 with a description of the impact conditions given in Table 2.

Test panel J-19 (Figure 18), with an 0.090-inch bumper placed flush on the hull plate, weighed 11.86 lb/ft². The 0.250-inch diameter by 0.094-inch thick cylindrical projectile traveling at 14,750 ft/sec (with several minute fragments) produced extensive damage to the bumper at the point of impact. Moreover, the hull plate was almost completely penetrated, and several cracks were produced in the bulge of disturbed material (one inch in diameter by 0.25-inch high) on the rear of the plate (Figure 19).

With the same test panel weight of 11.86 lb/ft², but with a 0.25-inch distance between the 0.090-inch bumper and hull plate, the projectile traveling at 15,200 ft/sec did not penetrate or crack (Experiment A-49) the aluminum hull plate (Figure 20). An 0.8-inch diameter and 0.05-inch high bulge of disturbed material was produced on the rear face of the hull plate. The fluid material leaving the crater in the hull plate can either cause petal formations in the bumper with zero spacing as seen in Figure 18, or can coat and produce the numerous small craters in a bumper spaced at a small distance from the main hull as seen in Figure 21, the reverse face of the bumper from test panel A-49.

The importance of spacing the bumper from the hull plate can also be seen from the additional photographs (Figures 22, 23, and 24) of test panels (10.15 lb/ft²) J-5, A-43, and J-6 with zero, 0.25-, and 0.50-inch spacing, respectively. The bumper of panel J-5 with zero spacing was petalled slightly, but not as much as J-19 (Figure 18), since the hull plate was completely penetrated, and most of the erupted hull plate material did not move back through the shear plug hole in the bumper. Consequently, confinement was less and a high back pressure was not produced. Test panel A-43 with an 0.25-inch spacing was not penetrated, but the hull plate was cracked (Figure 25), while panel J-6 with an 0.50-inch spacing prevented complete penetration or crack formation. Back splash of hull plate material, erupted from the crater onto the rear face of the bumper, can be seen in Figures 21, 25, and 26.

Test panel A-40 was subjected to impact from a projectile at 21,700 ft/sec. The bumper caused the projectile to fragment (Figure 27), but the projectile and shear plug fragments had sufficient mass and velocity to penetrate the hull plate as well as the 0.125-inch aluminum inspection plate placed four inches behind the target. Figure 28 shows the small craters on the reverse face of the bumper, that were caused from

* The data for experiment O-91 were not included in Figure 17 since the velocity was not measured.

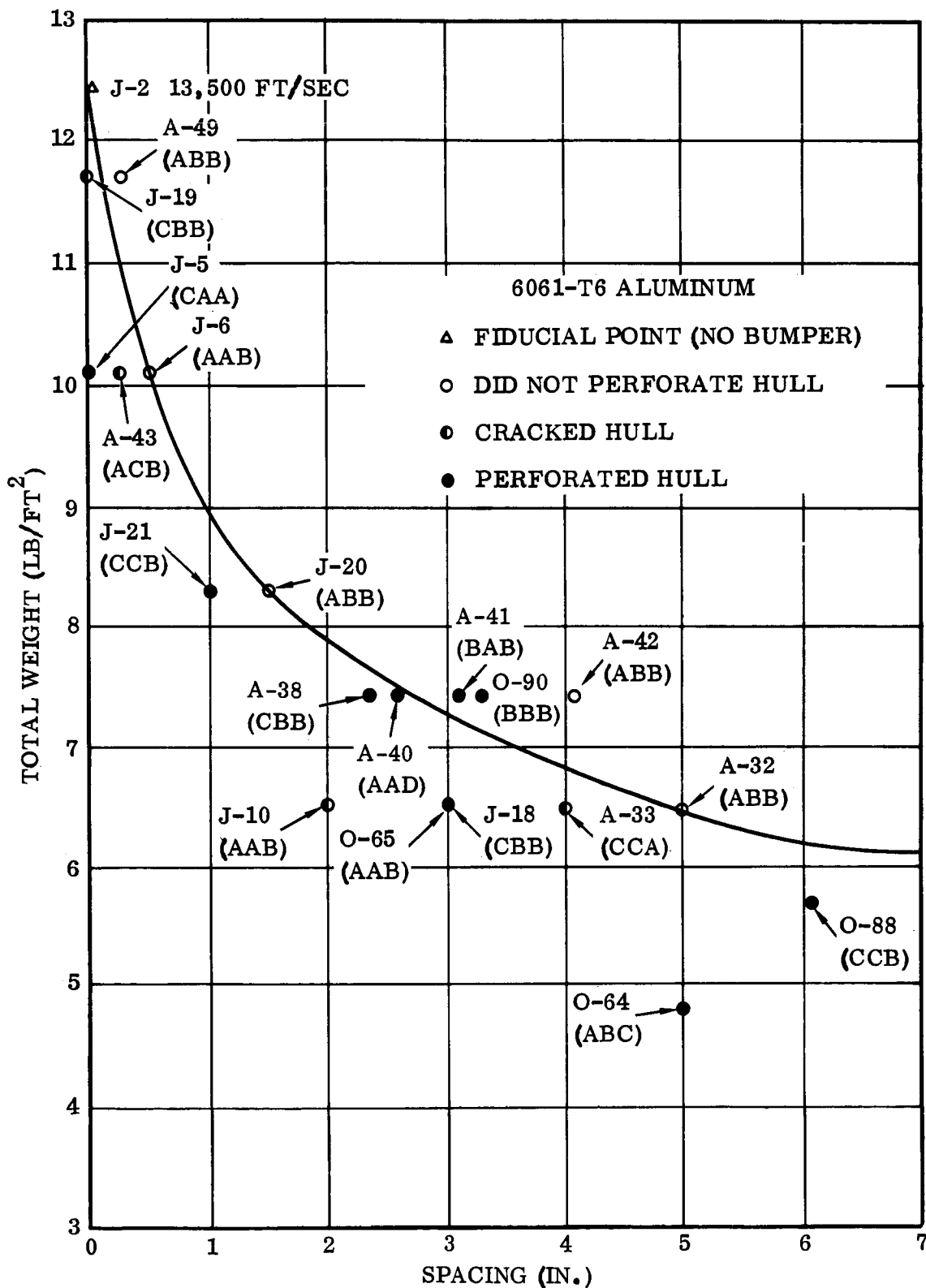


Figure 17. Test Panel Mass Versus Spacing (0.090-Inch Bumper)

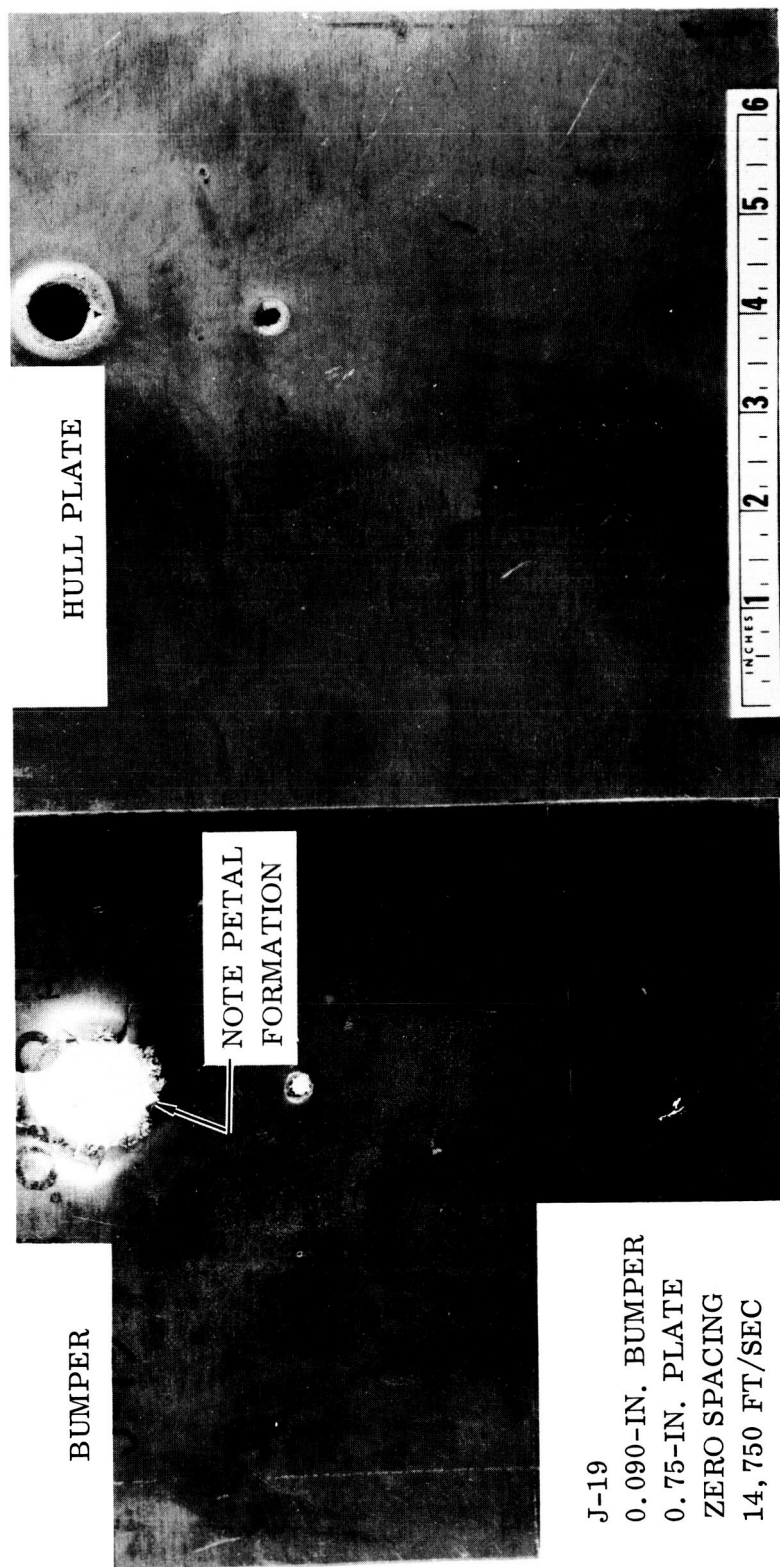


Figure 18. Aluminum Bumper With Zero Spacing (Panel J-19)

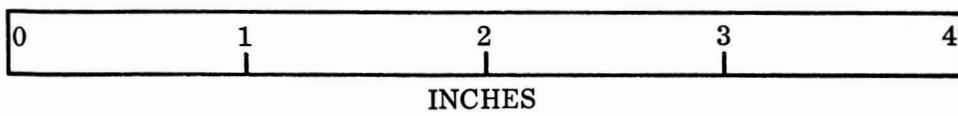
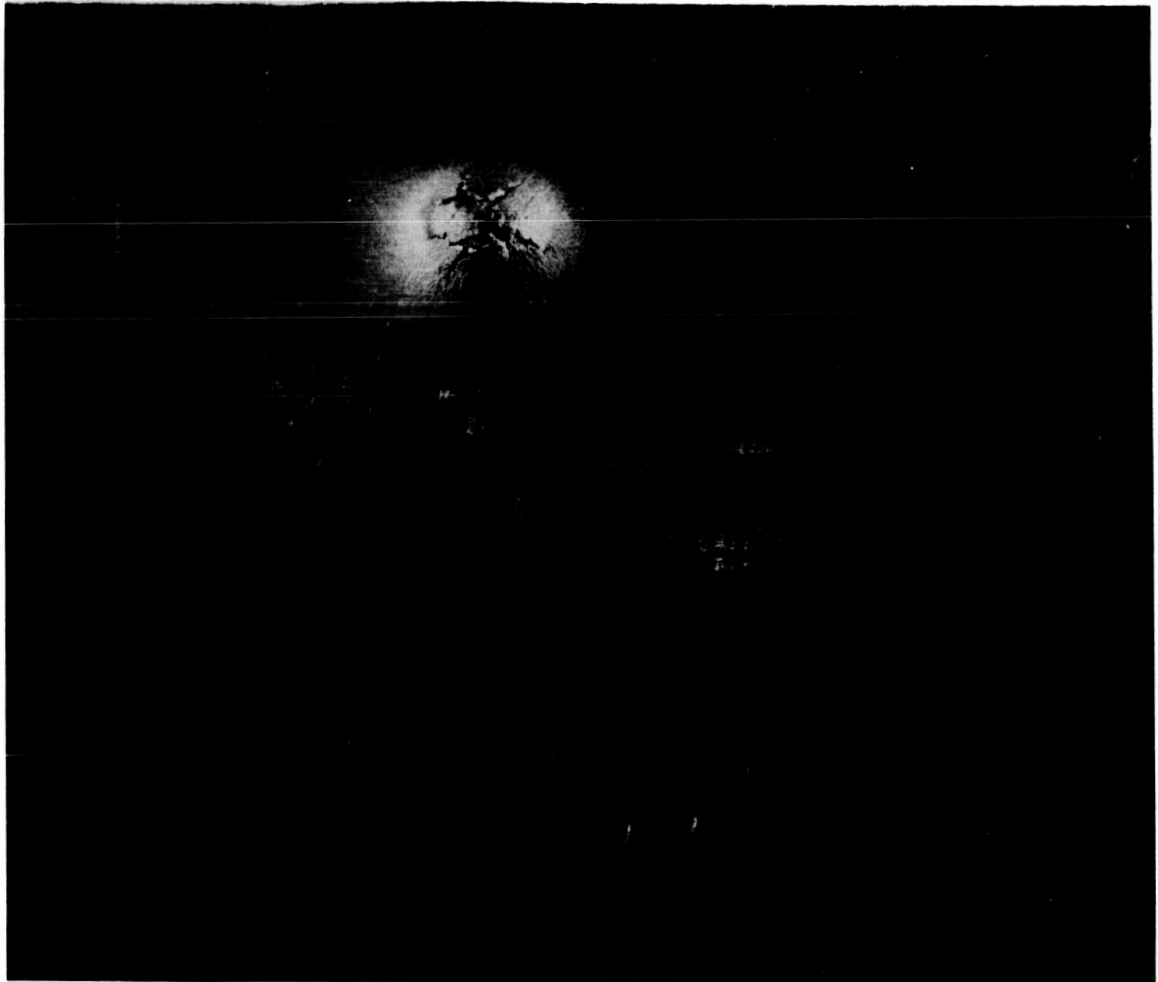


Figure 19. Reverse Side of Hull Plate (Panel J-19)

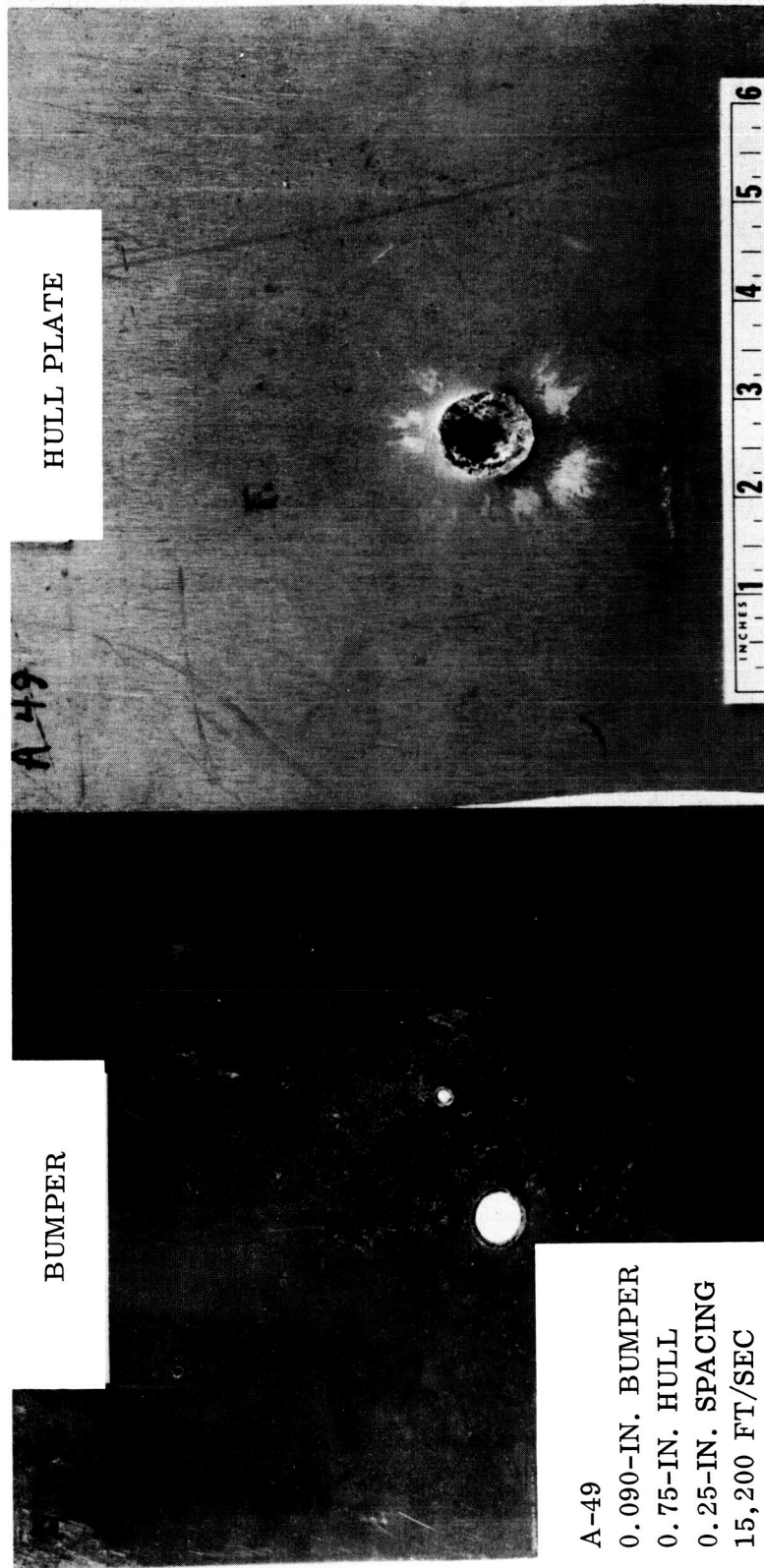


Figure 20. Aluminum Bumper With 0.25-Inch Spacing (Panel A-49)

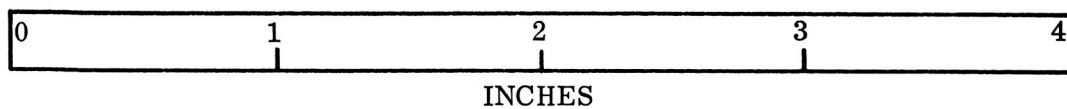


Figure 21. Reverse Side of Bumper (Panel A-49)

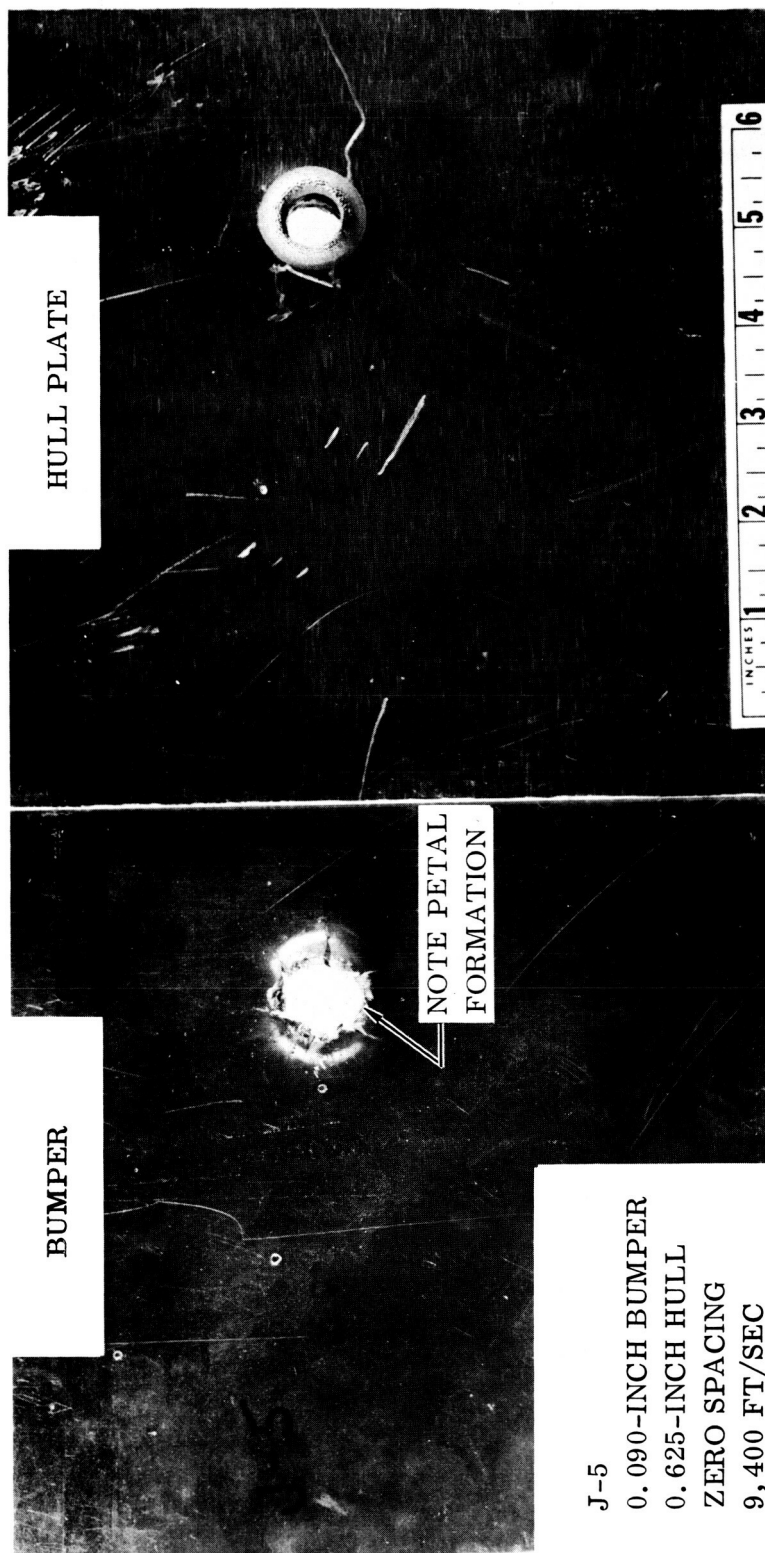


Figure 22. Aluminum Bumper With Zero Spacing (Panel J-5)

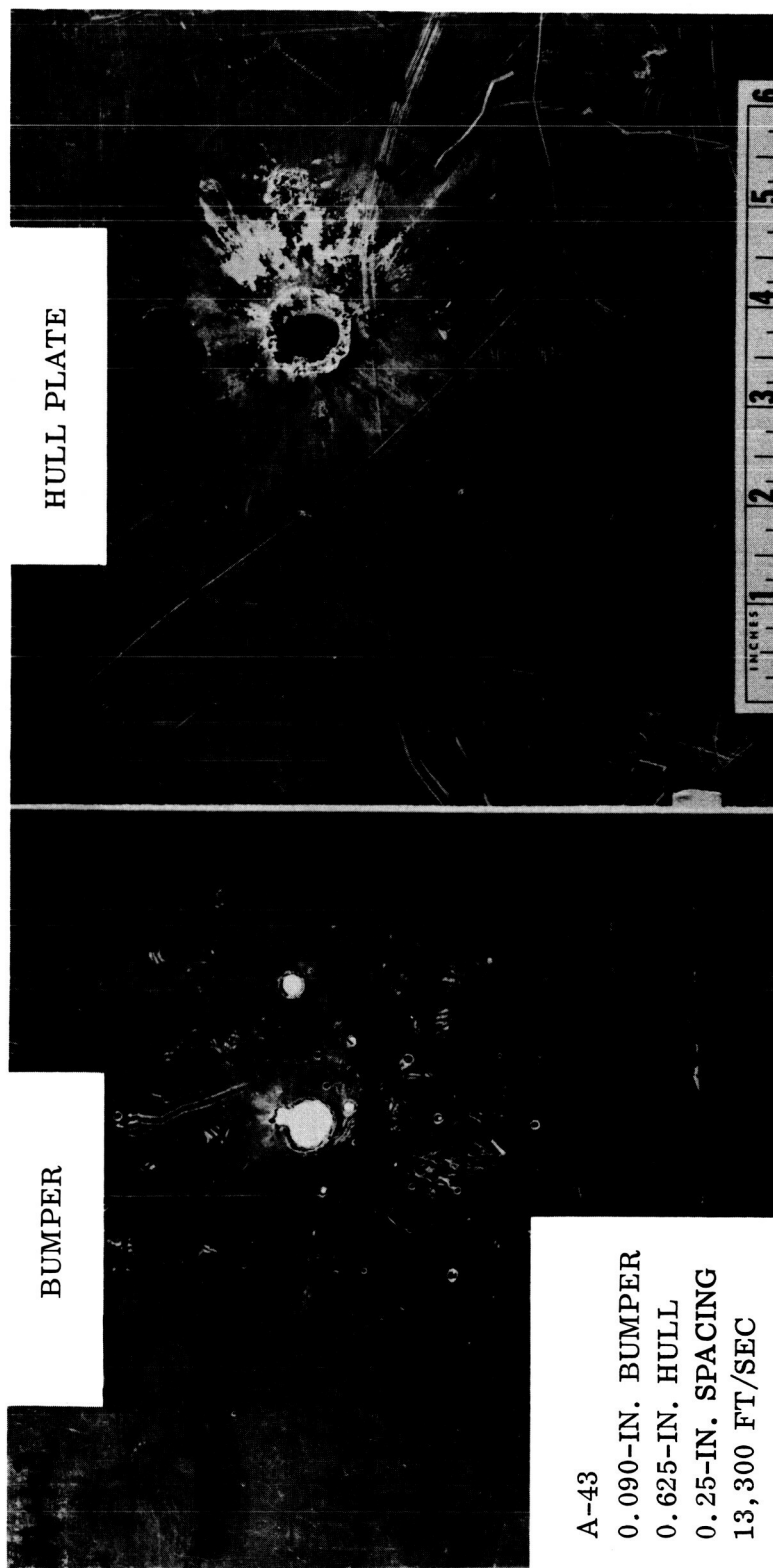


Figure 23. Aluminum Bumper With 0.25-Inch Spacing (Panel A-43)

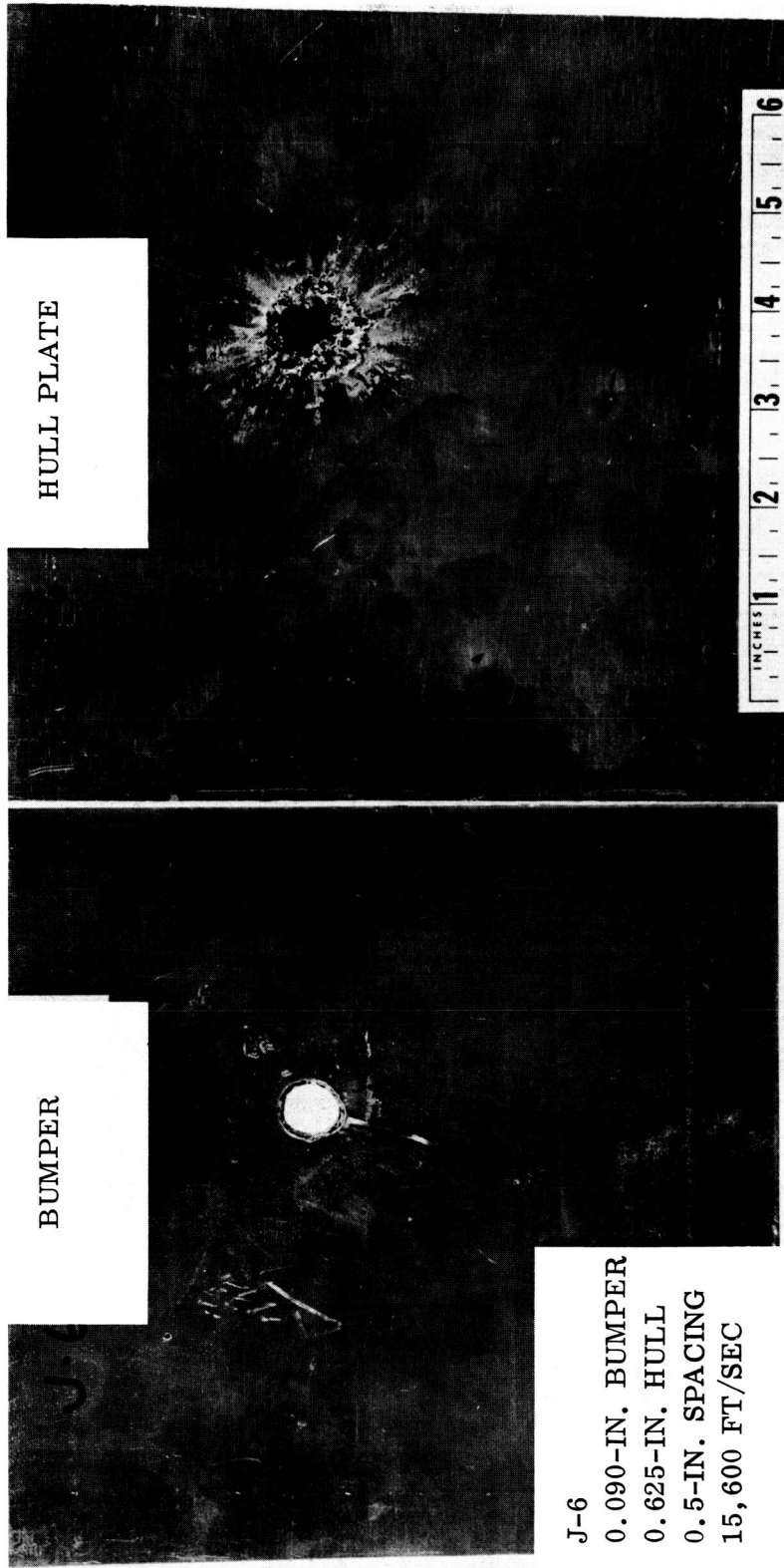


Figure 24. Aluminum Bumper With 0.5-Inch Spacing (Panel J-6)

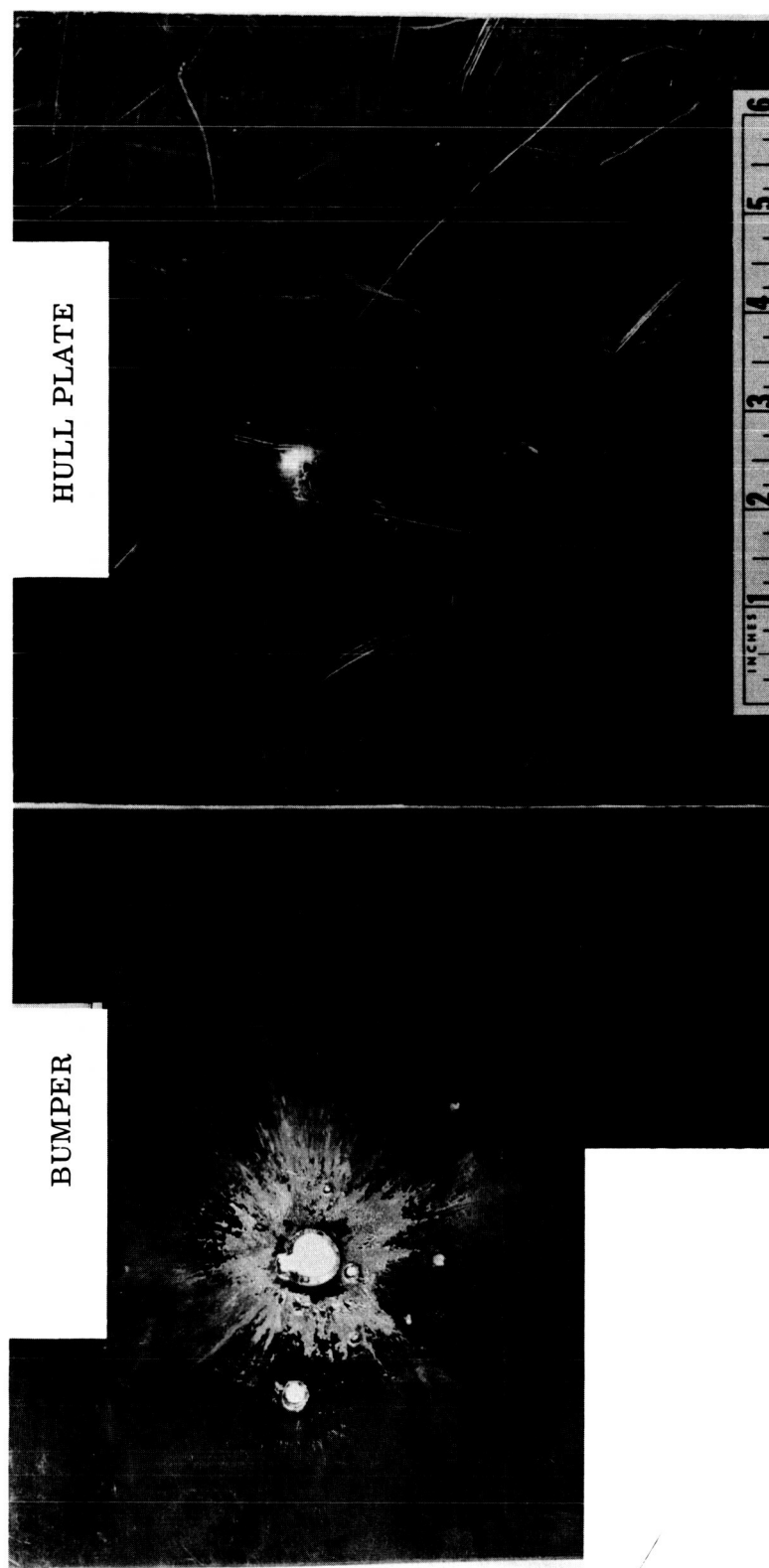
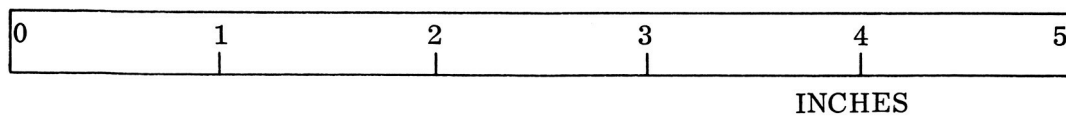


Figure 25. Reverse Side of Test Panel A-43



BACK SPLASH

Figure 26. Reverse Side of Bumper (Panel J-6)

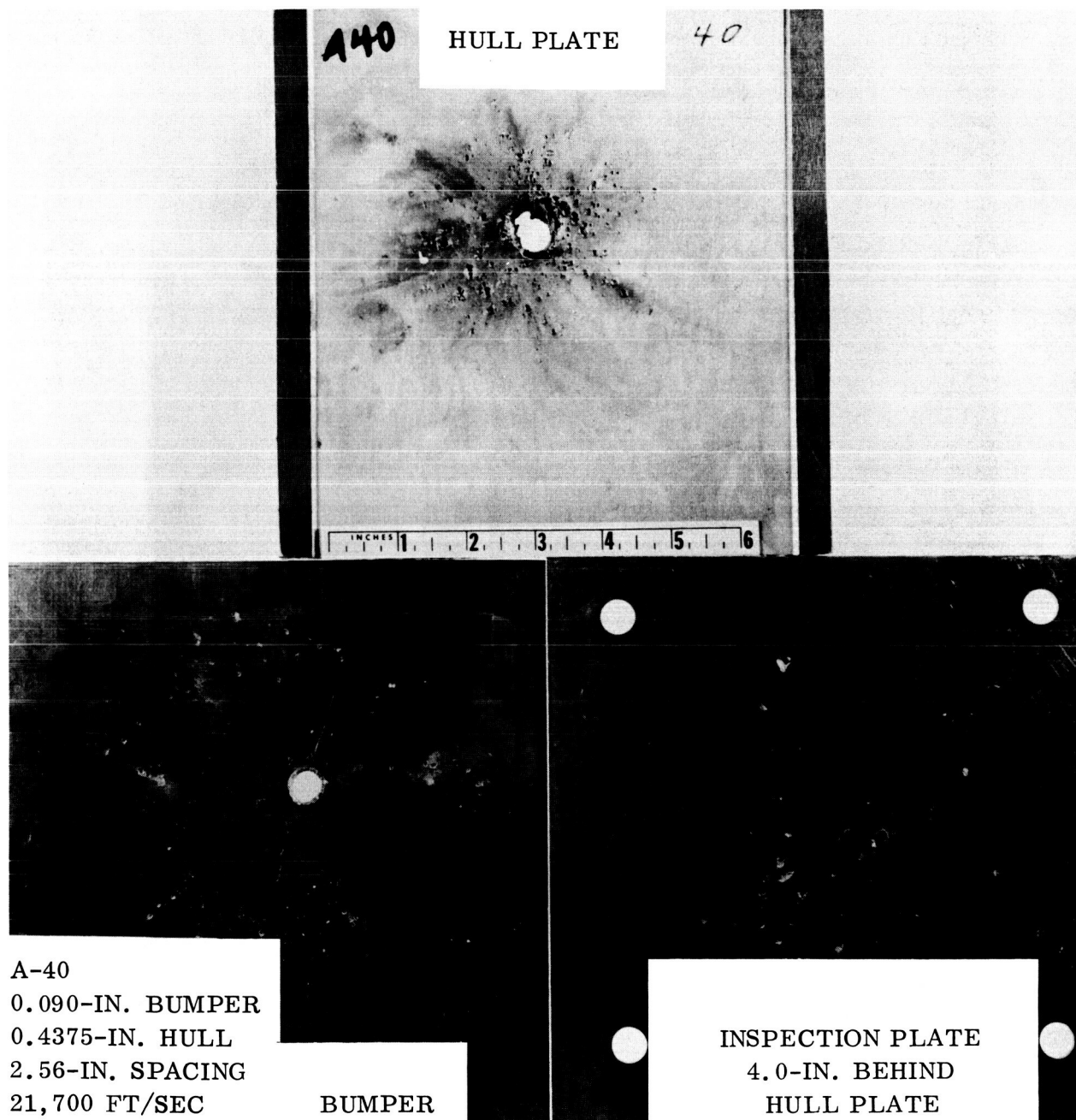


Figure 27. Aluminum Bumper With 2.56-Inch Spacing (Panel A-40)

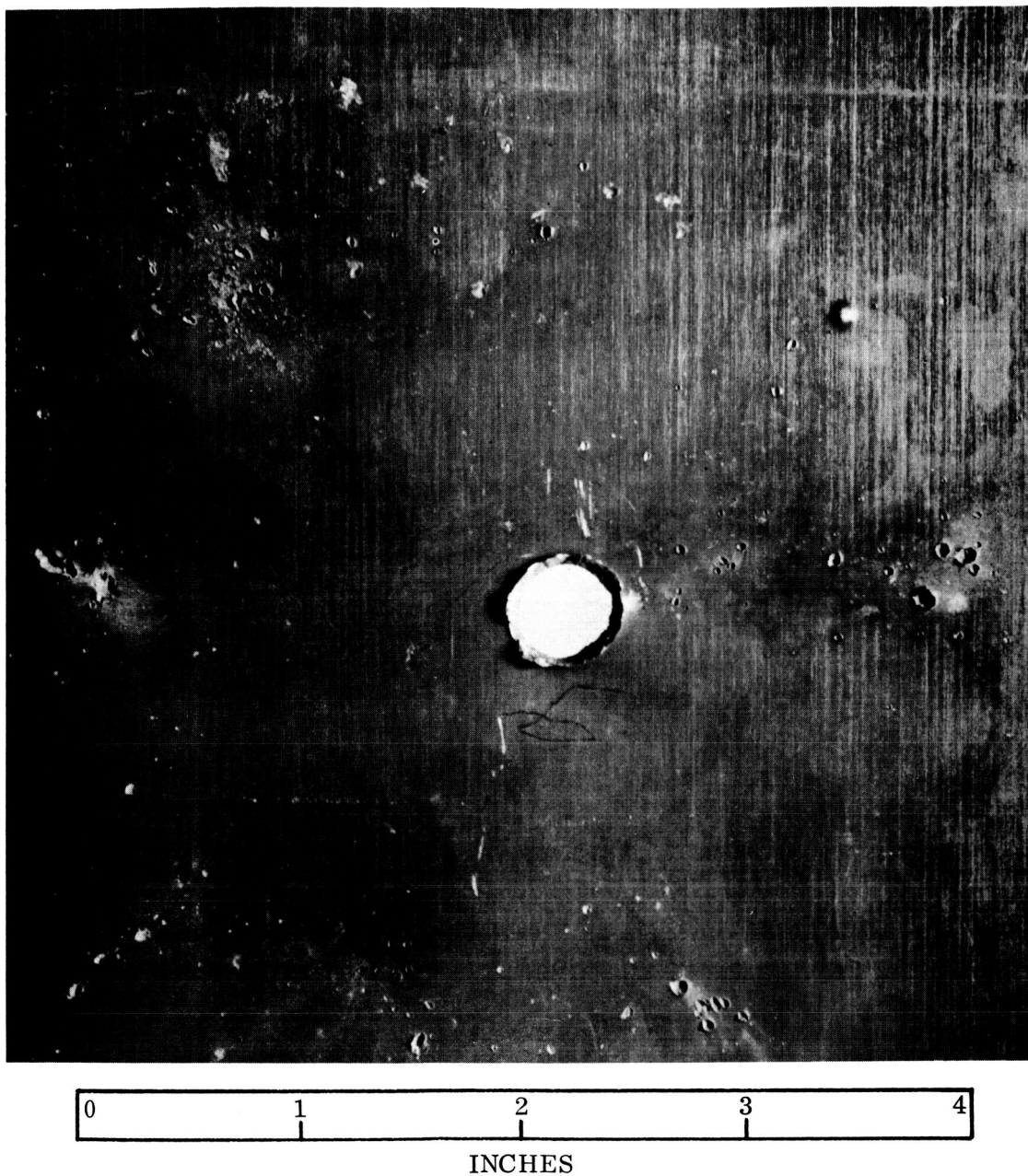


Figure 28. Reverse Side of Bumper (Panel A-40)

the material erupted (splashed back) from the small craters and the hole produced in the hull plate.

The bumper in test panel A-42 (Figure 29) was placed 4.06 inches in front of the target (total weight of 7.48 lb/ft^2), and it effectively fragmented the projectile traveling at 15,000 ft/sec. This can be seen from the numerous small craters in the hull plate. Moreover, the cone of the projectile or shear plug particles did not possess sufficient mass or velocity to completely penetrate the hull plate.

3.1.3 Aluminum Bumper, Type 6061-T6, 0.063 Inch Thick. Impact data obtained with 0.063-inch bumpers and the 0.57-gram projectile (Figure 30 and Table 4) are quite similar to those obtained with the 0.090-inch bumpers (Figure 17). For any given total weight, a critical minimum distance must be maintained between the 0.063-inch bumper and hull plate in order to permit the cone of projectile and shear plug fragments to expand and impact over a large hull plate area (momentum per-impact-area is diminished).

A spacing of 0.5-inch in test panel A-48 (Figure 31) was sufficient to prevent the projectile traveling at 14,700 ft/sec from completely penetrating the hull plate, but not from spalling and cracking the rear surface (Figure 32). Increasing the spacing from 0.5 inch to 0.75 inch, with the same total weight of 9.77 lb/ft^2 was adequate to prevent complete penetration or cracking of the hull plate (Figure 33).

The total weight of the test panel was decreased from 9.77 to 6.17 lb/ft^2 . When the spacing was increased to 3 inches (Figure 34), the projectile traveling at 16,000 ft/sec fragmented on contact with the 0.063-inch bumper, and the cone of particles expanded to the point where penetration of the vehicle hull plate was prevented.

3.1.4 Aluminum Bumper, Type 6061-T6, 0.032 Inch Thick

3.1.4.1 Steel Projectile; 0.57 Gram. The experimental impact data for 0.032-inch aluminum bumpers subjected to impact from the 0.57-gram steel projectile are summarized in Figure 35 and Table 4. Twelve experiments were made with test panels that weighed from 11.03 to 5.74 lb/ft^2 , and with a spacing from 0.25 to 4.0 inches.

Projectile orientation at the time of impact with the 0.032-inch bumper is very critical (see Section 9.5). This orientation manifests itself in the fact that any selected 0.032-inch bumper-vehicle hull system of fixed spacing and total weight per-unit-area will perform as designed, when the flat face of the projectile strikes the bumper, but penetration will occur when the edge of the projectile strikes the bumper. The total momentum for the projectile will be identical in all instances, and will not depend on whether the projectile strikes the bumper flat or on edge. However, the momentum

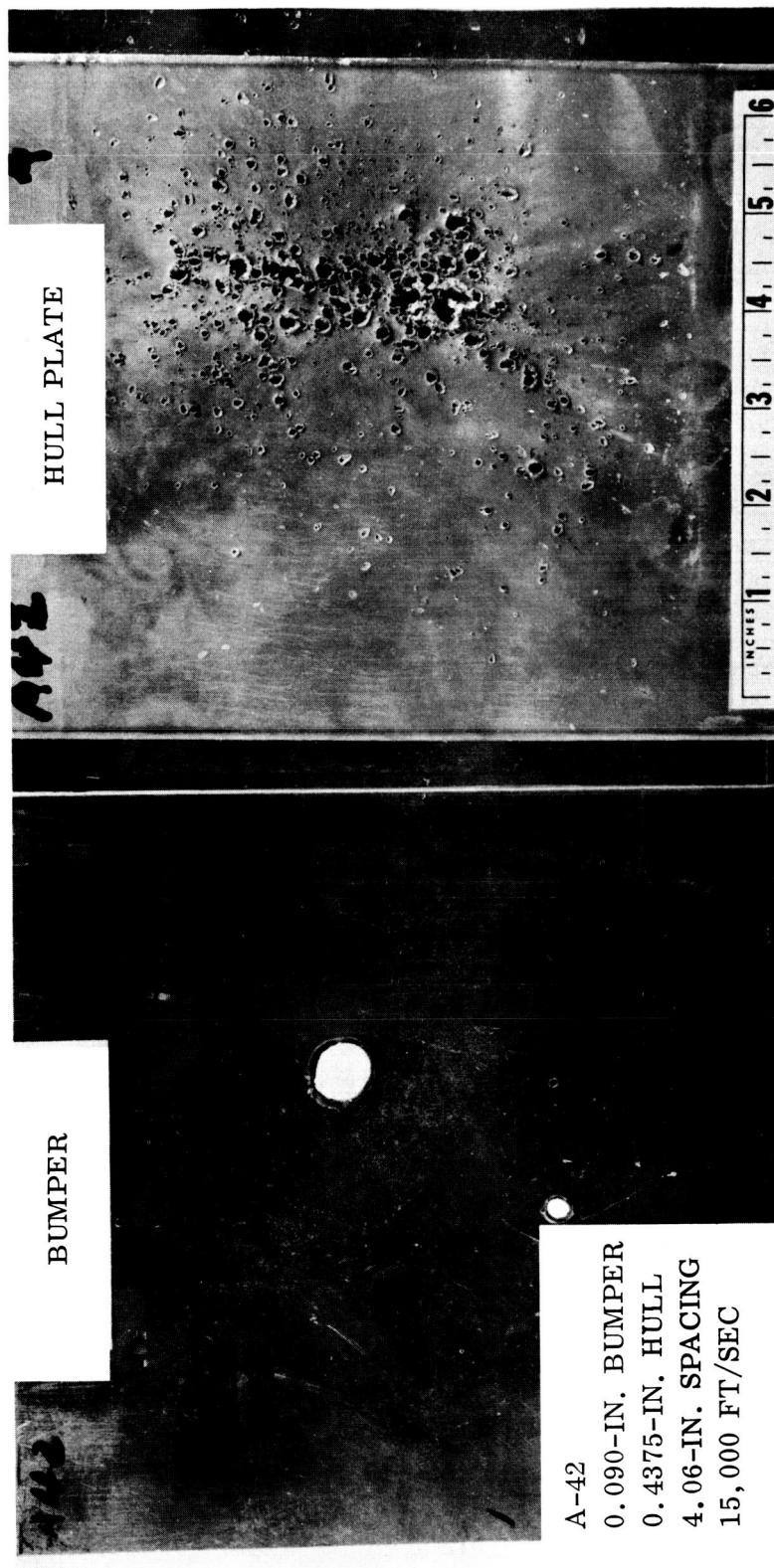


Figure 29. Aluminum Bumper With 4.06-Inch Spacing (Panel A-42)

April 1962

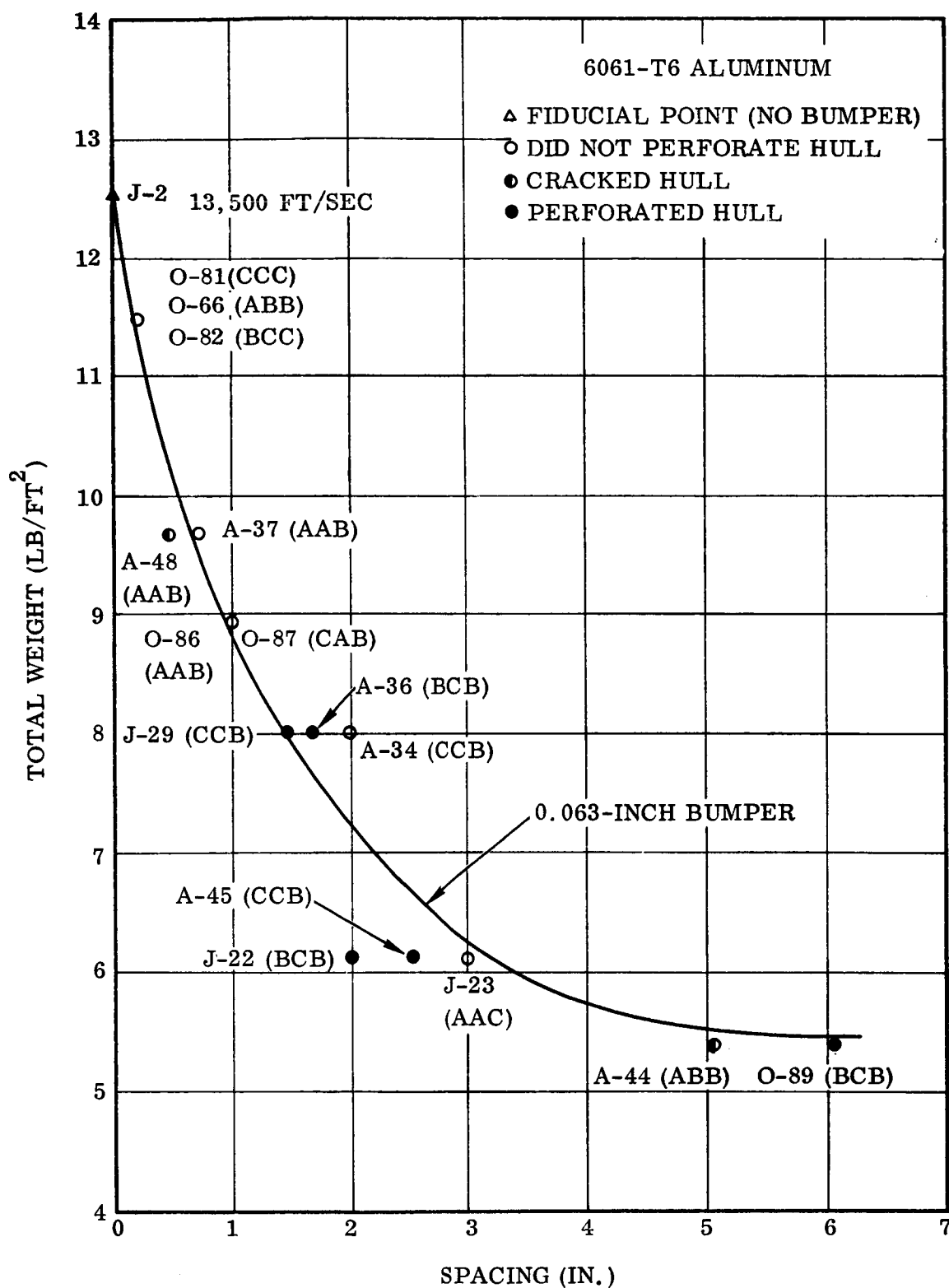


Figure 30. Test Panel Mass Versus Spacing (0.063-Inch Bumper)

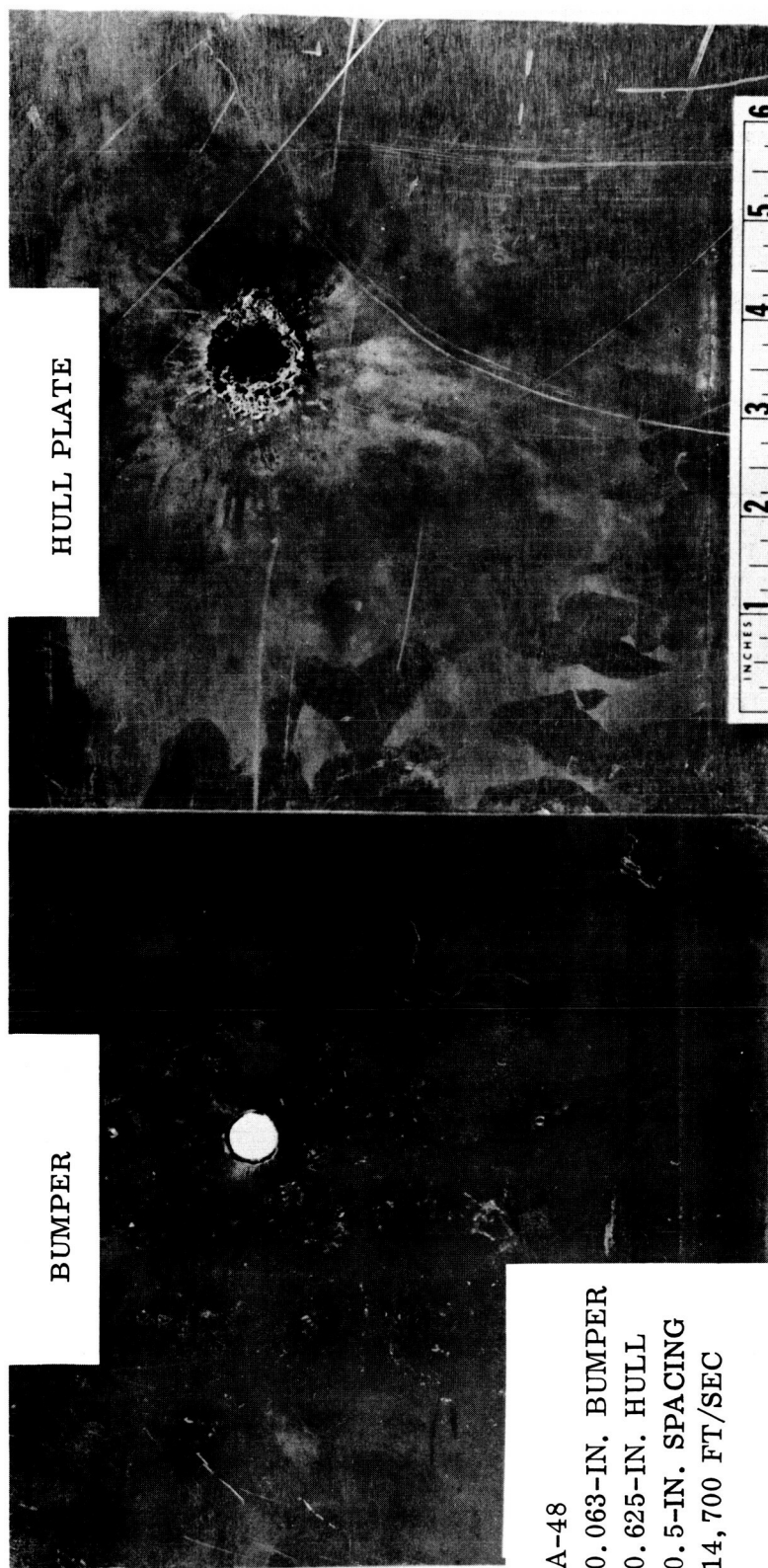


Figure 31. Aluminum Bumper With 0.5-Inch Spacing (Panel A-48)

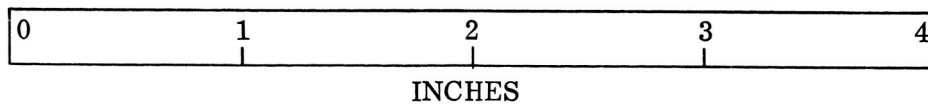
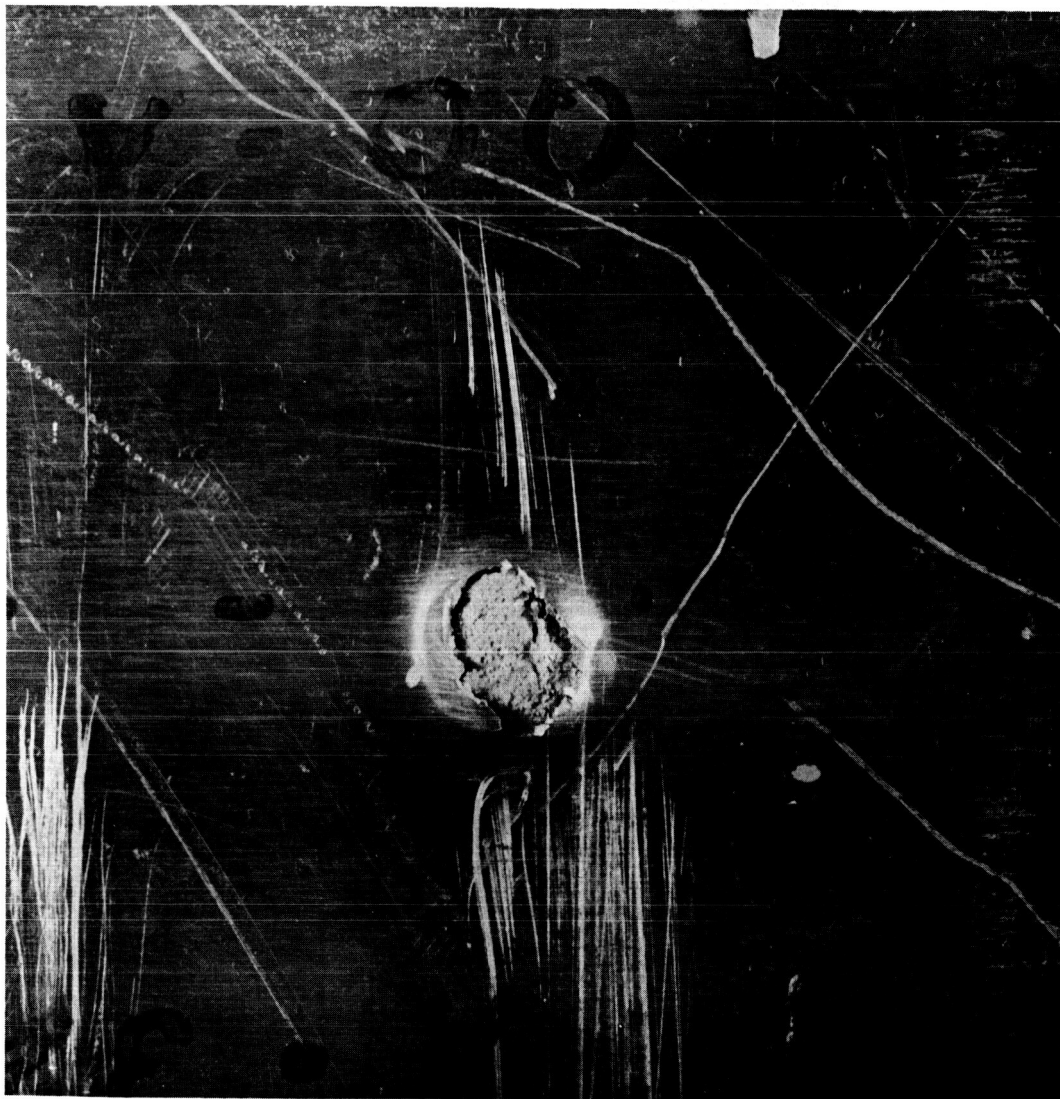


Figure 32. Reverse Side of Hull (Panel A-48)

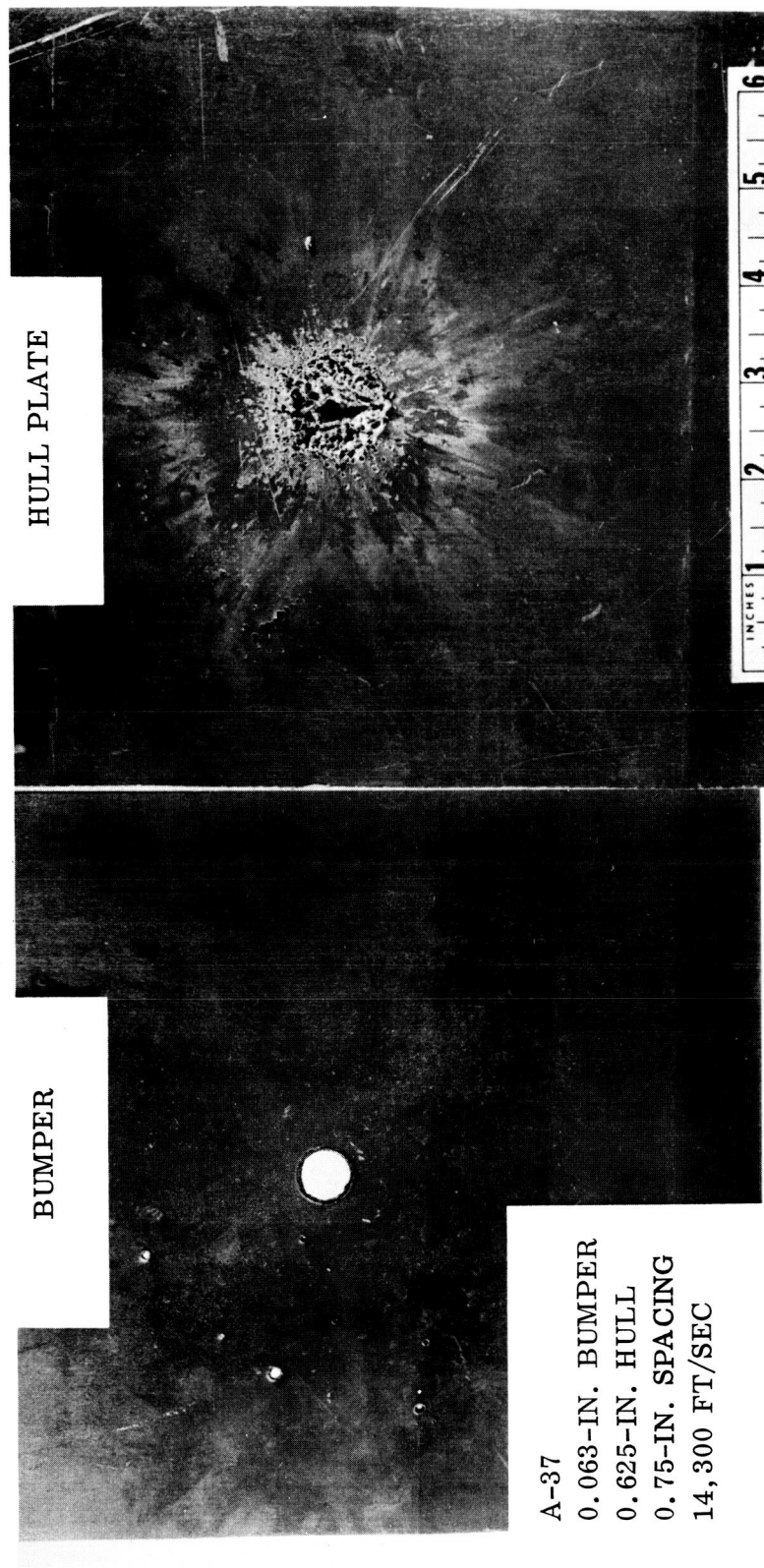


Figure 33. Aluminum Bumper With 0.75-Inch Spacing (Panel A-37)

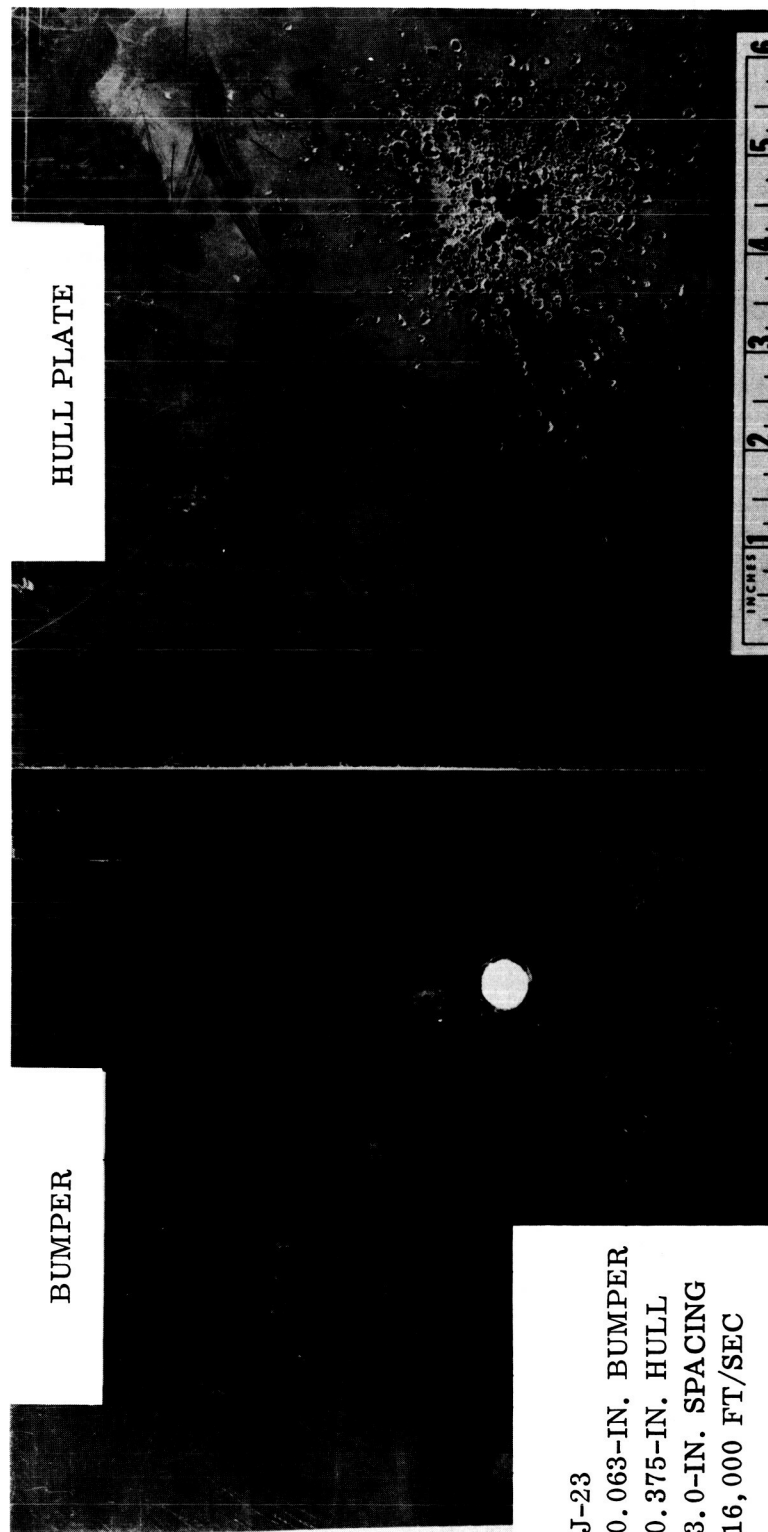


Figure 34. Aluminum Bumper With 3.0-Inch Spacing (Panel J-23)

April 1962

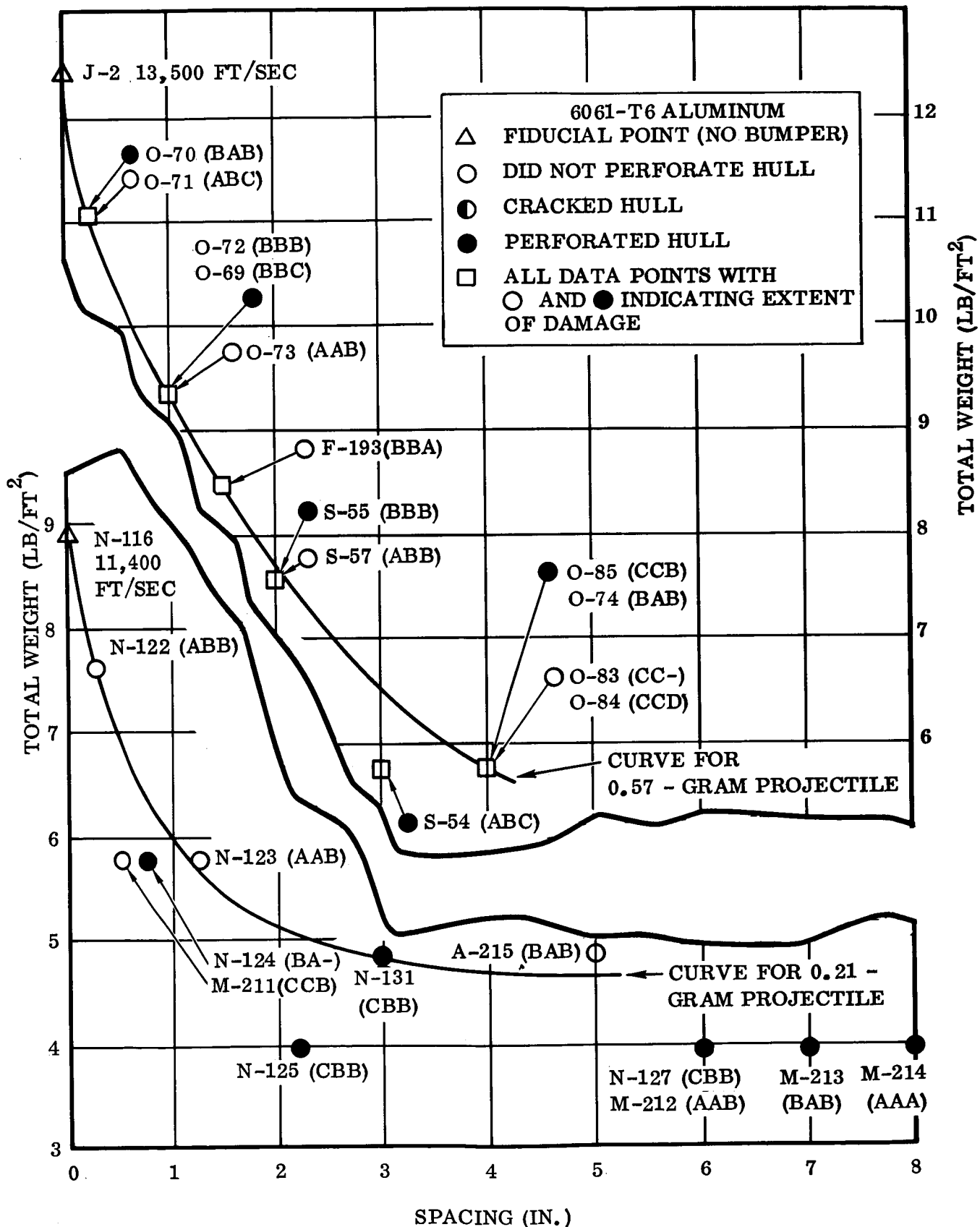


Figure 35. Test Panel Mass Versus Spacing (0.032-Inch Bumper)

Table 5. Summary of Bumper Impact Data: 0.21-Gram Cylindrical Steel and 0.34-Gram Spherical Steel Projectiles

ROUND NO.	RELIABILITY CODE	PROJECTILE			VELOCITY (FT/SEC)	BUMPER		SPACING BUMPER TO PLATE (IN.)	VEHICLE HULL PLATE THICKNESS (IN.)	TOTAL** WEIGHT OF TEST PANEL (LB/FT ²)	HOLE DIAMETER IN BUMPER (IN.)	SPRAY CONE DIAMETER (IN.)	PRINCIPLE CONE DIAMETER (IN.)	HULL PLATE			REMARKS
		MATERIAL	FORM	WEIGHT* (GM)		MATERIAL	THICKNESS (IN.)							DEPTH PENETRATION (IN.)	CRACKED	BULGE HEIGHT ON REVERSE FACE (IN.)	
N-116	-BA	4130-Steel	Cyl	0.21	11,400	None	---	---	0.625	8.87	---	---	---	0.48	No	0.04	0.4" dia , 0.08" lip
N-122	ACB	4130-Steel	Cyl	0.2135	14,000	Al	0.032	0.25	0.50	7.562	0.35	0.8	0.55	Cratered	No	Slight	Crater 0.55" dia.
M-211	CCB	4130-Steel	Cyl	0.2090	12,000	Al	0.032	0.50	0.375	5.742	0.25	---	---	0.35	No	0.05	
N-124	BAB	4130-Steel	Cyl	0.2143	13,600	Al	0.032	0.75	0.375	5.742	0.13 x 0.28	---	---	Punctured	---	---	0.45" dia puncture
N-123	AAB	4130-Steel	Cyl	0.2143	14,800	Al	0.032	1.25	0.375	5.742	0.3 x 0.35	1.2	---	Cratered	No	Slight	Good distribution of fragments
N-125	CBB	4130-Steel	Cyl	0.2135	12,500	Al	0.032	2.25	0.25	3.98	0.2 x 0.25	---	0.45	Punctured	---	---	0.45" dia puncture
N-131	CBB	4130-Steel	Cyl	0.2150	14,700	Al	0.032	3.0	0.3125	4.886	0.25	1.25 x 2.5	0.7 x 1.75	Punctured	---	---	0.3" x 0.4" puncture
A-215	BAB	4130-Steel	Cyl	0.1980	12,000	Al	0.032	5.0	0.3125	4.886	0.27 x 0.43	5.0	---	0.3	No	0.07	0.3" x 0.5" dia crater
N-127	CBB	4130-Steel	Cyl	0.2128	13,000	Al	0.032	6.0	0.25	3.98	0.23	---	0.4	Punctured	---	---	0.4" dia puncture
M-212	AAB	4130-Steel	Cyl	0.2153	12,600	Al	0.032	6.0	0.25	3.98	0.3	5.0	1.5	Punctured	---	0.05	0.25" and 0.2" diameter punctures--two.
M-213	BAB	4130-Steel	Cyl	0.2044	12,200	Al	0.032	7.0	0.25	3.98	0.15 x 0.22	---	---	Punctured	---	---	0.5" dia puncture
M-214	AAA	4130-Steel	Cyl	0.2115	11,800	Al	0.032	8.0	0.25	3.98	0.27	6.0	0.7	Punctured	---	---	0.30" x 0.4" dia puncture
N-129	BAB	4130-Steel	Cyl	0.2115	12,900	Al	0.090	2.0	0.25	4.81	0.25 x 0.35	3.0	---	Punctured	---	---	0.35" dia puncture
N-130	BB-	4130-Steel	Cyl	0.2140	---	Al	0.063	3.0	0.25	4.43	0.23 x 0.3	4.0	---	Punctured	---	---	0.4" dia puncture
F-181	AAA	Soft Steel	Sphere	0.34	5,250	None	---	---	0.75	10.58	---	---	---	0.5	No	0.05	Crater 0.3" dia; lip 0.08"
F-182	---	Soft Steel	Sphere	0.34	11,600	None	---	---	0.75	10.58	---	---	---	---	---	---	Projectile broke into about 8 closely grouped fragments
F-183	AAA	Soft Steel	Sphere	0.34	8,850	None	---	---	0.75	10.58	---	---	---	0.45	No	Slight	0.45" dia crater; lip 0.05"
F-184	---	Soft Steel	Sphere	0.34	11,900	None	---	---	0.75	10.58	---	---	---	---	---	---	Projectile broke into about six fragments
F-185	ABA	Soft Steel	Sphere	0.34	8,900	None	---	---	0.75	10.58	---	---	---	0.42	No	Slight	0.38" dia crater
F-192	AAB	Soft Steel	Sphere	0.34	12,500	Al	0.063	4.0	0.187	3.53	0.2 x 0.25	---	---	Punctured	---	---	0.32" dia puncture

* Accelerated Weight. ** The Test Panel Includes the Weight of the Bumper and Vehicle Hull.

per-impact-area will be considerably greater when the edge of the projectile strikes the bumper; consequently, projectile fragmentation will be less and damage to the main hull of the vehicle hull will be greater.

Due to the sensitivity of the 0.032-inch bumper system to projectile orientation, a series of experiments were made with each test panel combination (same total weight) in order to obtain valid results. A projectile striking an edge which failed to completely penetrate the hull, or a projectile striking flat which did completely penetrate the hull, would justify a change in spacing.

The open squares in Figure 35 indicate the total weight and spacing used, while the closed and open circles indicate the extent of test panel damage. This method of reporting the data was necessary, since the same test panel, depending on projectile orientation at the time of impact with the bumper, may or may not be penetrated.

3.1.4.2 Steel Projectile; 0.21 Gram. Test panels with an aluminum bumper, 0.032-inch thick and spaced from zero to eight inches from aluminum vehicle hulls of variable mass, have been subjected to impact from a 0.21-gram cylindrical steel projectile, 0.063-inch thick and 0.188 inch in diameter. All impact data are summarized in Figure 35 and Table 5. It should be noted that a new fiducial point was determined (N-116) for a single thick plate requiring 8.87 lb/ft^2 to prevent penetration, spallation, or cracking as a result of impact from the 0.21-gram projectile. This value can be compared to 12.43 lb/ft^2 required for the 0.57-gram projectile.

3.1.5 Aluminum Bumper, Type 6061-T6, 0.1875 Inch Thick. Three test panels (A-229, A-230, and A-232) with 0.1875-inch aluminum bumpers and 0.50-inch thick aluminum vehicle hull plates were subjected to impact from the 0.57-gram steel projectile. The data are summarized in Table 6. Impact velocities were 13,900, 14,800, and 14,700 ft/sec for separation distances 0.25, 0.125, and zero inch (flush), respectively. It should be observed that: a) none of the test panels were pierced completely; b) penetration into the vehicle plate decreased with increasing distance of separation from the bumper; c) the damage inflicted to the bumper was approximately the same in the three experiments; and d) none of the bumpers, even at the small separation distances, exhibited any evidence of petal formation.

3.1.6 Aluminum Bumper, Type 6061-T6, 0.090 Inch Thick; Copper Projectile. Six test panels with 0.090-inch aluminum (6061-T6) bumpers were subjected to impact (Table 7) with explosively accelerated copper projectiles, * that were 0.25 inch in diameter by 0.094 inch thick and weighed** 0.67 gram.

* The copper and 4130 steel projectiles are of identical geometry and have a mass of 0.67 gram and 0.57 gram, respectively. The electrolytic copper is 99.9 percent pure with the specification of QQC-502.

** Consult Table 7 for exact weights.

Table 6. Summary of Massive Bumper Impact Data: 0.57-Gram Steel Projectile

ROUND NO.	REL CODE	PRO-JECTILE WEIGHT (GM)	VELOCITY (FT/SEC)	BUMPER		SPACE BUMPER TO PLATE (IN.)	PLATE THICKNESS (IN.)	TOTAL WEIGHT SYSTEM (LB/FT ²)	HOLE DIA. BUMPER (IN.)	DEPTH PENETRATION IN PLATE (IN.)	BULGE HEIGHT REVERSE FACE PLATE (IN.)	REMARKS
				MATERIAL	GAUGE (IN.)							
A-222	BAB	0.5785	14,700	301 SS	0.063	0.75	0.50	9.72	0.35 x 0.55	0.2	Slight	Spray cone 1.7", main cone 0.9"
A-223	CCB	0.5780	14,300	301 SS	0.063	0.25	0.50	9.72	0.45 x 0.52	0.17	0.05	Crater diameter 0.8 x 0.9"
A-225	CC-	0.5770	---	301 SS	0.063	0.125	0.50	9.72	0.35 x 0.5	0.18	0.04	Crater diameter 0.7 x 0.8"
A-224	BBB	0.5625	12,000	301 SS	0.063	zero	0.50	9.72	0.32 x 0.43	Punctured	---	0.5 x 0.55" diameter hole. Spall 0.1" thick x 1.0" diameter
A-226	CBB	0.5730	12,900	301 SS	0.63	2.0	0.375	7.90	0.52 x 0.55	0.3	0.07	Spray cone diameter 4"; principal cone 0.8" x 1.0 diameter
A-229	CAB	0.5795	13,900	6061-T6 Al	0.1875	0.25	0.50	9.774	0.65 x 0.72	0.125	Slight	Crater diameter 0.9 x 1.0"
A-230	AAB	0.5770	14,800	6061-T6 Al	0.1875	0.125	0.50	9.774	0.62	0.12	0.03	Crater diameter 0.7"
A-232	CAB	0.5570	14,700	6061-T6 Al	0.1875	zero	0.50	9.774	0.65 x 0.7	0.3	0.125	Crater diameter 0.75"

Table 7. Summary of Impact Data: Copper Projectile; 0.090-Inch Al Bumper

ROUND NO.	REL CODE	PROJECTILE* WEIGHT (GM)	VELOCITY (FT/SEC)	SPACING (IN.)	VEHICLE HULL PLATE THICKNESS (IN.)	TOTAL** WEIGHT OF TEST PANEL (LB/FT ²)	HOLE DIA BUMPER (IN.)	SPRAY CONE DIA (IN.)	PRINCIPAL CONE DIA (IN.)	VEHICLE HULL PLATE			GENERAL REMARKS AND THOSE PERTAINING TO THE VEHICLE HULL
										PENE-TRATED (DEPTH) (IN.)	CRACKED	BULGE HEIGHT ON BACK FACE (IN.)	
D-150	--B	0.6819	14,000	---	0.875	12.43	---	---	---	No (0.44)	No	0.05	Crater dia 0.75" lip 0.12"
D-152	ABB	0.6355	13,200	0.25	0.625	10.15	0.45 x 0.5	0.9	---	No (0.38)	Yes	0.18	Crater 0.9" x 0.8" dia
D-147	ABB	0.6593	15,200	0.50	0.625	10.15	0.45 x 0.5	1.1	---	No (0.38)	No	0.05	Crater 0.7" dia
D-148	CBA	0.6603	10,400	1.5	0.50	8.39	0.31 x 0.4	2.25	1.0	No (0.38)	No	0.1	Crater dia 1.0"
D-146	AAA	0.6706	10,800	3.0	0.375	6.57	0.35 x 0.38	3.0	0.5 x 0.7	Yes	---	---	0.50 dia puncture
D-151	ABB	0.6330	12,600	4.0	0.375	6.57	0.45 x 0.5	5	0.3 x 1.2	Yes	---	---	2 perforations of plate 0.1" x 0.2" and 0.15" dia

* Accelerated Weight. ** The Test Panel Includes the Weight of the Bumper and Vehicle Hull.

April 1962

The data, in circles, are summarized in Figure 36 and can be compared with the data (solid line) obtained with the impact of a steel projectile on the 0.090-inch thick aluminum bumper (Figure 17). It should be noted that the same fiducial point was obtained with both the copper and steel projectiles. The excellent concordance between the two sets of data is obvious.

The craters produced by copper and steel projectiles can be seen in Figure 37 and the pertinent data are summarized in Table 8.

3.1.7 Magnesium - Lithium Alloy* (LA-141). Four experiments were made (Table 4, Figures 38 and 39) with Mg-Li alloy* bumper-aluminum (6061-T6) hull combinations. Both sets (0.063- and 0.095-inch thick bumpers) of data are in excellent concordance with the respective curves obtained with similar aluminum bumpers. The steel projectile weighed 0.57 grams prior to acceleration in air.

3.1.8 Stainless Steel, Type 301, 0.063 Inch Thick. Five test panels with 0.063-inch thick stainless steel bumpers and aluminum (6061-T6) vehicle hull plates were subjected to impact from the 0.57-gram steel projectile (Table 6). The aluminum hull in four test panels (A-222 to A-225) was 0.50-inch thick, and the separation distance from the stainless steel bumper was varied from zero (flush) to 0.75 inch. It should be observed that: a) the configuration with zero spacing was the only test panel completely pierced; b) penetration into the vehicle hull plate was about the same with separation distances of 0.125 to 0.750 inch; c) the damage inflicted to the bumper was about the same in the three test panels not pierced completely; and d) none of the bumpers, even with small separation distances, exhibited any evidence of petal formation.

The total weight of the fifth test panel was decreased from 9.72 to 7.90 lb/ft² and the separation distance was increased to 2.0 inches. This arrangement prevented the 0.57-gram steel projectile from completely penetrating the test panel. A bulge of 0.07 inch was raised on the reverse face of the hull plate.

3.2 GLASS BUMPERS. Four test panels with 0.094-inch plate glass bumpers were subjected to impact with explosively accelerated steel projectiles that weighed 0.57 gram. The data, in squares, are summarized in Table 4 and Figure 36 and can be compared with the data (solid line) obtained with the impact of a steel projectile on the 0.090-inch thick aluminum bumper (Figure 17). The glass bumper completely fragmented on impact making it impossible to determine the projectile orientation and integrity at the instant of impact. This necessitated coding (see Table 2 for symbol definitions) the impact data with glass bumpers as C-B, C-C, or C-D. The excellent concordance between the two sets (0.090-inch aluminum and glass bumpers) of data is obvious from Figure 36.

* Mg-14.1Li-1.5Al; density of 1.35 g/cc; Young's modulus of 6.5×10^6 psi.

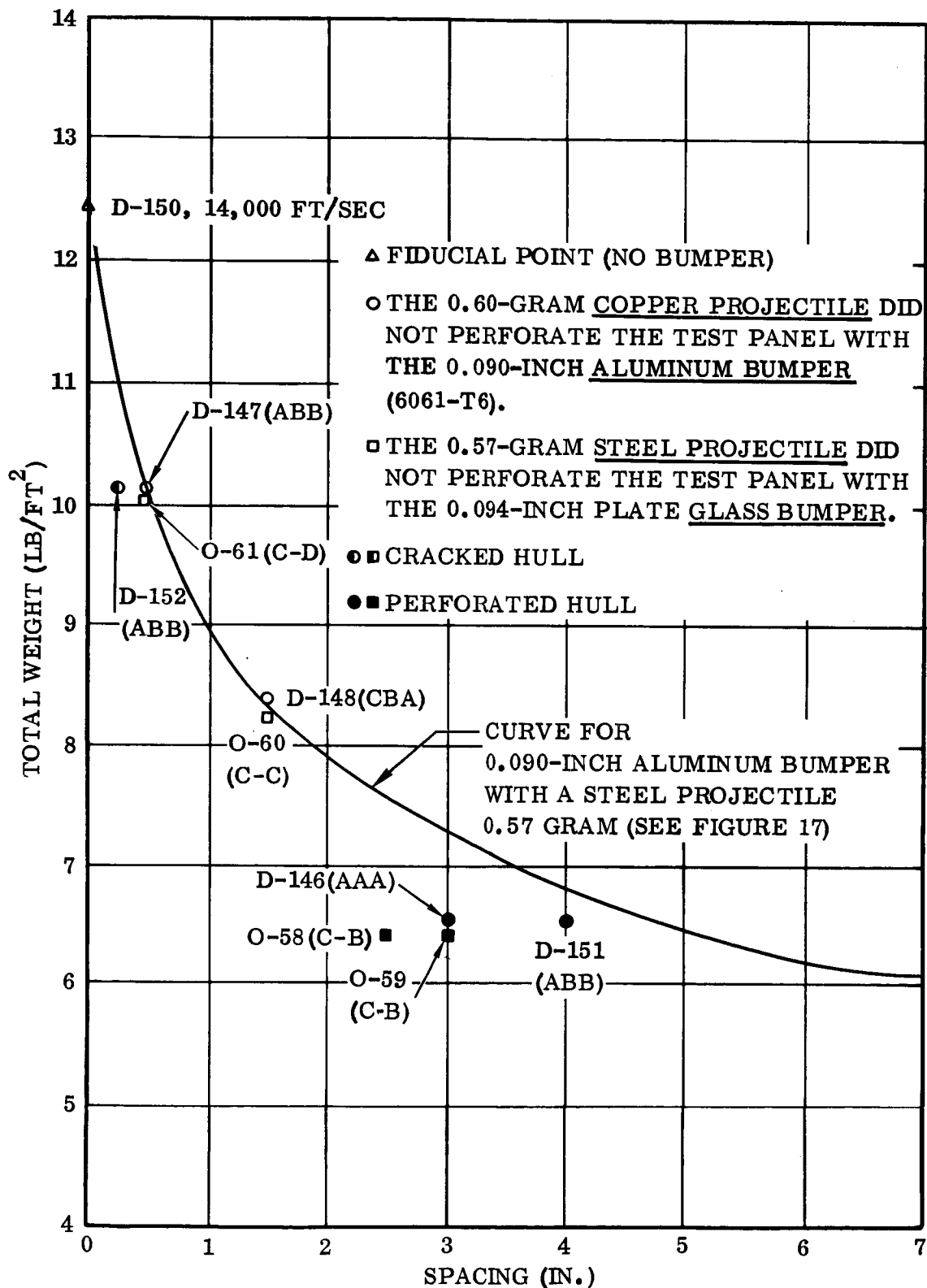
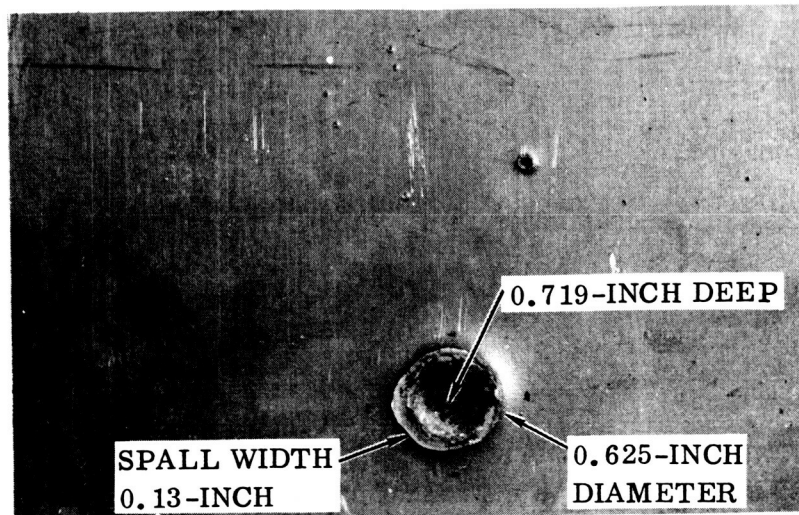
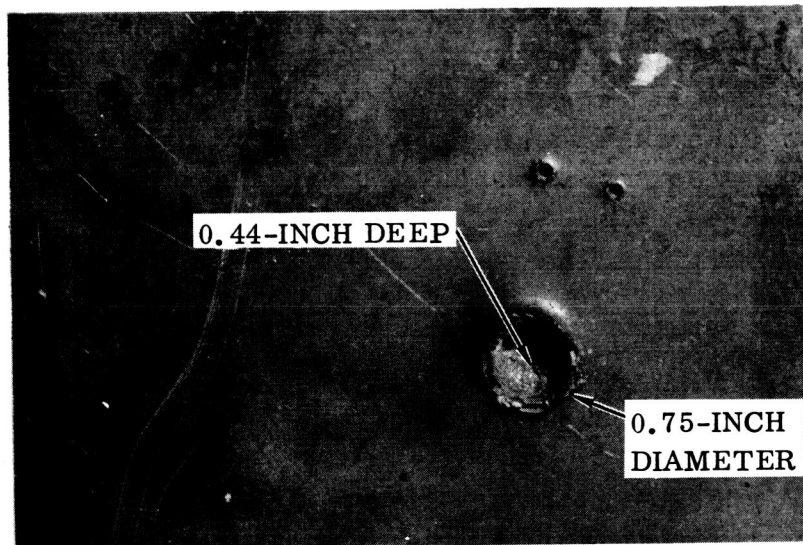


Figure 36. Test Panel Mass Versus Spacing (Aluminum and Plate Glass Bumpers)



J-2
NO BUMPER
0.875-INCH ALUMINUM
0.5742-GRAM STEEL PROJECTILE
13,500 FT/SEC



D-150
NO BUMPER
0.875-INCH ALUMINUM HULL
0.6819-GRAM COPPER PROJECTILE
14,000 FT/SEC

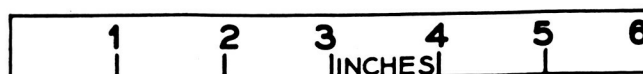


Figure 37. Craters Produced in Aluminum With Copper and Steel Projectiles

Table 8. Comparison of Craters in Aluminum Produced With a Copper and Steel Projectile

PROJECTILE					VEHICLE HULL		CRATER DIMENSIONS** IN VEHICLE HULL (IN.)		BULGE ON BACK OF VEHICLE HULL (IN.)		
ROUND NO.	MATL	SIZE	MASS* (GM)	VELOCITY (FT/SEC)	MATL	THICKNESS (IN.)	DIA	DEPTH	LIP	DIA	HEIGHT
J-2	Steel	0.25-inch diameter 0.094-inch thick	0.5742	13,500	Aluminum (6061-T6)	0.875	0.625	0.719	0.08	0.75	0.1
D-150	Copper	0.25-inch diameter 0.094-inch thick	0.6819	14,000	Aluminum (6061-T6)	0.875	0.75	0.44	0.12	1.00	0.08

* Accelerated mass.

** The crater is not amenable to precise measurement due to the irregularities in the crater wall, lip, etc.

April 1962

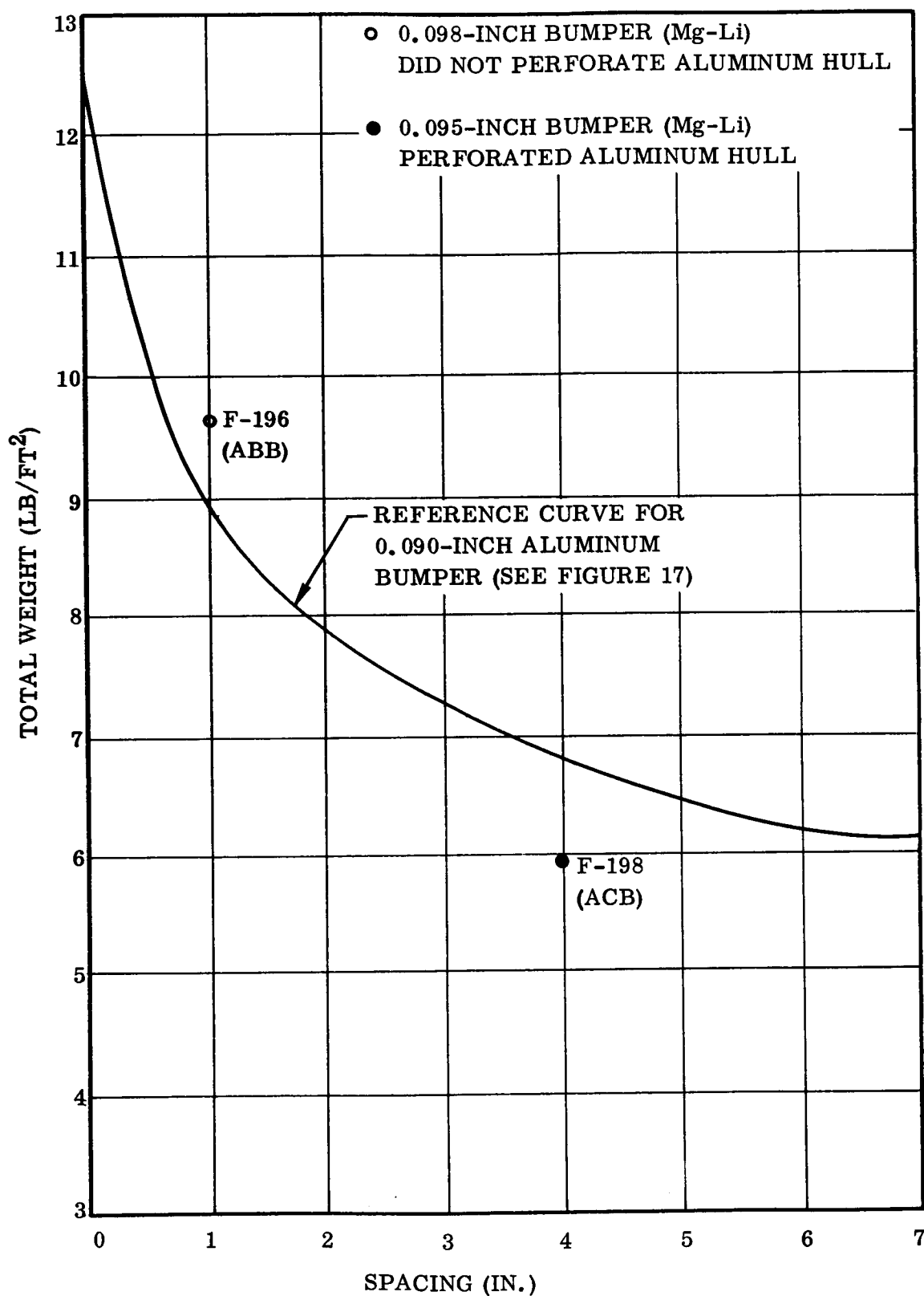


Figure 38. Comparison of Mass Versus Spacing for Magnesium-Lithium and 0.090-Inch Aluminum Bumpers

April 1962

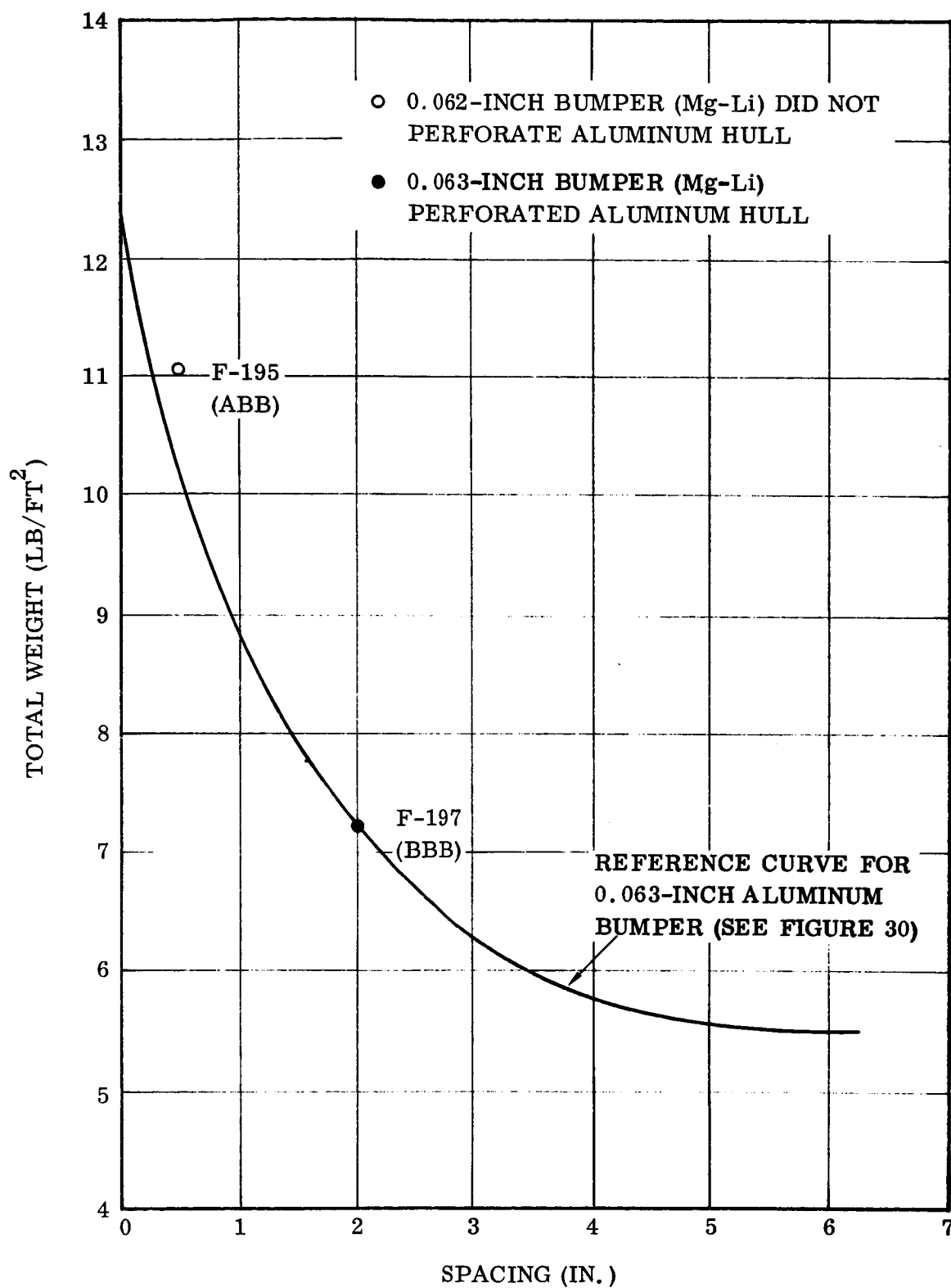


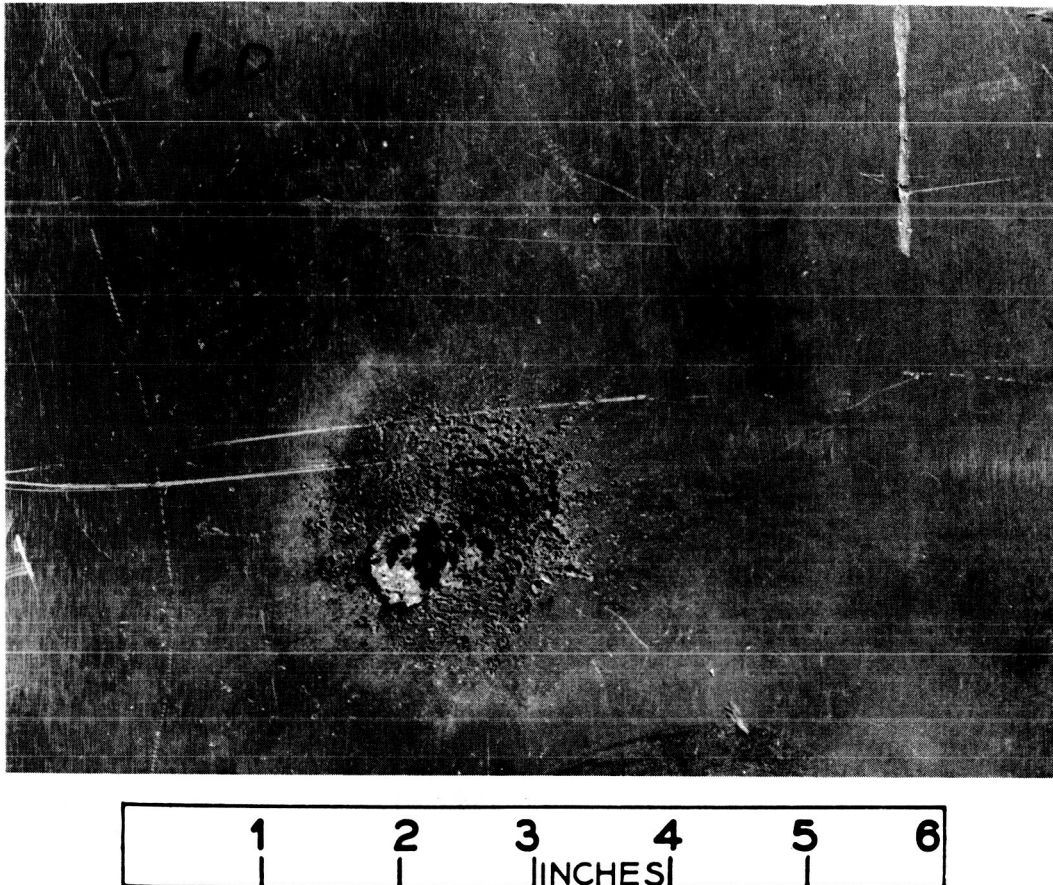
Figure 39. Comparison of Mass Versus Spacing for Magnesium-Lithium and 0.063-Inch Aluminum Bumpers

April 1962

The extent of damage inflicted on a main vehicle hull that was protected (Round No. O-60) with the 0.094-inch thick plate glass bumper spaced 1.5 inches from the hull is shown in Figure 40. This brittle and amorphous glass bumper material provided sufficient time and resistance to completely fragment the steel projectile traveling at 17,500 ft/sec. The crater in the vehicle hull was irregular and the area surrounding the crater was heavily pitted (see Section 9.5).

3.3 WIRE SCREEN BUMPERS. Sixteen-mesh, 0.028-inch aluminum screen was used as a bumper in two experiments (Table 4) with a 1.0-inch space between the bumper and main hull of the vehicle. The bumper in Experiment O-94 was composed of two layers of screen which were pressed together. Impact from the 0.59-gram steel projectile traveling at 15,200 ft/sec produced holes of 0.48-inch and 0.7-inch diameter in the first and second screens, respectively. The aluminum (6061-T6) vehicle hull was not penetrated, but a 0.4-inch circle of material was spalled from the back surface of the plate. The bumper in Experiment O-95 was composed of one layer of screen. The steel projectile, traveling at 14,300 ft/sec, produced a 0.48-inch by 0.50-inch hole in the screen. The main hull was completely penetrated with the formation of a 0.8-inch diameter shear plug which tapered to 0.4 inch.

The mesh of the wire screen was smaller than the projectile and permitted the steel projectile to partially fragment on impact. It should be noted that the wire screen had numerous impact holes, but many were produced by the spray of material splashed back from the 0.625-inch thick aluminum plate. This was determined from the direction in which the broken wires surrounding the hole were bent.



O-60
0.094-INCH PLATE GLASS BUMPER
0.50-INCH ALUMINUM HULL
1.5-INCH SPACING
17,500 FT/SEC

Figure 40. Vehicle Hull Protected With a Plate Glass Bumper

SECTION 4

PRESSURIZED STRUCTURES

Space vehicles will have components pressurized with fluid, gas and liquid fuel tanks at cryogenic temperatures, liquid working fluid for radiators where the temperature will be moderate to high, and gas for ambient temperature inflatable and manned structures. Pressurized structures, especially liquid filled components, present formidable protection problems due to the difference in materials and component behavior when subjected to hypervelocity impact.

The kinetic energy of a high velocity particle is delivered to a liquid pressurized tank at an extremely high rate. Since this energy supplements the hoop tension existing in the vessel wall, failure can be expected at the point of particle impact. This has been observed [2, 3] and the preliminary puncture (projectile velocity of approximately 17,000 ft/sec) will be followed by catastrophic ripping (Figures 41 and 42) of the vessel wall by stored energy due to the hoop tension stresses. Gas pressurized structures may behave in an entirely different manner (Figure 43). The kinetic energy is delivered to the vessel walls at a slower rate (relative to the liquid filled tank) due to the low gas density and low speed of sound. Therefore, failure can be expected via puncture, spall, and continued flight of the hypervelocity particles through the gas and out the opposite side of the tank. If, however, the crack or tear produced in the wall of the gas pressurized tank exceeds the critical crack length of the material for the wall stresses which prevail, catastrophic fracture of the tank wall may occur just as in the case of the liquid filled tank.

In addition to these obvious hazards, other perils exist which are frequently not recognized. For example, an astronaut may: a) experience shock and/or concussion; and b) be subjected to a flash explosion from the high velocity impact with an oxygen-rich pressurized space vehicle. Also, liquid-oxygen propellant storage tanks may explode since they will contain both liquid and gaseous oxygen.

In order to determine [2] the extent of damage as well as to study the impact flash and explosions resulting from meteoric particle impact on oxygen-rich pressure vessels, a 5-inch diameter by 6.75-inch long cylinder was fabricated (see Figures 13 and 14, and Table 3) with replaceable end diaphragms. These test containers were subjected to impact with explosively accelerated steel projectiles.

4.1 TEST PANEL NO. 1: 5Al-2.5Sn-Ti; 20-PSI GASEOUS OXYGEN. The front and back diaphragms (0.025 inch thick) of the test cylinder were fabricated from the 5Al-2.5Sn-Ti alloy, and the system was pressurized to 20 psi with pure gaseous oxygen. The 0.2110-gram* projectile, with an impact velocity of 15,900 ft/sec, formed the 0.33-inch diameter hole and the 0.75-inch diameter oxidized and burned area in the front diaphragm (Figure 44). Impact with the titanium alloy diaphragm

* Accelerated Mass

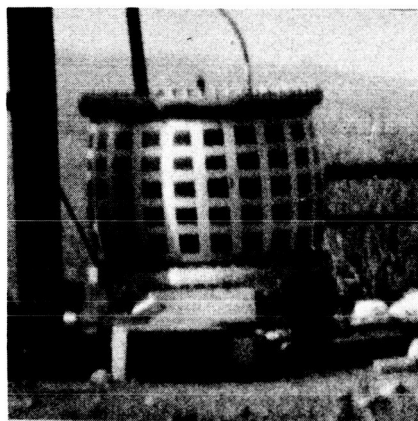
fragmented the projectile but did not prevent particles from penetrating the rear diaphragm. This rear diaphragm burned rapidly in the oxygen-rich environment and produced a burned-out area of about four inches in diameter. Ignition appears to have originated from at least three points.

4.2 TEST PANEL NO. 2: 301 FULL-HARD STAINLESS STEEL; 60-PSI GASEOUS OXYGEN. The front and back diaphragms (0.010 inch thick) of the test cylinder were 301 extra-full-hard stainless steel and the system was pressurized to 60 psi with pure gaseous oxygen. The 0.2154-gram projectile, with an impact velocity of 13,600 ft/sec, formed the 0.25-inch diameter hole (Figure 45) in the front diaphragm. Fragmentation of the projectile was extensive as evidenced from the numerous small holes in the rear diaphragm. An explosion was initiated as a result of the impact and the rear diaphragm was ruptured, but only after it was penetrated from the forward moving fragments. Two pieces of the rear diaphragm were found and these are shown in Figure 45.

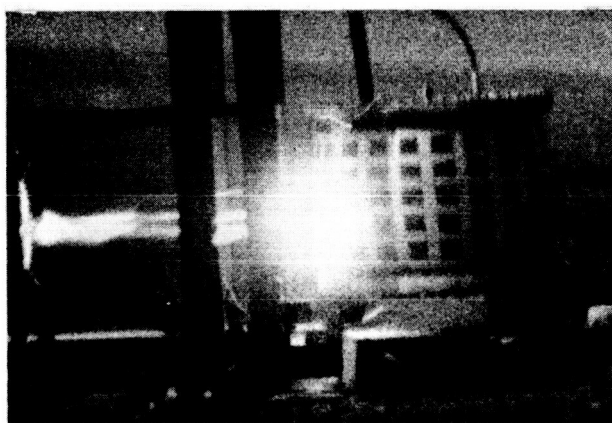
Photographs (not shown in this report) of one test cylinder were obtained at the rate of 25,600 frames-per-second (± 1000) with an exposure time of one microsecond, using a Beckman and Whitley, Model 326, Dynafax camera. The projectile broke in at least two pieces as evidenced from two flame jets. Details of the burning could not be followed since the entire area of the front diaphragm was obscured with the cloud of many fine particles of titanium alloy, titanium oxide(s), iron and iron oxide(s). Oxidation was quite rapid as evidenced from the progressive increase in illumination of this cloud of material.

4.3 TEST PANEL NO. 3: 6Al-4V-Ti; 60-PSI LIQUID OXYGEN. The front diaphragm of the titanium (6Al-4V-Ti) test panel ruptured from the impact of the 0.097-gram projectile traveling at 12,300 ft/sec. Frame A (Figure 46) shows the flap (Frame C) of titanium ripped from the front diaphragm (0.016 inch thick) as the liquid oxygen pressure was released. This flap of metal burned (about 10 percent burned) in the oxygen atmosphere, and the reaction can be seen in Frame B, which was taken 2.67 seconds after the impact. The rear diaphragm (0.016 inch thick) was neither pierced nor damaged (Frame D).

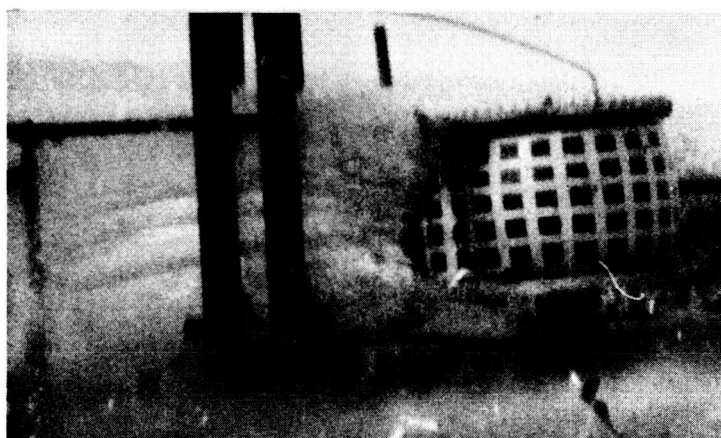
4.4 TEST PANEL NO. 4: ALUMINUM (2024-T3); 60-PSI LIQUID OXYGEN. The front and back diaphragms (0.016-inch thick) of the test cylinder were 2024-T3 aluminum, and the system was pressurized to 60 psi with liquid oxygen. The 0.097-gram projectile, with an impact velocity of 12,300 ft/sec, formed the two holes (0.20-inch and 0.10-inch in diameter) in the front diaphragm. There was extensive fragmentation of the projectile on impact, as evidenced from the numerous small holes (1 hole with a 0.15-inch diameter, plus 12 smaller holes) in the rear diaphragm (Figure 47). Slight oxidation occurred only at the rear diaphragm. Sequence photographs show the jet of oxygen escaping from the punctures produced in the rear diaphragm of the pressurized aluminum (2024-T3) structure.



TANK PRESSURIZED WITH WATER
PROJECTILE DIRECTION
→

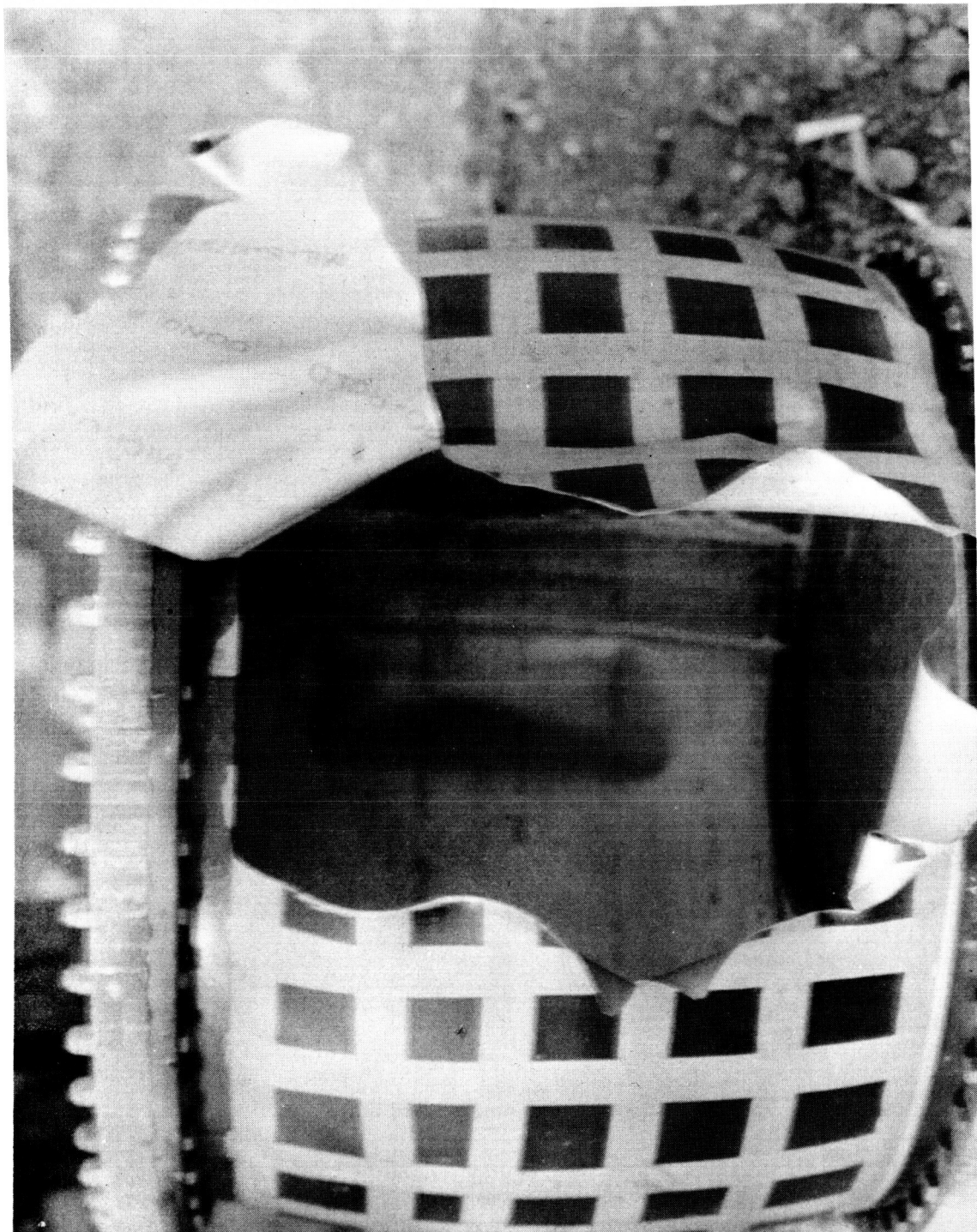


INSTANT OF IMPACT



THE PROJECTILE DID NOT PASS THROUGH
THE TANK, BUT THE TANK RUPTURED.

Figure 41. Liquid-Pressurized Tank During Impact [Ref 3]



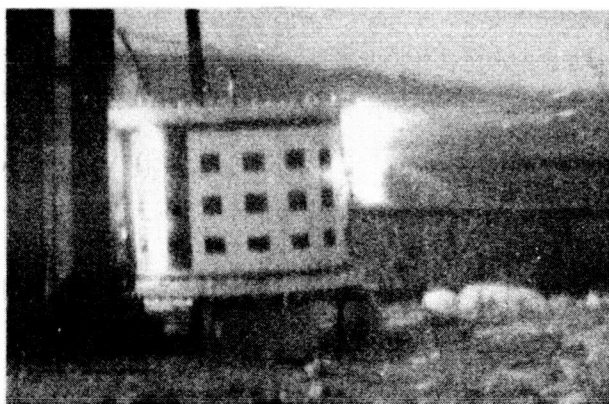
DAMAGE TO LIQUID PRESSURIZED TANK

Figure 42. Liquid-Pressurized Tank After Impact [Ref 3]



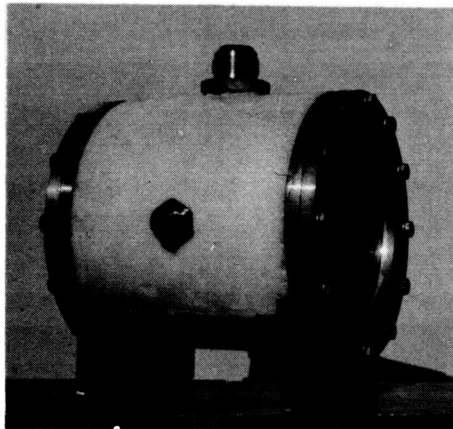
TANK PRESSURIZED WITH AIR AT INSTANT OF IMPACT

PROJECTILE DIRECTION

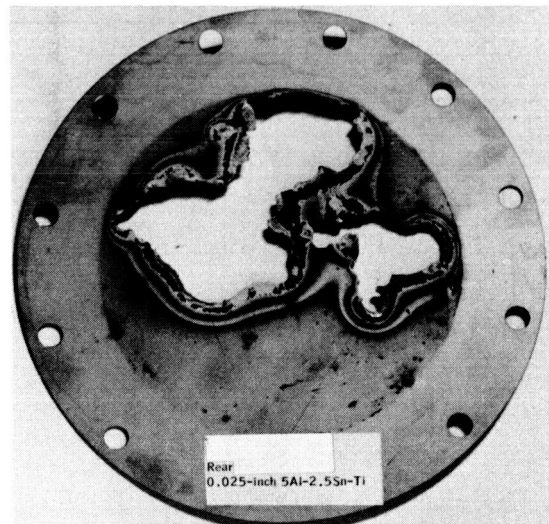
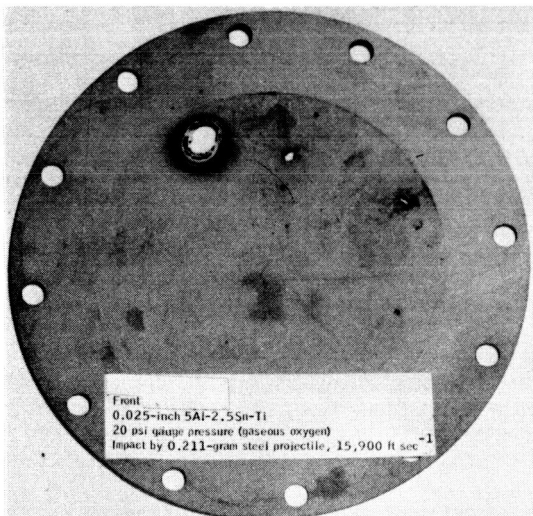


PROJECTILE PASSED THROUGH THE TANK

Figure 43. Gas-Pressurized Tank During Impact [Ref 3]



TEST CYLINDER



DIAPHRAGMS

Figure 44. Oxygen-Pressurized Tank: Test Panel No. 1 [Ref 2]

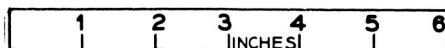
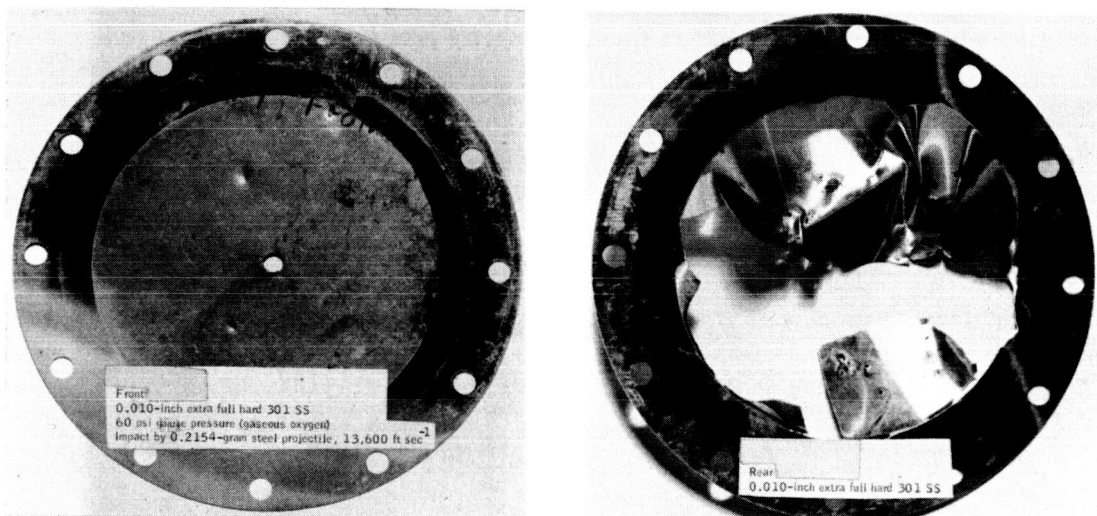
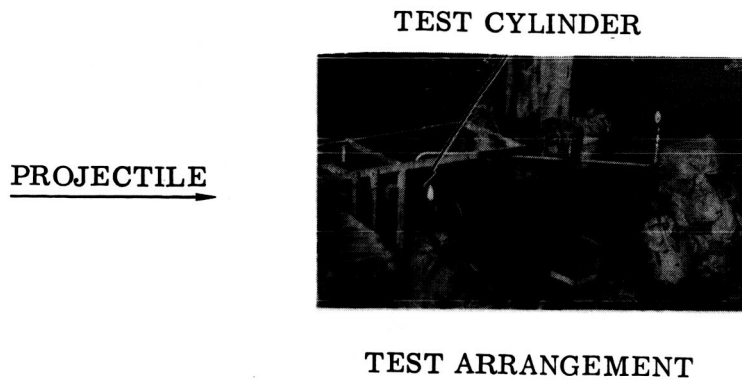
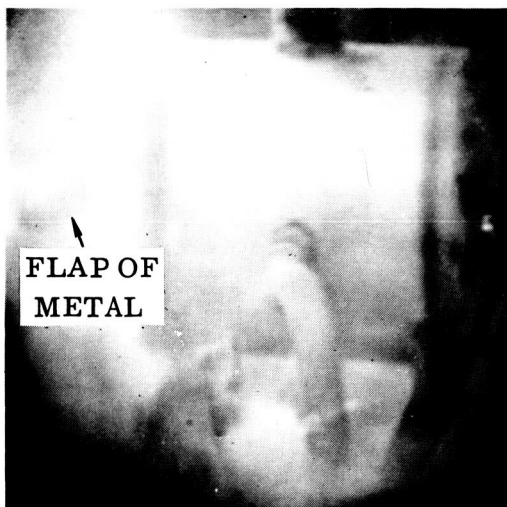
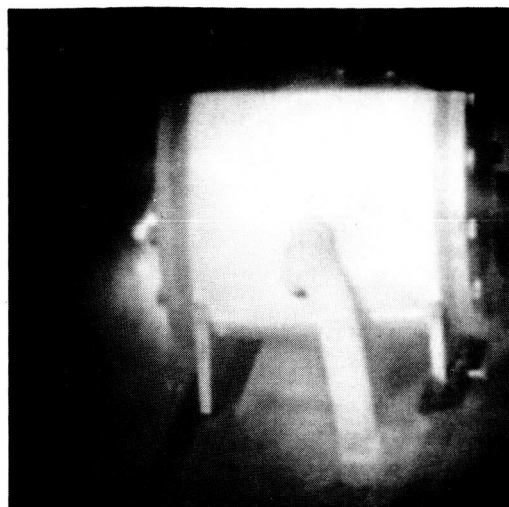


Figure 45. Oxygen-Pressurized Tank: Test Panel No. 2 [Ref 2]

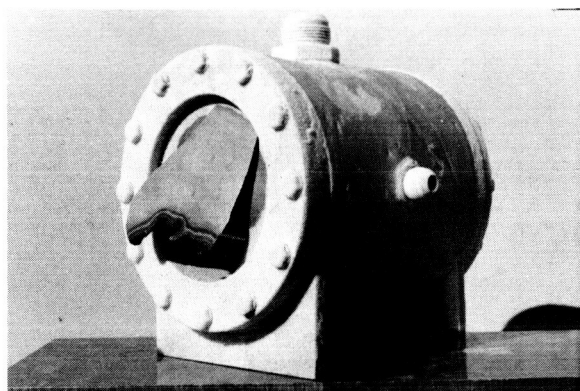
April 1962



FRAME A. FRONT DIAPHRAGM RUPTURED. NOTE FLAP OF METAL.



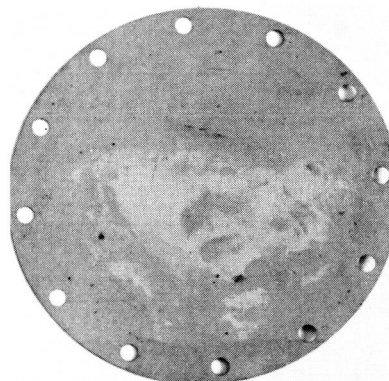
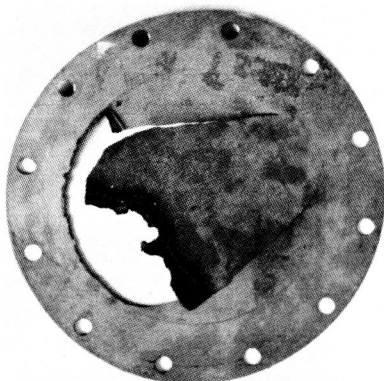
FRAME B. 2.67 SECONDS AFTER IMPACT.



FRAME C.

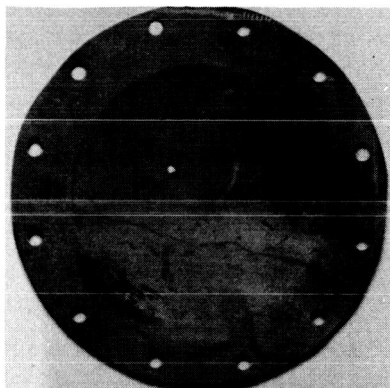
NO. 3 - FRONT DIAPHRAGM
0.016-INCH 6Al-4V-Ti
60 PSI GAUGE PRESSURE (LIQUID OXYGEN)
IMPACT BY 0.097-GRAM STEEL PROJECTILE,
12,300 FT/SEC

NO. 3 - REAR DIAPHRAGM
0.016-INCH 6Al-4V-Ti

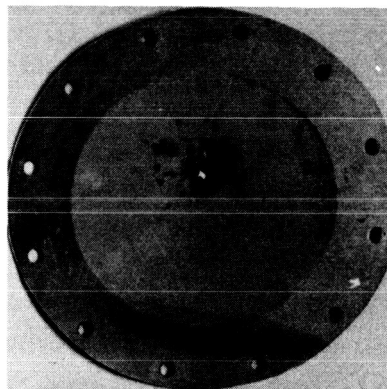


FRAME D.

Figure 46. Test Panel No. 3: 6Al-4V-Ti; 0.097-Gram Projectile; 60-psi Liquid Oxygen [Ref. 2]



FRONT DIAPHRAGM: 0.016-IN.,
2024-T3 ALUMINUM, 60-PSI
GAUGE PRESSURE (LIQUID
OXYGEN), IMPACT BY 0.097-
GRAM STEEL PROJECTILE,
12,300 FT/SEC

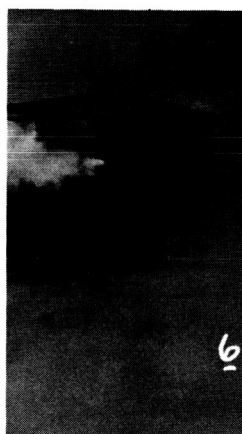


REAR DIAPHRAGM: 0.016-IN.,
2024-T3 ALUMINUM

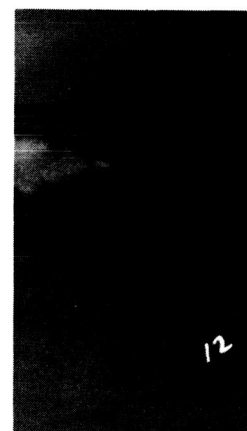
VIEW OF REAR DIAPHRAGM



PRIOR TO
IMPACT



0.20 SEC AFTER
IMPACT



0.44 SEC AFTER
IMPACT

Figure 47. Test Panel No. 4: 2024-T3 Aluminum; 0.097-Gram
Projectile; 60-psi Liquid Oxygen [Ref 2]

SECTION 5

ENERGY-ABSORBING CORE MATERIALS

Several energy absorbing or core materials were subjected to preliminary impact investigation with 0.57-gram steel projectiles. This material, located between the bumper and vehicle hull, was placed in contact with the vehicle hull in all experiments except F-167 (see Table 9). All test panels were fabricated from 6061-T6 aluminum, and the bumper thickness was held constant at 0.063 inch except in experiment D-159, where it was 0.032 inch.

The preliminary tests with energy-absorbing configurations subjected to impact from the steel projectile were limited to an experimental survey. All data (except Experiments D-159 and F-167) pertinent to the different energy-absorbing test panels are summarized in Table 8, and Figures 48 through 50. It should be observed that six different test panel configurations were used, and these, with the respective experiments, are summarized in Figure 51.

Two test panels were fabricated from a honeycomb-core material, which is a different type of energy absorber. Test panel 1 was composed of honeycomb with 0.75-inch cells* made from 0.005-inch commercial aluminum foil placed between 0.040-inch plates of 2024-T86 Alclad. The honeycomb was bonded to the skins with Aerobond adhesive 422. This panel (Figure 52) was subjected to impact (in air) from a 0.063-inch thick by 0.19-inch in diameter, 0.2144-gram steel projectile, traveling at 13,200 ft/sec. Two small fragments were broken from the projectile. The two fragments and the remainder of the projectile penetrated the entire panel, as well as the 0.125-inch aluminum (6061-T6) plate placed 6.75 inches behind the test panel. The honeycomb was deformed extensively due to the explosive impact of the projectile.

Test panel 2 was composed of honeycomb with 0.75-inch cells made with 0.005-inch commercial aluminum foil, placed between 0.050-inch plates of 5-ply Conolon 506. The honeycomb was bonded to the skins with Aerobond adhesive 422. This panel (Figure 53) was subjected to impact (in air) from the 0.063 inch thick by 0.19 inch in diameter, 0.2108-gram steel projectile, traveling at 16,100 ft/sec. The back skin was completely removed from the test panel as a result of the impact, and the projectile fragments penetrated the 0.125-inch aluminum (6061-T6) plate, placed 6.75 inches behind the test panel. The honeycomb was deformed extensively due to the explosive impact.

* Plastilock 620 was used for the intercellular adhesive.

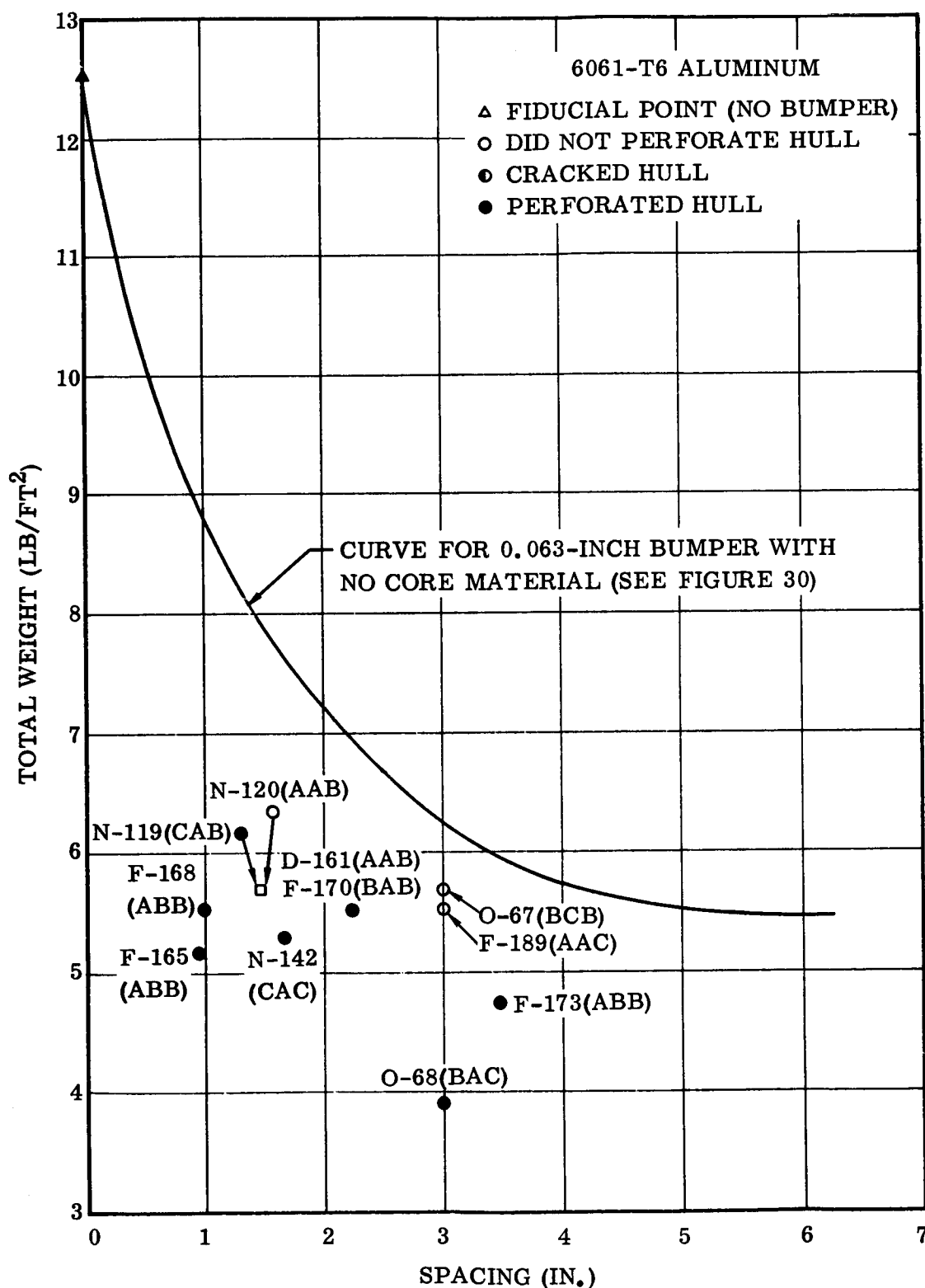


Figure 48. Mass Versus Spacing for Fiberglass Energy Absorber

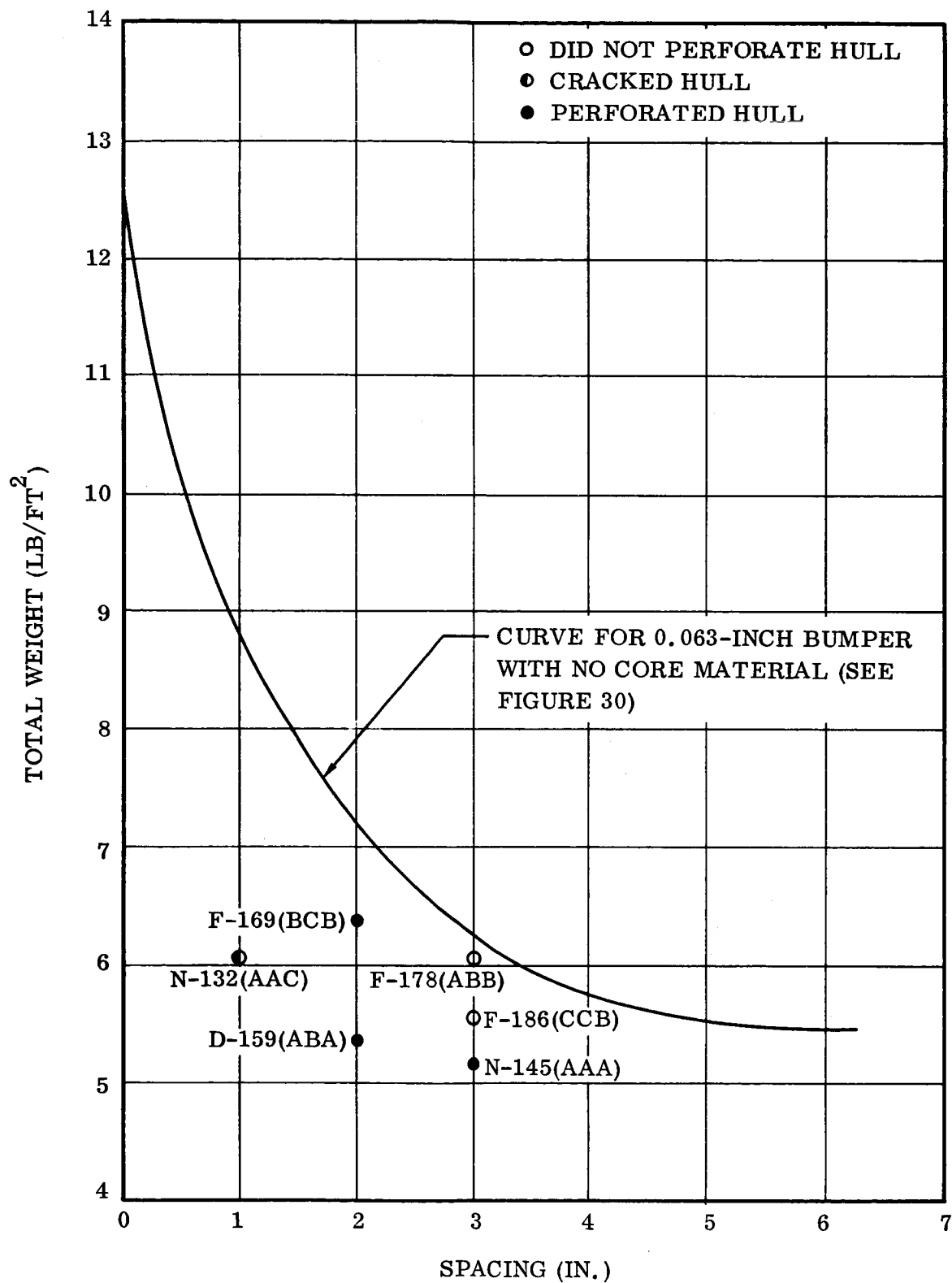


Figure 49. Mass Versus Spacing for MIN K-1300 Energy Absorber

April 1962

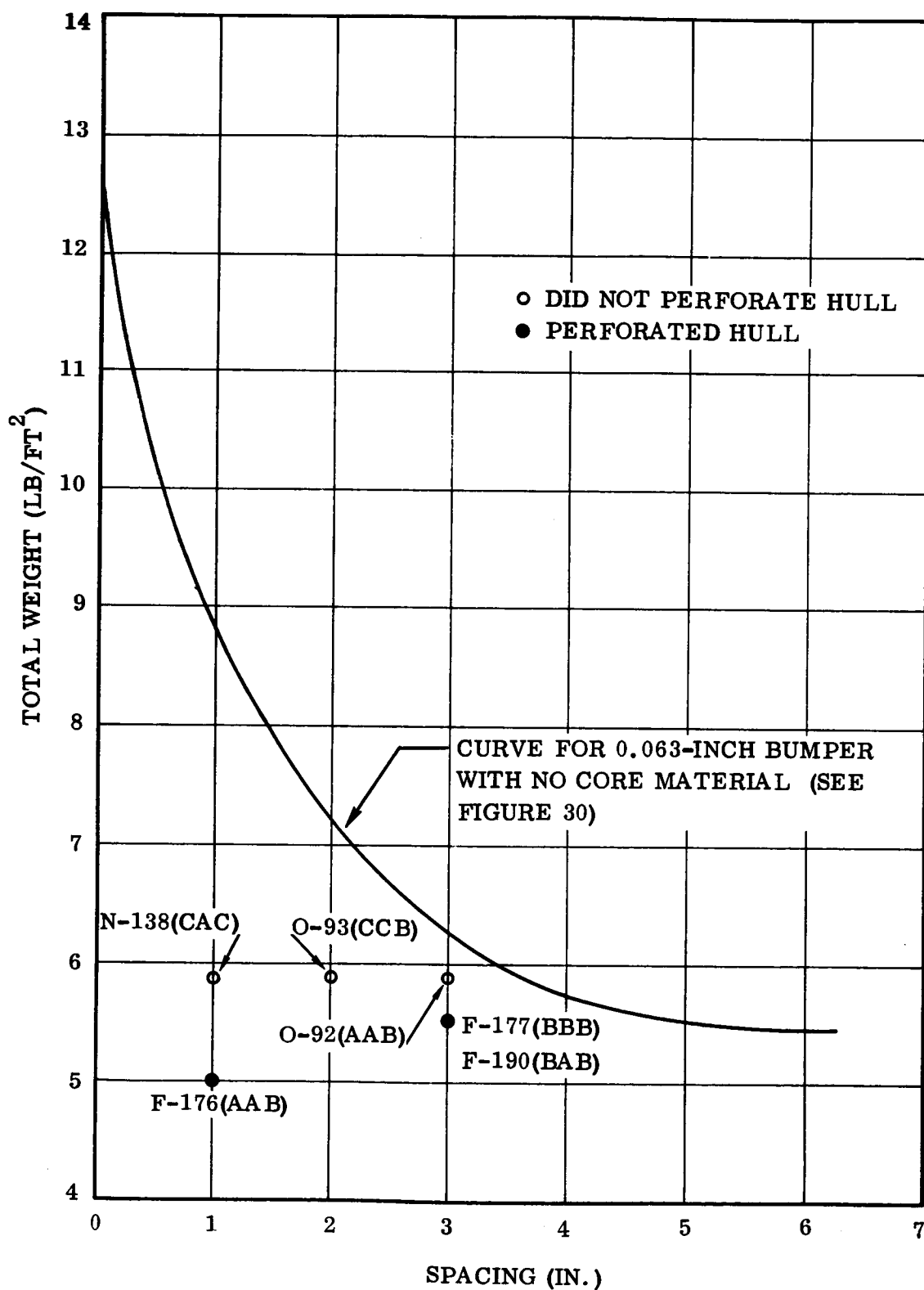


Figure 50. Mass Versus Spacing for Fibrous Potassium Titanate Energy Absorber

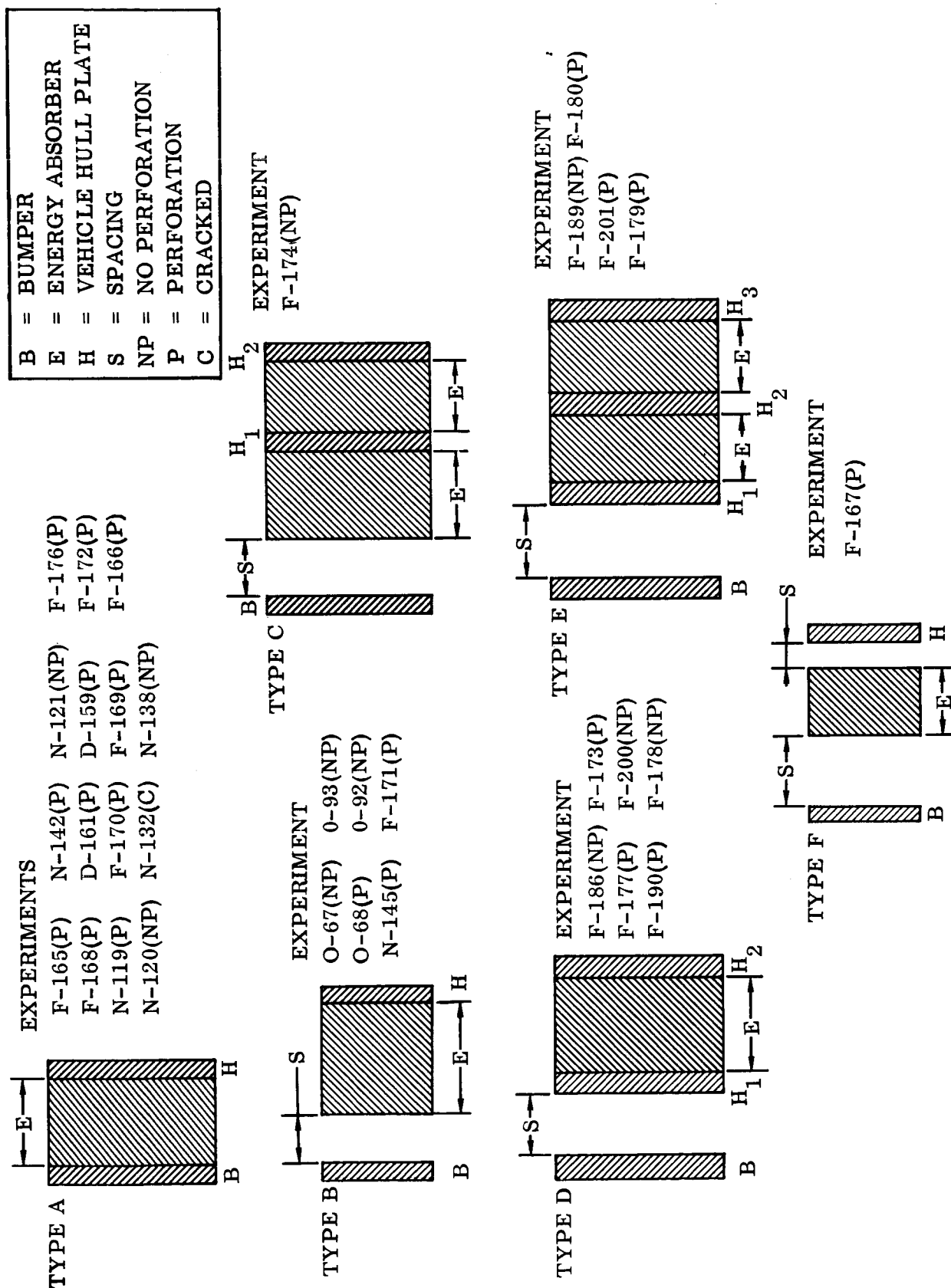
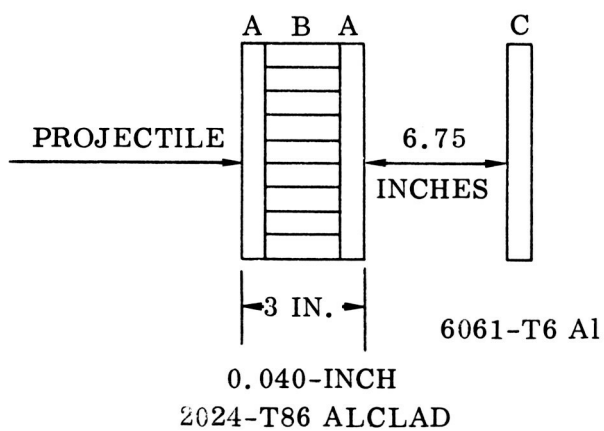
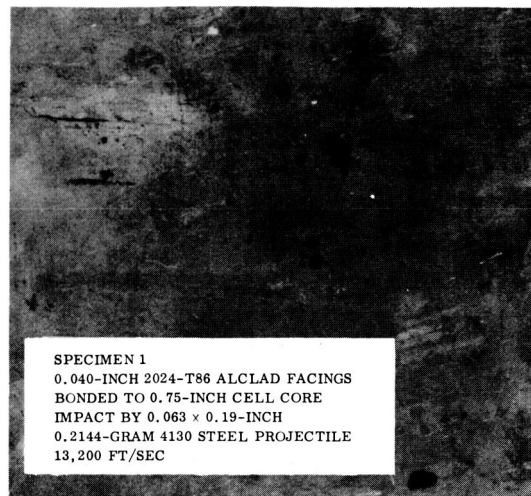


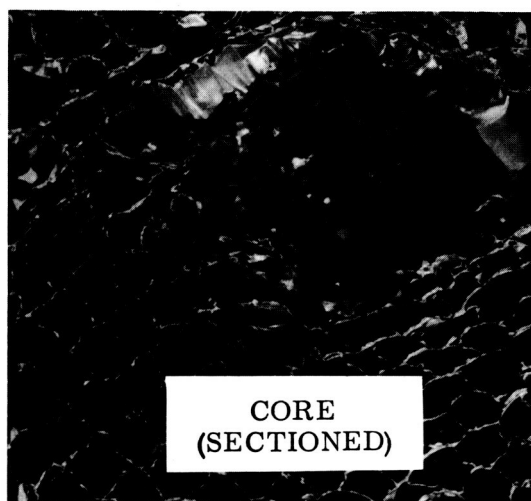
Figure 51. Energy Absorber Test Panel Configurations (See Table 9)



A



B



C

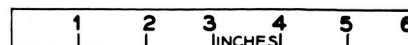


Figure 52. Honeycomb Panel No. 1

Table 9. Summary of Bumper Impact Data: Energy-Absorbing Core Materials and 0.57-Gram Steel Projectile (See Figure 51).

ROUND NO.	RELIA- BILITY CODE	PROJEC- TILE WEIGHT (GM)	VELOCITY (FT/SEC)	BUMPER THICKNESS (IN.)	SPACING BUMPER TO PLATE (IN.)	CORE			VEHICLE HULL PLATE THICKNESS (IN.)	TOTAL** WEIGHT SYSTEM (LB/FT ²)	HOLE DIA. BUMPER (IN.)	SPRAY CONE DIA. (IN.)	PRINCIPLE CONE DIA. (IN.)	VEHICLE HULL		REMARKS
						MATERIAL	ARRANGEMENT	THICKNESS (IN.)						DEPTH PENETRATED (IN.)	CRACKED	
O-67	BCB	0.5838	13,200	0.063	3.0	Fiberglass Insul. Board	1.5" space; 1.5" Fiberglass	1.5	0.25	\$,684	0.35 x 0.53	2 x 3	---	Not Appreciable	No	15 small craters
O-68	BAC	0.5838	17,200	0.063	3.0	Fiberglass Insul. Board	1.5" space; 1.5" Fiberglass	1.5	0.125	\$,914	0.17 x 0.4	1.25 x 1.5	0.45 x 0.52	Punctured	---	0.45" x 0.52" dia puncture
F-189	AAC	0.5750	16,100	0.063	3.0	0.032" Al; Edge grain F. 8#; 0.063" Al	2" space--0.032" Al--0.5" EGF 0.063" Al--0.5" EGF	1.0	0.1875	\$,553	0.4 x 0.45	3.0	1.2	Not Appreciable	No	Nicks
F-173	ABB	0.5785	15,200	0.063	3.5	0.063 Al; Edge grain F. 3; 6#	3" space--0.063" Al 0.5" EGF 3	0.5	0.1875	4,708	0.45 x 0.5	5.0	0.6 x 1.2	Punctured	Yes	0.1" dia puncture
F-200	CCB	0.5665	15,700	0.063	2.75	Linde S10 (Alter- nating layers glass fibers, foil)	2" space--0.063" Al--Linde S10 (28 glass fiber layers 30 Al foils)	0.75	0.1875	5,238	3 holes	3.0	1.0	Not Appreciable	No	
F-201	ABB	0.5795	14,300	0.063	3.0	0.032" Al; Refrasil	2" space--0.032" Al--0.25" re- frasil--0.032" Al --0.75" refrasil	1.0	0.1875	5,034	0.55	3.0	0.5 x 1.2	Punctured	---	0.2" dia puncture
N-132	AAC	0.5750	16,200	0.063	1.0	Min-K 1300	Filled Space	1.0	0.25	6,054	0.5 x 0.55	---	---	Not Appreciable	Yes	8 craters
N-121	BA	0.5718	---	0.063	1.5	Min-K 2000	Filled Space	1.5	0.25	6,834	0.3 x 0.43	1.0	---	Not Appreciable	No	7 craters
D-159	ABA	0.5726	10,900	0.032	2.0	Min-K 1300	Filled Space	2.0	0.125	5,332	0.3	---	---	Punctured	---	0.4" dia puncture
F-169	BCB	0.5705	15,700	0.063	2.0	Min-K 1300	Filled Space	2.0	0.1875	6,65	0.37 x 0.5	1.5	0.63 x 0.75	Punctured	---	0.25" x 0.35" dia puncture
N-145	AAA	0.5723	10,200	0.063	3.0	Min-K 1300	2" space--1" Min-K	1.0	0.1875	5,188	0.4 x 0.43	1.4 x 2.0	---	Punctured	---	2 punctures (0.25" x 0.3" and 0.18"); 2 craters
F-174	AAC	0.5714	17,200	0.063	3.0	Min-K 2000; 0.063" Al	2" space--0.5" Min-K--0.063" Al--0.5" Min-K	1.0	0.1875	6,064	0.5 x 0.62	1.75 x 2.25	1.0 x 1.5	Not Appreciable	No	0.04
F-178	ABB	0.5620	13,000	0.063	3.0	0.063" Al-- Min-K 1300	2" space--0.063" Al--1.0" Min-K	1.0	0.1875	6,084	0.45 x 0.5	2.5	1.2	Not Appreciable	No	None
F-186	CCB	0.5670	15,700	0.063	3.0	0.032" Al-- Min-K 1300	2" space--0.032" Al--1.0" Min-K	1.0	0.1875	5,632	0.32 x 0.44	2 x 3.5	0.5 x 1.25	Not Appreciable	No	0.03
F-179	BA	0.5645	---	0.063	3.5	0.032" Al; 3M inorganic paper	3" space--0.032" Al--0.25" 3M paper--0.032" Al --0.25" 3M paper	0.5	0.1875	5,028	0.3 x 0.43	1.5 x 4	0.6 x 1.0	Punctured	---	0.45" dia puncture

* Accelerated Weight. ** The System Includes the Weight of Bumper, Core, and Vehicle Hull.

Table 9. Summary of Bumper Impact Data: Energy-Absorbing Core Materials and 0.57-Gram Steel Projectile (See Figure 51). Contd

ROUND NO.	RELIABILITY CODE	PROJEC-TILE WEIGHT (GM)	VELOCITY (FT/SEC)	BUMPER THICKNESS (IN.)	SPACING BUMPER TO PLATE (IN.)	CORE			VEHICLE HULL PLATE THICKNESS (IN.)	TOTAL** WEIGHT SYSTEM (LB/FT ²)	HOLE DIA. BUMPER (IN.)	SPRAY CONE DIA. (IN.)	PRINCIPLE CONE DIA. (IN.)	VEHICLE HULL			REMARKS
						MATERIAL	ARRANGEMENT	THICKNESS (IN.)						DEPTH PENETRATED (IN.)	CRACKED	BULGE HEIGHT ON BACK FACE (IN.)	
N-138	CAC	0.5680	18,900	0.063	1.0	Tipersul (potassium titanate)	Filled Space	1.0	1.49	5.934	0.35 x 0.4	1.5	---	Not Appreciable	No	None	3 craters
F-176	AAB	0.5435	15,700	0.063	1.0	Tipersul	Filled Space	1.0	1.5	5.03	0.5 x 0.52	2.25	1.0	Punctured	---	---	0.4" dia puncture
O-93	CCB	0.5760	15,200	0.063	1.5	Tipersul	0.5" space--1.0" Tipersul	1.0	1.5	5.934	---	---	---	Not Appreciable	No	None	Premature projectile fragmentation
O-92	AAB	0.5744	14,700	0.063	3.0	Tipersul	2.0" space--1.0" Tipersul	1.0	1.5	5.934	0.48	2.5	---	Not Appreciable	No	None	Few minor nicks
F-177	BBB	0.5700	15,000	0.063	3.0	0.032" Al Tipersul	2.0" space--0.032" Al--1.0" Tipersul	1.0	1.952	5.482	0.28 x 0.42	2.2 x 3.5	0.5	Punctured	---	---	0.5" dia puncture
F-190	BAB	0.5760	12,200	0.063	3.0	0.032" Al Tipersul	2.0" space--0.032" Al--1.0" Tipersul	1.0	1.952	5.482	0.27 x 0.38	1.5 x 2.5	0.4 x 1.0	Punctured	---	---	0.5" dia puncture
F-172	ABB	0.5710	15,200	0.063	1.0	Al Wool 0.05" Rubber	Filled Space Wool 0.05" Rubber	1.0	0.933	5.265	0.48 x 0.52	3.0	1 x 1.4	Punctured	---	---	0.36" x 0.55" dia puncture
F-166	AAB	0.5680	15,700	0.063	1.31	Al Wool	Filled Space	1.31	0.5	4.934	0.47 x 0.53	3.0	0.8 x 1.6	Punctured	---	---	0.22" x 0.63" dia puncture
F-180	BAC	0.5495	17,300	0.063	3.0	0.032" Al Al wool	2" space--0.032" Al--0.5" Al Wool --0.032" Al--0.5" Al Wool	1.0	1.376	4.906	0.4 x 0.54	2.0 x 3.0	0.5 x 1.5	Punctured	---	---	2 punctures in plate 0.15" dia
F-171	ABB	0.5750	15,200	0.063	1.0	Al wire screen	0.5" space--0.5" Al screen	0.5	1.45	5.884	0.58 x 0.6	1.0 x 1.2	0.45 x 0.7	Punctured	---	---	0.2" x 0.3" dia puncture
F-167	AAC	0.5610	17,900	0.063	3.123	Cellular Magnesium	2" space--1" Cell Mg--0.125" space	1.0	3.7	5.504	0.63	1.63	---	Punctured	Yes	---	Two small holes
F-165	ABB	0.5770	13,900	0.063	0.94	TG 15000 10#	Filled Space	0.93	0.78	5.214	0.53	1.2 x 2.0	1.0	Punctured	Yes	0.125	Barely punctured
F-168	ABB	0.5750	15,900	0.063	1.0	TG 15000 10# 4 layers 181 glass cloth	Cloth--Fiberglass (Filled Space)	1.0	1.046	5.48	0.5 x 0.56	1.75	1.0	Punctured	---	0.03	0.1" x 0.3" dia puncture
N-119	CAB	0.5710	12,500	0.063	1.5	Edge grain F. (Spacecraft)	Filled Space	1.5	1.25	5.684	0.25 x 0.4	1.5	0.5	Punctured	---	---	0.45" dia puncture
N-120	AAB	0.5714	12,500	0.063	1.5	Edge grain F. (Spacecraft)	Filled Space	1.5	1.25	5.684	0.52 x 0.56	1.5	---	Not Appreciable	No	None	10 craters in plate
N-142	CAC	0.5762	16,200	0.063	1.7	EGF 13; 6# (Spacecraft)	Filled Space	1.7	0.85	5.284	0.3 x 0.4	1.0 x 1.8	0.4 x 0.6	Punctured	---	---	
D-161	AAB	0.5690	12,900	0.063	2.25	EGF 3; 6#	Filled Space	2.25	1.125	5.56	0.45	1.5	0.7	Punctured	---	---	
F-170	BAB	0.5640	15,000	0.063	2.25	EGF 3; 6#	Filled Space	2.25	1.125	5.56	0.4 x 0.5	1.0 x 2.0	0.7 x 1.0	Punctured	---	---	3 punctures (0.35"; 0.1"; 0.1")

* Accelerated Weight. ** The System Includes the Weight of Bumper, Core, and Vehicle Hull.

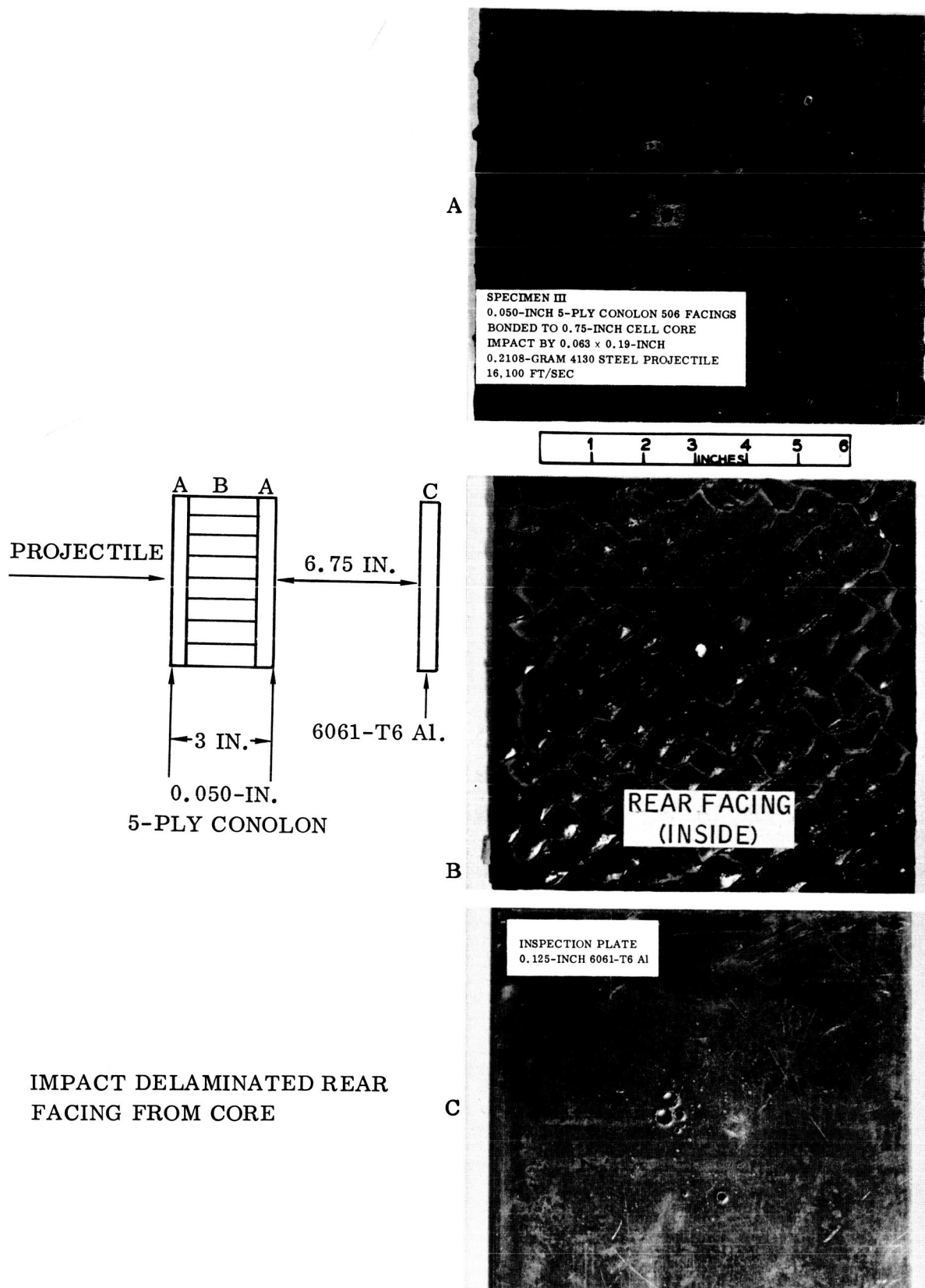


Figure 53. Honeycomb Panel No. 2

SECTION 6

PROJECTILES

6.1 DAMAGE RELATED TO PHYSICAL STATE: MASS, COMPOSITION, AND GEOMETRY

6.1.1 Physical State. Penetration dependence on impact velocity of solid aluminum [4], liquid[5], mercury, and water projectiles on 1100 and 2024 aluminum is given in Figure 54. Unfortunately, the maximum liquid-impact velocity is 2625 ft/sec. The penetration (P) damage in 2024 aluminum, at the impact velocity of 2231 ft/sec, is directly proportional to the projectile density (ρ); i. e., P/D values* of 0.101, 0.27, and 1.38, for water, aluminum, and mercury projectiles, respectively. This analogy cannot be carried out at high velocities due to the absence of any pertinent data for liquid projectiles.

6.1.2 Cylinders: Explosively Accelerated

6.1.2.1 Steel: 0.57 Gram. The behavior and damage inflicted by 0.57-gram steel projectiles has been discussed in Sections 3 and 5, and will be discussed again in Section 7.

6.1.2.2 Steel: 0.21 Gram. The behavior and damage inflicted by 0.21-gram steel projectiles to bumpered test panels and to pressurized vessels has been discussed in Sections 3 and 4, and the bumpered test panel data are summarized in Table 5.

6.1.2.3 Steel: 0.097 Gram. The behavior and damage inflicted by 0.097-gram steel projectiles to pressurized vessels has been discussed in Section 4.

6.1.2.4 Copper: 0.67 Gram. The behavior and damage inflicted by 0.67-gram copper projectiles to bumpered test panels has been discussed in Section 3 and summarized in Table 7.

6.1.3 Glass Spheres: 0.08 Gram. Spherical glass projectiles, 0.157 inch in diameter and weighing 0.075 gram, have been accelerated with a light gas gun and the data have been summarized in Table 10. Projectiles maintained their integrity during acceleration, and struck the aluminum (6061-T6) plate in vacuum. One projectile, traveling at 15,220 ft/sec, produced a crater that was nearly hemispherical; approximately 0.26 inch deep and 0.45 inch in diameter, with a 0.08-inch lip.

*Ratio: $\frac{\text{Penetration Depth}}{\text{Projectile Diameter}}$

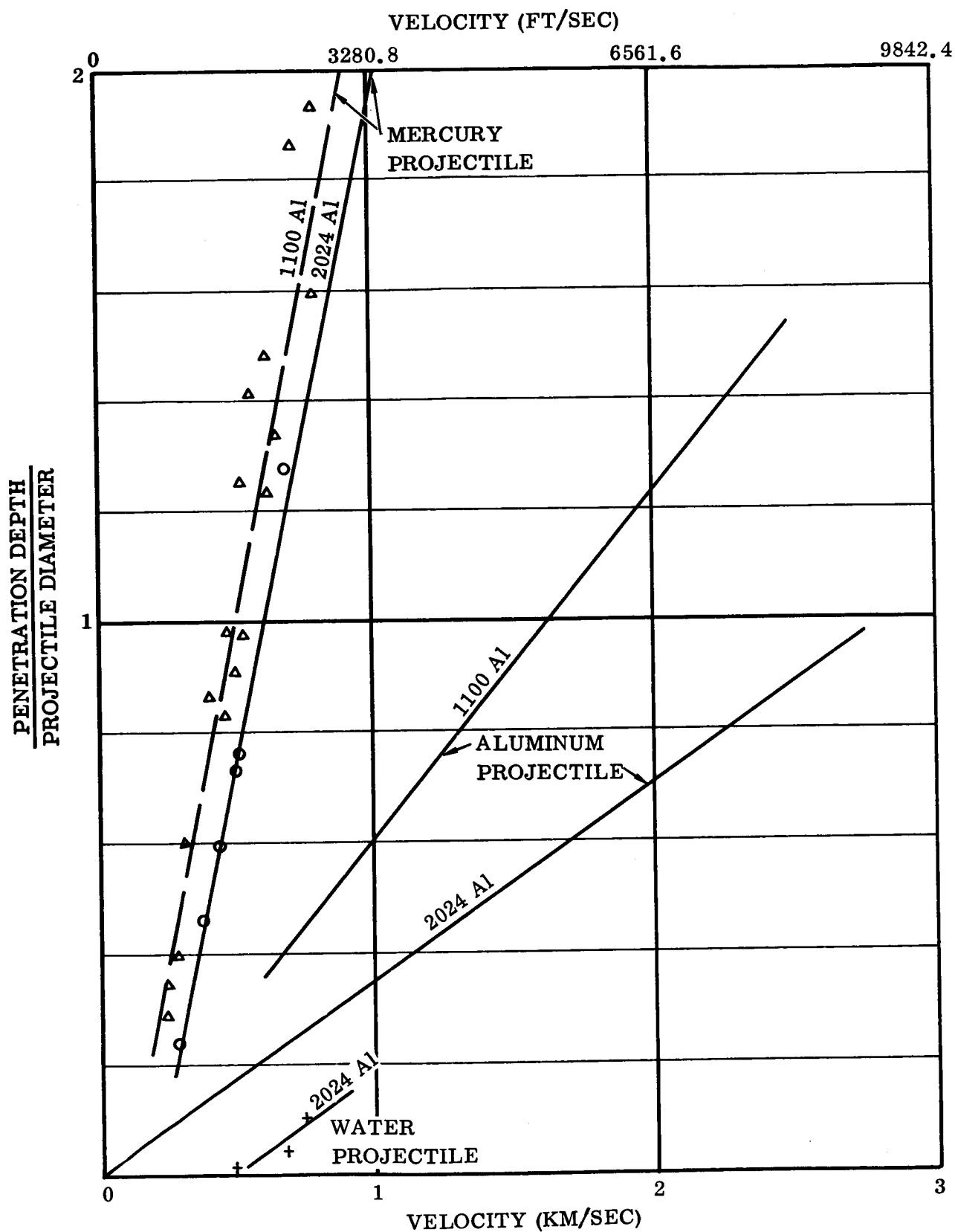


Figure 54. Penetration Dependence on Impact Velocity of Solid and Liquid Projectiles [Ref 5 and 13]

Table 10. Steel, Glass, and Nylon Projectiles (Light Gas Gun).

NO.	PROJECTILE			SYSTEM PRESSURE (MM HG)	VELOCITY (FT/SEC)	TARGET		CRATER		REMARKS
	MATERIAL	DIA (IN.)	WT * (GM)			TH (IN.)	MATERIAL	DIA (IN.)	LIP (IN.)	
27	Glass	0.157	0.08	22	3,000	0.25	6061T6	0.2	0.03	Bulge - Reverse Face 0.07" high
52	Glass	0.157	0.08	19	7,500	0.25	6061T6	0.32	0.03	
431	Glass	0.157	0.08	11	12,000	1.0	6061T6	0.4	0.07	
442	Glass	0.157	0.08	7	15,220	0.875	6061T6	0.45	0.08	
445	Glass	0.157	0.08	80	15,720	0.875	6061T6	0.42	0.07	
446	Glass	0.157	0.08	80	14,410	1.0	6061T6	0.45	0.08	Reverse Face: Scabbled - Bulge 0.45" high 1.25" dia.
447	Steel	0.125	0.12	105	14,010	0.875	6061T6	0.35 x 0.4	0.1	
438	Nylon	0.3125	0.299	7	17,800	0.875	6061T6	0.85	0.1	

*Accelerated weight is probably identical to impact weight since the particles were launched in low pressure.

April 1962

The formation of nearly hemispherical craters with impact velocities of 12,000, 14,410, 15,220, and 15,720 ft/sec have also been observed in experiments 431, 446, 442, and 445 (Figure 55), where the ratio of crater diameter to depth was observed to be 2.5, 2.05, 1.73, and 1.91, respectively. This ratio should be 2.00 for a hemispherical crater.

6.1.4 Nylon Spheres: 0.299 Gram. A spherical nylon projectile 0.3125 inch in diameter and weighing 0.299 gram*, has been accelerated to 17,800 ft/sec in vacuum with the light gas gun (Table 10). Damage to the test panel did not appear to be severe as evidenced from the wide (0.85 inch) but shallow (0.4 inch) crater, as seen in Figure 56. However, damage to the entire 0.875-inch thick aluminum test panel was more extensive than the damage observed on the front of the panel. The rear surface was bulged and cracked (Figure 56) due to the transmission of a strong compression wave produced by the impact of the projectile.

6.1.5 Accelerated Steel Spheres

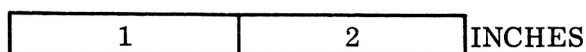
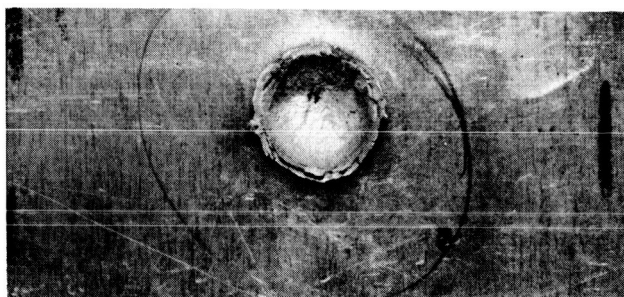
6.1.5.1 Light Gas Gun: 0.12 Gram. A spherical steel projectile, 0.125 inch in diameter and weighing 0.12 gram has been accelerated to 14,000 ft/sec in vacuum with the light gas gun (Table 10). The depth (0.38 inch) of the crater was almost equal to the diameter (0.35 by 0.40 inch). The crater can be seen in Figure 57.

6.1.5.2 Explosive Driver: 0.34 Gram. Four soft steel spherical projectiles (Table 5), 0.17 inch in diameter and weighing 0.34 gram, have been accelerated with the explosive driver. The velocity in one experiment (F-192) was 12,500 ft/sec, and the projectile produced a 0.2- by 0.25-inch diameter hole in the 0.063-inch thick aluminum bumper. This bumper was not adequate, in conjunction with the 0.187-inch thick aluminum vehicle hull and a four-inch spacing, to prevent complete penetration.

6.2 ORIENTATION AND FRAGMENTATION. In addition to the difficulties associated with the change in geometry and the loss of mass for projectiles accelerated in air (see the following section), there are orientation problems at the instant of impact. The cylindrical projectile may tilt (see Figure 7) or tumble during acceleration and flight to the test panel. Projectile orientation effects are diminished: a) when the test panel is thick and only a crater is formed; or b) if the projectile has a very high velocity. It should be observed that a projectile accelerated in air is surrounded by gas and, consequently, is in a state which does not resemble the condition of a meteoroid particle prior to or at the instant of impact on an aerospace vehicle.

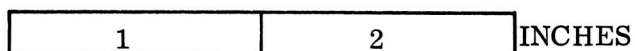
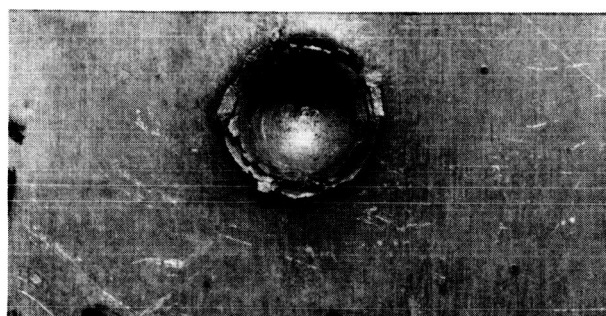
There are significant differences in the impact pattern(s) formed when the flat face (Figure 58) rather than the edge (Figure 59) of the projectile strikes the bumper. A flat-face impact will produce a circular hole. An edge impact, however, will pro-

* The accelerated and impact mass should be almost identical since the projectile was launched in vacuum.



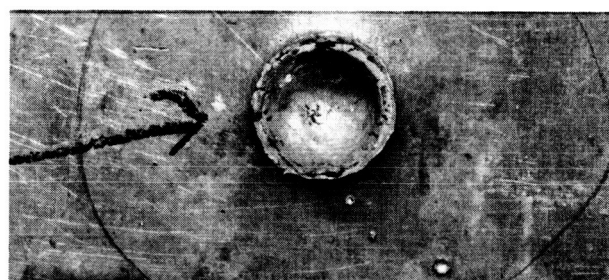
NO. 446
4-MM GLASS SPHERE (0.08 GRAM)
PRESSURE: 80-MM Hg
14,410 FT/SEC

EXPOSURE A



NO. 442
4-MM GLASS SPHERE (0.08 GRAM)
PRESSURE: 7-MM Hg
15,220 FT/SEC

EXPOSURE B

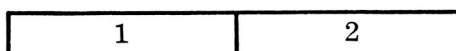
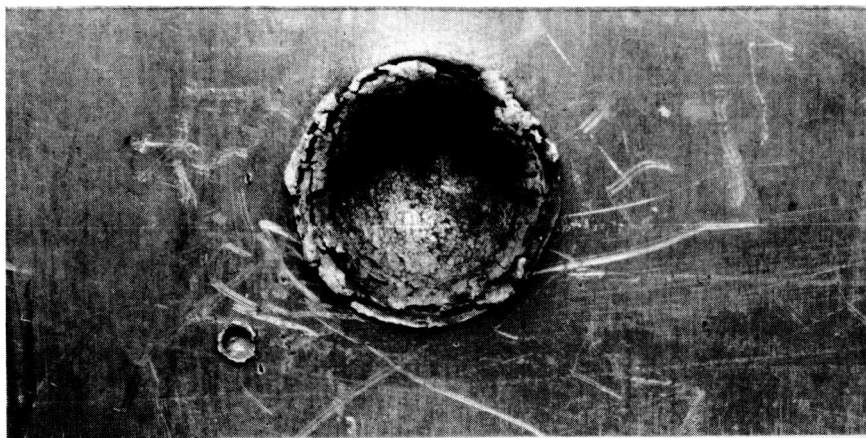


NO. 445
4-MM GLASS SPHERE (0.08 GRAM)
PRESSURE: 80-MM Hg
15,720 FT/SEC

EXPOSURE C

Figure 55. Glass Projectile Damage to Aluminum Panels

April 1962



INCHES

NO. 438

0.3125-IN. NYLON SPHERE

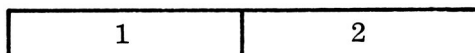
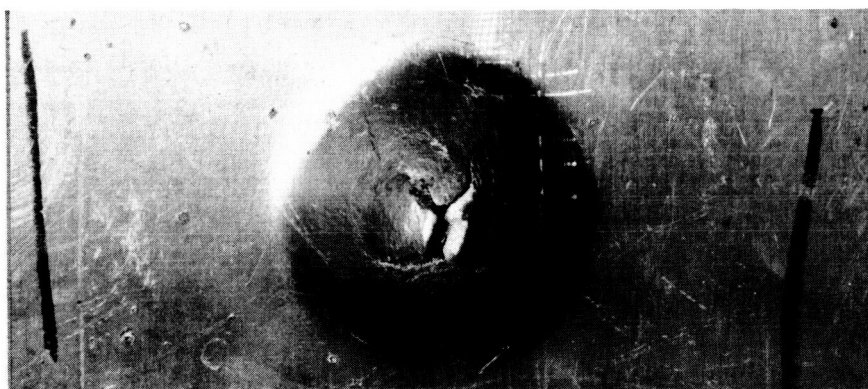
PRESSURE: 7-MM Hg

17,800 FT/SEC

VEHICLE HULL: 0.875 IN. THICK

PENETRATION DEPTH: 0.4 IN.

EXPOSURE A - FRONT



INCHES

BULGE

DIAMETER: 1.25 IN.

HEIGHT: 0.4 IN.

EXPOSURE B - REAR

Figure 56. Crater Formed in Aluminum With a Nylon Sphere



EXPERIMENT NO. 447

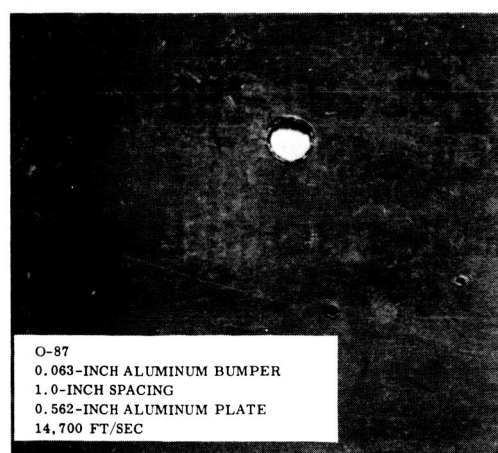
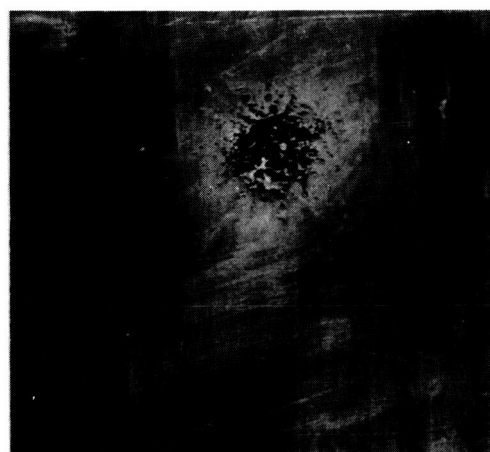
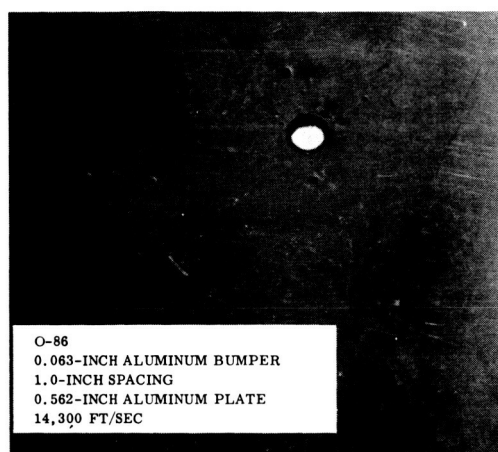
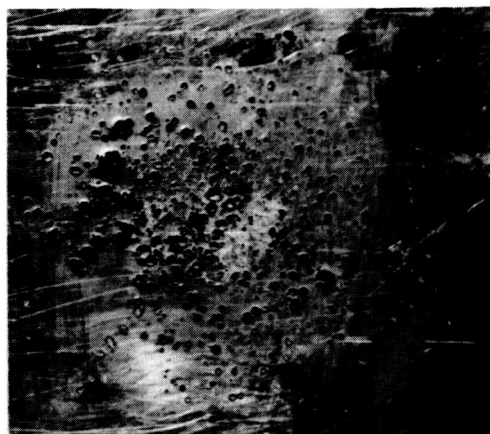
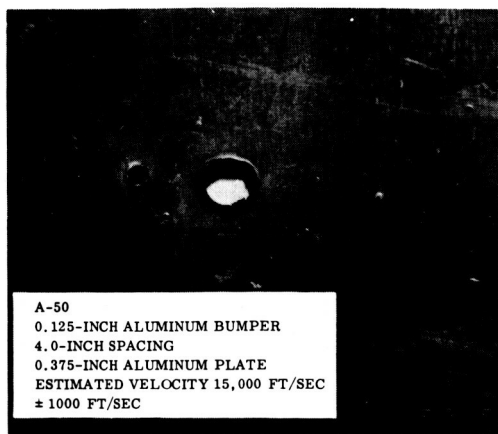
0.125-INCH STEEL SPHERE (0.12 GRAM)
PRESSURE: 105-MM Hg
14,010 FT/SEC

Figure 57. Crater Formed in Aluminum with a Steel Sphere

duce an elliptical hole in the bumper as well as an elliptical pattern of small craters in the vehicle hull. The major axis of the hole in the bumper does not coincide with the major axis of the crater pattern; i. e., the major dimension of the hole in the bumper and the crater pattern on the hull are rotated 90 degrees as seen in Figure 59. In addition, the particle distribution is not uniform, is concentrated in the central region, and results in greater penetration than observed with a flat-face impact.

Impact patterns on vehicle hulls protected by a bumper show craters which could only be produced by discrete particles. In a preliminary attempt to ascertain the fate of the steel projectile and the aluminum shear plug, an 0.57-gram projectile was fired through an 0.090-inch bumper. A block of paraffin was placed behind the aluminum plate. Three magnetic fragments were recovered (0.0341, 0.0253, and 0.0113 gram) as well as a quantity of gray magnetic paraffin. Microscopic examination of these three particles showed that melting occurred on one surface with jagged fracture on the opposite surface. These fragments evidently were from the perimeter of the projectile.

6.3 RECOVERY AFTER ACCELERATION. The original mass of the projectile is not accelerated intact with the explosive technique. There is a loss of material around the perimeter of the projectile due to aerodynamic effects, so that the accelerated or original mass of the projectile cannot be used in computing its striking momentum and energy. This mass loss, which varies with the explosive charge design, is apparently constant for a given charge design and experimental arrangement.



BUMPER PLATES

HULL PLATES

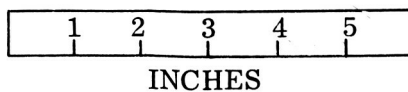
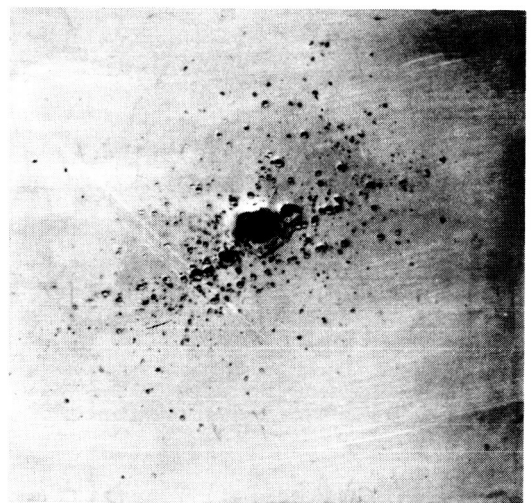
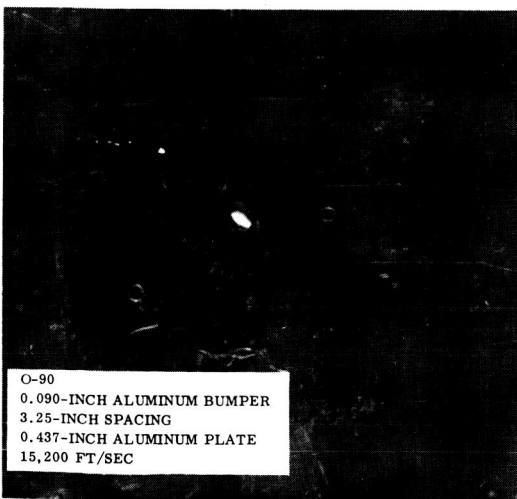
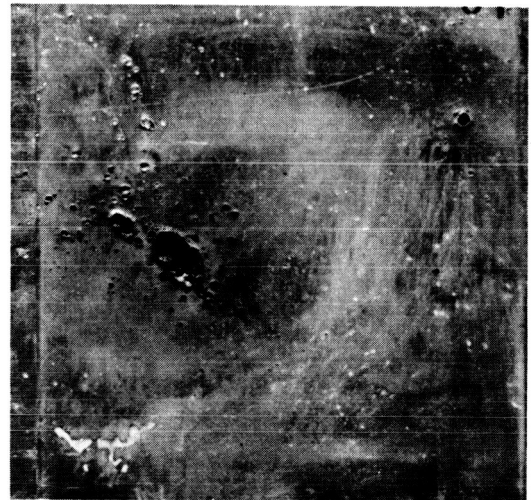
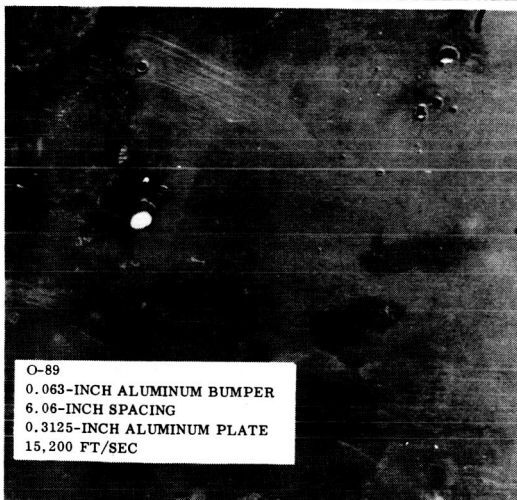
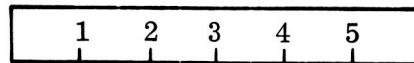
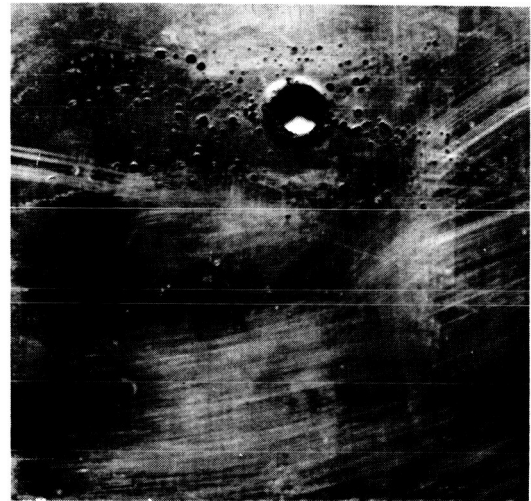
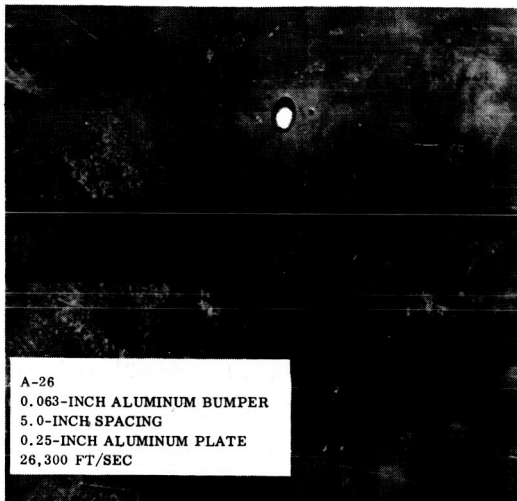


Figure 58. Fragmentation Behavior on Flat-Face Impact



BUMPER PLATES

HULL PLATES

Figure 59. Fragmentation Behavior on Edge Impact

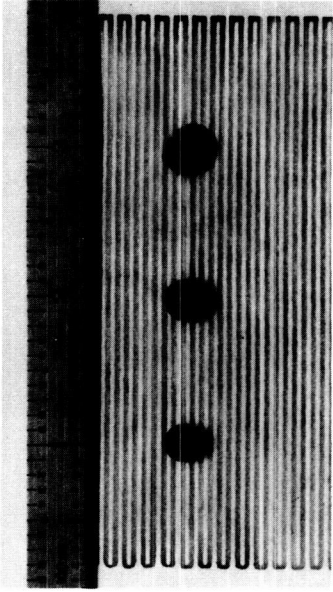
April 1962

To experimentally determine the actual projectile mass which strikes the test panel, several projectiles were accelerated into a projectile recovery material placed in the same position as the test panels (see Section 2) with the arrangement shown in Figure 60. This projectile recovery material consisted of eight inches of shaving cream positioned in front of two cakes of paraffin.

The projectile in experiment 221, 0.094 inch thick by 0.250 inch in diameter, and weighing 0.5628 gram, was accelerated to 9100 ft/sec. This projectile (Figure 60) was recovered intact after penetrating 1-1/2 inches into the first block of paraffin. The leading surface had 4 of the silver grid paper marks embossed in the steel. Also, the largest diameter (0.293 inch) appeared at the leading surface with the rear edge belled inward. This recovered projectile weighed 0.5506 gram which results in a 2.2 percent weight loss.

In Experiment 227 the 0.5760-gram projectile was accelerated to 12,960 ft/sec. This projectile was recovered intact and weighed 0.4538 gram (21.2 percent loss), was 0.048 inch thick and 0.35 inch in diameter (Figure 60). The leading edge was curved and the edges were colored blue from oxidation.

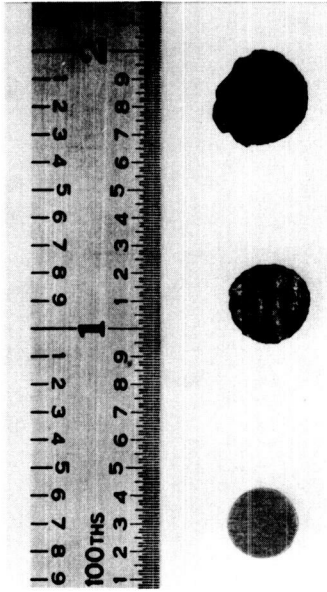
NOTE: PROJECTILES ARE NUMBERED
1 THROUGH 3 FROM LEFT TO
RIGHT IN ALL PHOTOGRAPHS



UNFIRED PROJECTILE:
(PROJECTILE NO. 1)

THICKNESS: 0.094 INCH
DIAMETER: 0.250 INCH
MASS: 0.570 GRAM

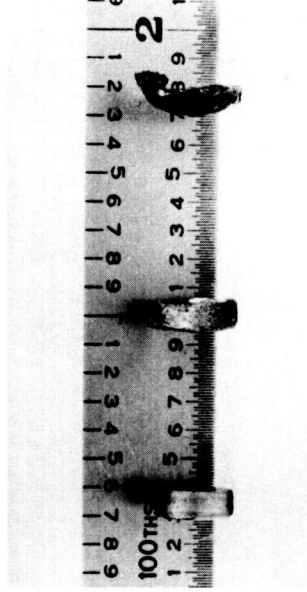
PROJECTILES PHOTOGRAPHED ON
SHEET OF PRINTED CIRCUIT PAPER.
NOTE PICKUP OF SILVER PARTICLES
ON PROJECTILES NO. 2 AND 3.



EXPERIMENT NO. 221:
(PROJECTILE NO. 2)

THICKNESS: 0.111 INCH
DIAMETER: 0.293 INCH
MASS: 0.5628 GRAM, INITIAL
0.5506 GRAM, FINAL

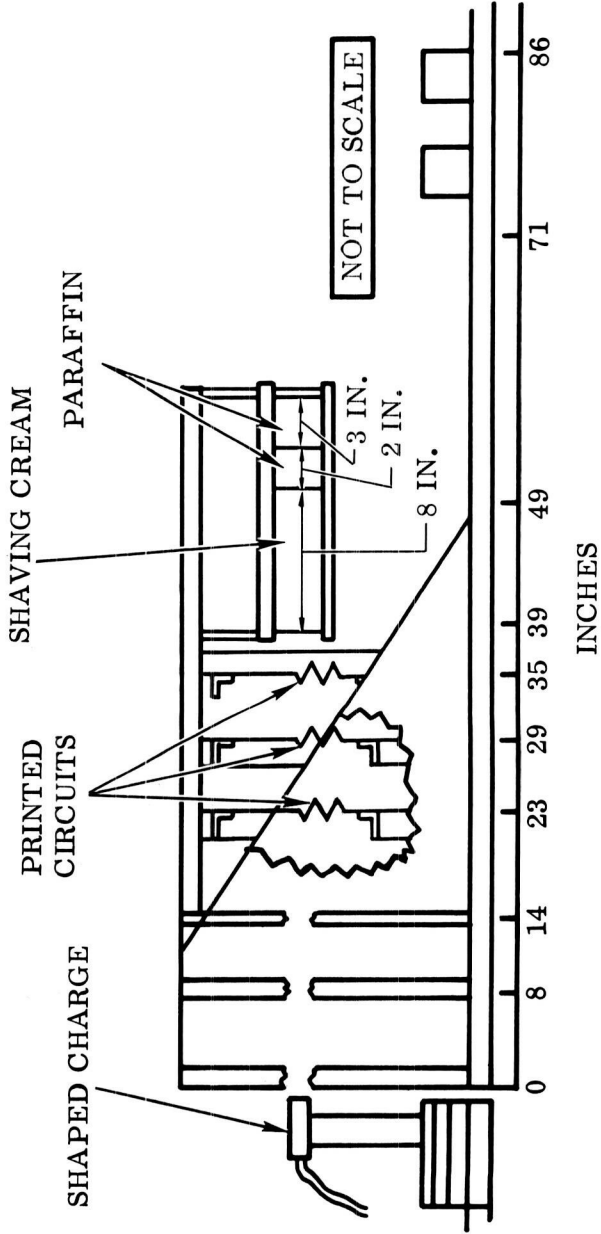
PROJECTILES PHOTOGRAPHED
AGAINST PLAIN BACKGROUND TO
SHOW DETAILS OF CONFIGURATION
AND PHYSICAL DIMENSIONS.



EXPERIMENT NO. 227:
(PROJECTILE NO. 3)

THICKNESS: 0.048 INCH
DIAMETER: 0.35 INCH
VELOCITY: 12,960 FT/SEC
MASS: 0.5760 GRAM, INITIAL
0.4538 GRAM, FINAL

PROJECTILES PHOTOGRAPHED IN
VERTICAL POSITION TO SHOW
DETAILS OF CONFIGURATION
AND PHYSICAL DIMENSIONS.



RANGE SCHEMATIC FOR PROJECTILE RECOVERY

Figure 60. Shooting Arrangement, Projectile Data, and Projectile Photos

SECTION 7

HOLE DIAMETER IN METAL PLATES

The diameter of the holes in the aluminum (2024-T3 unless designated as 6061-T6), titanium (75-A), magnesium (HK-31A), and full hard 301 stainless steel surfaces struck by the 0.57-gram high velocity steel projectile are given as a function of impact velocity in Figures 61 through 65. Over the very narrow velocity range considered, and near to the normal sonic velocity of about 16,500 ft/sec for these four metals, the hole diameter for a particular thickness appears to be linear and independent of impact velocity. It should be observed, also, that the distance between the projectile and hull plate in the initial experiments was 84 inches for HK-31A, 2024-T3 aluminum, titanium, and 40 inches in the last group of experiments with aluminum 6061-T6, LA-141, and 301 stainless steel.

The data summarized in Figures 66 and 67 were obtained with 0.21-gram and 0.097-gram cylindrical steel projectiles that were explosively accelerated. These data on thin panels of pressurized cylinders are not adequate to permit a statistical evaluation and are not precise enough to warrant further conclusions.

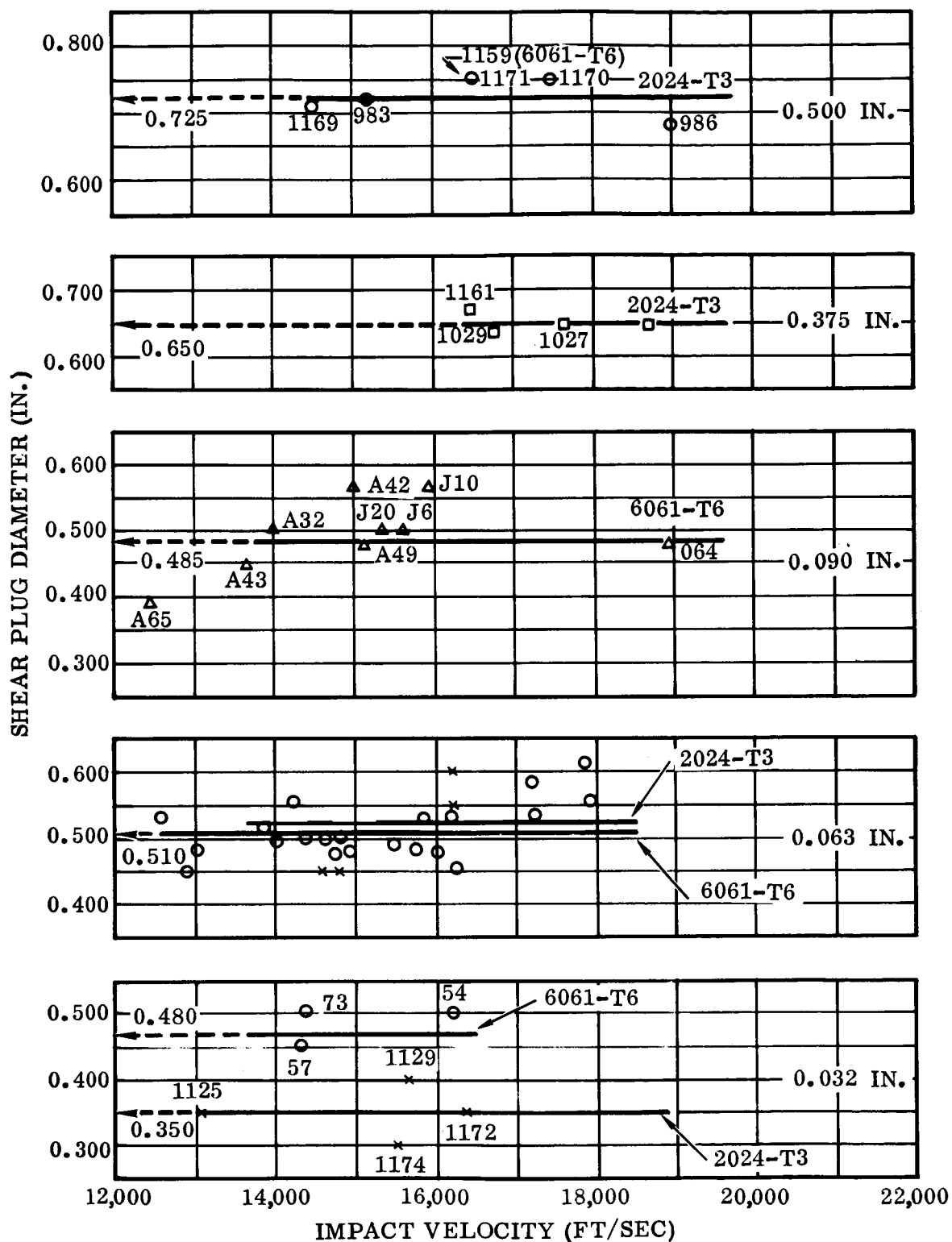


Figure 61. Shear Plug Diameter Dependence on Impact Velocity
(0.57-Gram Steel Projectile and Aluminum Plate)

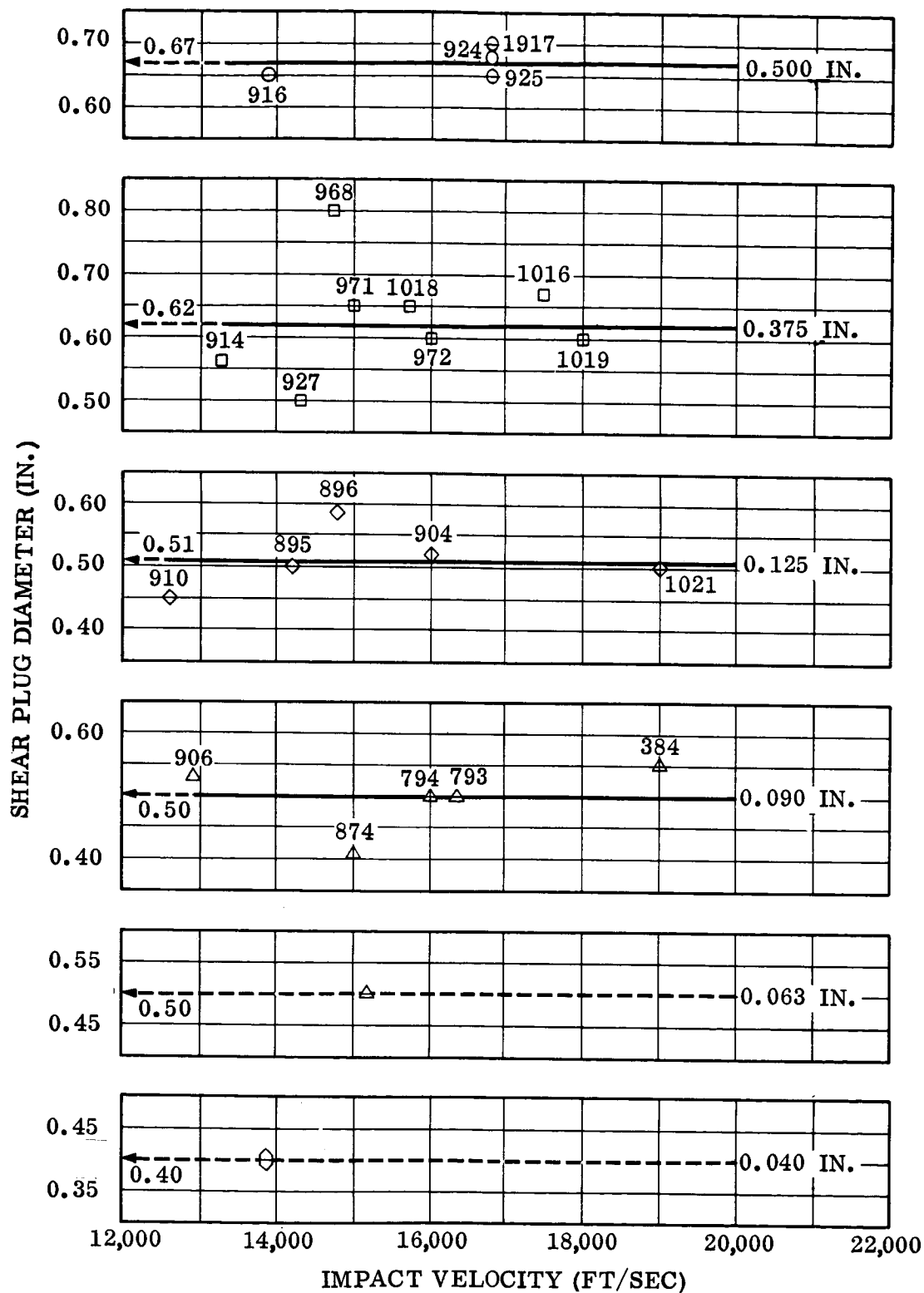


Figure 62. Shear Plug Diameter Dependence on Impact Velocity
(0.57-Gram Steel Projectile and Titanium Plate)

April 1962

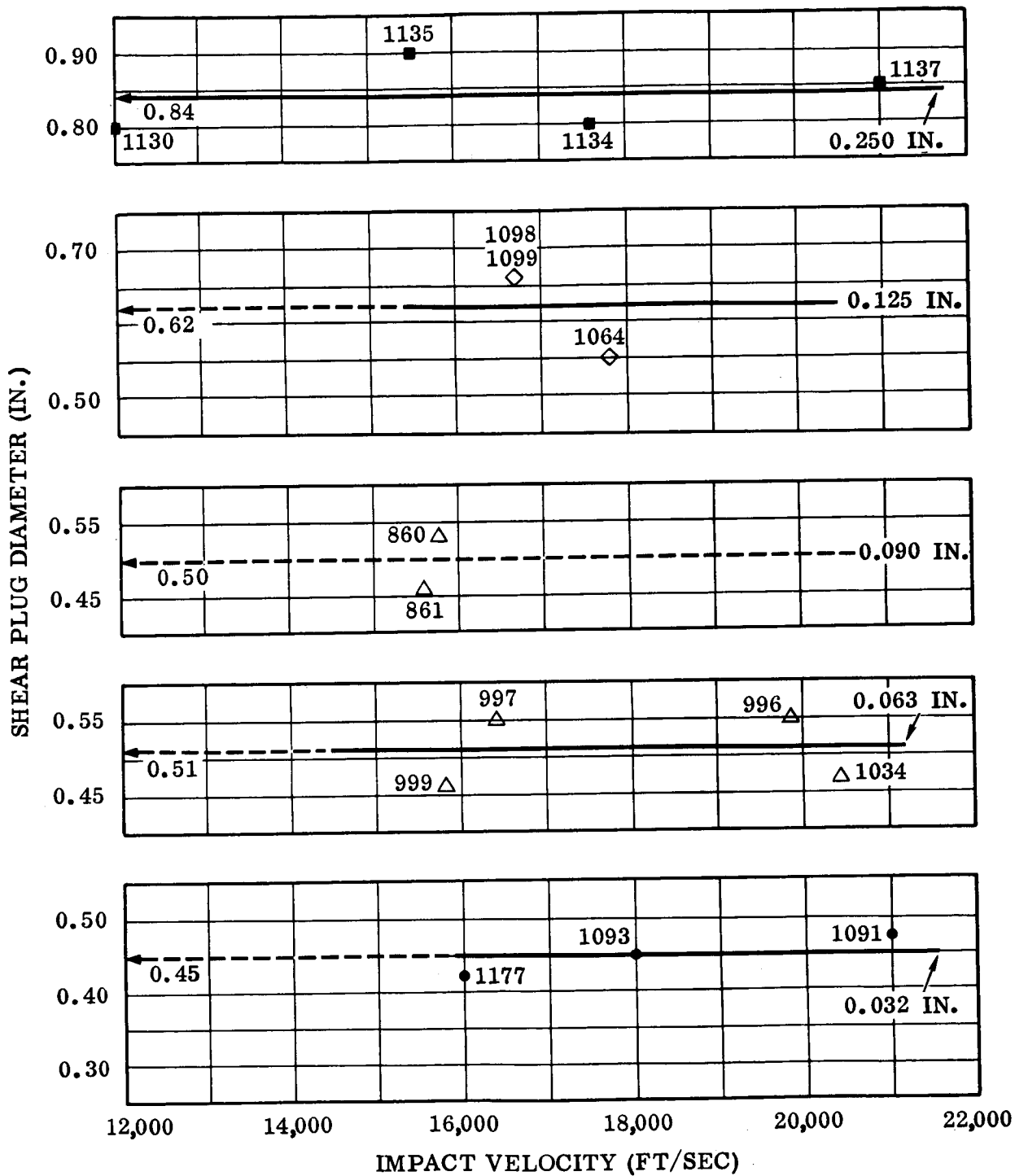


Figure 63. Shear Plug Diameter Dependence on Impact Velocity
(0.57-Gram Steel Projectile and Magnesium HK-31A Plate)

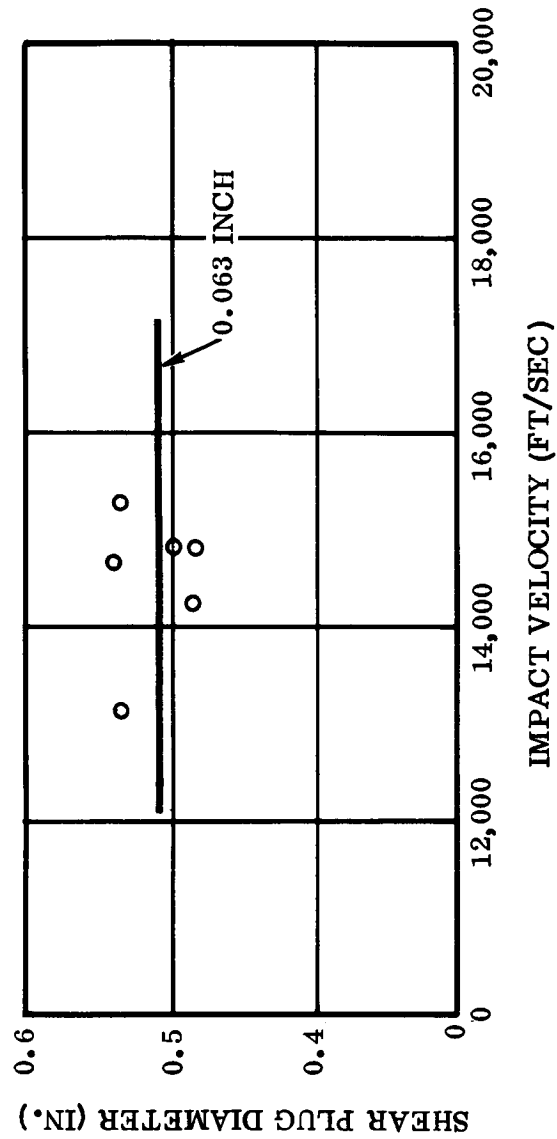


Figure 64. Shear Plug Diameter Dependence on Impact Velocity (0.57-Gram Steel Projectile and 301 Full-Hard Stainless Steel Plate)

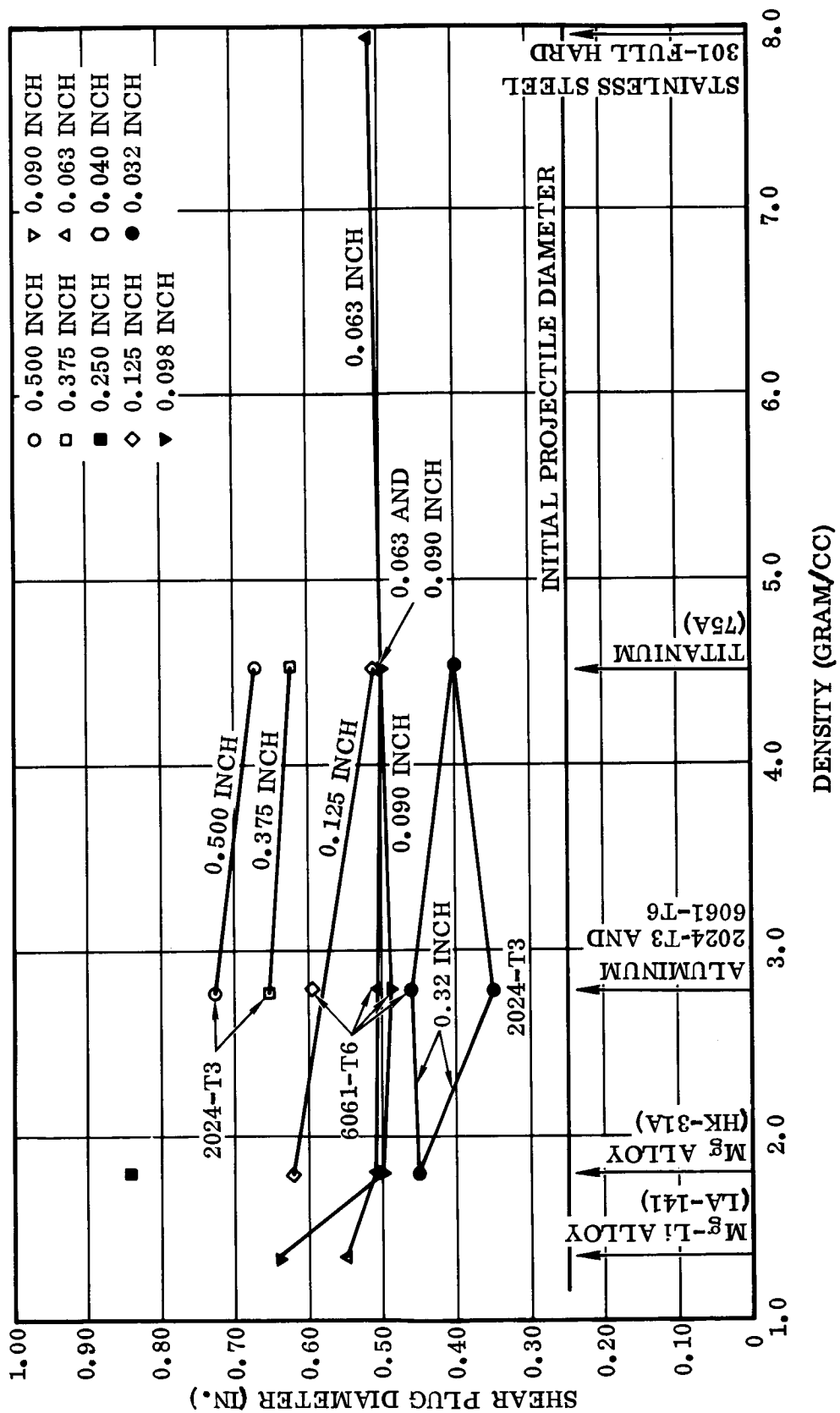


Figure 65. Shear Plug Diameter Dependence on Density (0.57 -Gram Projectile)

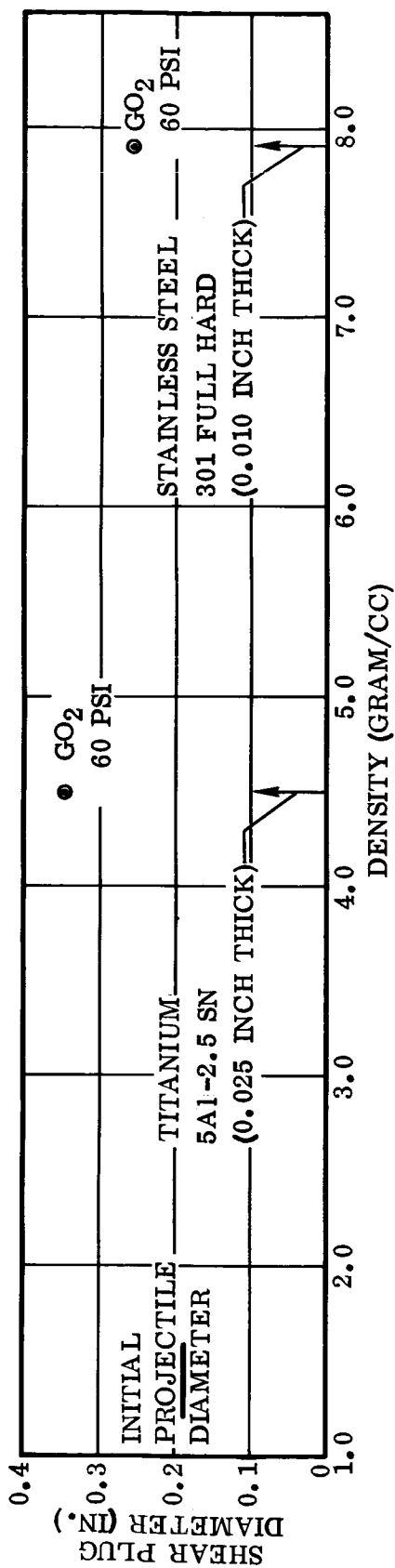


Figure 66. Shear Plug Diameter Dependence on Density (0.21-Gram Projectile)

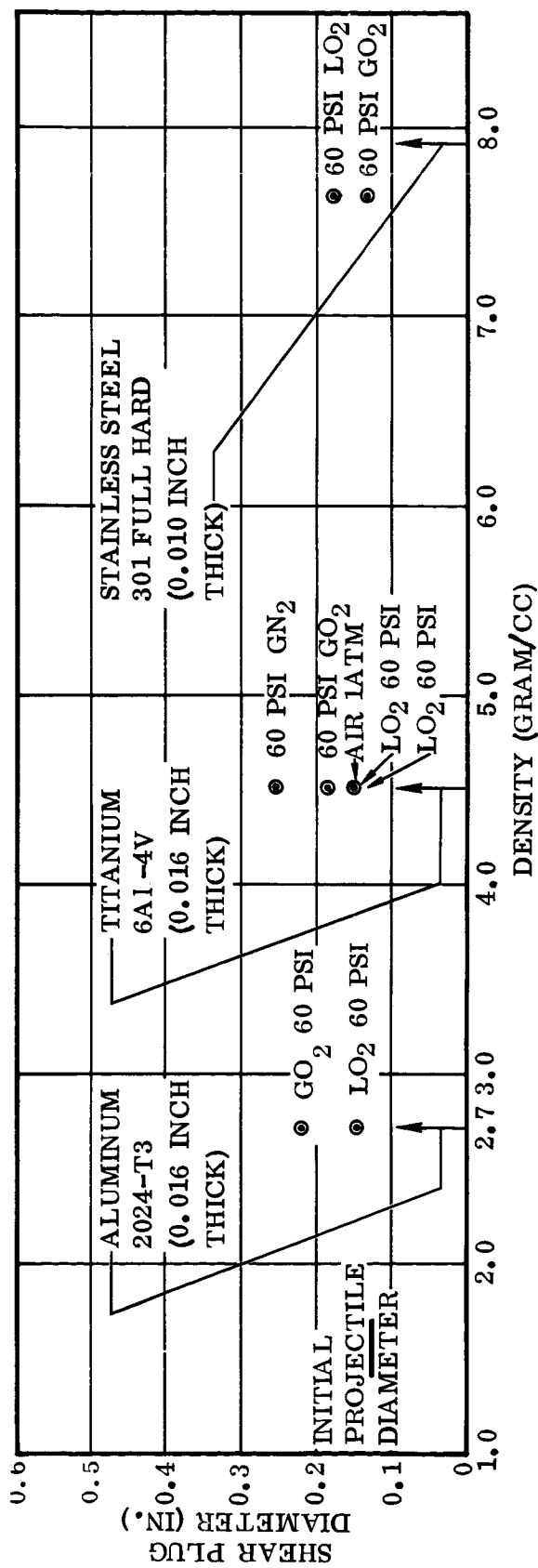


Figure 67. Shear Plug Diameter Dependence on Density (0.097-Gram Projectile)

SECTION 8

PHOTOGRAPHIC ANALYSIS OF IMPACT PHENOMENA

8.1 LOW SPEED PHOTOGRAPHS. The calibre .30-06 projectile, with a velocity of 3030 ft/sec, penetrated the 0.125-inch and the 0.250-inch aluminum (6061-T6) plates spaced four inches apart (Figure 68). The diameter of the holes in the first and second plates are 0.3 and 0.35 inch, respectively, and can be compared to the initial projectile diameter of 0.3 inch. The grooves in the wall of the hole in the first plate correspond to the rifling on the projectile. Photographs of the impact were taken at the rate of 2886 frames-per-second (Figure 69). Frame No. 1 shows the bullet and shear plug fragments passing through the first plate. Frame No. 2 shows: a) the spray of particles moving away from the front surface of the first plate at an angle of approximately 42°; and b) the impact flash and the bullet with the shear plug fragments moving through the second plate; and c) the lip formed on both faces of the first plate. It should be noted from Figure 68 that the second plate was struck with numerous small fragments as well as the projectile.

Sequence photographs of the behavior of pressurized (60-psi liquid oxygen) tanks when subjected to impact from a high velocity particle are given in Figure 47. These photographs were taken with a 70mm Hulcher camera at the rate of 25 frames-per-second and show the jet of oxygen escaping from the punctures produced in the rear diaphragm of the pressurized aluminum (2024-T3) structure.

8.2 MODERATE SPEED PHOTOGRAPHS. The flash resulting from the impact of the 0.55 gram, 15,800 ft/sec projectile on four spaced plates is given in Figure 70. Plates 1 and 3 were magnesium HK-31A, and plates 2 and 4 were aluminum 2024-T3. The luminosity produced is above the bright sunshine which appears as the black background. The four plates were completely penetrated. The extent of damage to each plate can be summarized as follows:

- a. Plate 1: Two holes; 0.58- and 0.18-inch diameter.
- b. Plate 2: Four-inch diameter of small perforations.
- c. Plate 3: Six-inch diameter of small craters and a 1.5-inch diameter of perforations.
- d. Plate 4: Four-inch diameter of small craters and a 2.5-inch diameter of perforations.

It can be seen that the impact flash at the surface of a plate is considerably greater in volume than at the exit side. For example, the size of the flash at the front of plate 2 is greater than at the reverse side and the same phenomena occurs at the opposite faces of plates 3 and 4. This can be attributed to the fact that the flash at

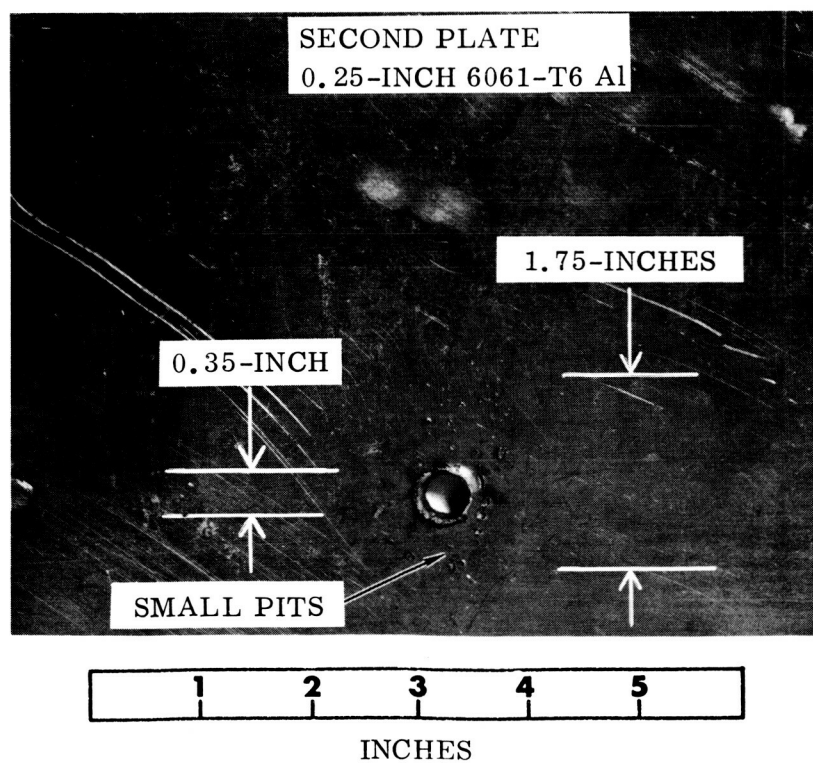
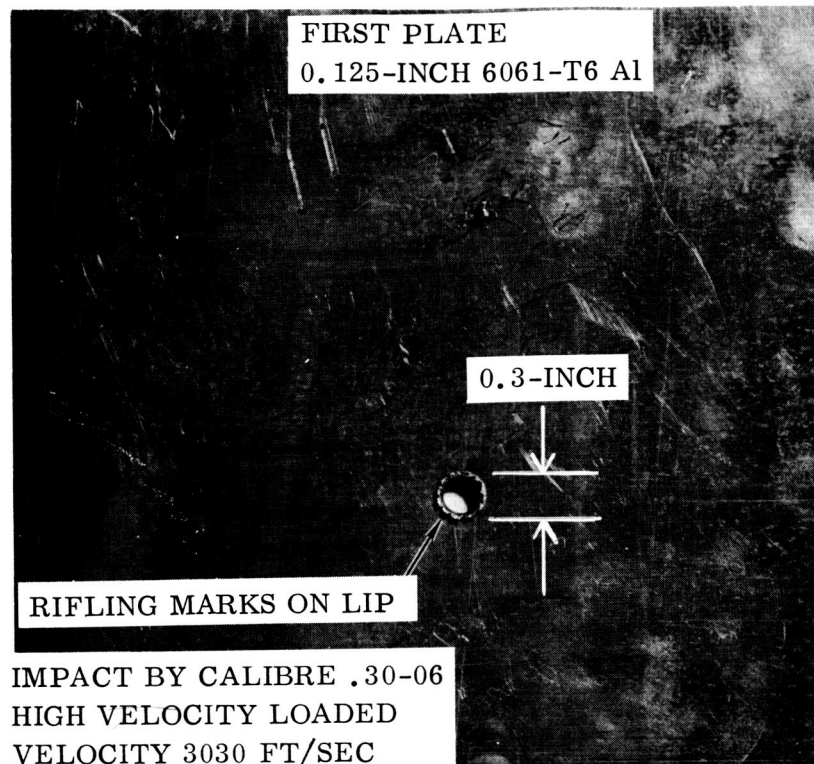


Figure 68. Damage to Aluminum Plates by a Calibre .30-06 Bullet

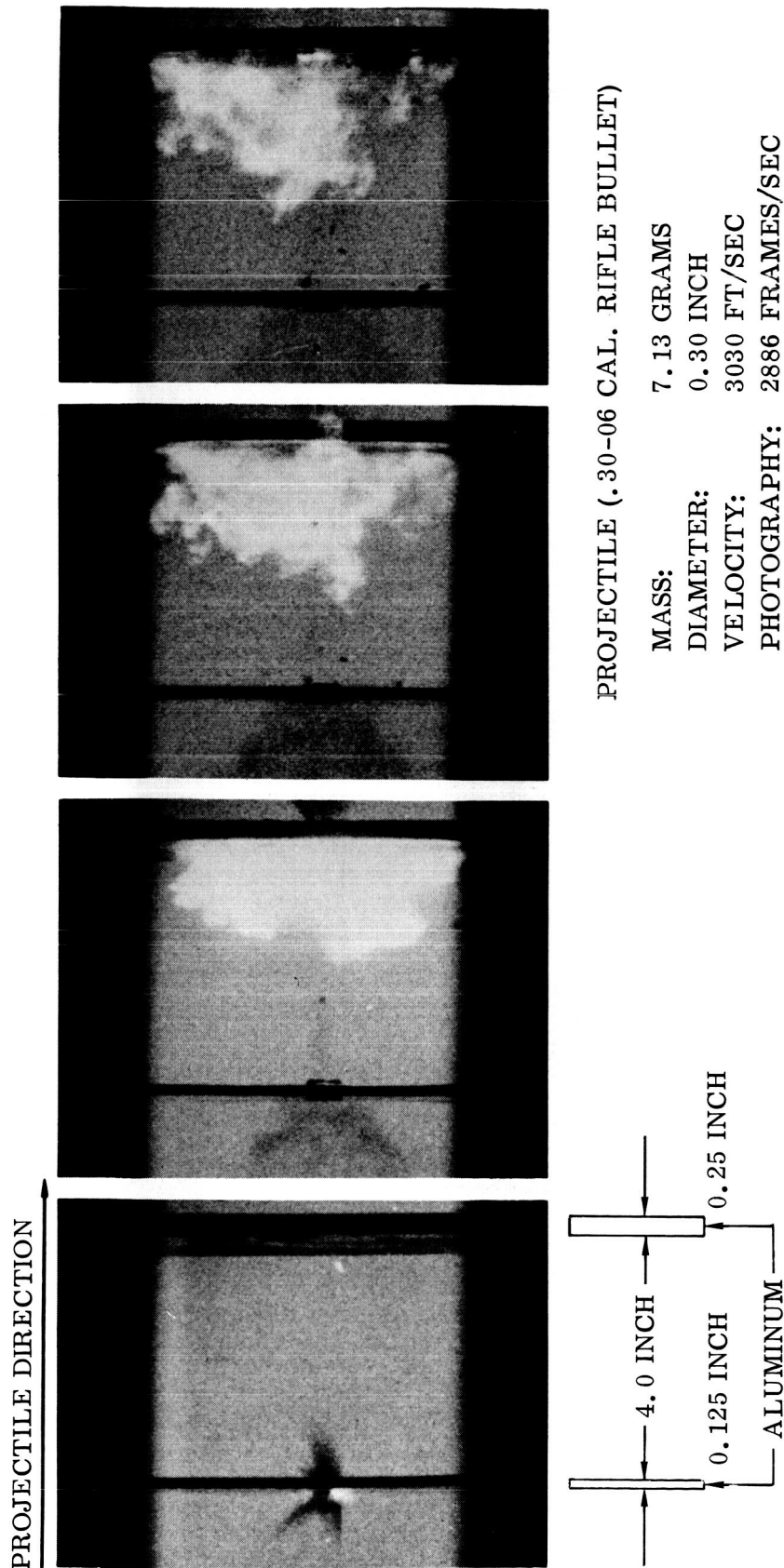


Figure 69. Slow Speed Impact Photographs

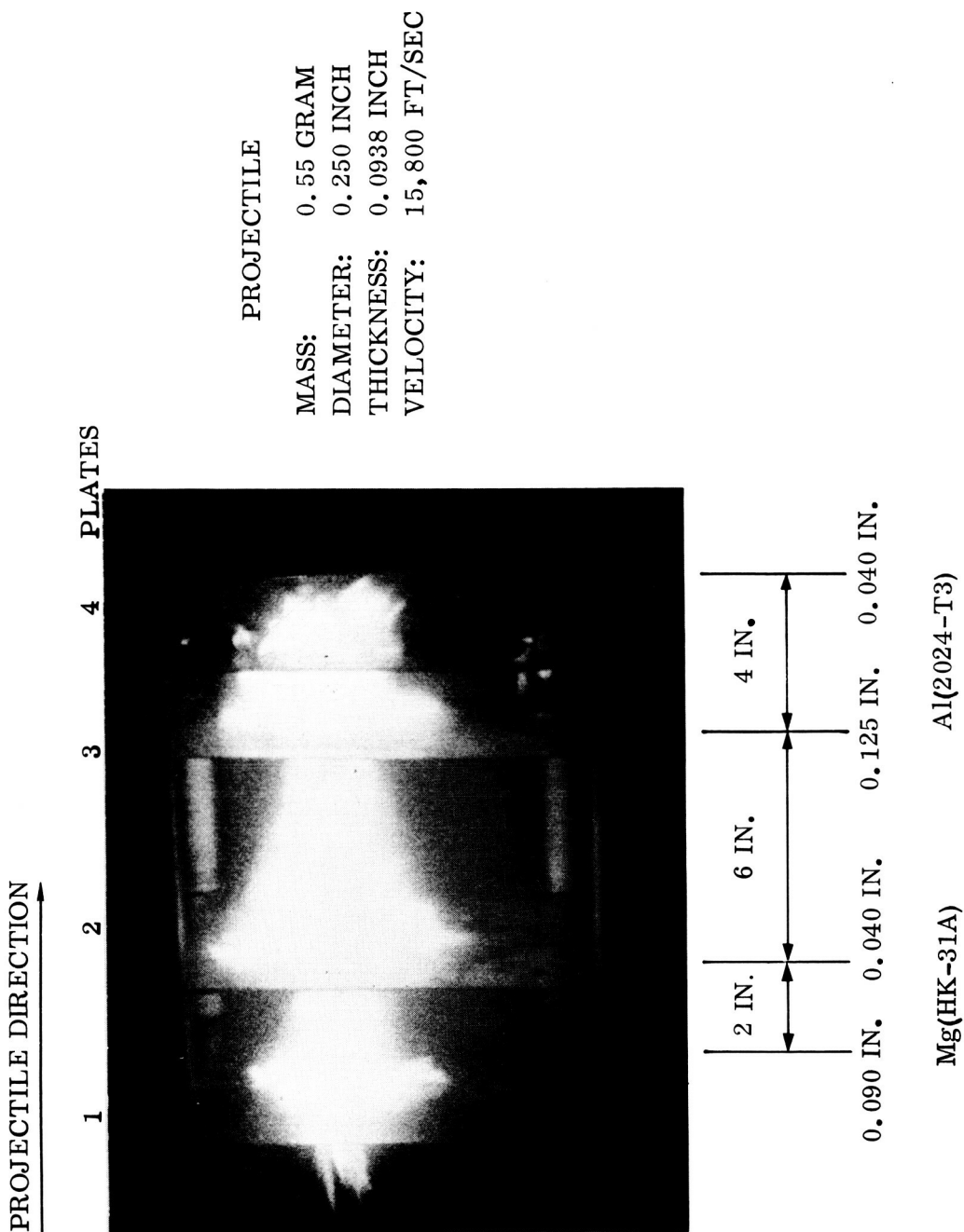


Figure 70. Impact Flash

the front of the plate is produced by the impact of many particles, and that not all particles penetrate the plate. The flash at the reverse side of the plate is produced by the particles which have penetrated the plate as well as those particles produced from the shear plug and via spallation. Some of the projectile and shear plug particles continue on a straight line trajectory, while some of the shear plug and spall material leaves the rear of the plate at an angle; this generates the luminous cone that is observed.

8.3 HIGH SPEED PHOTOGRAPHS. High speed photographs of the impact phenomena were taken after fixed periods of lapsed time with the Beckman and Whitley, Model 326, Dynafax camera. Two different, but representative, photographic sequences are shown in Figures 71 and 73.

The photographs shown in Figure 71 were taken at 26,500 frames-per-second (± 1000 frames-per-second). The impact velocity of the 0.58-gram projectile on the test panel was 9700 ft/sec. Three aluminum plates comprised this panel; the first two plates were 0.125 inch thick and spaced three inches apart, while plate 3 was 0.250 inch thick and placed one inch from plate 2.

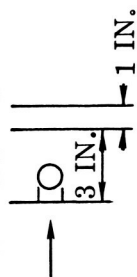
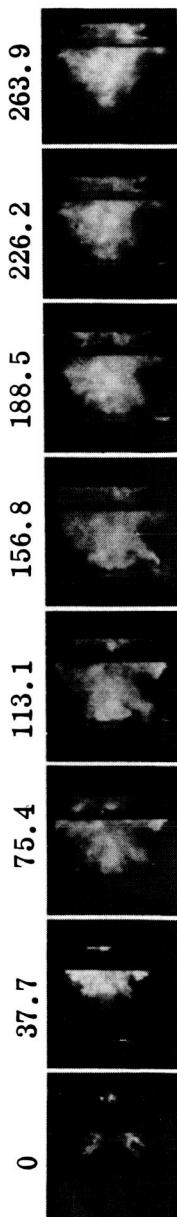
The projectile maintained its integrity (or if fragmentation did occur, the particles were fairly close together) on acceleration, as evidenced from the uniform impact flash (Frame 1 of Figure 71), and inspection of the front surface of the first bumper plate (Figure 72). The dimensions of the hole or shear plug varied from 0.329 to 0.422 inch. The ball of material (projectile plus shear plug), as seen in Frame 1 of Figure 71, was about 0.704 inch, which is almost twice the diameter of the hole. Thus, it can be deduced that either the projectile punched a hole in the bumper that was originally larger and there is rebound* in the bumper material as the elastic stresses in the main body of the bumper relax, that luminosity increases the image size, or that the ball of fragmentary material is increasing its volume. Although there is a luminosity effect, the latter deduction appears to be the most feasible, especially since the impact flash is spread over a 3.63-inch diameter circle (Figure 71) and the small craters and pit-marks over a 4.5-to 4.75-inch diameter circle of the second plate. These craters and pit marks are probably formed from the particles disrupted from the first plate. The main hole (0.47 inch) in the second plate was probably formed from particles of the original projectile, since the impact velocity (9700 ft/sec) was too low to completely fragment and disperse the particles of the incident projectile. Material passing through the second plate impinged on and cracked, but did not completely penetrate, the third plate.

The photographs shown in Figure 73 were taken at 25,800 frames-per-second (± 1000 frames-per-second). The impact velocity of the 0.57-gram projectile on the test panel was 28,600 ft/sec. Four aluminum plates, each 0.125 inch thick, with the

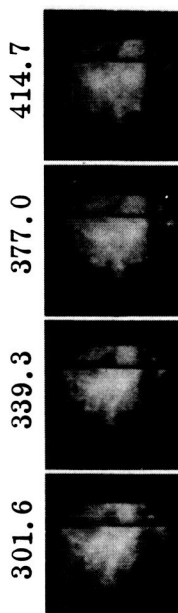
*Rebound may account for about 10 to 20 percent.

EXPERIMENT NO. 155

MICROSECONDS



MICROSECONDS

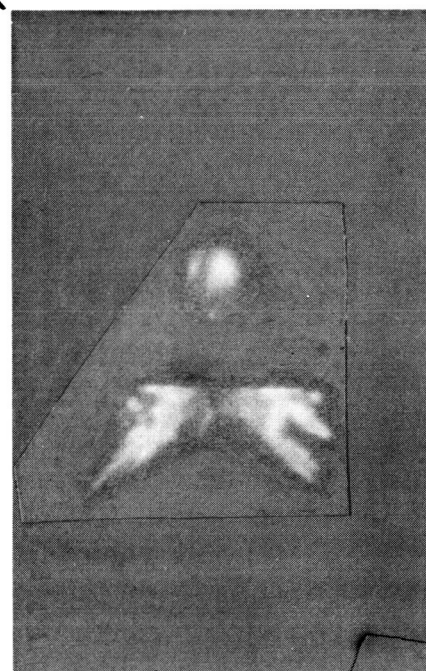
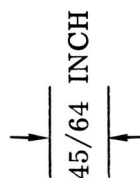


PROJECTILE

MASS: 0.5755 GRAM
SIZE: 0.094×0.25 INCH
VELOCITY: 9,700 FT/SEC
PHOTOGRAPHY: 26,500 FRAMES/SEC
DARK TIME: 36.7 ± 2.8 MICROSECONDS
EXPOSURE TIME: 1.0 MICROSECOND

TWO 6061-T6 ALUMINUM PLATES
EACH 0.125 INCH THICK AND THE
THIRD PLATE 0.250 INCH THICK

NOTE
SPHERE
OF SHEAR
PLUG
MATERIAL



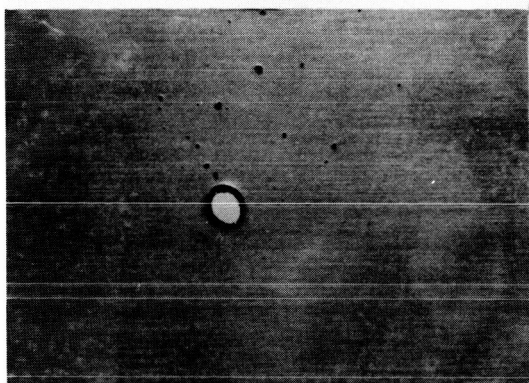
ENLARGEMENT OF FRAME 1



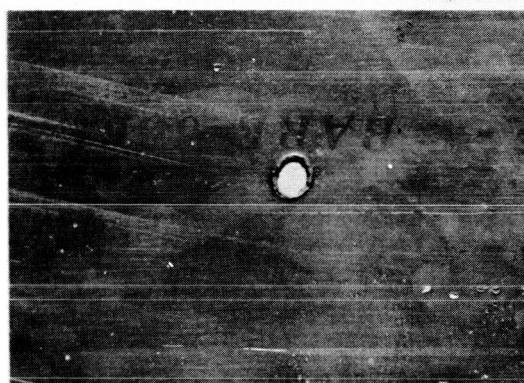
PLATE 1 PLATE 2 PLATE 3

ENLARGEMENT OF FRAME 2

Figure 71. Dynafax Photograph of Impact Phenomena Associated With Intermediate Speed Projectile



FIRST PLATE FRONT



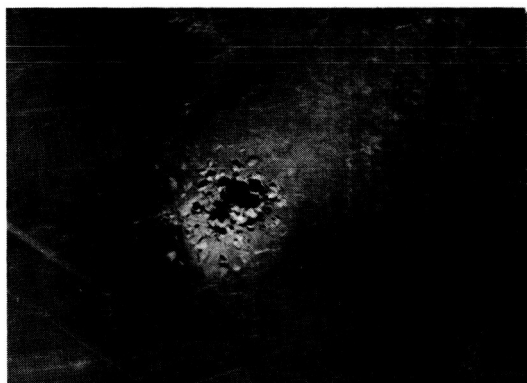
FIRST PLATE REAR



SECOND PLATE FRONT
SPACING 3 INCHES



SECOND PLATE REAR
SPACING 3 INCHES



THIRD PLATE FRONT
SPACING 1 INCH



THIRD PLATE REAR
SPACING 1 INCH

D-155
BUMPER AND TARGET(S) 6061-T6 AL.
PROJECTILE (4130 STEEL)

VELOCITY 9700 FT/SEC
MASS, 0.5955 GRAM
PLATE THICKNESS 0.125 INCH

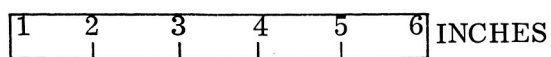
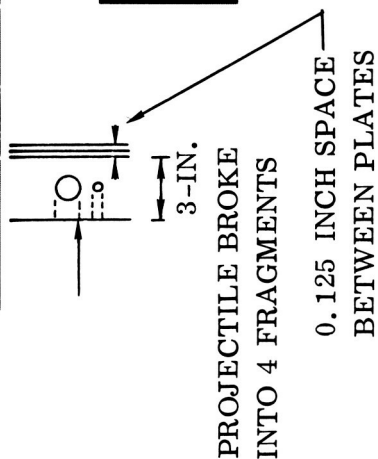
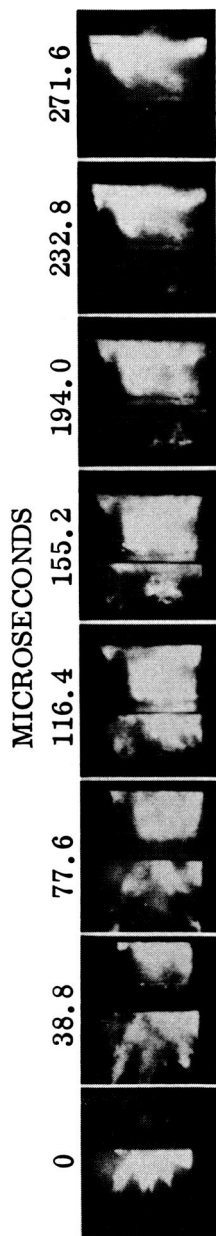


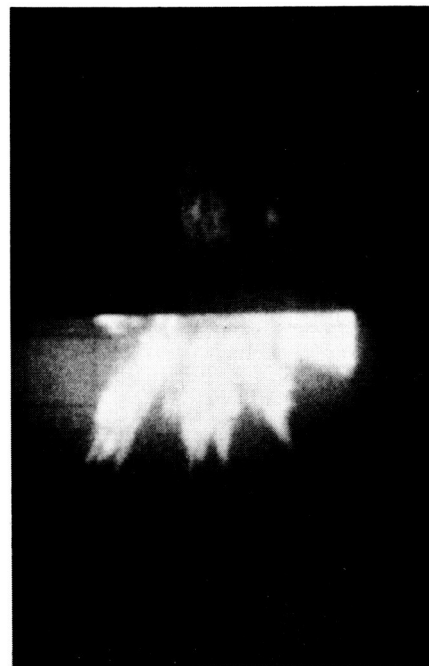
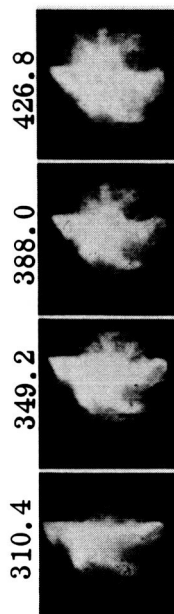
Figure 72. Aluminum Plates Used in Experiment D-155

EXPERIMENT NO. 157

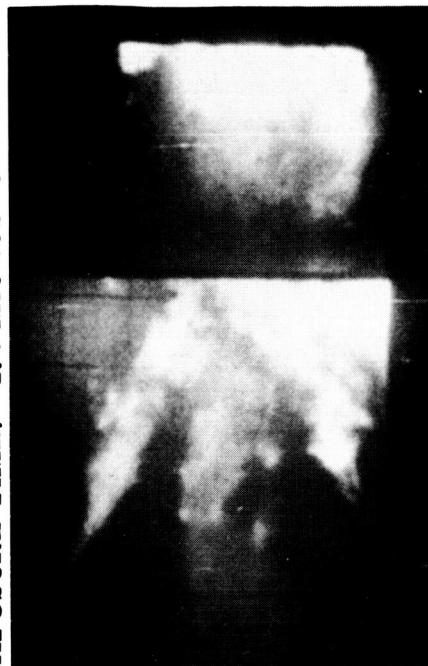


PROJECTILE:

MASS: 0.5714 GRAM
SIZE: 0.094 × 0.25 INCH
VELOCITY: 28,600 FT/SEC
PHOTOGRAPHY: 25,800 FRAMES/SEC
DARK TIME: 37.8 ± 3.0 MICROSECONDS
EXPOSURE TIME: 1.0 MICROSECOND



ENLARGEMENT OF FRAME 1
(GRIDS ARE SPACED ONE INCH APART)

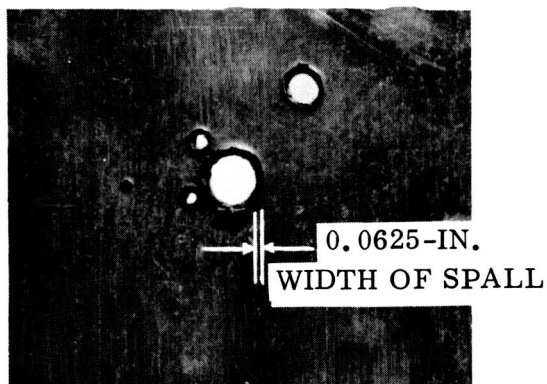


ENLARGEMENT OF FRAME 2

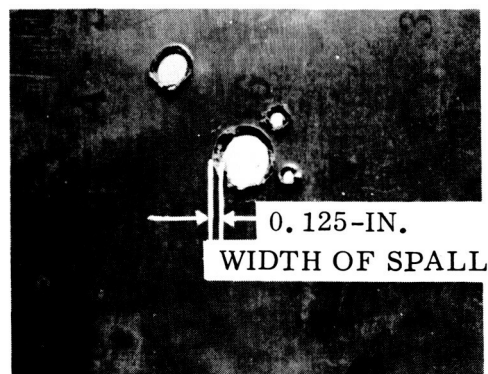
Figure 73. Dynafax Photograph of the Impact Phenomena Associated With a High Speed Projectile

April 1962

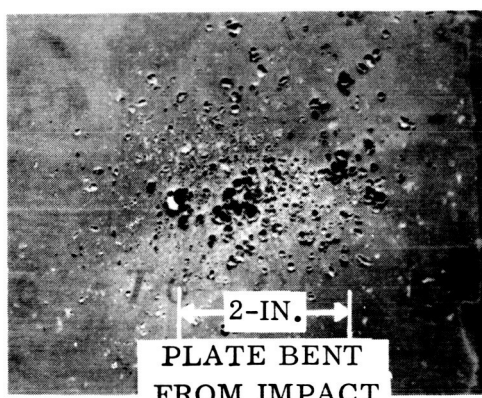
spacing indicated were used to form the test panel. The projectile broke into five fragments on acceleration as evidenced from inspection of the bumper plate (Figure 73). Four of these fragments penetrated the bumper; three of them very close together. These three fragments formed the large (one inch wide) cloud of material that can be seen between the bumper and Plate 2 in Frame 1 of Figure 73. The second cloud (0.44 inch wide) of material, directly below the large cloud, resulted from penetration of the bumper by the fourth projectile fragment. The incident particle velocity was sufficiently high to completely disrupt the integrity of the projectile particles so that the cloud of fragments was dispersed over a large area of the second plate. In fact, the momentum per-unit-impact-area was so low that the 0.125-inch plate was bent, and only three small holes were formed in the second plate. Two of these holes barely penetrated the second plate and produced small nicks on the surface of the third plate. The third hole in Plate 2 was produced with a fragment that formed a crater, but did not penetrate the third plate. The bottom of the crater in the third plate was pressed into the front surface of the fourth plate and produced the small indentation seen in the appropriate photograph of Figure 74. The third plate was not bent, and depth of the crater was 0.250 inch (0.125 inch in the plate plus the 0.125 inch in the gap between Plates 3 and 4).



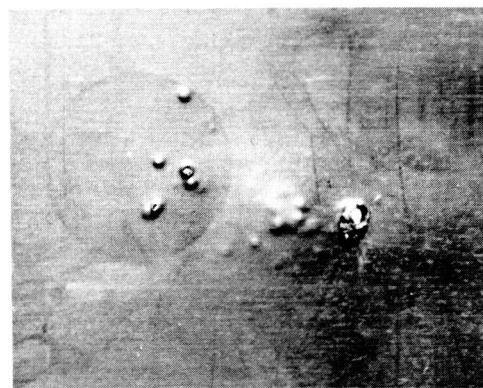
FIRST PLATE FRONT



FIRST PLATE REAR



SECOND PLATE FRONT
SPACING 3-INCHES



SECOND PLATE REAR
SPACING 3-INCHES

BUMPER AND TARGET(S) 6061-T6 Al
28,600 FT/SEC
0.5714-GRAM STEEL PROJECTILE (4130)

1-INCH

Figure 74. Aluminum Plates Used in Experiment D-157

SECTION 9

SUMMARY AND DISCUSSION

Many aspects and results that were obtained during this program were discussed phenomenologically in the appropriate sections. The summary and discussion of the results set forth in this section were directed toward relating and understanding the numerous phenomena observed. This summarization will be achieved by discussing the following topics in the order given: Prediction of Damage from Hypervelocity Crater Data; The 1.5 Times Rule; Meteoroid Bumpers; Pressurized Structures; Energy-Absorbing Core Materials; Projectiles; and Application of Scaling to Data in This Report. The principals of meteoroid protection will be delineated in the final section.

9.1 PREDICTION OF DAMAGE FROM HYPERVELOCITY CRATER DATA: THE 1.5 TIMES RULE. Impact data measurements, simulating meteoric particle impact, have been reported by a number of laboratories for a number of different projectile and target materials. Impact velocities usually are less than 30,000 ft/sec, with an abundance of data at impact velocities* less than 12,000 ft/sec. A considerable amount of the data is related to the formation of craters in semi-infinite plates**, rather than to impact phenomena related to thin sheets of material that will be utilized on aerospace vehicle protection systems. Semi-infinite crater measurements probably are not applicable for predicting damage to, or changes in, a typical vehicle hull configuration, which will include the outer skin, substructure, insulation components, etc. This inapplicability can be based on the fact that simple cratering does not comprise the full extent of damage inflicted by a high velocity meteoric particle. It should be noted that deformation, spallation, and rear surface cracking have been observed in thick plates where the depth of the crater was comparatively small (see Figure 56).

A frequently used empirical rule is that the thickness required for a high velocity particle to just penetrate a thin plate is 1.5 times the depth of a crater found in a semi-infinite plate of the same material. This 1.5 times rule does not appear to be reliable for all materials systems, or one for which extrapolation into the very high velocity range can be justified. Consequently, experimental verification must be established for specific material combinations of projectiles and vehicle hulls.

The impact of a 0.57-gram 4130 cylindrical steel projectile on a 1.5-inch thick 6061-T6 aluminum plate at 16,400 ft/sec formed a crater 0.625 inch deep (Experiment J-1).

* The lower velocities are insufficient for many combinations of projectile-target plate materials to behave in a fluid or hydrodynamic fashion and do not result in the formation of a hemispherical crater.

** A semi-infinite plate has sufficient thickness to eliminate all free surface effects.

April 1962

If the 1.5 times rule were valid under these experimental conditions, a plate 0.937 inch in thickness would be borderline between partial or complete penetration. It was experimentally observed that a 0.875-inch thick plate (Figure 15) was not completely punctured by an identical projectile with an impact velocity of 13,500 ft/sec (Experiment J-2). A bulge was formed on the rear surface. Plates thinner than 0.875-inch were cracked or completely punctured. The difference in thickness (6.6 percent less than predicted) may be attributed, in part, to the lower impact velocity (13,500 ft/sec) in the latter experiment. The data are in sufficient concordance to state that the 1.5 times rule is valid for the materials under the designated experimental conditions.

A 0.299-gram spherical nylon projectile with an impact velocity of 17,800 ft/sec struck a 0.875-inch thick 6061-T6 aluminum plate and produced a nearly hemispherical crater (0.85-inch diameter and 0.4 inch deep). If the 1.5 times rule were valid under these experimental conditions (Experiment 438 of Table 10), a plate 0.60 inch in thickness would be borderline between partial or complete penetration. It can be seen immediately that the prediction leads to an erroneous result since the rear surface of the 0.875-inch plate (1.46 times greater than the predicted required thickness) was scabbed by the impact. The diameter of the scabbed area was 1.25 inches (Figure 56).

Obviously, the impact damage to the 0.875-inch thick plates of 6061-T6 aluminum from the 0.57-gram steel projectiles traveling in air at 16,400 ft/sec, and the 0.299-gram nylon projectile traveling in vacuum at 17,800 ft/sec, do not follow the same pattern. It would be expected that the impact of a nylon sphere would be less severe than impact from the more dense steel projectile. However, damage to the aluminum plates indicates this expectation is not true. The crater shape, hemispherical for the nylon sphere and cylindrical for the steel cylinder, indicates in the specified hypervelocity environment that nylon is considerably less viscous than steel. The nylon must have offered very little resistance to flattening and in addition, set up a compression wave considerably stronger than the steel projectile. Not to be overlooked is the fact that the nylon projectile-aluminum target combination may behave in a fluid manner with impact velocities of 17,800 ft/sec, while the steel projectile-aluminum target combination may not be in the fluid impact region with particle velocities of 16,400 ft/sec.

Measurements of crater dimensions and their associations with particular conditions of hypervelocity impact, with suitable dimensional scaling, probably have a direct application to estimates of the surface erosion of space vehicles. Caution should be exercised in using such data for predicting structural damage from meteoric particle impact, since penetration and structural damage may not be synonymous. Structural damage involves some of the more complex and imperfectly understood behavior of materials when subjected to hypervelocity impact.

9.2 METEOROID BUMPERS. In 1946, Whipple [6] postulated that a very thin shield or meteoroid bumper surrounding a space vehicle would efficiently reduce meteoric particle impact damage. This postulate was based on the assumption that impact with the bumper would cause the meteoroid to break-up (fragment and/or vaporize) and these smaller particles of solid or fluid would be spread over a large area of the space vehicle surface. This fragmentation would greatly reduce the depth of penetration at any particular location, since the particle mass and velocity would be distributed over a greater area; i. e., momentum per-unit-area would be significantly reduced.

The term, "meteoroid bumper", includes any material that is used to protect the vehicle hull from impact damage. However, the term has been restricted to designate that part of the structure intended to change the condition of the impacting particle from a single compact solid to a cloud of dispersed particles (solid, liquid and/or gas) before the particles impact the vehicle hull.

From the standpoint of the meteoroid bumper concept, a space vehicle structure is composed of three components: a) the void (or core material sandwiched) between; b) the main hull of the vehicle; and c) the meteoroid bumper. For a high velocity particle, there is a bumper so thin there is very little decrease in total penetration*, a thickness which is optimum under the environmental conditions, and a bumper which is so thick** it cannot be penetrated completely by the particle.

A functional distinction is made, therefore, between the bumper, which permits some of the incident energy to be utilized in fragmenting the particle and the energy-absorbing (core) material which dissipates some of the kinetic energy before it can cause damage to the vehicle hull. This distinction is justified by the different physical characteristics of the materials that are required to efficiently perform the two functions: the bumper apparently should be compact and thin, with a moderately high density; the energy absorber, based on the experimental data, should be porous and thick with a moderately low density.

The bumper must be capable of fragmenting the meteoric particle and dispersing its energy over a large area of the main hull; the core material (if used) may reduce the velocity of the particles, and the main hull must have sufficient strength to transfer the momentum of the impacting particles without being penetrated completely. Actually, the two vehicle components (three when core material is used) function as an entity, but in order to simplify the analysis of engineering materials and structures during hypervelocity impact, each component must be considered phenomenologically.

* A bumper that is too thin will not provide the time necessary to utilize the energy released via impact in fragmenting the particle.

** A bumper that is too thick (but not semi-infinite) may produce large and numerous spall fragments, even though it is not completely pierced.

April 1962

Variables pertaining to the bumper such as composition, thickness, spacing from the vehicle hull etc., are difficult to separate since they are dependent. Separation of the variables has been made, in spite of the obvious redundancy, in order to provide a clear understanding of the significance of each variable.

9.2.1 Material or Composition. The material in the thin bumper at the point of impact can be assumed to have zero, or nearly zero, shear strength. The hydrodynamic model appears to be valid and with sufficient impact velocity, metals behave as though they were fluids. Consequently, mass rather than strength appears to be the important property of the bumper. Normal temperature strength characteristics are practically useless in the hypervelocity environment, since these physical properties do not exist during the time of fluid behavior. This applies only to penetration, and not to spallation*, a phenomenon which is related to both the material strength and ductility.

The effectiveness of the thin meteoroid bumper depends on its mass**. The thin bumper does not need to possess strength or toughness since the impact and shear processes are fluid. To obtain data supporting this "mass concept", or principle, has required a wide selection of bumper materials to be subjected to impact in air with the 0.57-gram*** steel projectile. Thin bumpers of aluminum (6061-T6), magnesium-lithium alloy (LA-141), plate glass, and stainless steel (301) have been found to be equally effective on the basis of total weight per-unit-area of the test panel. Total weight includes the weight of both the bumper and the aluminum (6061-T6) vehicle hull.

Pertinent data, taken from Figures 16, 17, 30, and 35 for those test panel configurations with bumpers of different thickness that were not completely penetrated, are summarized in Figure 75. It can be seen that test panels with a mass and spacing in the area: a) above the upper curve are not perforated or cracked; b) between the two curves may or may not be perforated or cracked; and c) below the bottom curve**** are always perforated or cracked under

* When the primary longitudinal wave, which is one of compression, strikes the opposite face of the plate, it is reflected and comes back as a wave of tension. If the wave is decaying in intensity, interference between the incident and reflected waves will cause a tensile stress to be built-up a short distance from the bottom of the plate. The tension may reach a high enough value to cause the plate to fracture.

** There is, however, a critical bumper thickness beyond which mass alone is not the important variable.

*** Note that 0.57 gram is the accelerated and not the impact mass.

**** See Section 3 and Figure 75.

April 1962

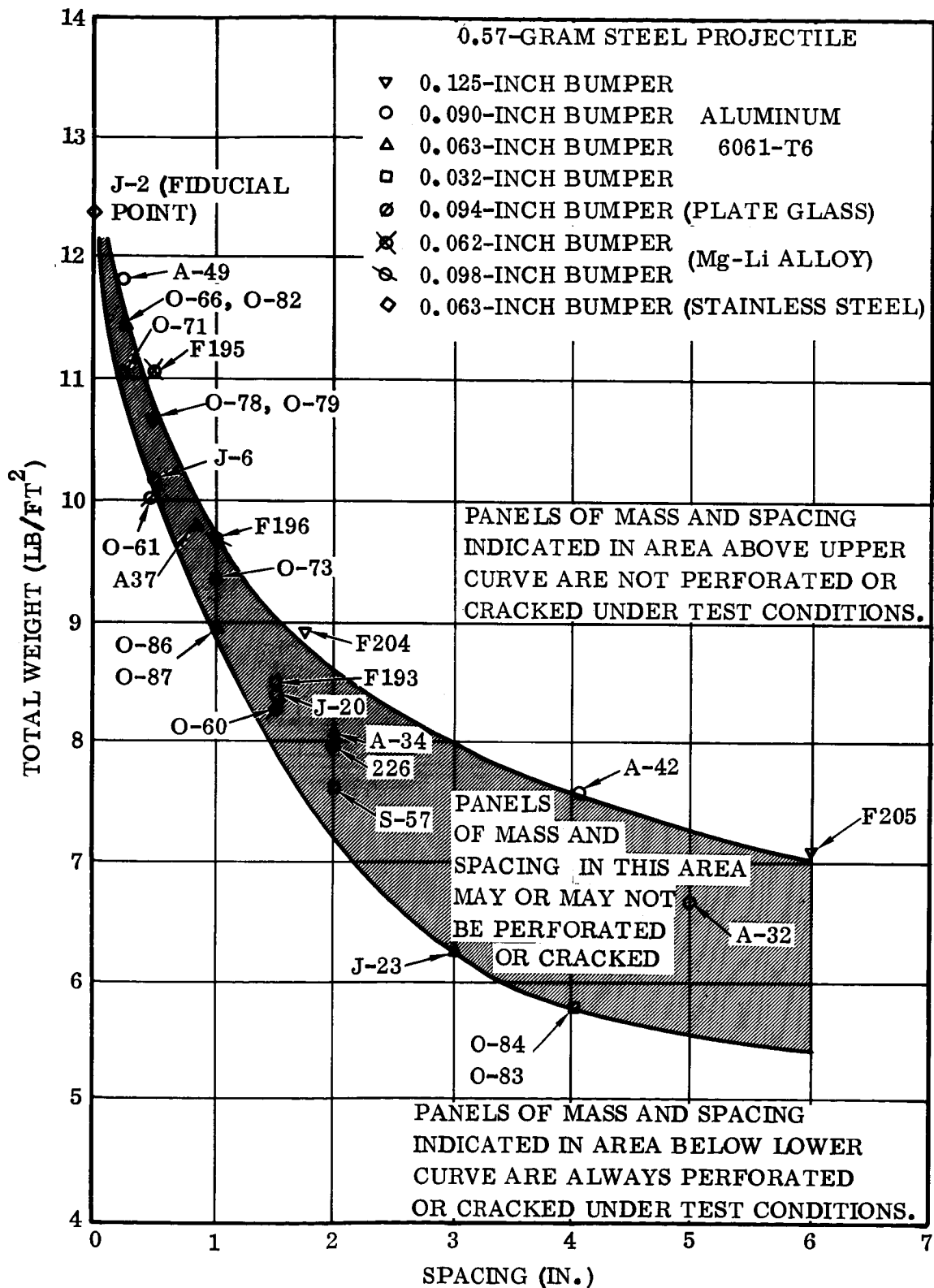


Figure 75. Test Panel Mass and Spacing: Bumpers of Aluminum, Plate Glass, Mg-Li Alloy, and Stainless Steel

April 1962

the test conditions. Thus, it can be concluded that bumpers fabricated from the five different materials with a thickness range from 0.032 to 0.125 inch provide the necessary impedance* or resistance to the steel projectile to bring about fragmentation, which prevented complete penetration of the vehicle hull. For any given aluminum hull thickness the corresponding minimum bumper mass may be obtained from the established relationships between total weight and spacing.

The area between the two curves merits several additional comments. Test panels with combinations of total weight and separation distance which fall in this area, yield conflicting data; i.e., the panels may or may not be completely perforated or cracked. This behavior can be attributed to several factors:

- a. There is definitely a dependence on impact velocity as shown in Section 9.2.5.
- b. The degree of particle fragmentation and the size and velocity of the fragments formed from the bumper will produce conflicting data. These effects can be related to the projectile orientation at the instant of impact.
- c. The larger the separation distance between the bumper and vehicle hull the greater the number of small fragments that will burn in the air environment. This will result in a decrease in the total impact momentum on the vehicle hull.

Experiments (A-222 to A-226; A-229, A-230 and A-232 of Table 6) with 0.063-inch thick stainless steel (2.61 lb/ft^2) and 0.1875-inch thick aluminum (2.66 lb/ft^2) bumpers placed in front of a 0.5-inch thick aluminum vehicle hull further indicates the importance of mass. These equivalent mass systems (steel and aluminum), with separation distances from zero to 0.25 inches, behaved** almost identically when struck with the 0.57-gram projectile. Additional discussion of these experiments will be made in the sections on "Thickness" and "Separation Distance".

Thus, it can be concluded that:

- a. The degree of brittleness or ductility does not appear to be an important property of the bumper, since plate glass, aluminum, and Mg-Li alloy bumpers function satisfactorily.
- b. Thin stainless steel and moderately thick aluminum plates, as well as plate glass and aluminum plates of equivalent mass, function in a similar manner.
- c. The "mass concept" permits a wide selection of materials.

* This is acoustical impedance.

** Damage to the aluminum vehicle hull protected by the aluminum bumper may be slightly less than the hull protected by the stainless steel bumper (see Table 6).

9.2.2 Thickness. Spaced plates offer more effective protection from meteoroids than either a stack of plates or a single plate of the same material and total mass. This improvement can be attributed to the fragmentation of the high velocity projectile on impact with the first plate, to reflection and refraction of the shock waves at the discontinuities (free surfaces) and to the expansion of the cone of projectile fragments and the disrupted shear plug material from the bumper.

The effect of two spaced plates, the bumper and the vehicle hull, has been previously shown in various Figures; i.e., 16, 17, 30, 35, and 75. The importance of spacing will be discussed in Section 10.

The effect of bumper thickness can be seen in Figure 76, a plot of total weight of the test panel for 0.032-, 0.063-, 0.090-, 0.125-, and 0.1875-inch aluminum bumpers with a spacing from 0.250 to 4 inches. The pertinent points shown in Figure 76 were taken from the smoothed curves given in Figures 16, 17, 30, and 35. Straight lines were used to represent the points due to the failure of the data to show a consistent pattern upon which the characteristics (slope) of the lines could be predicted.

In the thickness range from 0.032 to 0.125 inch, it appears from the isometric lines of Figure 76 that thinner bumpers require less weight in the vehicle hull to provide the same protection efficiency. Thus, with a 4 inch spacing the total weights are 5.74- and 7.17-lb/ft² and vehicle hull weights are 5.29- and 5.41-lb/ft² for the 0.032- and 0.125-inch bumper test panels, respectively. This weight advantage provided by the thinner bumpers is reduced as the space between the bumper and plate is decreased, and with a separation distance of one inch the total weight of the test panel is apparently the same when a 0.032- or 0.125-inch bumper is used.

It can also be seen from Figure 76 and Table 6 that aluminum bumpers 0.1875 inch thick require less weight in the vehicle hull than thinner bumpers at small separation distances, at least under the existing experimental conditions. The curve for the 0.250 inch spacing passes through a maximum with the 0.090-inch bumper. The total test panel weight of 11.86 lb/ft² for the 0.090-inch thick bumper at the maximum, can be decreased to 9.77 lb/ft² with a 0.1875-inch thick bumper, when the bumpers are placed flush with the vehicle hull plates.

Cognizance should be taken of the impact data from the three experiments* summarized in Table 11 and Figure 77. The 12.43 lb/ft² and 0.875-inch plate of aluminum used in Experiment J-2 can be considered as a bumper ** of sufficient thickness to prevent complete penetration or cracking. It can be expected that a bumper thickness

* Complete data are summarized in Table 4.

** In this instance the vehicle hull and bumper are identical since a single thick plate is used.

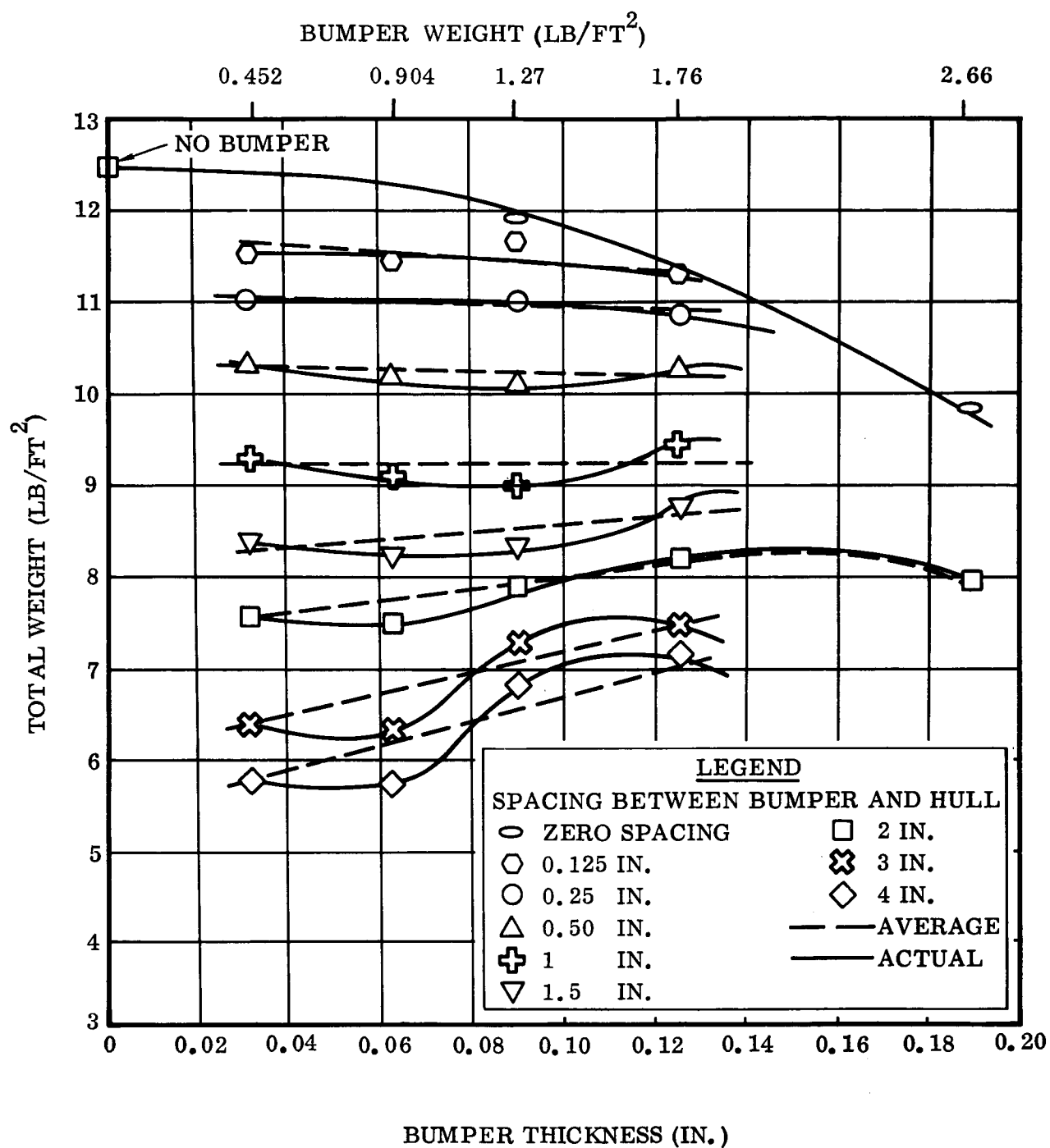
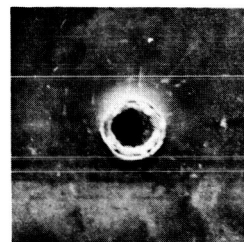
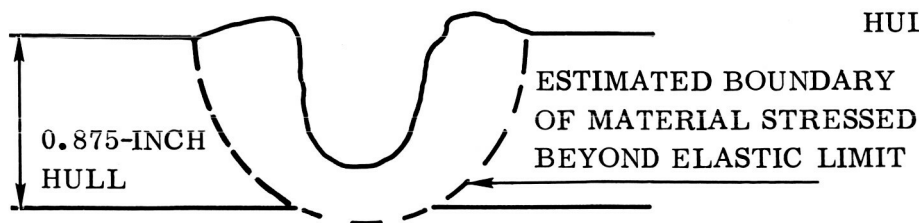


Figure 76. Total Weight Dependence on Aluminum Bumper Thickness (0.57-Gram Steel Projectile)

EXPERIMENT J-2

CRATER DEPTH: 0.719 INCH
CRATER DIAMETER: 0.625 INCH
IMPACT VELOCITY: 13,500 FT/SEC

VEHICLE
HULL

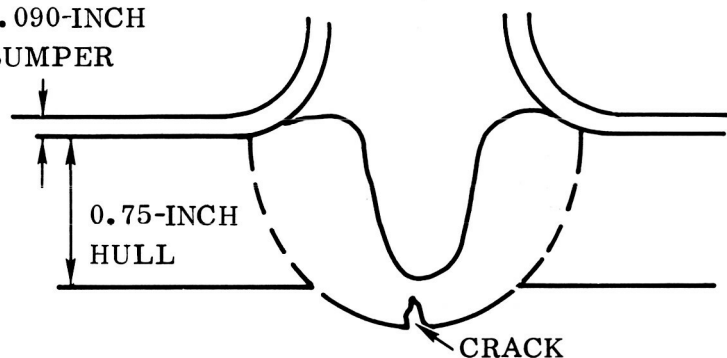


EXPERIMENT J-19

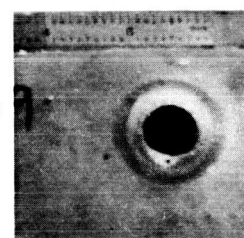
CRATER DEPTH: 0.75 INCH (IN HULL PLATE)
CRATER DIAMETER: 0.57 INCH
IMPACT VELOCITY: 14,750 FT/SEC

BUMPER

0.090-INCH BUMPER



VEHICLE HULL

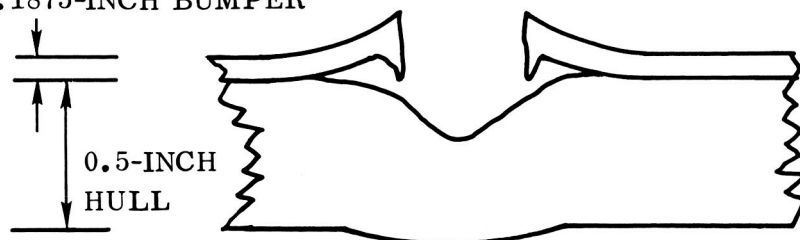


EXPERIMENT A-232

CRATER DEPTH: 0.3 INCH (IN HULL PLATE)
CRATER DIAMETER: 0.75 INCH
IMPACT VELOCITY: 14,700 FT/SEC

BUMPER

0.1875-INCH BUMPER



VEHICLE HULL

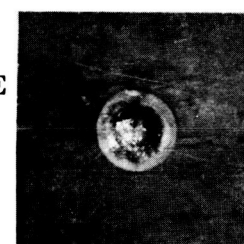
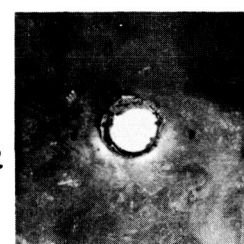


Figure 77. Effect of Bumper Thickness on Damage

Table 11. Effect of Bumper Thickness on Damage

ROUND NO.	BUMPER			TOTAL WEIGHT* OF TEST PANEL (LB/FT ²)	SPACING (IN.)	REMARKS
	MATERIAL	THICKNESS (IN.)	MASS (LB/FT ²)			
J-2	Aluminum	A single thick plate	---	12.43	A single plate 0.875 inch thick	0.625-inch diameter crater; 0.1-inch high bulge on rear face (see Figure 15).
J-19	Aluminum	0.090	1.28	11.86	Flush	0.57-inch diameter crater; 0.25-inch high bulge on rear face (see Figures 18 and 19).
A-232	Aluminum	0.1875	2.664	9.774	Flush	0.75-inch diameter crater; 0.125-inch high bulge on rear face.

* The test panel includes weight of the bumper and vehicle hull.

slightly less than 0.875 inch will be unsatisfactory and the panel would be completely pierced. The single thick panel (12.43 lb/ft²) does not provide the minimum test panel weight for a particular degree of protection from high velocity particles. This can be seen from the total weights of 11.86 lb/ft² and 9.77 lb/ft² for test panels with 0.090- and 0.1875-inch bumpers placed flush with the 0.75- and 0.5-inch thick vehicle hull in Experiments J-19 and A-232, respectively. It should be observed that the total weight of test panel J-19 should be increased slightly since a small crack was formed on the rear of the vehicle hull, while the total weight of test panel A-232 could be decreased slightly. Thus, it can be seen that:

- a. A stack of two plates provides the same amount of protection as a single thick plate but with less total weight.
- b. Several different thickness combinations between the bumper and vehicle hull (placed flush) can be selected which will provide the same protection.
- c. The thicker bumper appears to function satisfactorily with less total weight than required by thinner bumpers at small separation distances.
- d. A stack of two plates yields an advantage when the first plate is of a particular thickness relative to the impacting particle mass and velocity.
- e. Bumpers greater than 0.090 inch in thickness placed at a distance of 0.250 to zero inch from the vehicle hull offer the same amount of protection at the same total weight. Moreover, the isometric line will pass through a minimum and increase to a value of 12.43 lb/ft², as indicated in Figure 78.

The bumper thickness influences the diameter of the hole or shear plug produced from the impact of a hypervelocity particle and is treated phenomenologically, since there are insufficient data to justify definite conclusions. The inherent experimental problems associated with projecting a cylindrical particle of known mass and geometry, so that it strikes normal to the target surface, have not been solved. However, the data indicate certain trends and merit some discussion.

Importance of the shear plug size manifests itself in the total mass of material (and possibly size of particles) that will be removed from the bumper and may impinge* on the vehicle hull. Holes of different size are produced in thick plates of different materials by projectiles** of identical mass, size, geometry, and velocity.

* See Section 9.5 for a discussion of the significance of the mass and size of particles that impinge on the vehicle hull.

** The cylindrical steel projectiles lost mass and changed shape as a result of acceleration in air.

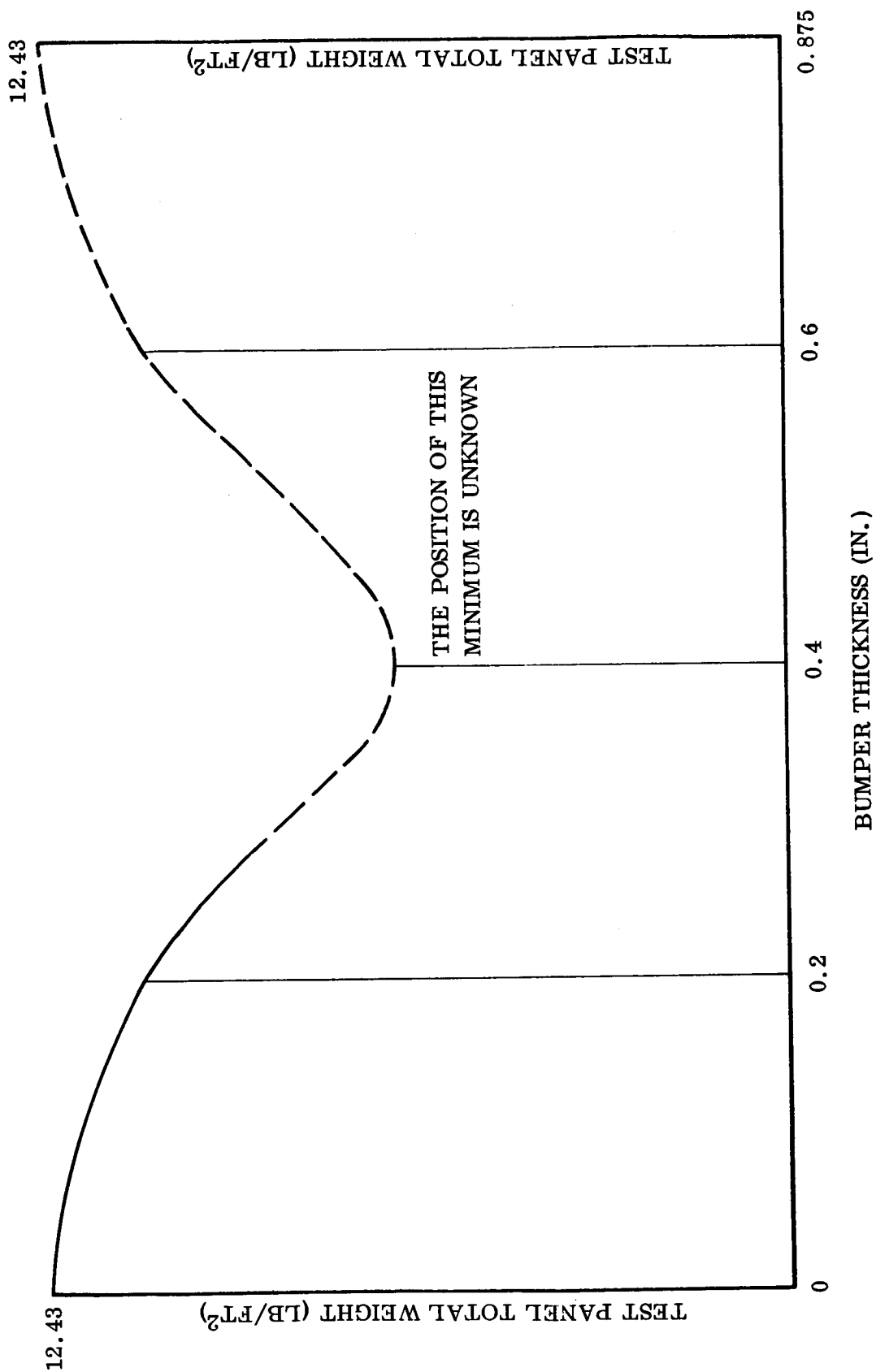


Figure 78. Predicted Total Weight Dependence on Thickness of Aluminum Bumper With Zero Spacing (0.57-Gram Projectile)

For example, the larger hole (Figure 65) in 0.375-inch aluminum in comparison to 0.375-inch titanium, and the larger hole in magnesium (0.250 inch thick) in comparison to aluminum (0.500 inch thick), may indicate that: a) more energy of the incident particle is consumed in forming the larger hole in magnesium; or b) with the same expense of incident energy a larger hole is formed in magnesium due to some intrinsic physical property.

The 0.375- and 0.500-inch aluminum (2024-T3) and titanium panels were sufficiently thick and a tapered hole was produced by the impact; a slightly tapered hole in the 0.375 inch, and a hole of greater taper in the 0.500-inch panel. Tapering can be attributed to the fact that these plates are approaching the thickness required to prevent complete penetration, i.e., the start of crater formation. Thus, the fluid impact process becomes of decreasing importance and the material strength begins to exert its influence. The shear plug diameter dependence on density for five materials is given in Figures 65 to 67, for projectiles with a mass* of about 0.57 gram, 0.21 gram, and 0.097 gram, respectively. It can be concluded that the thicker test panels, other factors being equal, yield the largest damage area in the surface struck with the high velocity projectile. The hole size appears to be constant (Figure 65) at about 0.5-inch diameter for sheets of HK-31A, aluminum, titanium, and stainless steel that range in thickness between 0.063 and 0.090 inch. This may indicate that materials of this thickness behave (under the designated experimental conditions) in a hydrodynamic manner when subjected to impact from a high velocity projectile. The shear plug is formed during the time period attributed to hydrodynamic behavior, and the target thickness does not permit the fluid impact to decay into the low velocity regime where material strengths are important. Panels less than 0.063 inch thick may yield holes with a diameter less than 0.50 inch when struck with the 0.57-gram projectile.

A possible explanation of the observed hole diameter data (Figures 61 to 67) can be made if the following observations are noted:

- a. The initial distance between the projectiles and hull plate was about 84 inches for HK-31A, 2024-T3 aluminum and titanium, and 40 inches for 6061-T6 aluminum, LA-141, and 301 stainless steel.
- b. The cylindrical steel projectile will lose mass and change its shape (increase diameter) as a result of acceleration in air (see Figure 60).

There are at least two points regarding the hole diameter data that should be discussed. The data, in regard to the first point given in Figures 61 to 64, indicate that the shear

* The exact mass is listed in the pertinent tables. This accelerated mass should not be confused with the actual impact mass.

April 1962

plug diameter for a fixed plate thickness is independent of impact velocity over the range from 12,000 to 20,000 ft/sec. It would be predicted that the hole diameter should increase with an increase in the impact velocity for particles of identical mass, geometry, etc. The reason this prediction was not observed in this program can be attributed to observation b; i.e., with increasing velocity the projectile lost an increasing amount of mass with the simultaneous increase in the projectile diameter. These two effects tend to cancel out as well as produce the observed scatter in the data.

The second point pertains to the apparent anomalous behavior (Figure 65) of 0.032-inch sheets of 6061-T6 and 2024-T3 aluminum alloys. It appears that a larger hole is formed in the 6061-T6 (0.475 inch) than in 2024-T3 (0.35 inch) alloy. This apparent discrepancy can be attributed to observation a; the different distances between the projectile and hull plate. The 6061 plate was about 44 inches closer to the projectile than the 2024 plate. Consequently, with the greater distance of travel, the projectile lost more mass with a simultaneous decrease in diameter, and the hole diameter in the 0.032-inch 2024-T3 aluminum was correspondingly smaller. For this reason, only those data obtained at a fixed distance between the projectile and hull plate should be compared.

9.2.3 Separation Distance from the Vehicle Hull. A summary of total mass and bumper spacing for 0.032-, 0.063-, 0.090-, and 0.125-inch thick aluminum bumpers is given in Figure 79. These curves were drawn from the data obtained from the isometric lines given in Figure 76. The following observations can be made for impact data obtained with the 0.57-gram cylindrical steel projectile:

- a. The curves for aluminum bumpers of various thickness apparently cross so that less total test panel weight is required for: 1) thicker bumpers at very small separation distances; and 2) thinner bumpers with increasing distance of separation.
- b. With the experimental system and aluminum bumpers in the thickness range from 0.032 to 0.125 inch, the total test panel weight - separation distance curves are about the same (or may cross) at a spacing from zero to 0.50 inch and diverge significantly at distances greater than 0.50 inch.
- c. With a total test panel weight of 7.0 lb/ft^2 , a 3-, and 4-inch spacing is required for 0.081-, and 0.123-inch thick aluminum bumpers, respectively.

When the space between the bumper and hull plate is very small, a thin bumper may be extensively damaged from material erupted or splashed back from the crater in the vehicle hull. The importance of the 0.25 inch distance between the bumper and hull plate can be seen from the fact there was: a) less total penetration into the hull plate in comparison to Experiment J-19 with zero spacing; and b) less damage to the bumper from back splash. For example, a one-inch diameter by 0.25-inch high petal

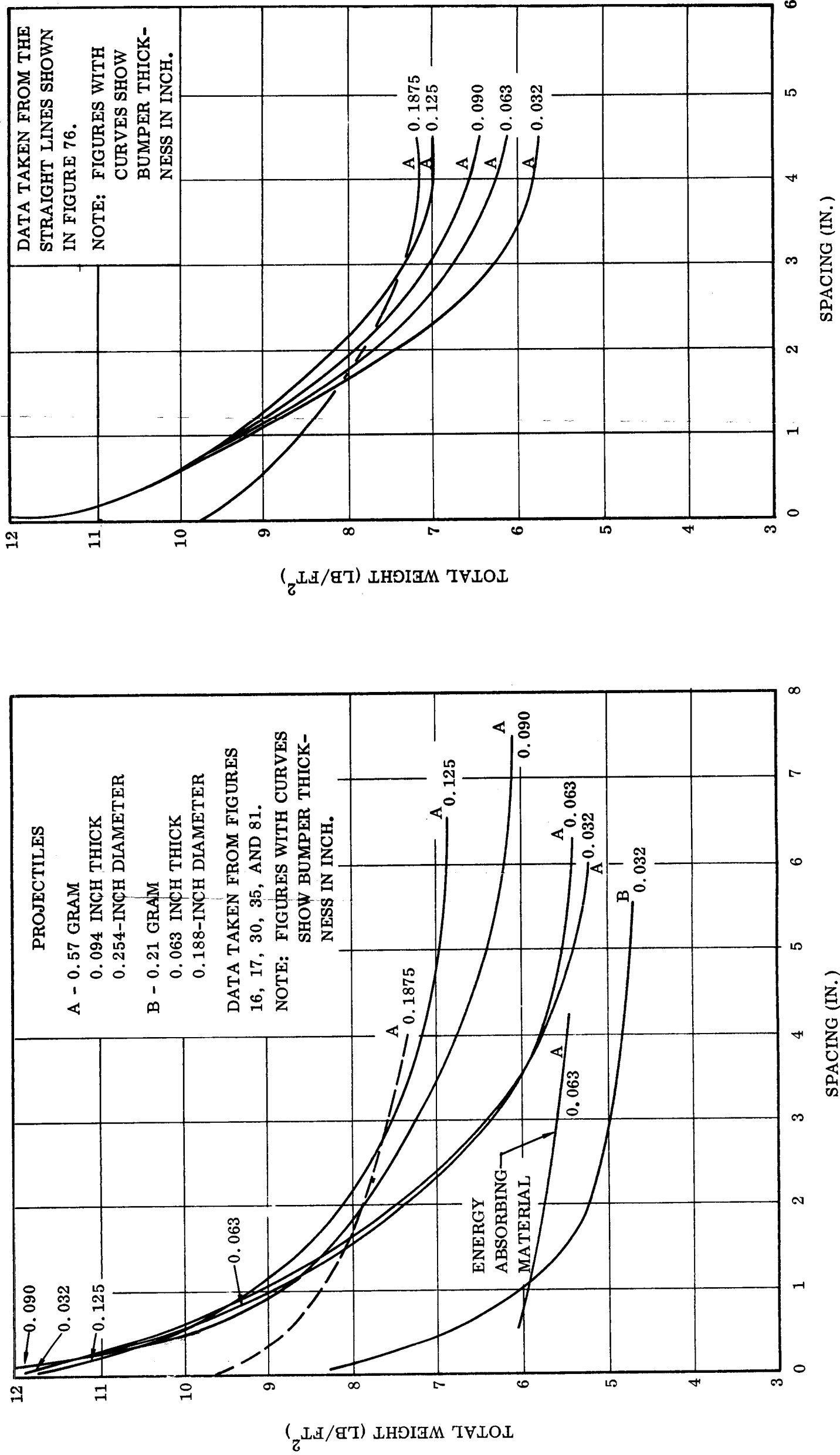


Figure 79. Summary of Total Mass and Bumper Spacing

April 1962

was found in the bumper placed flush (Figure 18) to the vehicle hull, while an 0.45- by 0.50-inch hole (shear plug) with no petal formation was found in the bumper (Figure 20) spaced 0.250 inch from the vehicle hull. The large area of damage and petal formation in the thin bumper placed flush to the hull plate can be attributed to the insufficient strength of the bumper, to withstand the pressure generated by the confinement of material erupted from the crater in the hull plate. The fluid material or particles leaving the crater in the hull plate move at high velocities, but not necessarily normal from the hull plate surface toward the rear face of the bumper.

The splash back of the hull plate material does not constitute a major problem with very thick bumpers, (see Section 3.1.5, where the 0.1875-inch thick bumper did not petal) since they exert sufficient strength to overcome the peak pressures that are generated. However, very thin bumpers must necessarily be spaced at a greater distance from the hull plate to prevent extensive damage. This damage may not be critical to the continued performance of the bumper, unless the bumper is used to protect a space radiator and the radiating surface must be maintained at some critical value.

Distance between the bumper and the vehicle hull will permit the cone of fragmented meteoric particles and shear plug material passing through the hole in the bumper to expand, so that momentum per-particle-contact-area on the vehicle hull will be significantly diminished. A large distance cannot be tolerated, since this will impose severe volume difficulties on the vehicle system. On the other hand, the distance cannot be too small, since material splashed back from the main hull will cause extensive damage to a thin bumper.

The diameter of this pattern of small craters depends, among other things, on the distance between the bumper and the vehicle hull. A circular cone* of material is formed, with a right circular section of the cone at the rear face of the bumper and the cone base at the front face of the vehicle hull. The farther the two plates are apart, the greater the area of the cone base; consequently, the distributed particles impact over a larger area on the vehicle hull. This decrease in impact momentum per-unit-area of vehicle hull manifests itself by reducing the damage to the hull.

Fragmentation has not been found to conform to a single type of behavior. However, there is an apparent tendency for the larger fragments to impact the vehicle hull near the center of the impact pattern. Occasionally, an impact pattern is found in which there is an even gradation of crater size, with the size diminishing uniformly with increasing distance from the impact pattern center. The non-reproducibility of this effect may be attributed to the tumbling action of the cylindrical projectile.

* See Section 9.5 on projectiles for a more detailed discussion.

9.2.4 Dependence on Projectile Mass. The previous data with the 0.57-gram projectile striking 0.032-inch thick aluminum bumpers can be compared with the 0.21-gram projectile (Figures 35 and 79). These data must be considered preliminary, but the following tentative statements can be made: a) penetration is less severe with the smaller projectile (a decrease of 0.36 gram, 0.031 inch in thickness and 0.062 inch in diameter) than with the 0.57-gram projectile; and b) the total weight per-unit-area for any given distance of separation between the bumper and vehicle hull appears to be proportional to the thickness of a given steel projectile. For example, the thickness of the 0.57-gram projectile (0.094 inch) is about 1.5 times that of the 0.21-gram projectile (0.063 inch), and the total weight per-unit-area to prevent penetration of the 0.57-gram projectile is about 1.5 times greater at separation distances of about two inches. The two curves for 0.032-inch bumpers appear to approach the same total test panel weight at a separation distance of about 5 inches.

9.2.5 Dependence on Impact Velocity. Total penetration into a test panel will depend on the impact velocity and mass of the particle. It should be observed that high particle velocities in air will result in a large loss of particle mass and possibly an increase in diameter. Moreover, particle fragmentation at impact should be more complete for high impact velocities. Data for impact velocities in the range of 16,000 to 21,700 ft/sec are summarized in Figure 80. Scatter in the data do not permit an accurate assessment of the impact velocity parameter, but it should be observed that the curve given in Figure 80 for bumpers in the thickness range from 0.032 to 0.094 inch, subjected to the higher impact velocities, is in excellent concordance with the bottom curve given in Figure 75.

9.3 PRESSURIZED STRUCTURES. Fluid (gas and/or liquid) pressurized components to be required on aerospace vehicles will range from the: a) low temperature cryogenic propellant tanks; b) ambient temperature compartments for astronauts and delicate instruments; and c) moderate to high temperature space radiators. The design and materials used in these various pressurized systems will be dictated by the operating pressures, temperatures, and the environment in which they must perform.

Power plants and cooling systems that must operate for extended periods of time in space must reject excess heat by radiation to space. Finned tube radiators have attracted considerable attention due to their low weight as well as their reduced area of meteoroid vulnerability in comparison to non-finned radiators. The working fluid may be a liquid such as sodium, rubidium, cesium, rhodium-potassium alloy, etc. Regardless of the ultimate design, or the materials used, space radiators will contribute most of the weight to the larger space power systems. Consequently, it is necessary to minimize the weight of the radiator through optimum design weight from the standpoint of heat transfer and protection from meteoroids.

April 1962

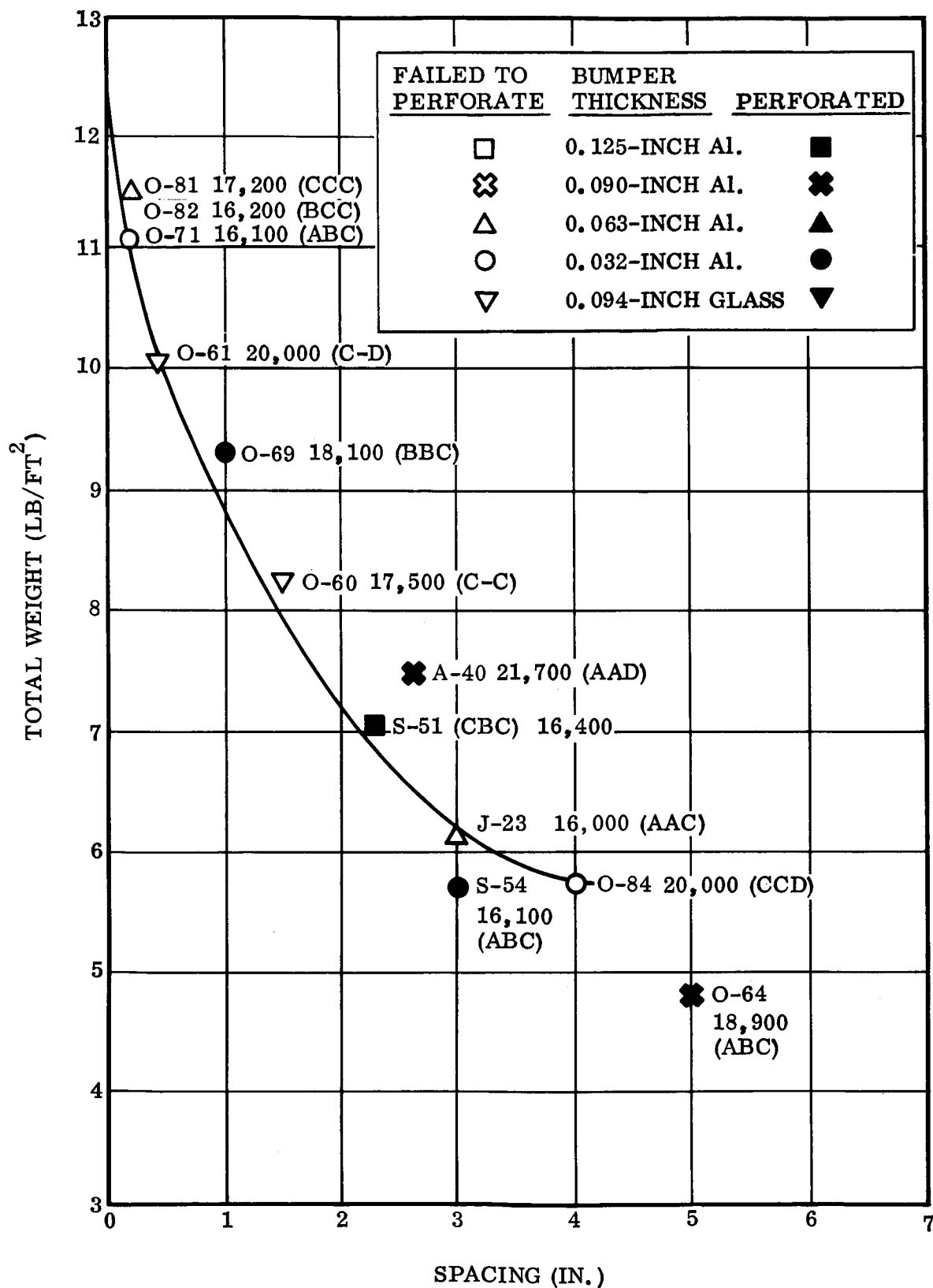


Figure 80. Curve for Those Experiments With Velocities From 16,000 to 21,700 Ft/Sec

Perils other than penetration are frequently neglected. For example: a) a flash explosion may result from a high velocity impact with an oxygen-rich pressurized aerospace vehicle; b) an astronaut may experience shock and/or concussion; or c) be subjected to catastrophic decompression resulting from the rapid loss of environment. Liquid oxygen propellant storage tanks may explode and/or burn since they will contain both liquid and gaseous oxygen.

In addition to the obvious hazards of burning to the vehicle or its passengers, the somewhat hidden dangers of removal of material or change of temper should be considered. Both can contribute to catastrophic failure by either: a) reducing the net area of the structure causing an increase in stress level and approaching the critical crack length-stress combination; or b) reducing the strength of the structural material by uncontrolled heat treating, resulting in a smaller crack length being required for rapid propagation and failure of the structure.

The impact conditions that form a puncture must be below the critical crack level, or catastrophic failure will occur. Repair of a non-catastrophic type puncture will prevent vessel failure that could be induced by an increase in pressure or load, or by further extension of the puncture damage by additional impacts that would extend the crack to its critical length.

In addition to the hazards resulting from structures burning in the oxygen environment, there is also the possibility of explosive decompression. Even though stainless steel and aluminum structures pressurized with oxygen will not burn when pierced by a hypervelocity particle, these structures may explode. Fracture of a pressurized vessel can occur if a perforation or crack is formed at 60 psig, providing the crack is propagated to its critical crack length.

The following can be concluded from pressurized structure impact data:

- a. Pressurized structures that have been tested would not rupture or lose pressure, when subjected to the shock wave generated with a one-pound explosive charge located a distance of four and one half feet from the structure.
- b. Steel projectiles accelerated to high velocity will not cause all pressurized structures to fail catastrophically. Catastrophic failure is dependent upon structure material, stress level, fluid medium, area of hole, compression wave set up in the medium, and reactivity between the medium and structural material.

Aluminum alloy 2024-T3 and full-hard 301 stainless steel do not react, while titanium alloys (5Al-2.5Sn-Ti) do react catastrophically with gaseous or liquid oxygen, when thin diaphragms pressurized to 60 psi are struck with steel projectiles weighing 0.097 to 0.21 gram, traveling at a velocity up to 13,000 ft/sec.

April 1962

The 0.016-inch aluminum and 0.010-inch 301 stainless steel successfully fragmented the high velocity steel projectile with only one of the diaphragms rupturing.

9.4 ENERGY-ABSORBING CORE MATERIAL. The energy-absorbing or core material placed between the bumper and the vehicle hull may insulate, support, stiffen, and hold the bumper and hull plates in their respective positions. From the standpoint of protection from meteoric particles, this energy-absorbing material is to be sacrificed to save the vehicle hull. The core material may be fibrous such as glass fibers, Refrasil (H. I. Thompson Fiber Glass Co.), Min-K (Johns-Manville), Linde S-10 (Linde Company), Tipersul (E. I. Dupont de Nemours), Crystal-M (Minnesota Mining and Manufacturing Company), metal wools, or it may be sponge or foam such as cellular magnesium (Dow Chemical Company).

The energy-absorbing material must have moderate compressive and shear strength, low density, directionality of mechanical properties, and low ablation rates. In addition, the material must not measurably contribute to the shock cone or to the fast moving fragments. Also, it should be capable of reducing the velocity of all particles moving toward the main hull. Thermal stability, moderate toughness, and a uniform texture are also desirable.

The preliminary experiments that were made with energy absorbers in conjunction with the 0.063-inch aluminum (6061-T6) bumper system given in Figures 48 to 50, are summarized in Figure 81, and compared with all the bumper data in Figure 79. These experiments show that insulating materials increase the protection from meteoric particles when used as core materials in the bumpered systems. The exact principle whereby fibrous material furnishes this increased protection has not been determined.

On the basis of these preliminary data, it can be concluded that energy-absorbing material placed between the bumper and the main hull of the vehicle will significantly reduce the weight per-unit-area of the meteoroid protection system. For example, the total weight per-unit-area can be lowered from approximately 8.8 to 5.9 lb/ft² with the incorporation of a one-inch thick pad of fibrous potassium titanate (Figure 50) placed flush with both the bumper and vehicle hull. It should be recognized that further improvement may be forthcoming, since panel N-138 (Figure 82) may not represent the minimum spacing for the 5.93 lb/ft² panel.

Differences in impact behavior for the same total weight of several test panel configurations can be attributed to projectile fragmentation on acceleration, mode of projectile impact (flat face versus edge), as well as changes in test panel design.

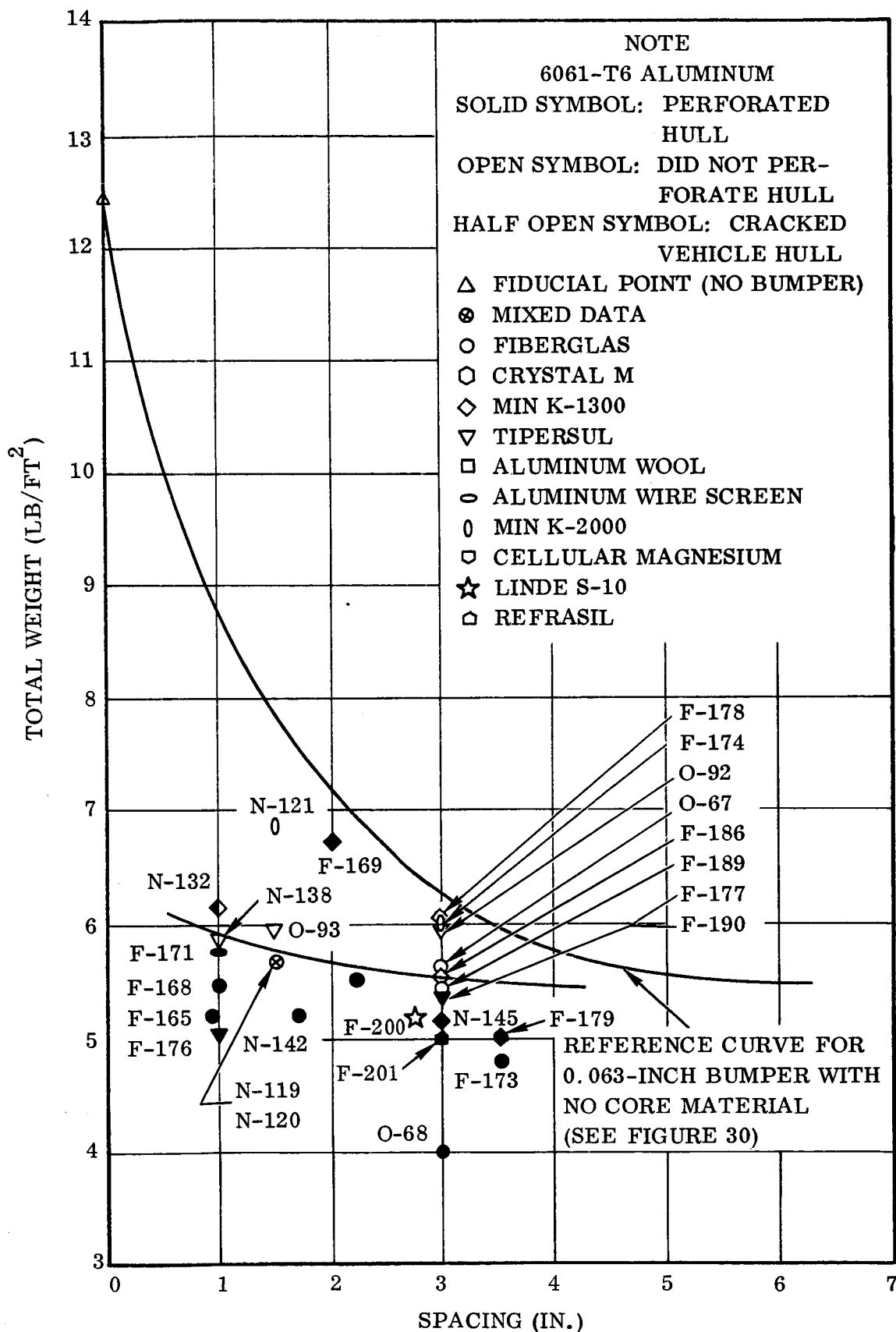
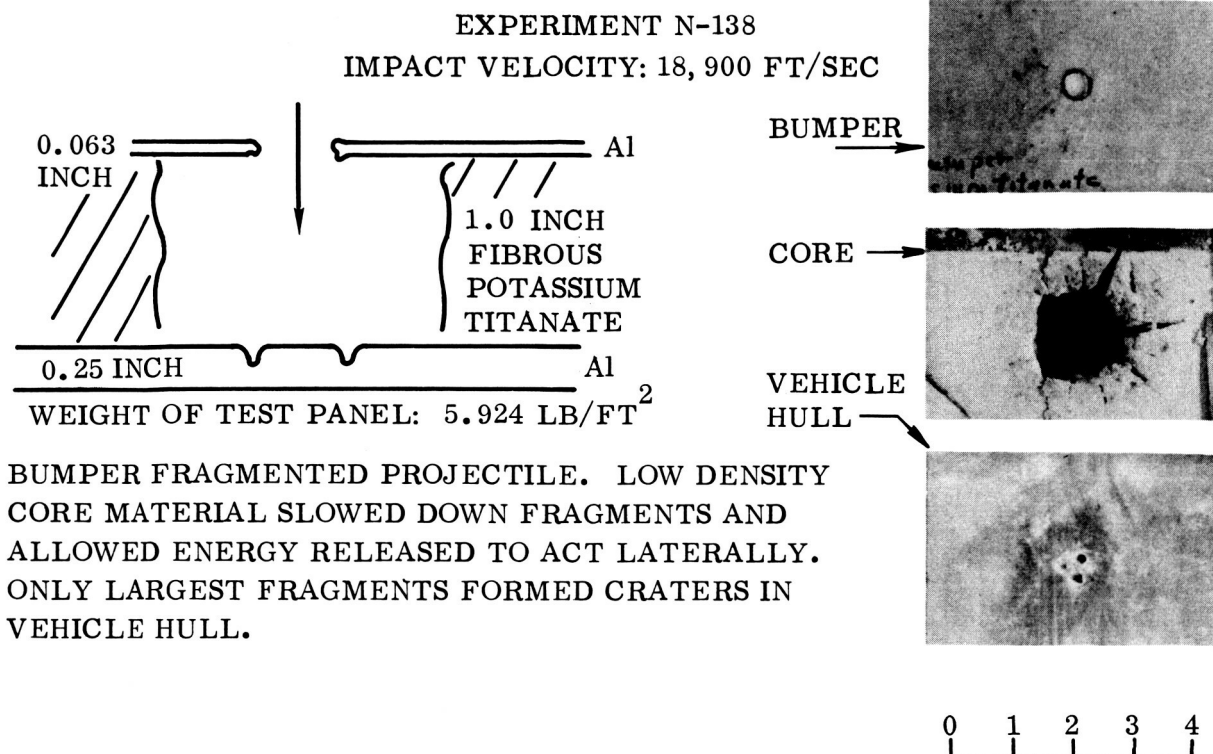


Figure 81. Summary of Energy Absorbing Material

April 1962



BUMPER FRAGMENTED PROJECTILE. LOW DENSITY CORE MATERIAL SLOWED DOWN FRAGMENTS AND ALLOWED ENERGY RELEASED TO ACT Laterally. ONLY LARGEST FRAGMENTS FORMED CRATERS IN VEHICLE HULL.

Figure 82. An Experiment Which Shows the Advantage of Energy Absorbing Core Material in Certain Configurations.

For example, panels N-119 and N-120 were identical, since they were fabricated from 1.5-inch thick pads of edge-grain fiberglass with a density of 10 lb/ft³. The projectile impact velocity was 12,500 ft/sec. Panel N-120 was not penetrated, since the projectile did not fragment prematurely; it struck the bumper flat (the hole in the bumper was almost circular; 0.52 by 0.56 inch) which caused the projectile to fragment and distribute the total impact momentum over a large area. However, panel N-119 was penetrated since the projectile struck the bumper on edge (the hole in the bumper was oval; 0.25 by 0.40 inch) which resulted in a large momentum per-impact-area.

Other differences in configuration behavior can be observed in test panels O-67 and O-68. A 1.5-inch thick pad of fiberglass was placed in contact with the vehicle hull, and a 1.5-inch spacing was provided between the fiberglass and the bumper. Panel O-67, with a 0.25-inch thick vehicle hull prevented the projectile from completely piercing the structure, while panel O-68 with a 0.125-inch thick vehicle hull was completely penetrated. These results were not unexpected, since the vehicle hull in panel O-68 with a 0.125-inch vehicle hull was not thick enough, and the total weight of the test panel was too low. Moreover, in this experiment, the projectile struck the bumper on edge, and edge impact always results in greater depth of pene-

tration. In the case of Panel O-67, the projectile was moderately fragmented during acceleration, and the momentum per-unit-impact-area was reduced to the point where the particles could not pierce the 0.250-inch vehicle hull plate.

Cognizance should be taken of test panel F-169 where a two-inch spacing was maintained between the bumper and vehicle hull. The entire two-inch spacing was filled with core material (Min-K-1300). This test panel was completely penetrated, since too large a fraction (46.9 percent) of the total weight (6.65 lb/ft²) was contributed by the core material (3.12 lb/ft²).

Apparently, materials such as pressed fine fibers and foams transfer or accept momentum or energy from the particles moving from the bumper toward the hull plate. Any reduction in particle velocity corresponding to the momentum transfer may release large quantities of kinetic energy. This reduction in velocity indicates that large amounts of the kinetic energy associated with the velocity change must be consumed in melting, vaporizing, and/or pulverizing the core material. Fine fibers provide large surface areas to absorb energy as well as to reflect and refract the impact shock waves. Furthermore, the fine material eliminated the possibility that the forces of impact would remove and accelerate large solid fragments of core material toward the vehicle hull.

The spray pattern when a fibrous material was placed between the bumper and vehicle hull, was masked somewhat by the material destroyed, and by gases and fragments rebounding from the surface of the plate. However, there were usually three to ten closely grouped small craters or nicks in the vehicle hull. The impact pattern was usually very small (see Figure 82) in comparison with similar test panels in which core material was not used (Figure 83).

The following trends were noted and are pertinent for the planning of future experimental programs:

- a. Energy-absorbing systems apparently provide a greater savings in total weight with the same degree of protection than systems without energy absorbers. For example, with a spacing of one inch between the 0.063-inch bumper and vehicle hull, the test panel total weight of 9.0 lb/ft² can be reduced to 5.9 lb/ft² with energy-absorbing material.
- b. Most of the energy-absorbing materials surveyed were fibrous. No absolute basis was established for a preference of either a fibrous or cellular type of material.
- c. Commercial insulating materials appear to behave as well as the more exotic types. Future experimental work may provide a basis for refinements of certain physical properties of materials.

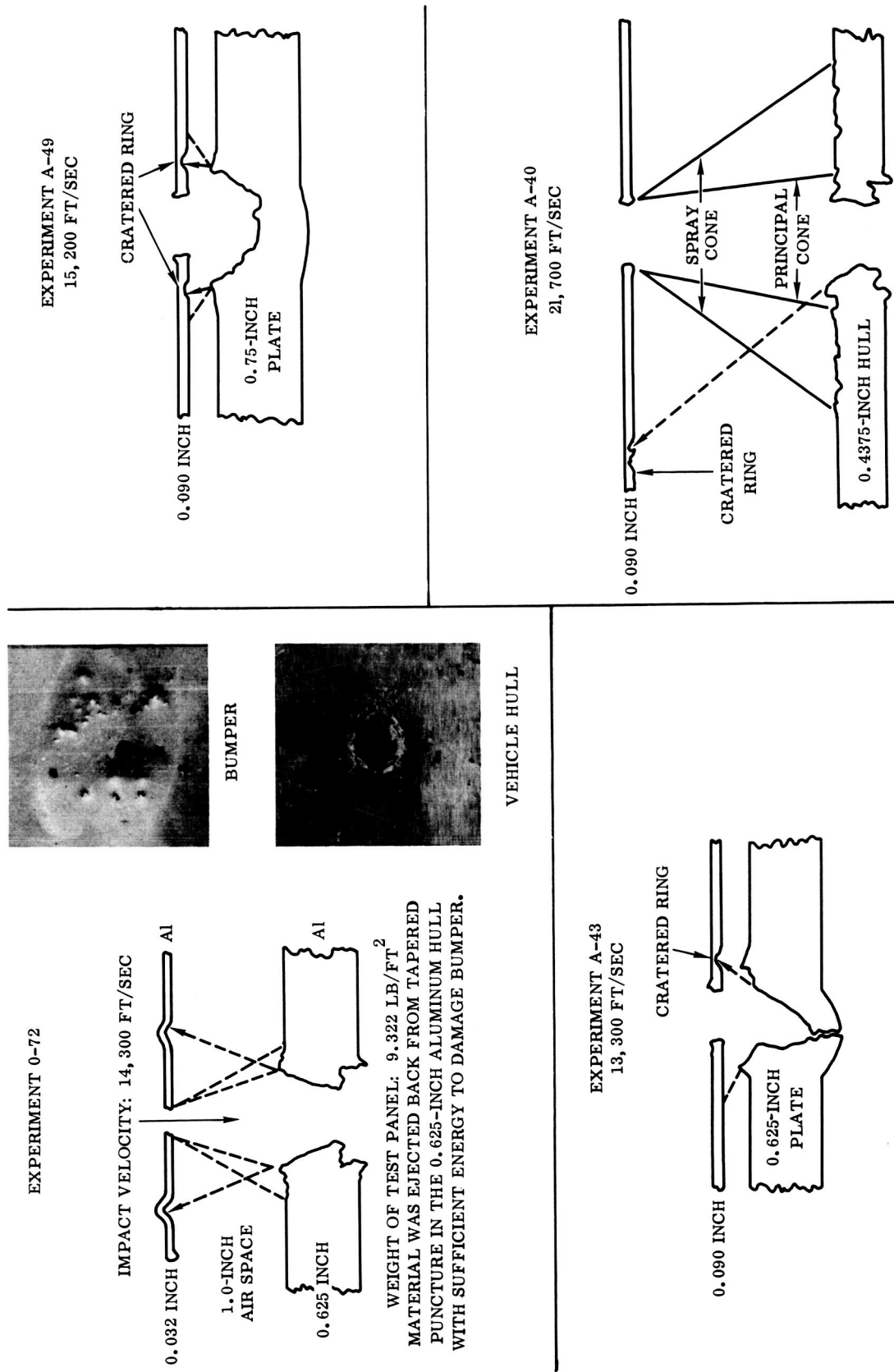


Figure 83. Cross Sections of Bumpered Systems Showing Locations of Spray Cone of Fragments

April 1962

- d. There appears to be an optimum density and thickness for the core material. Under the test conditions, the optimum density is apparently greater than 10 and less than 45 lb/ft³. The optimum thickness of this sacrifice material is evidently not greater than one inch under the test conditions.
- e. Core materials* with densities less than 10 lb/ft³ apparently are unsatisfactory. Increasing the thickness of 6 lb/ft³ core material from 1.7 inches (Experiment N-142) to 2.25 inches (Experiments D-161 and F-170) did not improve the protection efficiency.
- f. Thin aluminum plates were used with insulating material, essentially as part of the core material, to increase the mean core density, or to adjust the total weight of a system. These plates were very effective. Used in conjunction with the low density core material, the combination gave acceptable performance. However, it should be recognized that such plates do not appear to improve the performance over those systems that use higher density core material.
- g. Performance of the bumpered system was improved by substituting core material of the proper density for part of the mass of the vehicle hull; i. e., a thinner hull plate was used. It appears that substitution of core material must be limited to less than half of the mass of the vehicle hull replaced. Under experimental conditions, it was observed that fibrous core material could be substituted for 33 to 50 percent of the thickness of the vehicle hull, with either a 15 percent saving in total weight or a 75 percent saving in thickness. The steel projectile can be stopped with a 0.25-inch thick aluminum plate (3.53 lb/ft³) and a one-inch thick block of Tipersul (1.22 lb/ft³) substituted for a 0.375-inch thick aluminum plate (5.29 lb/ft³) with a spacing between the 0.063-inch bumper, and the face of the hull plate reduced from three inches (for the 0.375-inch plate with no core material) to one inch for the combination. For a maximum saving in total weight by retaining the three inch spacing, a 0.188-inch thick vehicle hull (2.65 lb/ft³) and a one-inch thick block of insulating material (1.85 lb/ft³) could be substituted for the 0.375-inch vehicle hull.
- h. The core material may alter momentum transmitted to the vehicle hull plate and therefore change the conditions of impact. When two thin plates separated by a layer of fibrous material were used as part of the core material, it was noted that the impacted area on the second plate showed characteristics typical of a low velocity impact; i. e., there was severe petal formation.

*Tipersul, Min-K, and Fiberglas TG-1500 have densities of 10 lb/ft³ or greater.

April 1962

- i. The effectiveness of density increases of core material by insertions of thin sheets of aluminum is evidently not dependent on the thickness of the aluminum sheets; 0.032-inch and 0.063-inch aluminum sheets were very effective for this purpose. This is also true of the 0.0015-inch aluminum foil that was used between the glass fiber layers in the S-10 insulating material.

Based on these observations it can be hypothesized that the core material:

- a. Slows down the particles moving from the bumper to the vehicle hull.
- b. Permits kinetic energy to be released without excessive confinement.
- c. Must have a particular density (minimum mass) to effect the release of kinetic energy.
- d. Must not be so dense that kinetic energy is confined.
- e. Must be sufficiently thick so that particles of a particular energy moving through the core material will be decelerated to a velocity too low for the core material to provide additional effectiveness. Thickness beyond this optimum will not be required.

9.5 PROJECTILES. The mechanism by which the air cavity explosive charge provides greater acceleration of the projectile than is usual with a plane-ended charge is probably a combination of two effects. These effects are: a) an attenuation of the peak pressure and a lengthening of its duration for shallow cavities; and b) the formation of a high velocity gas jet (Monroe effect) with deeper cavities. The magnitude and relative importance of the two effects is controlled by the cavity depth. The first effect may account for the increased projectile velocity, depending on the magnitude of the pressure (P) increase and the time of application, since the total impulse applied to the projectile is the integral of Pdt , integrated within the limits of zero and any time (t). The jet effect obtained by increasing the cavity depth probably contributes to the total impulse, and the peak dynamic pressure may be applied at the center of the projectile which causes the projectile to shatter. In some instances, the center of the projectile may be removed. This problem may be alleviated by making the projectile smaller in diameter than the cavity, and using a surrounding material (collet) to position the projectile. Another explanation for removing the center of the projectile, is that the radial compression on the projectile by the surrounding explosive is focused on the center of the projectile, weakens the structure of the projectile, and a hole is produced because of failure in tension when the compression wave is reflected at the center.

Projectiles with a small thickness (or length) to diameter ratio (T/D) can be explosively projected at a higher velocity, and with better integrity, than can projectiles with a T/D ratio of about one.

An example of this behavior can be seen from the data given in Table 1, where the maximum velocity obtained with acceptable integrity using a 0.196-gram projectile with a T/D equal to 1 is 10,800 ft/sec. But the velocity can be increased to 13,000 ft/sec with a 0.097-gram projectile with a T/D of 0.504; to 15,000 ft/sec with a 0.215-gram projectile with a T/D of 0.333; and to a velocity of 17,400 ft/sec with a 0.5-gram projectile having a T/D of 0.375. A possible explanation for this projectile behavior is that thicker projectiles fail in axial tension, because the initial compression wave is reflected from the free front surface; a situation similar to the effect which produces spallation of the back surface of thick target plates when subjected to hypervelocity impact.

There is no particular geometrical configuration associated with meteoric particles. Cylindrical and spherical projectiles are used to study the impact behavior of materials so that meteoric particle impact damage to aerospace vehicles can be predicted. The cylinder or disc used in this experimental program is not the most desirable projectile geometry, since the cylinder may tilt or tumble, (Figure 7) lose mass via ablation (in air), and change shape due to fusion and liquid flow as a result of acceleration to high velocity (Section 6). Because of these undesirable effects, the original mass of the projectile cannot be used in computing its striking momentum or energy per-unit-impact-area. The sphere is probably the best representation of the mean statistical form of meteoric particles. In addition, tumbling of a sphere does not affect the impact behavior and the data obtained with spherical projectiles are more reproducible than are data from projectiles with other geometries.

Cylindrical configurations are used instead of spherical when the particle acceleration is attained by the explosive driver technique, since cylindrical projectiles lend themselves to higher accelerations without fragmentation. A sphere is found to be more difficult to explosively accelerate than a cylinder with the same T/D ratio; i.e., T/D equal to one. Thus, in order to attain the highest particle accelerations with a discrete particle of known mass, size, etc., the mass of the projectile must be decreased with an increase in surface area and force applied. This is accomplished by using a flat cylinder (or disc) with a low T/D ratio; i.e., the projectile is very thin with a large diameter.

There can be no doubt that the orientation of the explosively accelerated cylindrical projectile is unstable since it tilts or tumbles in flight as pointed out in Section 3.1.4, and observed in the flash X-ray photograph shown in Figure 7. In addition, the center of the projectile is subjected to higher forces than the perimeter so there is an apparent bulge in the center. Not to be overlooked is the fusion resulting from aerodynamic heating, which permits material to flow at the leading edge, decreasing the thickness with a simultaneous increase in the diameter of the original projectile, as shown in Figure 60.

April 1962

There is no observable orientation impact effect when a thin cylindrical projectile impacts a massive plate at very high velocity; i.e., damage at the surface of the plate is circular even though the crater is not hemispherical (note, Experiments: J-1 and J-2, of Table 4; D-150 of Table 7; and N-116 of Table 5). However, the penetration and shear plug diameter that results when the flat face of a cylindrical projectile traveling at 12,000 to 17,000 ft/sec strikes a thin bumper are different from those observed when the projectile strikes the bumper on edge. These differences can be seen in Figures 58 and 59. When the flat face of the disc or cylindrical projectile strikes the bumper (Figure 58) at a velocity of about 15,000 ft/sec, the hole in the bumper is circular, and the impact pattern on the vehicle hull plate spaced one or more inches behind the bumper is also circular. Moreover, an edge impact produces deeper penetration and more extensive damage than a flat face impact. These impact patterns on the vehicle hull plate give the appearance of two distinct areas; one area* in the center is heavily cratered, while that area around the periphery is more lightly cratered. The difference in cratering can be attributed to the expansion of the material as it leaves the rear surface of the bumper; i.e., a circular cone (Figure 83) of material is formed with a right circular section of the cone at the rear face of the bumper, and the cone base at the front face of the vehicle hull. This damage pattern can be attributed to a greater concentration of material (projectile and bumper) in the center of the cone** emerging from the rear of the bumper.

The concentration gradient was so pronounced that the cone appeared to be composed of an inner and outer segment. The expansion of material passing through the bumper was not as large as expected for steel projectiles in the velocity range from 12,000 to 20,000 ft/sec. There appeared to be a concentrated core of fragmented material that had a diameter of about one inch, after it traveled about three inches beyond the bumper toward the vehicle hull. This central or inner core is probably composed of material from the projectile plus material from the bumper that was directly in the path of the projectile. The most heavily damaged section of the vehicle hull is in the inner cone, which conforms to the size of the cloud of fragmented particles that has been observed by high speed photographs showing the ball or cloud of luminous particles emerging from the rear of the bumper (Figures 71 and 73). The size of this cone of material depends on the projectile impact velocity; the lower the velocity the more compact the cone of material and the greater the damage inflicted to the vehicle hull. The outer part of the cone or spray pattern on the vehicle hull plate must be due to fragments removed from the bumper. The appearance of impact patterns on aluminum vehicle hulls obtained by projecting steel projectiles through glass bumpers (Figure 40) supports this hypothesis.

*The diameters of the central and heavily cratered areas are reported in the pertinent tables under the heading, "Principal cone diameter."

**The core of material is composed of numerous fragments of projectile and bumper material. At about 28,600 ft/sec, all holes in 0.125-inch bumper plates are round (Figure 74).

April 1962

When the cylindrical projectile strikes the bumper on edge an oval hole is formed (Figure 59). The impact pattern on the plate behind the bumper is elongated with its longer axis 90° to the longer axis of the oval hole in the bumper. The particle distribution is not uniform, is concentrated in the central region, and results in greater total penetration than observed with a flat face impact.

The impact pattern of a spherical projectile on a bumper protected target plate indicates there is a higher concentration of particles at the center of the impact pattern on the vehicle hull than when a cylindrical shaped projectile strikes on its flat side (Experiment F-192 of Table 5). Thus, the spherical projectile with its concentration of particles in a small impact area will permit a greater momentum transfer per-impact-area so that damage to the vehicle hull will be greater.

The orientation effects of a projectile at high velocity manifest themselves in the extent that the projectile is fragmented when it strikes the bumper and, in turn, fragmentation manifests itself in the total damage inflicted to the vehicle hull. A projectile that strikes on its flat face rather than on its side will be fragmented to a greater extent. The greater the number of fragments produced as a result of contact with the bumper, the less damage inflicted to the vehicle hull; i.e., concentration of momentum per-unit-impact-area is diminished, since the particles are numerous, but small, and are distributed over a greater area.

The craters produced in aluminum (6061-T6) by the copper and steel projectiles of identical size and shape, but with a slightly different mass (the copper was 18.8 percent heavier than steel), can be compared from the data given in Table 8 and Figure 37. The non-hemispherical, somewhat cylindrical* crater produced by the steel projectile was 0.625 inch in diameter and 0.719-inch deep; however, the copper projectile produced a rather shallow crater that was nearly hemispherical* (0.75-inch diameter and 0.44-inch deep). Copper, by virtue of its low melting point and greater plasticity than steel, behaved as a semi-viscous fluid during penetration, thus developing the essentially semi-hemispherical crater which is normal for this penetration mechanism.

It should be observed, also, that 0.075-gram spherical glass projectiles produced nearly hemispherical craters in aluminum plates. Thus, glass (Figure 55), nylon (Figure 56), and copper (Figure 37) projectiles impacting on aluminum form nearly hemispherical craters, while steel projectiles form cylindrical craters. This difference in impact behavior may be explained by the following reasoning. The breaking force is an inverse function of time in which the force acts and all solids can be visualized as liquid with high viscosities. For example, glass is an amorphous solid

*The crater is not amenable to precise measurement due to the irregularities in the crater wall, lip, etc.

April 1962

which is known to be a liquid of high viscosity, and nylon is an organic solid with a high viscosity, and crystalline materials such as metals exhibit properties of ordinary and non-Newtonian liquids. For example, stressed metals can undergo cold flow. Thus, the degree to which a hemispherical crater is approached in an aluminum plate may depend on the viscosity of the projectile material during the cratering process. Thus, steel projectiles would be expected to form hemispherical craters at higher impact velocities.

9.6 APPLICATION OF SCALING TO DATA IN THIS REPORT. The data on meteoroid bumpers and on core material given in this report are based on the use of a 4130 cylindrical steel projectile with a mass of 0.57 and 0.21 gram. These data include a factor for the effects of the projectile shape and orientation at the instant of impact with the bumper. The probability of impact with a meteoric particle with a mass of 0.57 gram is not as great as the probability of encounter with particles in the mass range of 10^{-2} to 10^{-7} gram. It is imperative, therefore, to investigate the applicability of scaling laws.

An appropriate size-scaling law* for impact can be stated [7] as follows: "If two impact conditions are identical in all but size, then they are mathematically identical when expressed in units derived from the same fundamental stress (e.g. Young's modulus) and velocity (e.g. bulk wave velocity) and a fundamental length proportional to the linear dimensions of the projectile." Thus, it can be seen that crater depth varies directly as the cube-root** of the projectile volume.

Data with the 0.57- and 0.21-gram steel projectiles impacting aluminum plates may be amenable with the cube-root scaling law. A plate thickness of 0.875 inch was required to defeat the 0.5742-gram steel projectile, traveling at 13,500 ft/sec (Experiment J-2 of Table 4), while a thickness of only 0.625 inch was required for the 0.210-gram projectile traveling at 11,400 ft/sec (Experiment N-116 of Table 5).

The value of 2.734 for the cube of the projectile mass ratio $\left(\frac{0.5742}{0.210}\right)^{\frac{1}{3}}$, can be compared to the value of 2.744 for the cube of the plate thickness ratio $\left(\frac{0.875}{0.625}\right)$, or the value of 2.750 for the cube of the total weight per-unit-area ratio. The latter two ratios are equivalent. The following facts should be observed:

- a. The height of the bulges on the reverse faces of the two plates were different; 0.10 and 0.04 inch for Experiments J-2 and N-116, respectively.
- b. The two different mass projectiles can be expected to lose different quantities of mass and change their geometry as a result of aerodynamic heating.

*This is Hopkinson's rule for explosions.

**Cube-root or Lampson scaling.

April 1962

The cube-root factor for scaling down from a 0.57-gram to 0.011-gram particle is about 3.7; i.e., the cube root of the mass ratio. This leads, with the data in this report, to the following vehicle structure that would be considered adequate for protection from meteoric particles with an impact up to 20,000 ft/sec:

Bumper: 0.016-inch aluminum (6061-T6)	0.226 lb/ft ²
Core: 0.5 inch	0.5 lb/ft ²
Vehicle hull: 0.070-inch aluminum (6061-T6)	1.0 lb/ft ²
	<hr/>
Total thickness of 0.586 inch for the structure	1.726 lb/ft ² *

The thickness of the core material is double the computed value to incorporate a margin of safety.

A reliable prediction of the effect of impact velocities in excess of 20,000 ft/sec on this structure cannot be made on the basis of the available data. However, the bumper is expected to be more efficient in fragmenting the projectile at higher impact velocities. This would permit the use of thinner bumpers but due to the greater momentum transfer, the vehicle hull plate would be increased in thickness. The greater kinetic energy associated with higher impact velocities would probably necessitate an increase in the core thickness and/or separation distance between the bumper and vehicle hull.

These data and estimates are based on particle impact normal to the bumper surface; an impact condition which is the most severe but not the most probable. There is, therefore, a possibility that a nominal increase in total weight of the structure, given in the previous example, would offer a system providing reasonable protection against puncture by micrometeoroids with very high impact velocities.

The data reported in this program were obtained with steel projectiles. Micro-meteoroids are expected to be somewhat frangible, and densities greater than that of steel are not expected to be encountered by a space vehicle. It can be expected that particle densities will be about 2.5 to 2.8 g/cc with bulk densities as low as 0.05 g/cc. Normal impact from fragments with a low bulk density may lead to wide craters that are not hemispherical.

In general, it appears that the requirements to prevent complete puncture of a vehicle by meteoric particles can be solved by the correct selection and arrangement of materials. Most of these materials are also needed to meet the design structural and thermal requirements. Thus, attention should be focused on the development of minimum weight multipurpose structures; i.e., structures to simultaneously provide protection from meteoric particles, radiation, etc. It should be noted that the example derived by application of the cube-root scaling law may barely fulfill the minimum structural requirements, and fails to meet the thermal insulation requirements by a considerable margin.

*This weight does not include fasteners for holding together the bumper and vehicle hull.

SECTION 10

PRINCIPLES OF METEOROID PROTECTION

The influence of material strength in semi-infinite targets is of prime importance in the low impact velocity or unbroken projectile region, but is greatly diminished at the impact velocity* of approximately 4,000 ft/sec. Impacts at this velocity are in the transition or broken projectile zone, which immediately precedes the fluid impact region (Figure 84). With a further increase in impact velocity, the effect of target strength continues to lessen. At approximately 10,000 ft/sec, the penetration in soft copper is only 12 percent greater than in hard copper. Impact at this velocity is well into the fluid impact regime, and extrapolation of the observed data indicates that penetration would be affected very little by target strength at velocities of the order of approximately 20,000 ft/sec.

A single thick plate of material cannot be considered for use in the construction and protection of a space vehicle, since the vehicle would be too heavy to move from the earth's atmosphere. In addition, a single thick plate does not furnish the maximum protection for its thickness and weight per-unit-area, because of the spallation hazard. This paradox can be attributed to the propagation of shock waves through materials, and to the reflection of shock waves at free surfaces which may lead to spallation. Material spalled from the inside surface can have moderately high velocity and can also cause extensive damage to the interior of a vehicle.

Conserving axial momentum in the inelastic collision of a high velocity meteoric particle with any material, in this case the meteoroid bumper, will result in a large loss of kinetic energy. Neglecting sound and light, as well as shock energy in the bumper, leaves very few mechanisms remaining for energy absorption.

An energy exchange occurs when a high velocity projectile strikes any material. The strong shock waves set up in the projectile will cause the projectile to fracture or deform and mush-out as a fluid as the target material impedes the forward motion of the projectile. The fluid projectile tends to turn itself inside out, which increases the diameter and results in the eruption and dispersion of some of the particles in the opposite direction of the incident projectile. The vehicle hull plate material, when subjected to the impact from the high velocity projectile, will initially behave as a fluid with almost zero shear strength. Two cases must be considered.

*The velocity at which these transitions occur depends on the material comprising both the target and projectile.

April 1962

10.1 CASE I: THE RELATIVELY THIN* SINGLE PLATE. Projectile impact** at about 20,000 ft/sec on a relatively thin* single target plate will lead initially to projectile dispersion and/or fragmentation, and initially the target will behave similar to a fluid (Point A, Figure 84). A large amount of energy is transferred from the projectile to the target, and therefore, the target material must be displaced under the directed hydrodynamic forces. With the relatively thick plate or mass of material impeding this fluid motion, the displaced fluid material is forced to move from the impacted free surface and a crater starts to develop, since the vehicle hull is not completely penetrated. In the confined space of the cavity, the release of energy accompanying the impact acts on the material with explosive violence. Material is ejected from the cavity backward in the direction from which the projectile came. A momentum equal to but opposite in direction to that of the ejected material is added to the shock wave advancing in front of the cavity.

Concurrently, the projectile, and some of the disrupted target material, is still expanding and moving deeper into the target but at a slower velocity than the incident projectile; i.e., the advancing particles of the projectile and target have a steadily decreasing velocity corresponding to points A, B₁, B₃, C₁, and 0 of Figure 84. At any particular instant, the target material will resist the forward motion of the incident particles. Since the forward motion or particle velocity is steadily decreasing with time, the target material is forced to behave first as a fluid (A to B₃, Figure 84), then undergo the transition corresponding to particle velocities from B₃ to C₁, and then exert its strength properties in the particle velocity region from C₁ to zero.

Spallation occurs around the inside of the crater in a brittle material due to the stress of the tension wave. In a ductile material, a ridge or lip is formed around the crater. In the proximity of the crater there is an area of material which has been stressed beyond its elastic limit.

10.2 CASE II: THE SINGLE METEOROID BUMPER. The material in the bumper at the point of impact can be assumed to have zero, or nearly zero, shear strength. The hydrodynamic model appears to be valid, and with sufficient impact velocity metals behave as though they were fluids. In the high-speed perforation process, the stress waves cannot radiate any significant distance from the point of impact. Large amounts of energy will be transmitted to the particles in the region of the impact point and these particles will be pulverized and/or become fluid.

*"Relatively thin plate" in contrast to a semi-infinite plate, refers to the minimum thickness that cannot be punctured by a given particle.

**Projectile impact will be considered normal to the target surface.

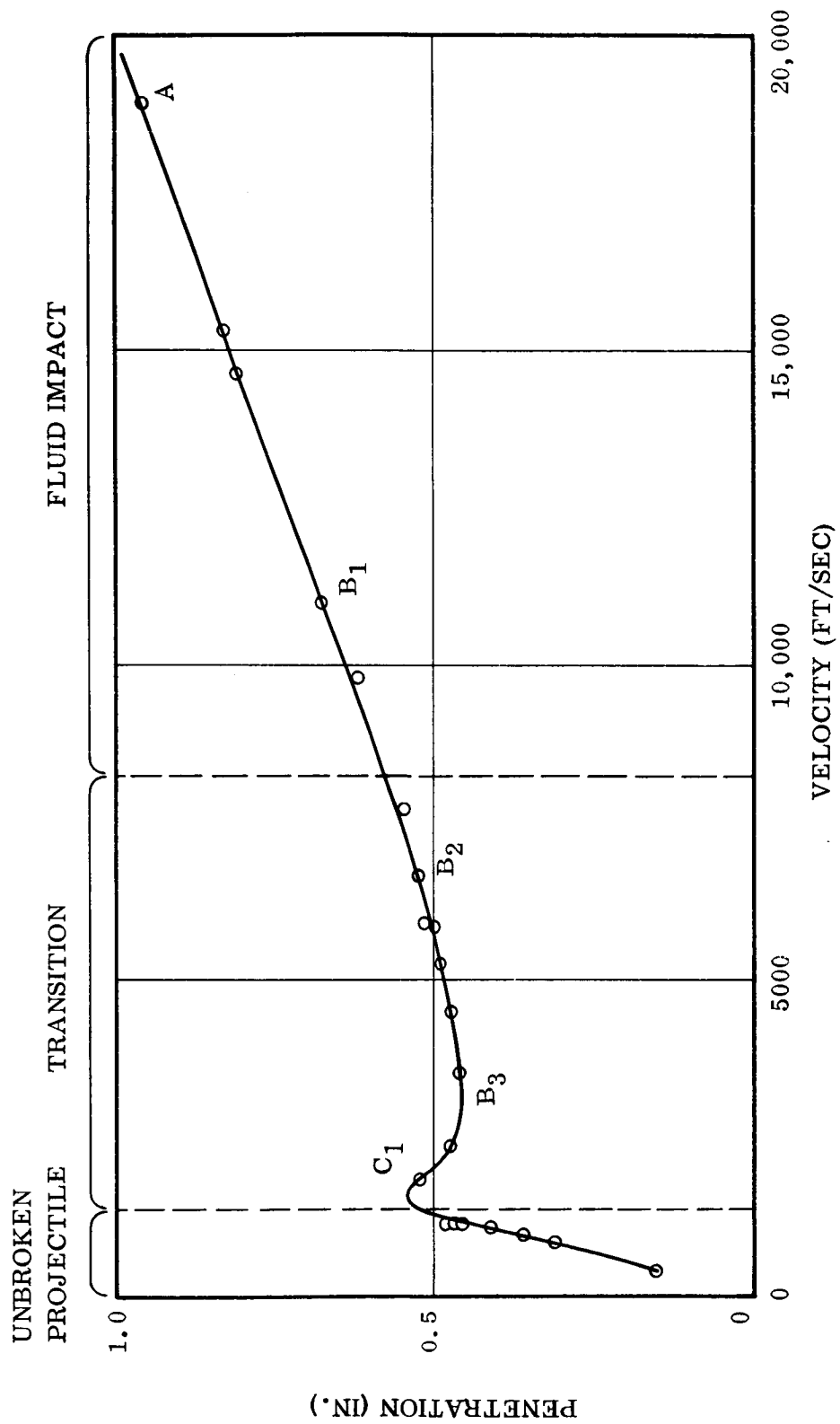


Figure 84. Impact Regions [Ref 52]

April 1962

Movement, or motion of the meteoric particle, is opposed [6] by the inertia of the bumper. Total momentum probably is not significantly changed, but the added mass of the shear plug reduces the particle velocity,

$$v_f = \beta v_i$$

where

$$\beta = \frac{M}{M+m}$$

M = projectile mass

m = shear plug mass

v_i = initial velocity

v_f = final velocity

This reduction in velocity results in a release of energy and if \bar{E} is the average internal energy-per-gram of material, then, from the conservation of energy we have,

$$KE = \frac{1}{2} m v_i^2 = (M+m) \bar{E}_{int.} + \frac{1}{2} (M+m) v_f^2$$

Combining these two equations, we arrive at the equation expressing the internal energy,

$$\bar{E}_{int.} = \frac{v_i^2 \beta (1 - \beta)}{2}$$

Part of this energy is available to destroy the meteoric particle or projectile via fragmentation and vaporization and part to disrupt the shear plug.

Since available materials behave as though they have nearly zero strength under hypervelocity impact, it becomes apparent that mass rather than strength is the important property of the material in the bumper. Normal temperature strength characteristics are practically useless in the hypervelocity environment since these physical properties do not exist during the time of fluid behavior. This applies only to penetration and not to spallation, a phenomenon which is related to both the strength and ductility.

Projectile impact at about 20,000 ft/sec on a simulated vehicle structure, composed of a meteoroid bumper and main hull, will lead to projectile dispersion and/or fragmentation. The material in the bumper will behave as a fluid (Point A, Figure 84).

The time for energy exchange between the projectile and bumper plate is limited since the bumper plate is thin and is readily penetrated; however, the time is sufficient to permit the projectile to lose its integrity, although the resistance presented by the bumper is insufficient to decelerate the particles from the high- to the low-velocity region. That is, penetration of the thin bumper is always in the fluid impact region and particle velocities will range from the initial impact velocity of Points A to B₃ of Figure 84. The projectile particles and shear plug material leaves the bumper and moves into the void* between the bumper and the vehicle hull. Total momentum at the instant the particles move by the rear face of the bumper is still quite high, but momentum per particle is quite low due to the large number of particles produced.

This void permits the forward moving particles to disperse** into a more or less conical spray before contacting the vehicle hull. This dispersion of the particles will result in a drastic reduction of the momentum per-impact-area on the vehicle hull, although the total momentum will be almost unaffected. Consequently, damage to the vehicle hull from these numerous moderately high velocity (but very small) particles will be reduced.

If the void is filled with an energy-absorbing or sacrifice material, the velocity of the particles passing by the rear face of the bumper may be significantly reduced before they contact the vehicle hull. The low density of the core material provides time and distance for impact energy to be released during particle deceleration, and this energy can be utilized in pulverizing, melting, or vaporizing the core material. Moreover, the core material, due to its low density, does not severely confine the action of the energy in a lateral direction. Particle velocity may be reduced from the range of Points A to B₃, down to C₁, or lower (Figure 84). In this case, the momentum and energy per-unit-impact-area of the forward moving particles contacting the vehicle hull is lowered by the particle dispersion as well as the reduction in impact velocity. Consequently, the material comprising the vehicle hull may be exposed to numerous particles with velocities in the range of Point C₁ or lower, and the vehicle hull should have high strength in order to absorb, without being penetrated, all the energy of the impinging low-velocity particles.

It can be deduced that a void filled with energy-absorbing material provides a discontinuity in the penetration-impact velocity curve of Figure 84. Due to this discontinuity, the total weight per-unit-area of the vehicle can be reduced. With this concept, the meteoroid bumper must have mass, with no strength requirements, while the vehicle hull must have high strength to prevent penetration from the relatively low velocity particles.

*This void may or may not be evacuated and filled with an energy-absorbing material.

**Increase the distance between the particles.

SECTION 11
BIBLIOGRAPHY

1. T. A. Dana, Light Gas Gun and Ballistic Range for Physics Research, General Dynamics/Convair Report No. PH-203-M, August 1961.
2. R. F. Rolsten, H. H. Hunt, and J. N. Wellnitz, Hypervelocity Impact on Pressurized Structures (Part I), General Dynamics/Astronautics Report No. AE62-0207, Contract AF18(600)-1775, 31 January 1962.
3. H. L. Lovelace, Preliminary Results of an Investigation of Ballistic Missile Vulnerability to Hypervelocity Fragment Impact, General Dynamics/Convair Report No. T-HI-2, 15 April 1960.
4. R. L. Bjork, Paper Presented at the Hypervelocity Impact Symposium, Denver Colorado, 1961.
5. D. E. Hurd and R. F. Holmes, A Study of Rain Erosion Testing Methods for Supersonic Speed. WADC Technical Report 53-173, Part VI, January 1960.
6. F. L. Whipple, Possible Hazards to a Satellite Vehicle, Project RAND, Douglas Aircraft Corporation, Santa Monica, California, 1946.
7. H. G. Hopkins and H. Kolsky, Mechanics of Hypervelocity Impact of Solids, A.R.D.E. Report (B) 12/60, November 1960, ASTIA AD-246757.
8. A. A. Broyles, Damage to X-Ray Detectors by Meteorites, The Rand Corporation Memorandum RM-2314, 1959.
9. Proceedings of the Rand Symposium on High-Speed Impact, Edited by J. H. Huth, R. D. Holbrook, and H. M. Dye, 1 May 1955.
10. Proceedings of the Second Hypervelocity and Impact Effects Symposium, U.S. Naval Research Laboratory and Air Research and Development Command, Washington, D. C., Volumes I and II, May 1957.
11. Proceedings of the Third Symposium on Hypervelocity Impact, Armour Research Foundation of Illinois Institute of Technology, Chicago, Illinois, Volumes I and II, February 1959.

12. Fourth Hypervelocity Impact Symposium, Sponsored by the U. S. Army, U. S. Navy, and U. S. Air Force, Air Proving Ground Center, USAF, Eglin Air Force Base, Florida, April 1960.
13. Hypervelocity Techniques Symposium, Co-sponsored by the University of Denver, Denver Research Institute, and The Institute of the Aeronautical Sciences, Denver, Colorado, October 20-21, 1960.
14. R. L. Bjork, Numerical Solutions of the Axially Symmetric Hypervelocity Impact Process Involving Iron, Proceedings of the Third Symposium on Hypervelocity, Volume II, February 1959.
15. R. L. Bjork, Effects of a Meteoroids Impact on Steel and Aluminum in Space, Rand-P-1662, December 1958.
16. R. L. Bjork, Meteoroids Versus Space Vehicles, Rand-P-1963, 4 April 1960; ARS Journal, pp 803-807, June 1961.
17. R. E. Henderson and P. Stanley, The Effect of Micrometeorites on Reflecting Surfaces, Proceedings of the Institute of Environmental Sciences, Los Angeles, California, pp 109-118, April 6-8, 1960.
18. F. L. Whipple, The Dust Cloud About the Earth, Nature 189, 127-128, 1961.
19. E. J. Öpik, Physics of Meteor Flight in the Atmosphere, Interscience Publishers, Inc, New York City, N.Y., 1958.
20. D. W. R. McKinley, Meteor Velocities Determined by Radio Observations, Astro J., 113, No. 2, 225-267, 1951.
21. L. A. Manning and V. R. Eshleman, Meteors in the Ionosphere, Proc. IRE, 47 186, 1959.
22. G. S. Hawkins and R. B. Southworth, The Statistics of Meteors in the Earth's Atmosphere, Smithsonian Contribution to Astrophysics, 2, No. 11, Smithsonian Institution, Washington, D. C., 1958.
23. F. L. Whipple and G. S. Hawkins, Handbuch der Physik, Group XI, Astrophysics, 52, 1959.
24. O. E. Berg and L. H. Meridith, Meteorite Impacts to Altitudes of 103 Kilometers, J. Geophys. Res., 61, 751, 1956.

25. E. R. Manring, Micrometeorite Measurements from 1958 Alpha and Gamma Satellites, Planet Space Sci., 1, 27-31, 1959.
26. H. L. Martin, Micrometeorite Distribution Measured by Several Rockets and Satellites, Army Ballistic Missile Agency, Redstone Arsenal, Huntsville, Alabama, Report No. DV-TN-4-60, 29 February 1960.
27. R. F. Rolsten, Meteoroid Bumpers for Space Craft, General Dynamics/Convair Report No. ZS-MT-014.
28. H. L. Martin, Micrometeorite Distribution Near the Earth, George C. Marshall Space Flight Center, Huntsville, Alabama, MTP-M-RP-61-2, 1 February 1960.
29. H. A. Bethe, An Attempt at a Theory of Armor Penetration, Ordnance Laboratory Report, Frankford Arsenal, Pa., May 1941.
30. G. I. Taylor, The Formation and Enlargement of a Circular Hole in a Thin Plastic Plate, Quart. J. Mech. Appl. Math., 1, 103-124, 1948.
31. W. T. Thompson, Approximate Theory of Armor Penetration, J. Appl. Phy., 26, 80-82, 1955.
32. Idem, 26, 919-920, 1955.
33. M. Zaid and B. Paul, Armor Penetration, Ordnance, 41, 609-611, 1957.
34. Ibid., Mechanics of Thin Plate Penetration, Proc. Second Fuze Symposium, Diamond Ordnance Fuze Laboratories, Washington, D.C., March 1956.
35. Ibid., Mechanics of High-Speed Projectile Perforation, J. Franklin Inst., 264, 117-126, 1957.
36. B. Paul and M. Zaid, Normal Perforation of a Thin Plate by a Truncated Projectile, Idem., 265, 317-335, 1958.
37. M. Zaid and B. Paul, Oblique Perforation of a Thin Plate by a Truncated Conical Projectile, Idem., 268, 24-45, 1959.
38. G. Grimmer, Probability that a Meteorite Will Hit or Penetrate a Body Situated in the Vicinity of the Earth, J. Appl. Phy., 19, 947-956, 1948.

39. J. L Bohn and O. P. Fuchs, High Velocity Impact Studies Directed Towards the Determination of the Spatial Density, Mass, and Velocity of Micrometeorites at High Altitudes, Contract AF19(604)-1894, Scientific Report No. 1, ASTIA AD 243106.
40. M. Zaid, An Analytical Approach to Hypervelocity Impact Mechanics, Fourth Hypervelocity Impact Symposium, Sponsored by the U. S. Army, U. S. Navy, and U. S. Air Force, Air Proving Ground Center, USAF, Eglin Air Force Base, Florida, Volume III, Paper No. 31, April 1960.
41. Penetration by Hypervelocity Particles, Ibid., Technik Incorporated, Research Analysis Development, Garden City, N.Y., Contract DA-30-069-507-ORD-2674, November 1960.
42. F. L. Whipple, The Meteoric Risk to Space Vehicles, in Vistas in Astro-nautics, Pergamon Press, New York City, N.Y., pp 115-124, 1958.
43. N. H. Langton, The Thermal Dissipation of Meteorites by a Bumper Screen, Bericht über der V. Internationalen Astronautischen Kongres, August 1954.
44. C. E. McDermott, E. T. Canon, and R. W. Grow, Temperature Studies and Effects in Penetration of Thin Aluminum Targets, University of Utah Technical Report UU-3, May 1959.
45. M. A. Lavrent'yev, The Problems of Piercing at Cosmic Velocities, NASA-TT-F-40, May 1960.
46. K. P. Stanyukovich and V. V. Fedynskiy, The Destructive Action of Meteorite Impacts, Doklady Akademii Nauk SSSR, 57, No. 2, 129-132, 1947.
47. K. P. Stanyukovich, Concerning the Impact of Solids at High Velocities, Soviet Physics JETP, 9, 1141, 1959.
48. G. Birkhoff, D. P. MacDougall, E. M. Pugh, and G. Taylor, Explosives with Lined Cavities, J. Appl. Phy., 19, 563-582, 1948.
49. E. Öpik, Researches on the Physical Theory of Meteor Phenomena: Theory on the Formation of Meteor Craters, Tartuensis Obs. Pub. 29, No. 5, 1937; Acta et Comm. University Tartuensis A, 33, 1939.
50. M. A. Cook, Mechanism of Cratering in Ultra-High Velocity Impact, AFOSR-TN-57-486, AD 136479, Contract AF-18(603)100.
51. D. C. Pack and W. M. Evans, Penetration by High Velocity (Munroe) Jets, Proc. Phy. Soc., London, England, B64, 298-302; 303-310, 1951.

52. A. C. Charters, High-Speed Impact, Scientific American, 203, No. 4, 128-140, 1960.
53. W. W. Atkins and H. F. Swift, Hypervelocity Capability and Impact Research, Semi-annual Progress Report, NRL Memo. Report 1115, December 1960.
54. J. L. Summers, Investigation of High-Speed Impact: Regions of Impact, and Impact at Oblique Angles, NASA-TN-D-94, October 1959.
55. F. J. Willig and H. W. Semon, A Multi-Staged H. E. Actuated Hypervelocity Gun, Proceedings of the Third Symposium on Hypervelocity Impact, Armour Research Foundation of Illinois Institute of Technology, Chicago, Illinois, Vol. I, pp 501-508, February 1959.
56. J. O. Funkhouser, A Preliminary Investigation of the Effects of Bumpers as a Means of Reducing Projectile Penetration, NASA-TN-D-802, April 1961.
57. W. H. Kinard and R. D. Collins, Jr., An Investigation of High-Velocity-Impact Cratering into Nonmetallic Targets and Correlation of Penetration Data for Metallic and Nonmetallic Targets, NASA-TN-D-726, 1961.
58. W. H. Kinard, C. H. Lambert, Jr., D. R. Schryer, and F. W. Casey, Jr., Effect of Target Thickness on Cratering and Penetration of Projectiles Impacting at Velocities to 13,000 Feet-Per-Second, NASA MEMO. 10-18-58L, 1958.
59. A. E. Olshaker, Jr., Experimental Investigation in Lead of the Whipple Meteor Bumper, J. Appl. Phy., 31, No. 12, 2118-2120, 1960.
60. D. B. Lull, Analysis of Impact of Hypervelocity Pellet with a Thin Shield, MEMO. of A. D. Little Corporation, Cambridge, Massachusetts, 29 December 1959; Case 62509-1.
61. R. D. Collins and W. H. Kinard, The Dependency of Penetration on the Momentum Per-Unit-Area of the Impacting Projectile and the Resistance of Materials to Penetration, NASA-TN-D-238, May 1960.
62. W. S. Partridge and H. B. VanFleet, Similarities Between Lunar and High-Velocity-Impact Craters, Astrophysical Journal, 128, 416-419, 1958.

April 1962

63. W. S. Partridge, High-Velocity Impact, Proceedings of the Fifth Sagamore Ordnance Materials Research Conference, Materials-in-Space Environment, Sagamore Conference Center, Racquette Lake, New York, September 16-19, 1958, PB-151900, pp 303-322.
64. S. M. Halperson and R. H. Fuller, Hypervelocity Kill Mechanisms Program: Impact Damage Phase, ARPA Order No. 149, NRL Prob. No. FO4-11B, First Quarterly Report, Period Ending 20 December 1960.
65. J. Wm. Gehring, Jr., Observations on the Phenomena of Hypervelocity Impact, Fourth Hypervelocity Impact Symposium, Sponsored by the U. S. Army, U. S. Navy, and U. S. Air Force, Air Proving Ground Center, USAF, Eglin Air Force Base, Florida, Volume II, Paper No. 29, April 1960.
66. J. B. Feldman, Jr., Volume-Energy Relation from Shaped Charge Jet Penetrations, Ibid, Paper No. 26.
67. J. H. Kineke, Jr., An Experimental Study of Crater Formation In Metallic Targets, Ibid, Volume I, Paper No. 10.
68. F. E. Allison, K. R. Becker, and R. Vitali, Effects of Target Temperature on Hypervelocity Cratering, Ibid, Paper No. 14.
69. E. P. Palmer, R. W. Grow, D. K. Johnson, and G. H. Turner, Cratering; Experiment and Theory, Ibid, Paper No. 13.
70. A.C. Charters and G. S. Locke, Jr., A Preliminary Investigation of High-Speed Impact: The Penetration of Small Spheres into Thick Copper Targets, NACA-RM-A58B26, 1958.
71. G. H. Turner, E. P. Palmer, and R. W. Grow, Projectile Effects and Substitute Disturbance in High-Velocity-Impact Cratering in Lead, University of Utah Technical Report UU-5, 2 August 1960.
72. D. Humes, R. N. Hopko, and W. H. Kinard, An Experimental Investigation of Single Aluminum Meteor Bumpers, Presented at the Fifth Hypervelocity Impact Symposium, Denver, Colorado, October 1961.

APPENDIX A

HYPERVELOCITY IMPACT: LITERATURE SUMMARY*

A-1 INTRODUCTION. A concerted effort [1-72]** is currently directed toward defining the meteoric particle environment and elucidating the: a) mechanism(s) of hypervelocity impact; b) energy and/or momentum transfer processes; c) interaction between the projectile and target; and d) behavior of aerospace vehicle materials. The majority of programs have concentrated on the impact phenomena occurring between like materials, and with semi-infinite*** plates, in order to reduce the number of variables in a very complex system. Impact velocities have varied from a few hundred to about thirty thousand feet-per-second, with projectile masses from 10^{-6} to several grams, and projectile densities from about two to eight grams per-cubic-centimeter.

The relative importance of the various complex processes that occur during impact between a projectile**** and target plate***** will determine the nature of the target plate damage and the stress-wave patterns produced in the projectile and the target. The nature of an impact at any velocity for a specific configuration of projectile and target depends [7] on the relative importance of five distinct material properties of the target and projectile. These properties are:

- a. Elastic stress-strain behavior.
- b. Plastic stress-strain behavior.
- c. Density (Hydrodynamic impact).
- d. Decrease of compressibility with increasing pressure (Sonic impact).
- e. Thermal (Explosive).

The relative importance of these properties on impact phenomena indicates a change from (a) to (e) with increasing velocity. Hopkins and Kolsky [7] made a further

* This literature summary is not intended to be exhaustive.

** Numbers in brackets refer to the reference given in the bibliography.

*** A semi-infinite plate has sufficient thickness to eliminate all free surface effects.

**** Projectile refers to a meteoric particle in space, as well as particles accelerated to high velocity on Earth for purposes of studying hypervelocity impact.

***** Target plate refers to the structure of a space vehicle, as well as the small test panels used on Earth for purposes of studying hypervelocity impact.

April 1962

division in which the impact is "quasi-static" or "dynamic" depending on the proportion of the projectiles' kinetic energy that is transferred to the target. Impacts in regimes (a) and (b) are generally considered as "quasi-static", and regimes (c), (d), and (e) are dynamic.

A-2 THEORIES OF PENETRATION AND/OR CRATERING. Theoretical analysis of high velocity cratering and penetration can be divided into at least four groups. This arbitrary division can be made on the basis of the assumptions involved.

A-2.1 Rigid Projectile. Several theories on penetration by armor-piercing projectiles have been proposed. These theories include:

- a. Penetration [29] of relatively thick plates by finding the work required to form a hole equal to that of the projectile. Plane stress was assumed.
- b. Penetration [29, 30] of relatively thin plates with appreciable thickening of the target material near the hole. Plane stress was assumed.
- c. Penetration [31, 32] of very thin plates which bend out of their plane as a result of projectile impact. Bending will not occur until the hole diameter is 7 to 10 times the thickness of the plate.
- d. Penetration [33 to 37] of thin plates which petal. The impacted section of the target takes the shape of the projectiles' surface while the non-impacted section remains undisturbed. This behavior can be attributed to the fact that the plastic waves do not have sufficient time to radiate any appreciable distance.
- e. Grimminger [38] assumed that the rigid projectile was slowed by a drag force (drag coefficient was assumed to be 1 for high Mach numbers) during the fluid phase of penetration, and estimated the remaining low velocity penetration with an empirical armor-penetration law.
- f. Bohn and Fuchs [39] also assumed a fluid drag (dynamic) force with an additional static force proportional to the Brinell hardness of the target material.
- g. Zaid [40, 41] considered that the shock waves in the projectile and target cannot propagate at high enough velocity to move from the projectile-target interface, and therefore, both can be regarded as rigid. Moreover, the rigid projectile is separated from the rigid target by a thin layer of an incompressible fluid, composed of both projectile and target materials. Penetration depends on the assumptions made.

A-2.2 Thermal Penetration. In the thermal penetration theories, it is assumed that penetration occurs via fusion and/or vaporization of the target by the energy released from the incident projectile. These theories include:

- a. Whipple [42] assumed that all the initial kinetic energy was converted into heat, and the crater was a right circular cone with a total apex angle of 60 degrees.
- b. A theory similar to Whipple's [42] was proposed by Langton [43], and four possible assumptions were considered.
 1. Neither projectile nor the target melt.
 2. The projectile melts.
 3. The target melts.
 4. Both projectile and target melt.
- c. McDermott, Canon, and Grow [44] assumed that the projectile did not melt or deform, but that a hole equal in diameter to the projectile formed in the target via fusion.
- d. The Lavrent'yev [45] analysis is idealized by considering the media to consist of a set of infinitesimally thin layers of incompressible material, which impact inelastically.

A-2.3 Explosive Impact. Stanyukovitch [46, 47] has proposed that crater formation due to high-velocity impact is similar to crater formation by high explosives. The pressure on the front of the shock wave caused by the impact drops sharply with increasing distance from the point of initiation, and the mechanism of cratering changes from vaporization to melting and pulverization of the material.

A-2.4 Hydrodynamic. It has been suggested [15, 48] that the pressures produced in high-velocity impact are so much greater than the shear strengths of the projectile and target that the shear strengths can be neglected, and the projectile and target can be considered as inviscid fluids. Based on this assumption, the resistance to penetration stems entirely from the inertial forces required to accelerate the target material.

- a. Bjork [15] integrated the two-dimensional equations of motion of a compressible inviscid fluid, together with an entropic equation of state of the solid material, that relates the internal energy, pressure, and specific volume, but neglects the shear strength of the material.
- b. In the theory proposed by Opik [49] in 1936, an allowance was made for the yield strength of the target material. The projectile is considered to be incompressible.
- c. Similar incompressible theories have been proposed [48, 50 and 51] to explain the penetration produced by a shaped-charge jet. The jet and target material are regarded as incompressible fluids.

A-3 IMPACT PHENOMENA RELATIVE TO VELOCITY. The impact of a spherical steel projectile (10,000 to 25,000 ft/sec) in a massive aluminum target is announced by a brilliant flash of light (Figure A-1). As the front of the sphere moves into the target, a spray of fine particles squirts (about twice the impact velocity) out the side. This is followed by a shock wave [52] which propagates from the point of impact, and compresses and accelerates the target material to make room for the onrushing sphere. Another wave backs up into the sphere, decelerates the projectile so that both the sphere and target materials move together along a common boundary. A crater starts to form, and as the target material flows radially from the point of impact, a hemispherical cavity forms. As the crater grows, the angle of the jet steepens, the velocity of the ejected particles decreases, and the sheath takes the shape of a flower petal.

During the process of crater formation the initial shock wave rushes ahead. The expanding crater follows close behind, and between the shock wave and the crater is a hemispherical shell of hot matter, which is simultaneously compressed by the shock wave and stretched by the expansion of the shell. The shock wave weakens as its volume of action increases and as it is overtaken by tension waves connecting free surfaces with the material moving away underneath.

The crater expands for a significant period of time after the impact and a considerable quantity of material is ejected from the crater. The material appears to be ejected by a mechanism of hydrodynamic flow along the walls of the crater. While the velocity of this ejected material is less than that of the impacting projectile, it is quite high, and represents a significant quantity of momentum.

Ultimately, the strength of the target material takes over and all fluid flow ceases. At this point, the craters' surface rebounds slightly as the elastic stresses in the main body of the target relax. The final volume is about fifteen percent less than the maximum reached before rebound.

There appear to be three regions of thick target cratering. These are the low velocity impact regions where the projectile remains intact, the transition region where the projectile undergoes major deformation or shattering, and the region of hypervelocity impact. Thus, a low velocity projectile does not lose its integrity on contact with a target, and will maintain its shape while forming a relatively deep narrow cavity of approximately the same diameter as the projectile. Penetration into a target material increases [52] steadily with the four-thirds power of the projectile velocity.

At some higher velocity, the projectile starts to deform and/or break into pieces. The velocity at which projectile fragmentation occurs depends on the mechanical properties of both the projectile and target. Charters [52] observed that tungsten carbide spheres with a velocity of about 1500 ft/sec started to fragment when impacting semi-infinite plates of lead. With velocities exceeding the 1500 ft/sec critical or transition point,

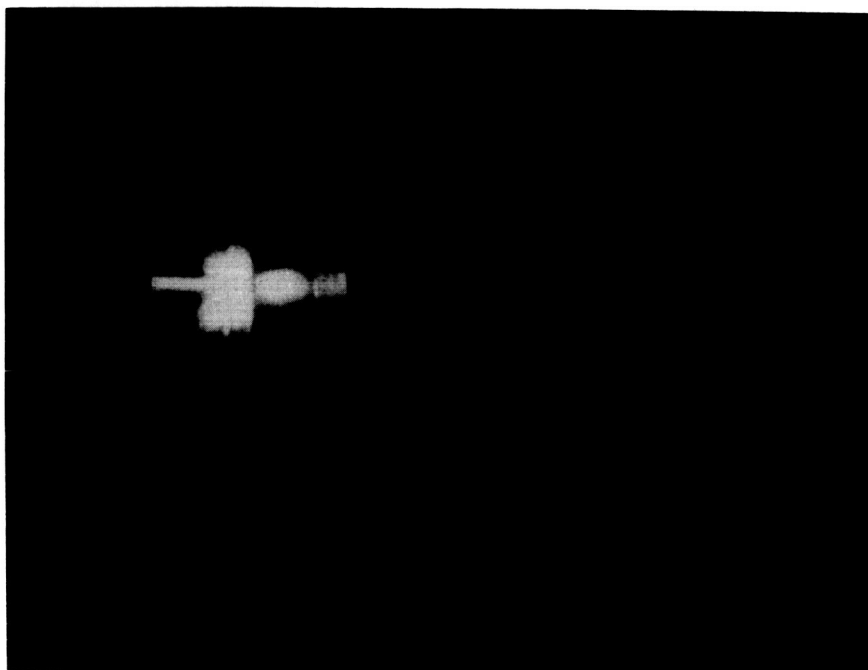


Figure A-1. Impact Flash

April 1962

a ductile projectile mushrooms in front (deforms as though it were trying to turn inside out). A brittle projectile will fragment into smaller pieces. Penetration will decrease slightly, pass through a minimum (Figure A-2), and then start to increase with increasing velocity. The crater widens and begins to approach a hemispherical shape, since the projectile has more kinetic energy to be utilized in increasing the crater volume rather than increasing the depth of penetration.

Under the experimental conditions reported by Charters, the crater becomes almost perfectly hemispherical at about 8000 ft/sec. At velocities greater than 8000 ft/sec, the depth of penetration (p) increases with increasing velocity (v) and, although the rate (dp/dv) is constant, it is less than in the unbroken projectile region. Penetration now varies with the two-thirds power of the velocity, and doubling the velocity will increase penetration by a factor of about 1.6. Charters points out that a transition zone has been crossed. This can be seen in Figure A-2 where the three impact regions are shown as: a) low velocity or unbroken projectile; b) medium velocity or transition; and c) high velocity or fluid behavior.

The ratio of p/d (target penetration divided by the projectile diameter) is shown [53] as a function of impact velocity in Figures A-3 and A-4. The projectile-target combination is given with each curve. All projectiles were spherical, with acceleration masses of 1.27 grams for aluminum, 2.009 grams for 0.25-inch diameter tungsten-carbide and 0.25 gram for the 0.125-inch diameter tungsten-carbide. The shattering of the projectile in the low-velocity region is evident, and this shattering results in an actual decrease in penetration. With increasing projectile fragmentation resulting from an increase in velocity, the depth of penetration increases. The slope of the curves (Figures A-2, A-3, and A-4) is much less after projectile break-up than it is for the unbroken projectile region of penetration.

In the early stages of impact in the high-velocity region, forces or stresses are set up which are considerably greater than the mechanical strength of either the projectile or target. Under these conditions, materials will behave as though they possess no strength. A material with little or no strength to resist a change in shape is a fluid, and it can be expected that both the projectile and target materials will flow under the stresses of impact and during the process of cavity formation as though they were fluids. The material in ductile metal targets continues to flow as a fluid throughout the entire cratering process. Around the crater circumference is a thin wall of metal resembling splashed-up material.

The preceding description of impact phenomenon on semi-infinite targets may be applied with certain restrictions (see following paragraph) to impact on thin plates. The principal differences being that, a thin plate does not afford the mass, depth, or time to permit a crater to form. Consequently, impact behavior and data on semi-infinite targets are not directly applicable to the thin plate structures from which the space vehicles will be fabricated.

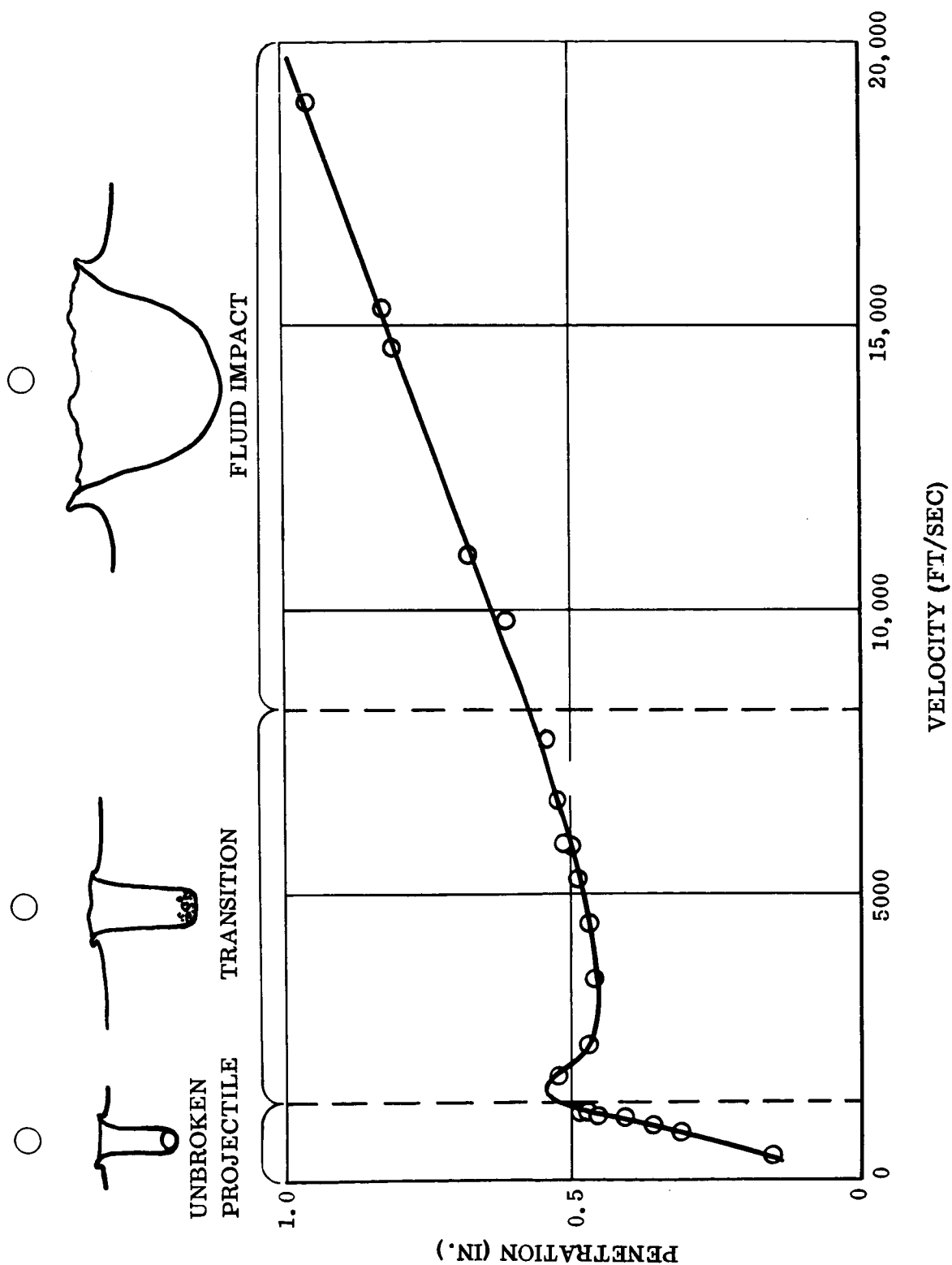


Figure A-2. The Effect of Velocity on Penetration [Ref 52]

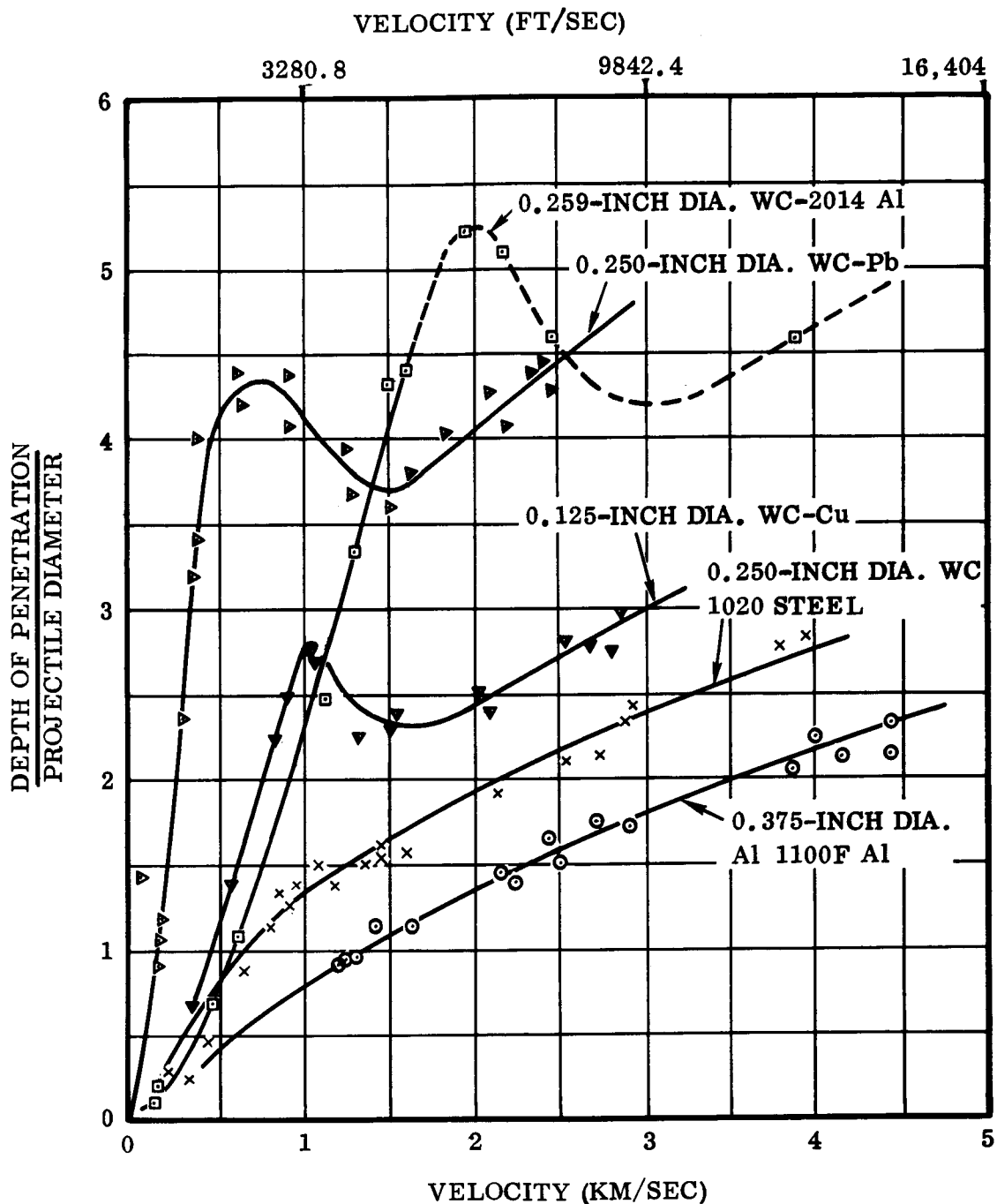


Figure A-3. Penetration into Thick Targets Divided by Projectile Diameter as Function of Velocity [Ref 53]

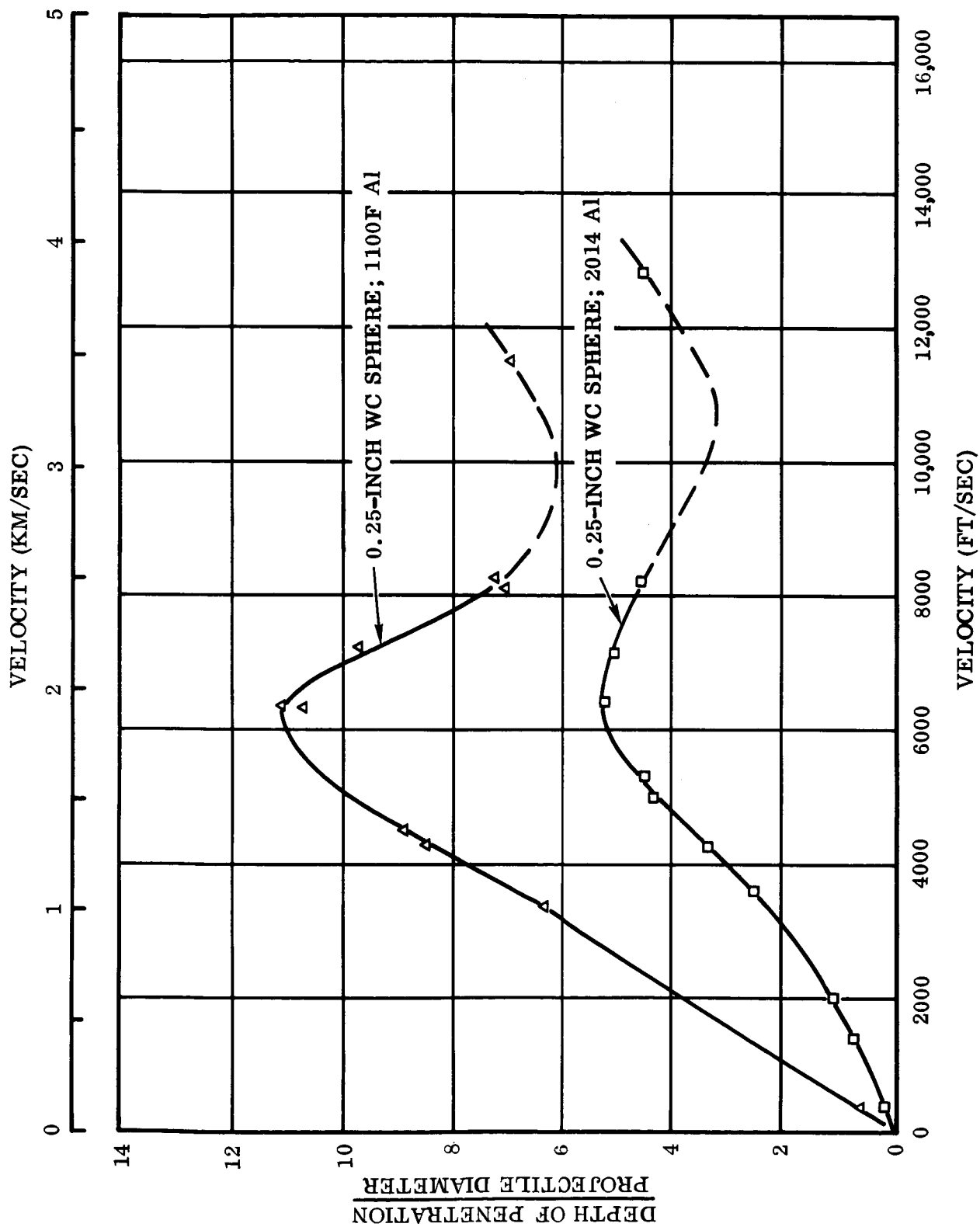


Figure A-4. Ratio of Crater Depth/Projectile Diameter Versus Velocity
for Two Types of Aluminum [Ref 53]

April 1962

The massive resistance, or thick shield approach to protection from meteoric particles, is prohibitively heavy and makes it imperative that attention be focused on other protection concepts.

It has been estimated [8] that a particle that penetrates a sheet may produce a hole with a radius as large as three times the particle radius. This leads to a hole of area,

$$a = 9 \pi \left(\frac{3m}{4\pi\rho_p} \right)^{2/3}$$

where

a = area

m = mass of particle

ρ_p = density of particle

If the crater formed is assumed to be hemispherical, the area of the target surface destroyed by the crater can be expressed by,

$$a = 2 \left(\frac{V}{h} - \frac{\pi h^2}{6} \right)$$

where

V = volume

a = area

h = depth of penetration

Broyles [8], quoting Bjork [14], estimated the area of material punched out (shear plug) by penetrating meteoric particles, and related the thickness (t)* of a sheet of material having density (ρ_t) penetrated by a particle of radius (r) and density (ρ_p) and striking at normal incidence with velocity (v) in km/sec. The equation is:

$$t = 8r \left(\frac{\rho_p}{\rho_t} \right)^{1/2} \left(\frac{v}{c} \right)^{1/3}$$

It should be noted that many empirical equations give a velocity dependence of the two-thirds power, but these experiments lie below velocities of 10,000 ft/sec. Bjork's formula is based on three calculations made with two-dimensional hydrodynamics, and

*This minimum thickness is required for the particle to just penetrate the sheet material.

April 1962

with cylindrical iron projectiles striking iron targets, and aluminum projectiles striking aluminum targets, at velocities ranging from 9842 ft/sec to 229,658 ft/sec. He has been able to compare his formulae with experiment (Figure A-5) at a velocity of 22,211 ft/sec and gets very good agreement. The two formulae are:

$$\text{Al on Al: } p = 0.429 (mv)^{1/3}$$

$$\text{Fe on Fe: } p = 0.238 (mv)^{1/3}$$

where

p = penetration depth in inches into a semi-infinite plate

m = mass in grams

v = velocity* in km/sec

The shaded area and the $v^{1/3}$ line in Figure A-5 can be compared to the arbitrarily placed $v^{2/3}$ line.

Summers [54] observed that, for the same particle mass, the penetration depth varies inversely proportional as the $1/3$ power of the density of the impacting particle. This would give, for iron impinging on aluminum,

$$p = 0.606 (mv)^{1/3}$$

Theory and experimental data indicate that a thin plate, which is $1.5p$ inches thick, would be punctured by a meteoric particle which would form a crater " p " inches deep in a thick plate. This results in the equation for iron impinging on aluminum,

$$t = 0.909 (mv)^{1/3}$$

where " t " is the thickness in inches of a plate which would be penetrated by a meteoric particle of mass (m) in grams.

In 1946 Whipple [6] postulated that a very thin shield or meteoroid bumper surrounding a vehicle would efficiently reduce meteoric particle impact damage. This postulate was based on the assumption that impact with the bumper would cause the meteoroid to break up (fragment and/or vaporize), and these smaller particles of solid or fluid would be spread over a large area of the vehicle surface. This fragmentation would greatly reduce the penetration at any particular location, since the particle mass and velocity would be distributed over a greater area; i. e., momentum per-unit-area would be significantly smaller.

*One km/sec is equivalent to 3280.83 ft/sec.

April 1962

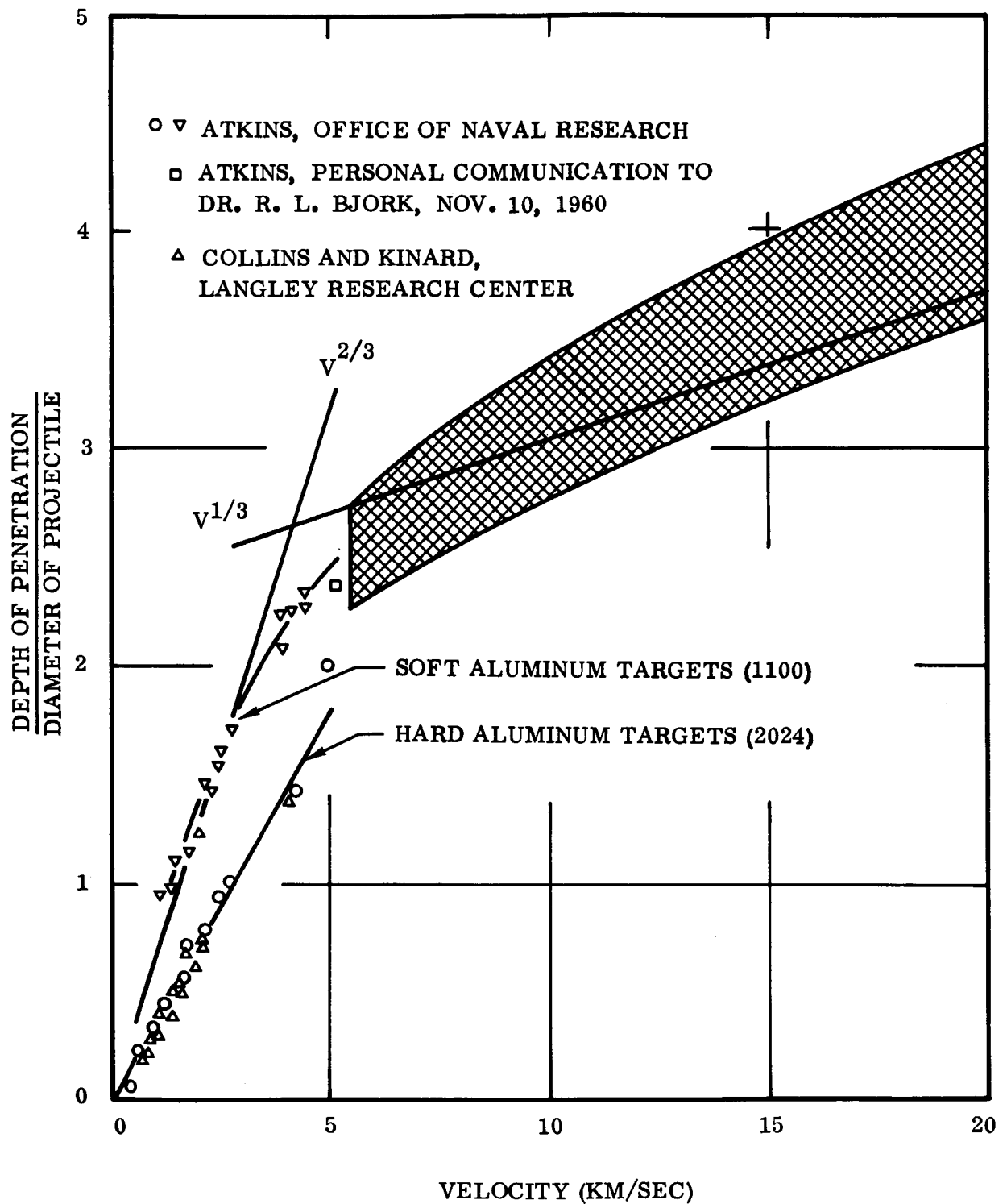


Figure A-5. Aluminum Impact on Aluminum [Ref 4]

The Whipple meteoroid bumper concept has been under investigation. Willig and Semon [55] fired several preliminary shots at aluminum (2024) shields at 15,000 ft/sec. The 0.240-inch long by 0.250-inch diameter aluminum pellet produced, in the thick aluminum plate, a cavity almost an inch in diameter and a half-inch deep. However, impact from a similar projectile on an aluminum target protected by a 0.250-inch thick aluminum 2024 plate spaced: 1) 1 inch; and 2) 0.125 inch from the target, showed that the target was not penetrated, although severely pocked.

Funkhouser [56] related the total penetration (bumper plus target) to the projectile velocity before impact with the bumper (Figure A-6). Velocities up to about 11,000 ft/sec were attained with 0.062-inch diameter (0.0183 gram) copper spheres. The aluminum (2024-T4) bumper spacing and thickness was held at one inch and 0.031 inch, respectively. The broken line in Figure A-6 represents the general penetration data [57] for a semi-infinite unprotected target, and is valid to velocities of 20,000 ft/sec. Impact data with the bumper (solid line) show greater penetration [58] than for the unprotected target, at projectile velocities less than 6,000 ft/sec, and less penetration for projectile velocities greater than 6,000 ft/sec. This can be attributed to the partial breakup of the projectile in impact with the bumper. In the velocity region between 8,000 and 9,000 ft/sec, the projectile completely fragments, as evidenced by the sharp change in slope. For the velocity range covered by Funkhouser, the slope of the penetration data for the target plus bumper is only about one-twelfth the slope of the penetration data for the unprotected target in the region after target breakup. At 11,000 ft/sec, total penetration with the bumper combination is less than half that of the quasi-infinite target with no bumper.

A-4 PENETRATION DEPENDENCE ON BUMPER THICKNESS. Funkhouser [56] studied the relationship between total penetration and bumper thickness. The thickness of the aluminum bumper was varied from 0.001 inch to 1 inch, while the bumper spacing was held constant at 1 inch with a projectile velocity of $11,500 \pm 1,000$ ft/sec. Total penetration was approximately constant with 0.001- to 0.01-inch thick bumpers. Projectile disintegration occurred with a bumper thickness somewhere between 0.01 and 0.02 inch as evidenced by the change in slope in Figure A-7. With a further increase in bumper thickness, total penetration increases to a maximum, and at this point (~ 0.25 inch), the bumper will not be penetrated and will function as the target.

Beyond this maximum, the total penetration decreases as the bumper, due to its thickness, begins to behave as a semi-infinite target. Similar results [59] have been obtained in the study of 0.125-inch steel (0.133 gram) and lead (0.188 gram) projectiles impacting at 8400 ft/sec on lead, and these data are also given in Figure A-7. The difference in minimum penetration between the lead and aluminum bumpers and targets can be attributed to dissimilarities in bumper materials and spacing, as well as projectile velocity, mass, size, and material. Even with these variations, the general trend and importance of the bumper thickness with respect to total penetration damage

April 1962

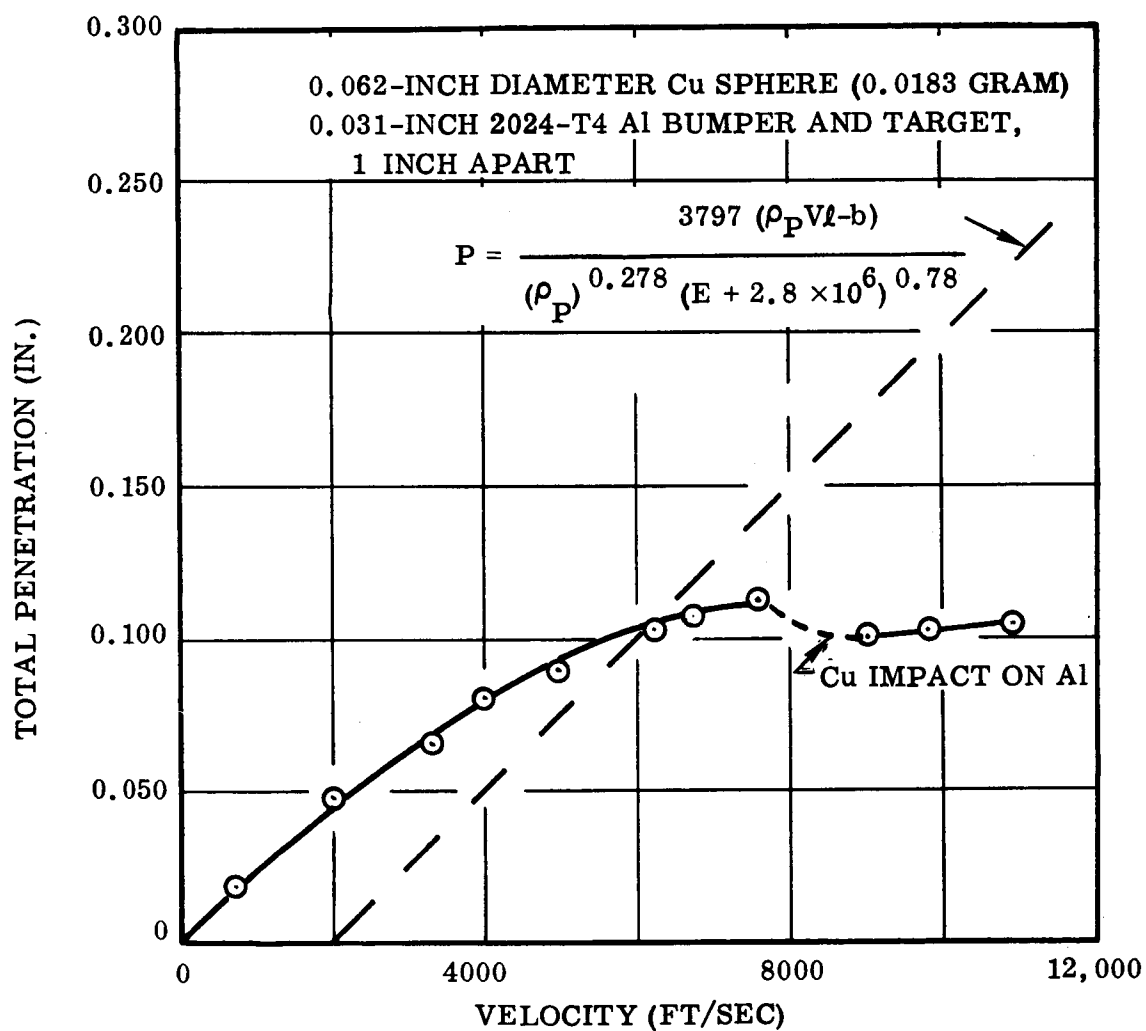


Figure A-6. Total Penetration Versus Impact Velocity [Ref 56]

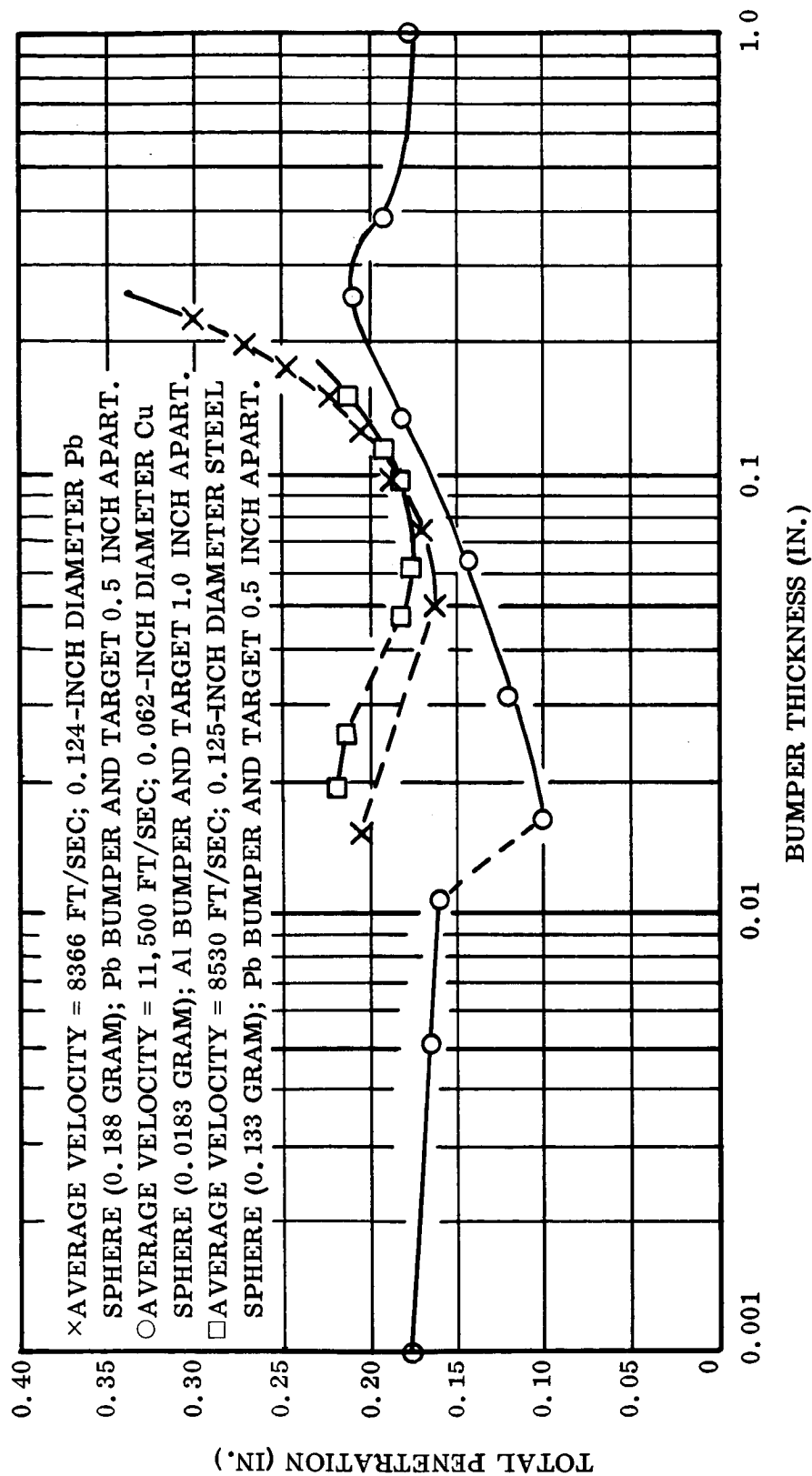


Figure A-7. Total Penetration Versus Bumper Thickness [Ref 56 and 59]

is obvious. There is a bumper thickness below which there is very little decrease in penetration, a thickness which is optimum under the experimental conditions, and a bumper which is so thick that it behaves as the target.

A-5 PENETRATION DEPENDENCE ON BUMPER SPACING. Figure A-8 shows the dependence of the total penetration on the distance between the bumper and target. The spacing of the bumper in front of the target surface was varied: a) from zero to 6 inches with a constant aluminum bumper [56] thickness of 0.031 inch, and projectile mass and velocity of 0.0183 gram and 12,000 ft/sec, respectively; and b) from 0.25 to 1.49 inch with a constant lead bumper [59] thickness of 0.054 inch, and projectile mass and velocity of 0.188 grams and 8366 ft/sec, respectively. There is a rapid decrease in total penetration in aluminum from zero spacing to a spacing of 2 inches; and with greater distances the total penetration is almost constant. The decrease in total penetration in lead with a 0.50-inch spacing is even more pronounced than with aluminum.

A-6 ANGLE OF FRAGMENT DISPERSION. Lull [60] equated the excess kinetic energy to the spherical, radial expansion of the projectile fragments. This indicated that the half angle of spray (θ) is a function of only the shield thickness and is independent of the distance between the plates. The predicted [60] solid angle variation (curve in Figure A-9) can be compared to the angles measured [59] from the crater diameters of the constant lead shield separation data.

A-7 HOLE DIAMETER. Olshaker [59] reported the dependence of the diameter of the hole in a lead target to the thickness of the lead bumper (Figures A-10 and A-11). Projectile velocities of 8400 ft/sec were obtained with 0.125-inch diameter steel and lead spheres. At low velocities, there was very little difference in the hole diameter formed with the steel or lead projectile. However, at higher velocities, the heavier lead (0.188-gram lead and 0.133-gram steel) produced a larger hole.

Collins and Kinard [61] observed (Figure A-12) that the ratio of crater diameter to projectile diameter in semi-infinite aluminum targets could be correlated to the impact velocity. It appears that the diameter ratio increases with increasing velocity and is independent of projectile size or configuration.

A-8 DEPENDENCE ON INCIDENCE. * Identical projectiles impacting the surface of identical semi-infinite target plates at equal velocities, hit with varying angle-of-incidence, will result in a decrease of crater volume with an increase in the angle-of-incidence [54, 62]. Nearly hemispherical craters are also formed in oblique impact up to some critical angle. Beyond the critical angle, the crater becomes asymmetrical,

*Angle-of-incidence is defined as the angle between the trajectory of the projectile and a perpendicular to the plane of the target at the point of impact.

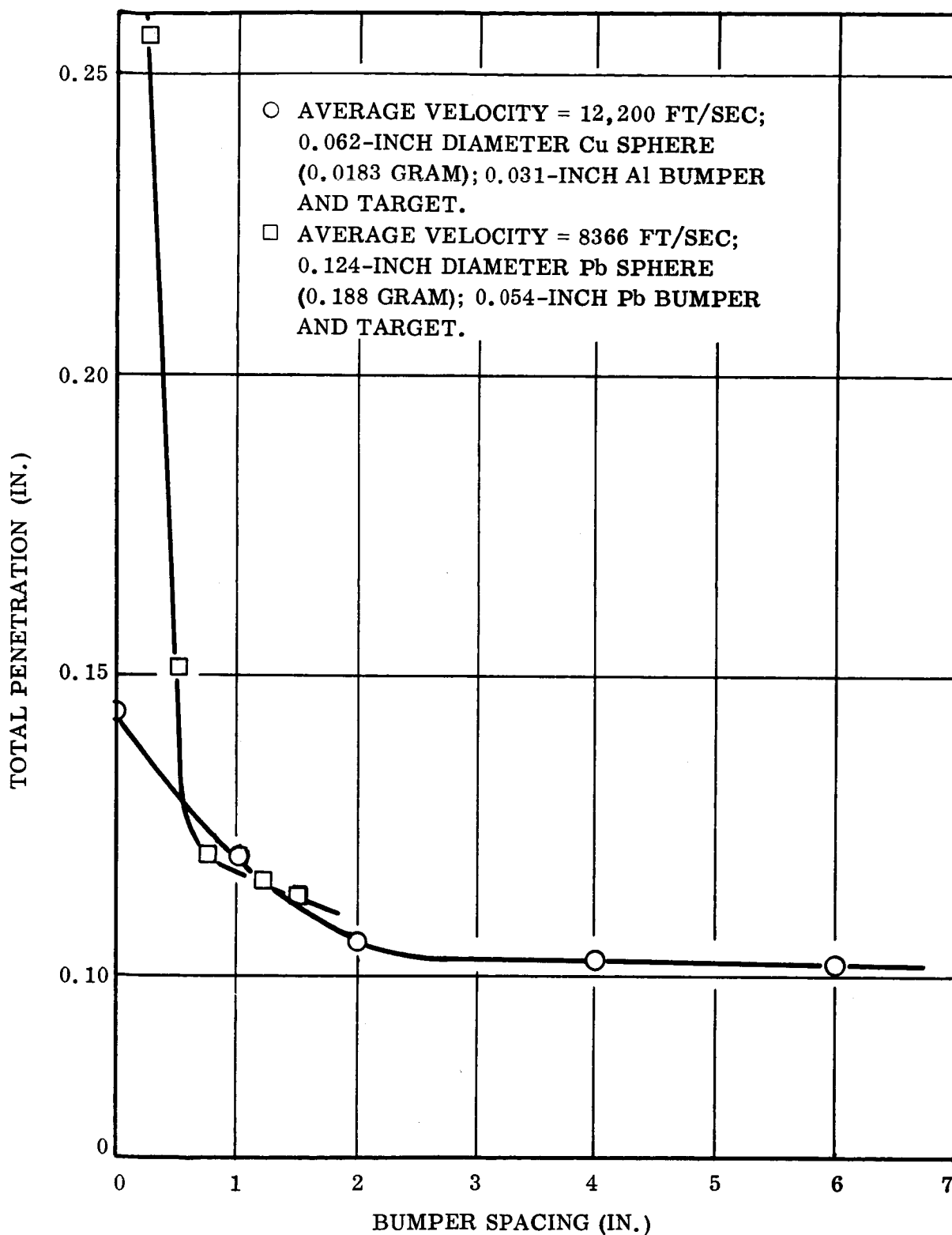


Figure A-8. Dependence of Total Penetration on Bumper Spacing [Ref 56 and 59]

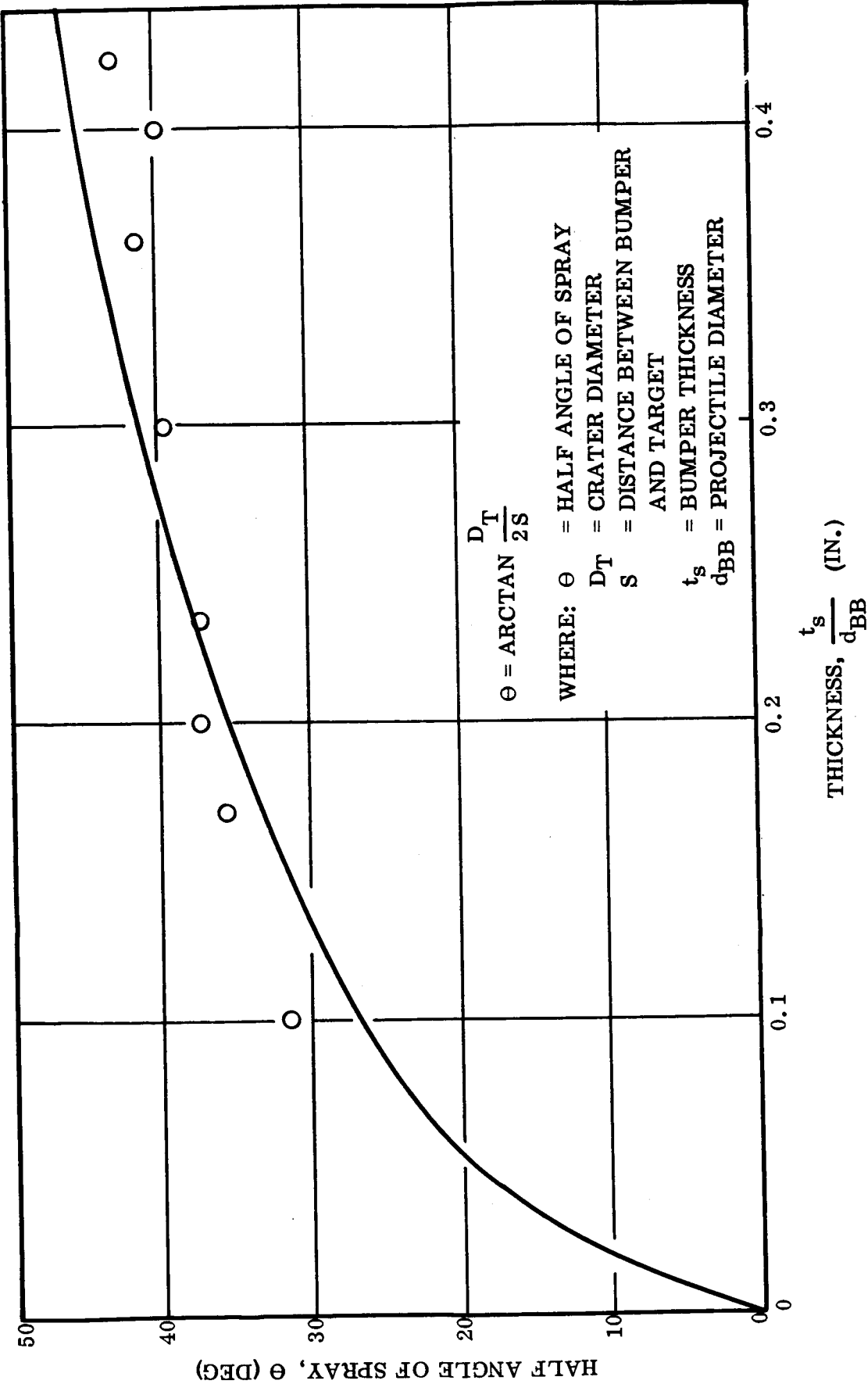


Figure A-9. Half Angle of Spray Dependence on Target Thickness [Ref 59]

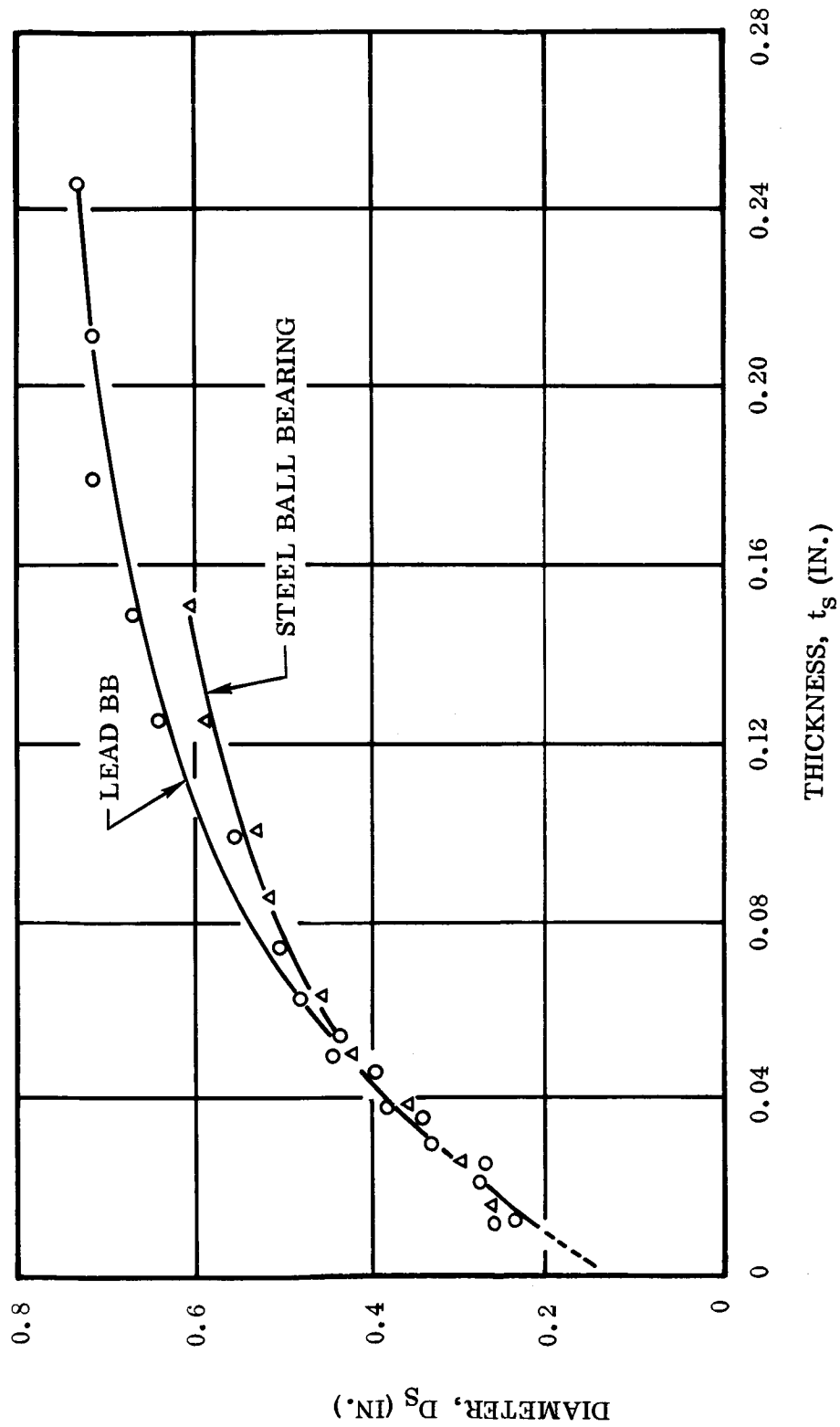


Figure A-10. Bumper Hole Diameter Versus Bumper Thickness [Ref 59]

April 1962

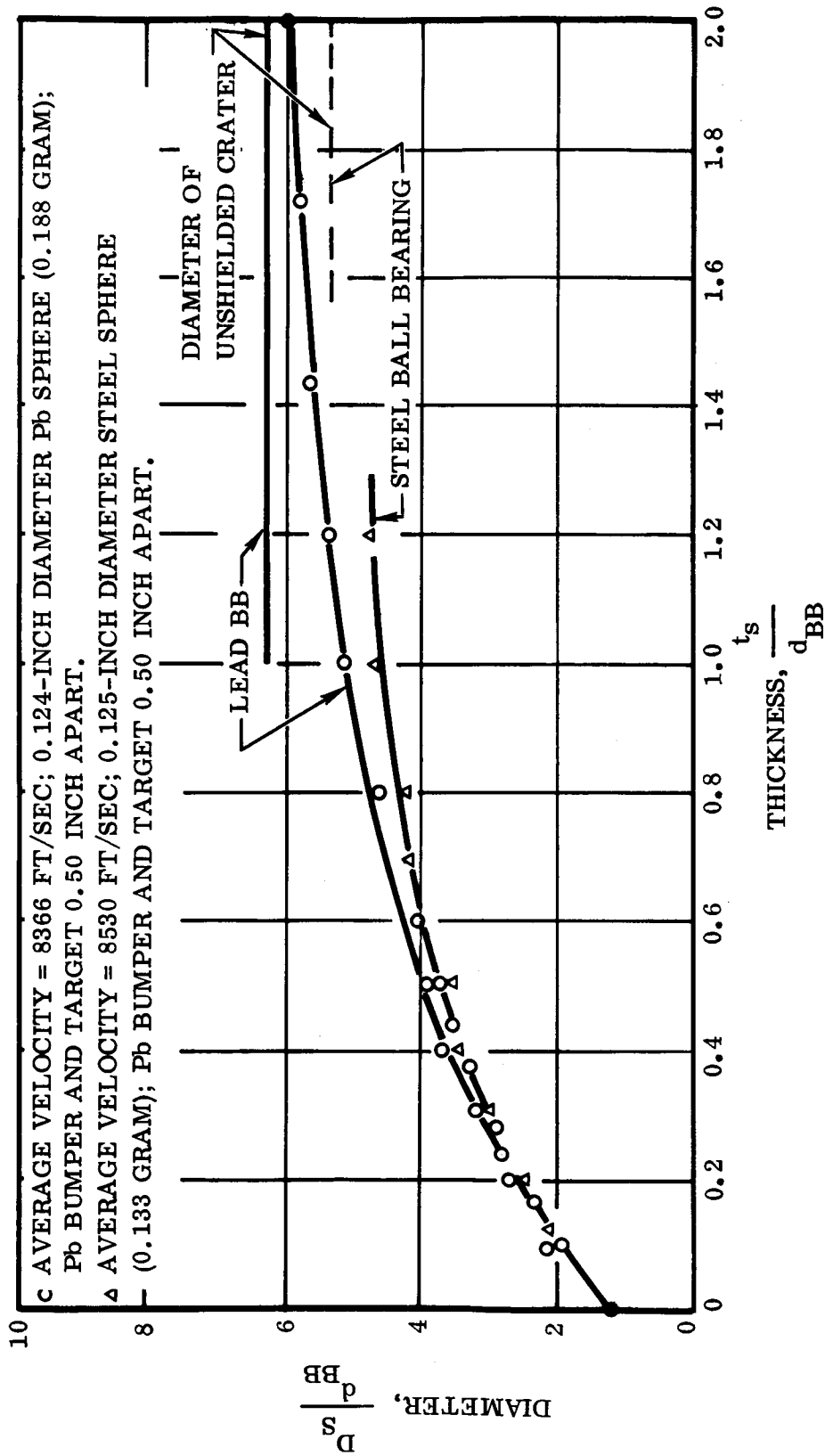


Figure A-11. Diameter Ratio to Thickness Ratio [Ref 59]

April 1962

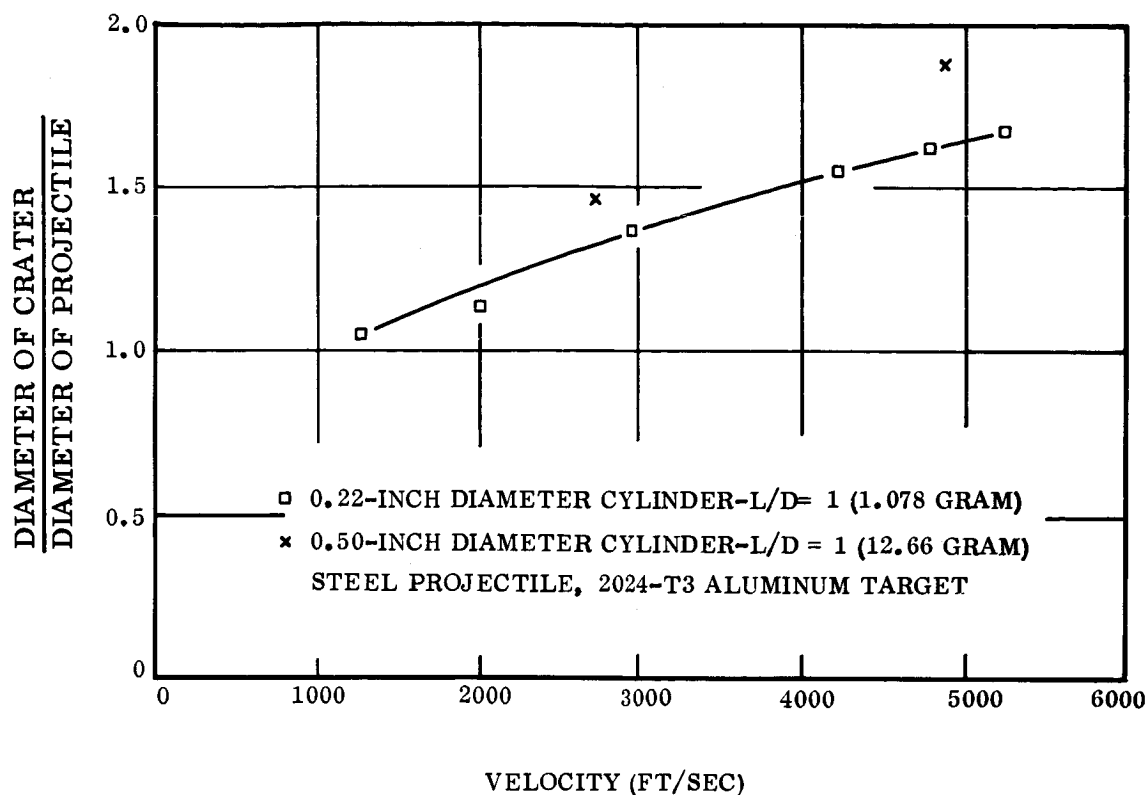


Figure A-12. Crater Diameter Dependence on Velocity [Ref 61]

with greater depth and steeper sides towards the direction from which the projectile approached. At grazing incidence, the crater becomes very elongated and the projectile ricochets.

Partridge [63] plotted the volume of the crater against the square of the cosine of the angle-of-incidence ($\cos^2 \theta$), as shown in Figure A-13. The quantities are directly proportional, as expected, since $\cos^2 \theta$ is proportional to the vertical component of the energy of the impacting particle.

Halperson and Fuller* [64] also studied the effect of the angle-of-incidence on the penetration of thin metal plates. A 0.25-inch aluminum (5052) plate was struck at an angle of 10° from the plane of the plate, by a cylindrical aluminum projectile (0.2 gram). The measured penetration was compared with that calculated by the semi-empirical penetration equation.

$$p = \left(\frac{3}{4\pi K} \right)^{1/3} m^{1/3} (v \sin \theta)^{2/3}$$

* Halperson and Fuller measured their angles from the plane of the target, consequently, their measured angles must be subtracted from 90° to obtain values for the angle-of-incidence.

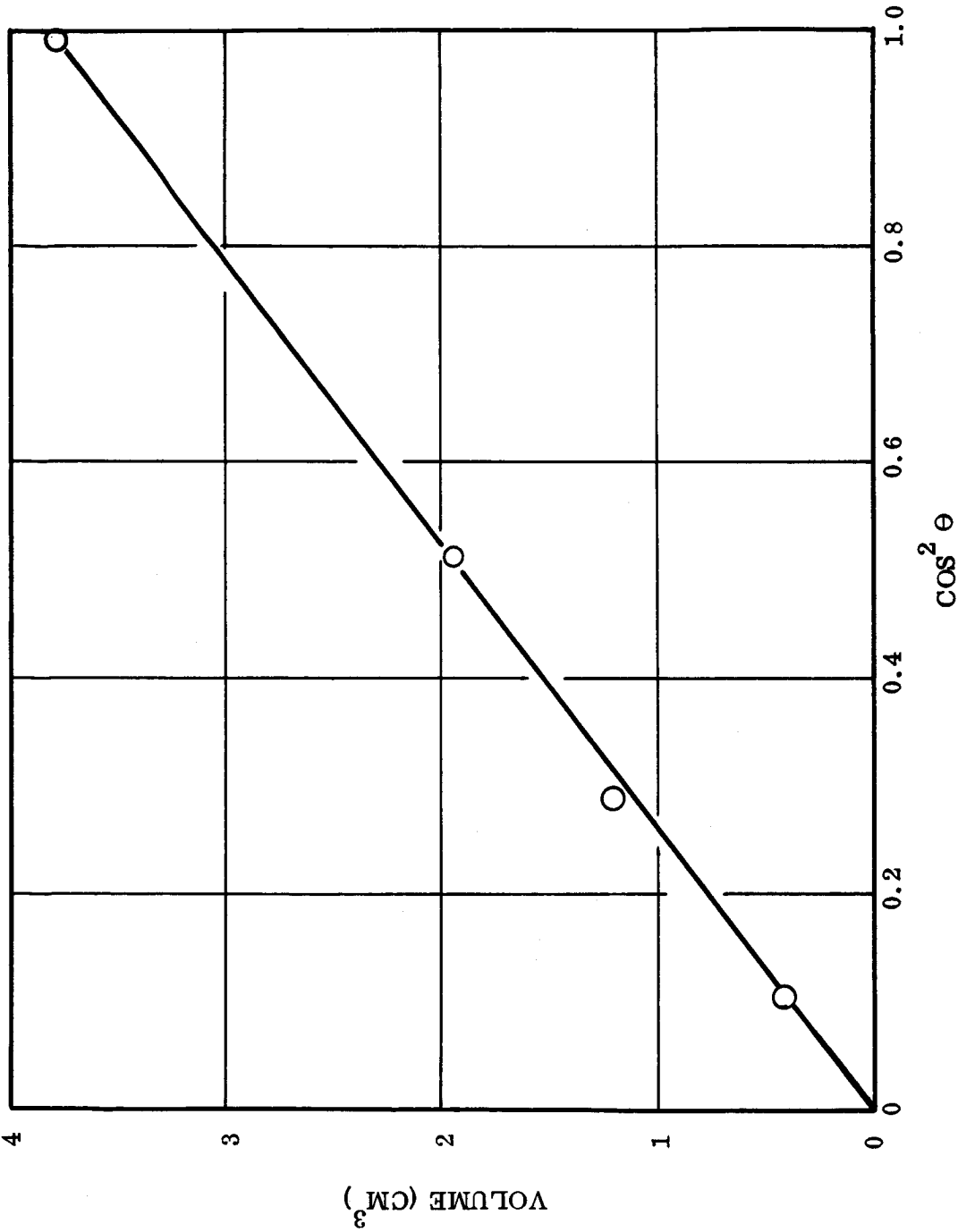


Figure A-13. Crater Volume Plotted Against the Cosine Square of the Angle-of-Incidence [Ref 63]

where K is the energy-per-unit volume (E/V) for the projectile-target combination, m is the projectile mass, v the impact velocity, and θ the angle of its obliquity to the plane of the target. This equation is based [53] on the formation of a hemispherical crater with a constant impact energy-per-unit volume. Hemispherical craters are usually formed in metal targets, even at small angles, if the velocity component normal to the target is in the hypervelocity region [65]. A K value of 680 joules/cc was used for 5052 aluminum. This value was obtained [64] from the measurement of the Brinell Hardness Number and use of the Feldman relation [66]. It has been shown that frictional effects and variations in aluminum projectile shear-out can cause up to a 50 percent decrease of fragment mass. Therefore, penetrations of 0.4 and 0.5 cm were calculated for 0.1- and 0.2-gram projectiles, respectively. The measured penetration was 0.34 cm, which results in an error of between 15 and 32 percent. The observed crater was not hemispherical, as expected, since the normal velocity component was only 4462 ft/sec.

Kineke [67] fired cylinders of (0.50 inch diameter by 0.04 inch thick) steel projectiles into lead targets. Impact velocity was 16,400 ft/sec and the data are shown in Figure A-14. Summers [54] fired 0.125-inch diameter copper spheres into semi-infinite copper targets. Since the normal component of velocity also decreased with an increase in the angle-of-incidence, the data were reduced by measuring the penetration normal to the target surface, and computing the impact Mach number from the component of velocity normal to the target surface. The velocity component parallel to the target surface was assumed to contribute nothing to the target penetration. Oblique * penetration data are compared with the normal penetration data in Figures A-15 and A-16. The normal penetration data were obtained by varying the projectile velocity, and the oblique penetration data were obtained by varying the angle-of-incidence with a constant projectile velocity of 7,000 ft/sec in one case, and 11,000 ft/sec in the other. For the lower velocity, the targets were of hard copper; for the higher velocity, the targets were of soft copper. It can be seen that for both impact velocities, the oblique penetration correlates well with the normal penetration to a value for the angle-of-incidence as great as 50° for the higher impact velocity. Summers [54] suggested that if the impacting body has a very high velocity, the crater formed will be hemispherical** regardless of the angle-of-impact. The oblique impact data departs from the normal impact data at about the same critical angle at which the crater ceases to be hemispherical.

A-9 DEPENDENCE ON TEMPERATURE. The importance of temperature on material behavior during impact has been investigated with relatively thick targets; i.e., cratering, rather than complete penetration. Although impact behavior of thin plates is required, available data on thick plates can be used to give a relative indication of

* Angle of obliquity refers to any acute angle which may or may not be equal to the angle-of-incidence.

** This may be true for moderately high bulk densities; but particles with a density of about 2.8 g/cc, with a bulk density of about 0.05 g/cc, may form a large diameter and shallow crater.

April 1962

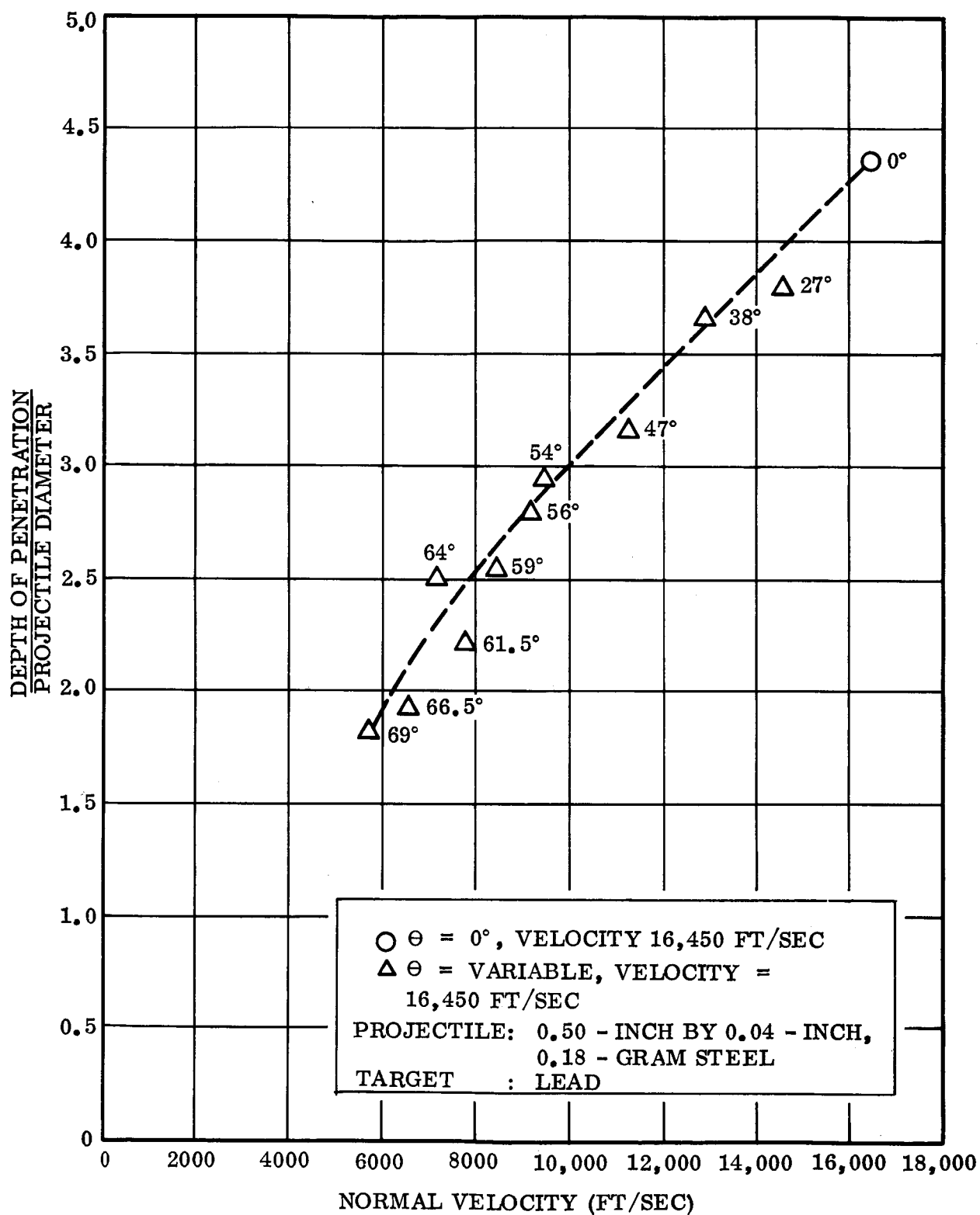
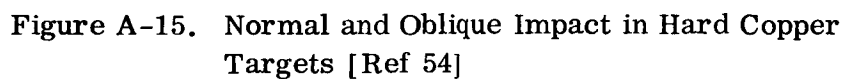
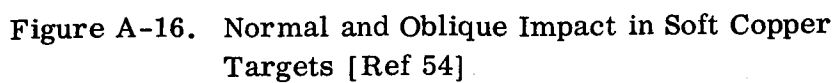


Figure A-14. Normal and Oblique Impact in Lead Targets [Ref 67]





the magnitude and importance of target temperature. Allison, Becker, and Vitali [68] studied the impact behavior of copper (300° to 873° K), lead (77° to 550° K), cadmium (77° to 425° K), and zinc (77° to 650° K); the data are summarized in Figure A-17. The velocity of the 0.18-gram steel fragment was 16,440 ft/sec.

The crater diameter in lead was observed to increase linearly over the temperature range of 77° to 550° K. Due to this linear change in which lead behaves in a ductile fashion at all temperatures, the crater dimension could be correlated with any one of a large number of physical properties that also vary linearly with temperature. Crater volumes in copper targets appear to be independent of temperature, at both the highest and lowest temperature studied, and indicate a dependence on the softening or annealing temperature as shown in Figure A-18. The crater volumes for both zinc and cadmium are given in Figure A-17, and in the case of zinc, the impact behavior has been correlated with the brittle to ductile transition (Figure A-19).

The transition temperature depends on the rate of strain; a higher transition temperature being associated with a higher strain rate. Since the strain rate varies over such a wide range during crater formation, the transition region will be very broad, perhaps several hundred degrees centigrade. Therefore, Allison, Becker, and Vitali [68] concluded that zinc behaves in a brittle fashion below 42° C, and in a ductile fashion above 300° C, with the intermediate range representing a mixture of brittle and ductile behavior depending on the local rate of strain. From these studies, it can be seen that the cratering process is a complex phenomenon in which the bulk mechanical and metallurgical properties play an important role. Their importance arises from the fact that a true hydrodynamic situation, in which the densities and velocities are primary variables, exists during a very small fraction of the time required to form the entire crater.

A-10 TARGET STRENGTH. Summers [54] observed that the influence of target strength (semi-infinite targets) is greatly diminished at the impact velocity of 4,000 ft/sec, since the penetration of a copper projectile in a soft copper target is about 25 percent greater than that in the hard target. The impacts at this velocity are in the transition zone, or at the beginning of the fluid impact region (Figure A-2). With a further increase in impact velocity, the effect of target strength continues to lessen, and at 10,000 ft/sec, the penetration in the soft copper is 12 percent greater than that in the hard copper. Impact at this velocity is in the fluid impact region. Extrapolation of the observed data indicates that penetration would be affected very little by target strength at velocities of the order of 20,000 ft/sec.

Collins and Kinard [61] observed that the penetration of high velocity (up to 11,000 ft/sec) metal projectiles of aluminum, copper, lead, and steel into aluminum, copper,

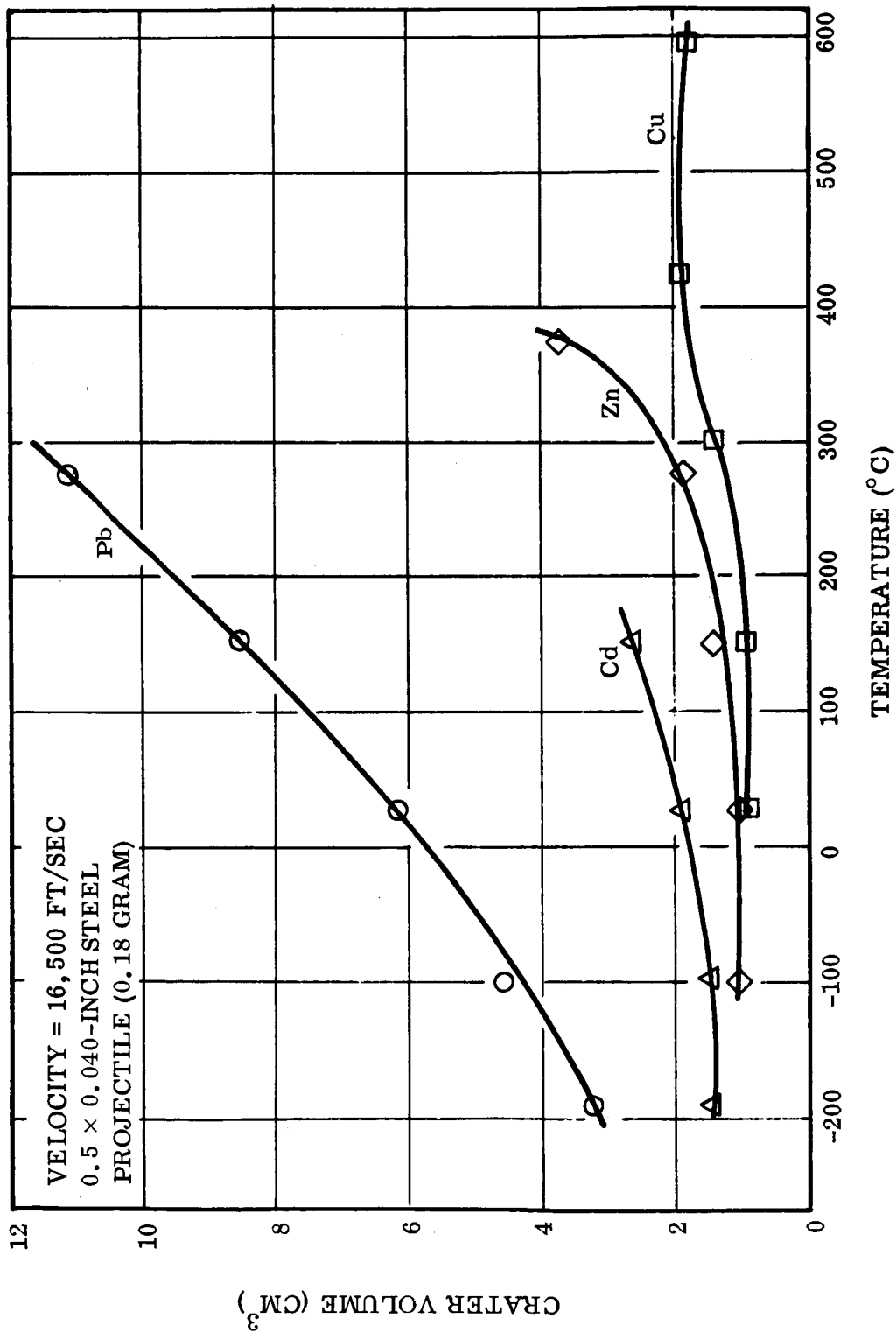


Figure A-17. Effect of Temperature on Crater Volume [Ref 68]

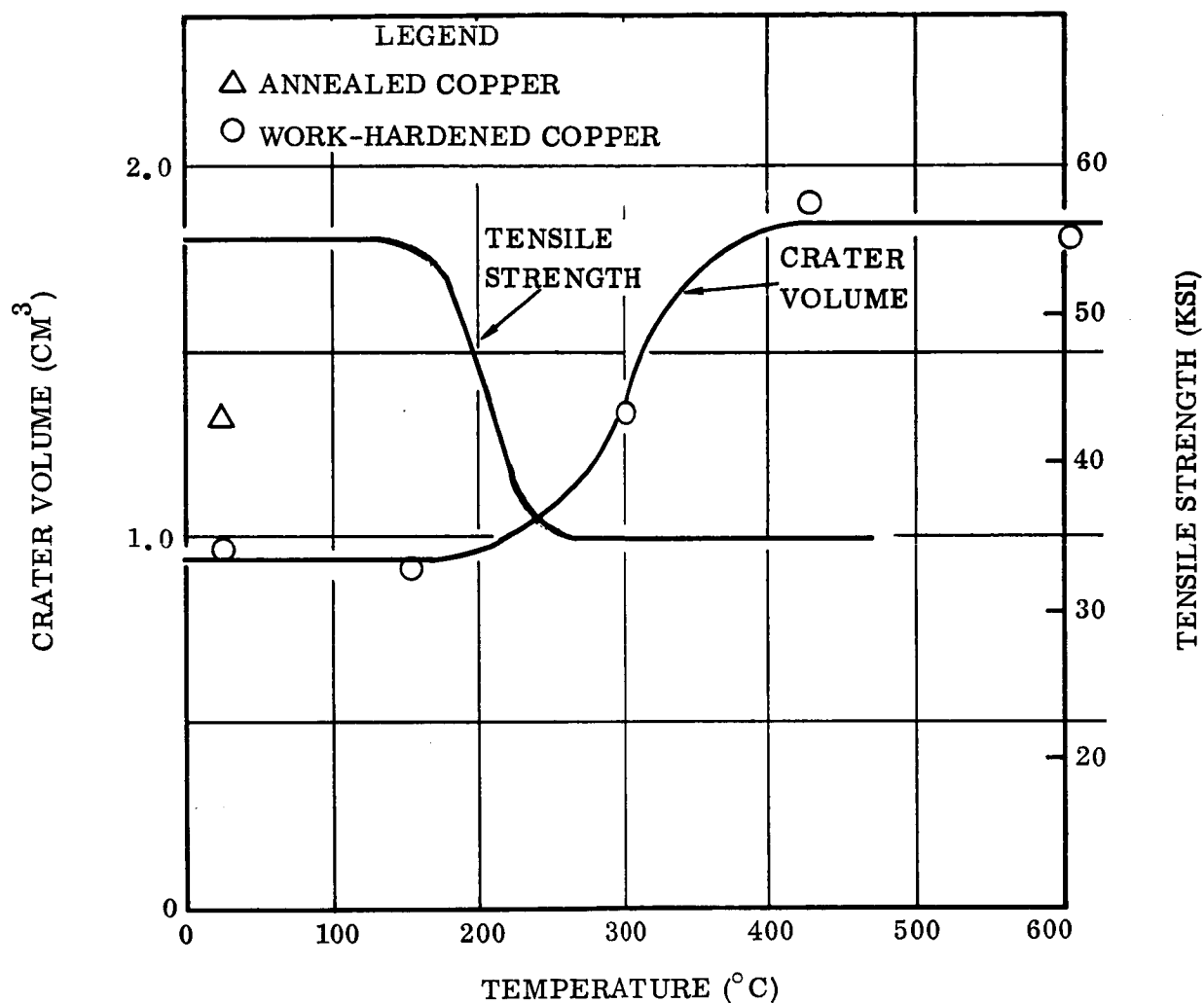


Figure A-18. Comparison of Crater Volume With Temperature and Tensile Strength With Annealing Temperature [Ref 68]

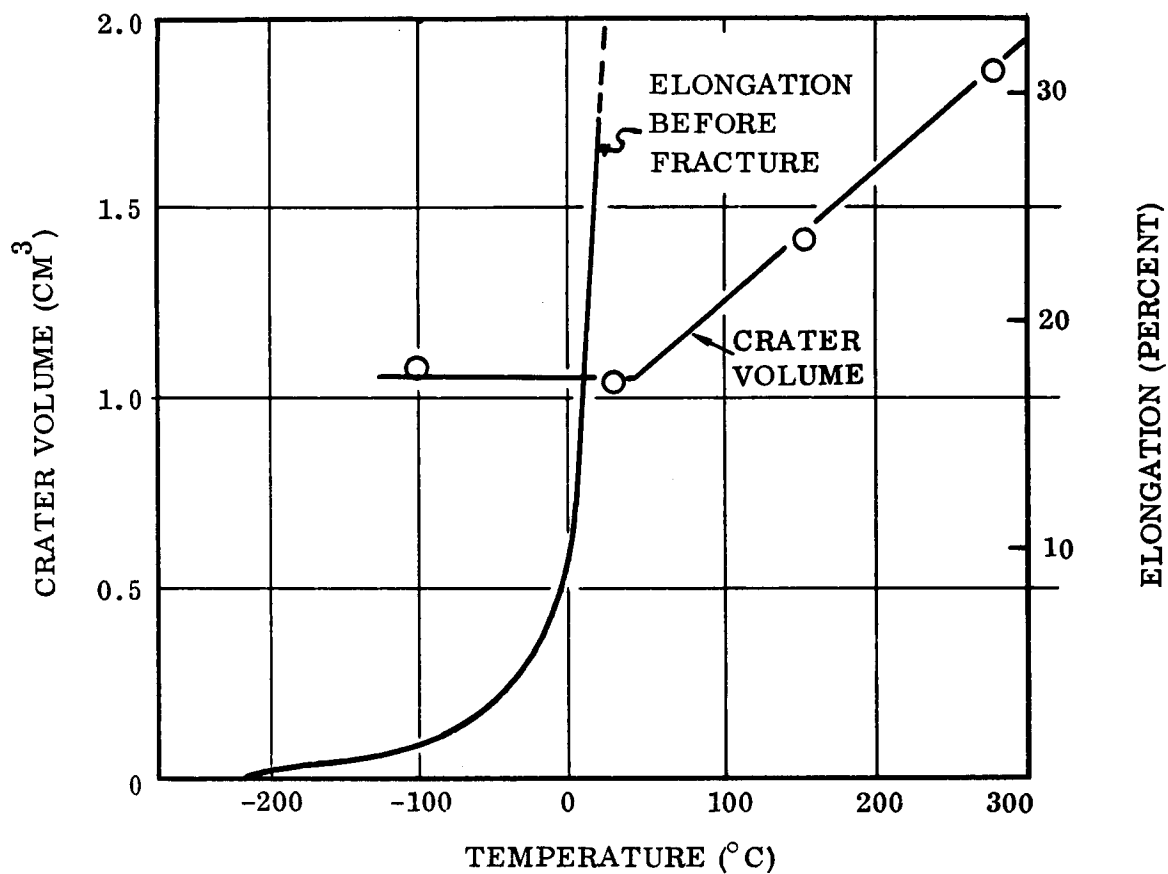


Figure A-19. Comparison Between Crater Volume Temperature and the Elongation of Zinc Before Fracture [Ref 68]

April 1962

and steel targets, could be correlated* as a function of the maximum momentum per-unit-area of the projectile, by the equation,

$$p = (\rho_p vL) = \frac{\text{lb. -sec.}}{\text{in.}^2}$$

where

p = penetration, inches

ρ_p = mass density, slugs in.⁻³

v = projectile velocity, ft/sec

L = maximum length of projectile normal to the point of impact

In order to produce permanent penetration, enough momentum must be available in the $\rho_p vL$ parameter to exceed the elastic limit of the target material.

If the physical properties (except density) of the projectile-target combination are unimportant during the entire penetration process, the curves of P/d versus velocity (i.e., Figures A-3 and A-4) should merge into one. However, if strength properties of the target material are important, as might be the case in the latter stages of crater formation, these curves will not converge.

A-11 DENSITY

A-11.1 Projectile. Palmer, et al. [69], observed that the crater volume in lead was proportional to projectile energy with velocities up to 2.5 km/sec (8202.1 ft/sec). There was, however, a considerable difference in the value of V/E when comparing different projectile materials, and V/E is approximately proportional (Figure A-20) to the square root of projectile density.

Penetration in semi-infinite slabs is directly affected [61] by the density of the projectile. For an equivalent momentum per-unit-area, the maximum penetration will be obtained by the lowest density projectile, and will decrease in the order of increasing density. If a material is desired for optimum design of projectiles of a fixed diameter, such that the projectile can achieve the maximum penetration per projectile weight, it appears that the lowest density material should be used.

If the material comprising the projectile is less dense than that of the target, the crater has the appearance of a broad but shallow spherical segment. When the material

*The lead targets produced a nonlinear curve of penetration plotted against momentum per-unit-area.

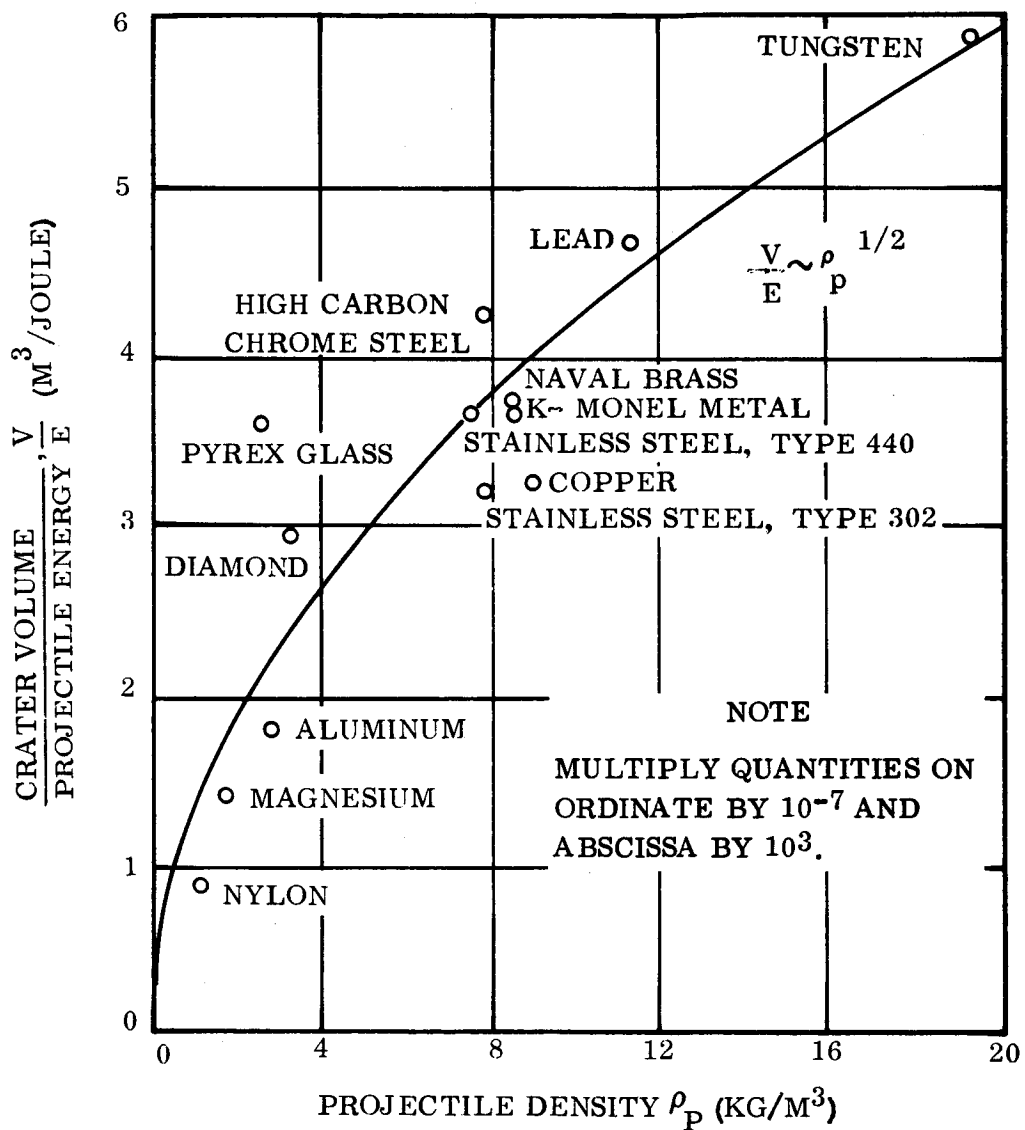


Figure A-20. Crater Volume Per-Unit-Projectile Energy Versus Projectile Density for Impact into Lead [Ref 69]

comprising the projectile is more dense than that of the target, the cavity has a deep penetration compared to the crater radius at the target surface.

A-11.2 Target. Palmer, et al. [69], observed that projectile fragmentation can be used as a measure of the maximum pressure produced in the impact. If the stagnation pressure (P_s) on the projectile is assumed to be given by the Bernoulli equation ($P_s = 1/2\rho_T v^2$), where ρ_T is the target density and v is the impact velocity, then P_s is almost equal to 574,000 lb/in.² for all cases. This can be seen in Figure A-21, where v is plotted against ρ_T for the point of projectile break-up in each target material. The stagnation pressure (P_s) at break-up is twice the value of 287,000, given by the manufacturer of the ball bearing projectiles. There are several possible explanations why the stagnation pressure is not the same as the ultimate stress of the steel projectile. One is that the stagnation pressure for flow in a metal may not be given exactly by Bernoulli's equation. Another is that the ultimate stress of the steel is increased under the dynamic conditions of cratering. A third possibility is that geometric configuration of the steel ball increases the ultimate strength over that measured by conventional methods in testing machines.

A-12 KINETIC ENERGY. The crater volumes were found [61] to be a linear function of the total kinetic energy possessed by the projectile; the largest craters formed in semi-infinite target materials having the lowest strength, and the lowest speed of sound.

Charters and Locke [70] related the crater volume and projectile kinetic energy ($1/2mv^2$) by assuming that the target crater was hemispherical, with a radius equal to the penetration (p). This results in the equation,

$$\left(\frac{\rho_T c^2}{2}\right) \left(\frac{2}{3} \pi p^3\right) = k \left(\frac{\rho_P}{\rho_T}\right) \left(\frac{mv^2}{2}\right)$$

where

$$\frac{2}{3} \pi p^3 = \text{crater volume}$$

c = speed of sound in the target material; the velocity of propagation of a plane longitudinal wave in a slender prismatic bar

ρ = mass density

T = target

P = projectile

E = kinetic energy.

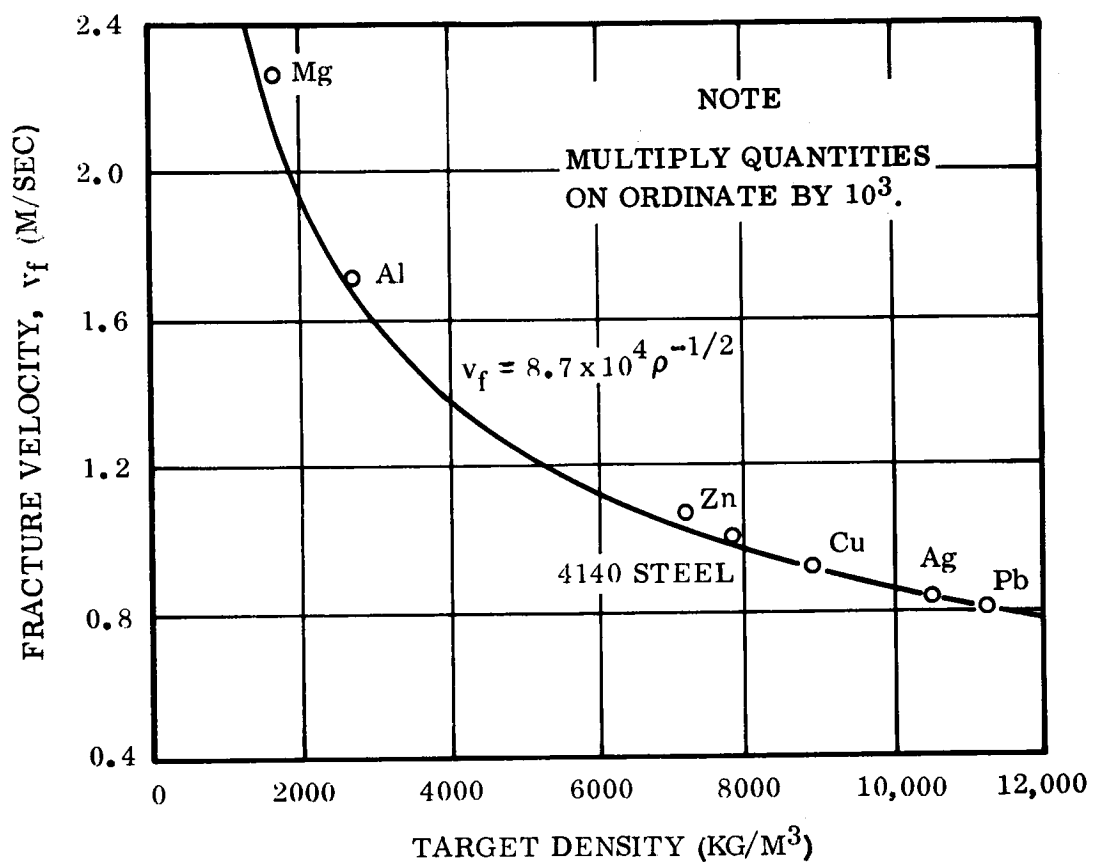


Figure A-21. Projectile Fracture Velocity Versus Target Density for Impact of Hardened Steel Spheres into Various Targets [Ref 69]

Summers [54] actually measured the volume of the target craters, and observed that the crater volume varied as the $3/2$ power of the density ratio and the second power of the impact mach number. The ratio of crater volume to projectile volume can be expressed by the equation,

$$\frac{V_T}{V_P} = k \left(\frac{\rho_P}{\rho_T} \right)^{3/2} \left(\frac{v}{c} \right)^2$$

It can be seen that V_T is proportional with $\frac{E_P}{E_T}$.

Atkins and Swift [53] observed that crater volume varied linearly with the impact energy, and the data are shown in Figure A-22. The scatter in the data was attributed to variations in the projectile mass. Volume-energy relationship for several projectile-target combinations are shown in Figures A-23 and A-24. Based on these limited data, each curve, with the exception of WC-Pb, is either linear and intersects the origin, or becomes linear as the impact energy is increased. Figure A-25 is a plot of the impact energy per-unit-of-crater volume as a function of impact velocity. For the Al -1100F aluminum and WC-Cu curves, the ratios of E/V are constant at 690 joules/cm³, and 1100 joules/cm³, respectively. For the remaining curves in Figures A-23 and A-24, the volume-energy curves are not linear in the low impact energy regions. The solid curves (Figure A-25) indicate the region of experimental data; the dash extensions are extrapolations which indicate the ultimate value of E/V , when the impact is actually in the hypervelocity region. From a practical point of view, these ratios become constant.

Atkins and Swift [53] assumed that in the hypervelocity region, the craters are hemispherical, the volume versus energy relations are linear (except for WC-Pb), and they obtained the following penetration expression:

$$P = \left(\frac{3}{4\pi K} \right)^{1/3} m^{1/3} v^{2/3}$$

where

K = energy/unit volume for a given projectile-target combination

m = projectile mass

v = impact velocity

A summary of calculated and experimental penetration data is given in Table A-1.

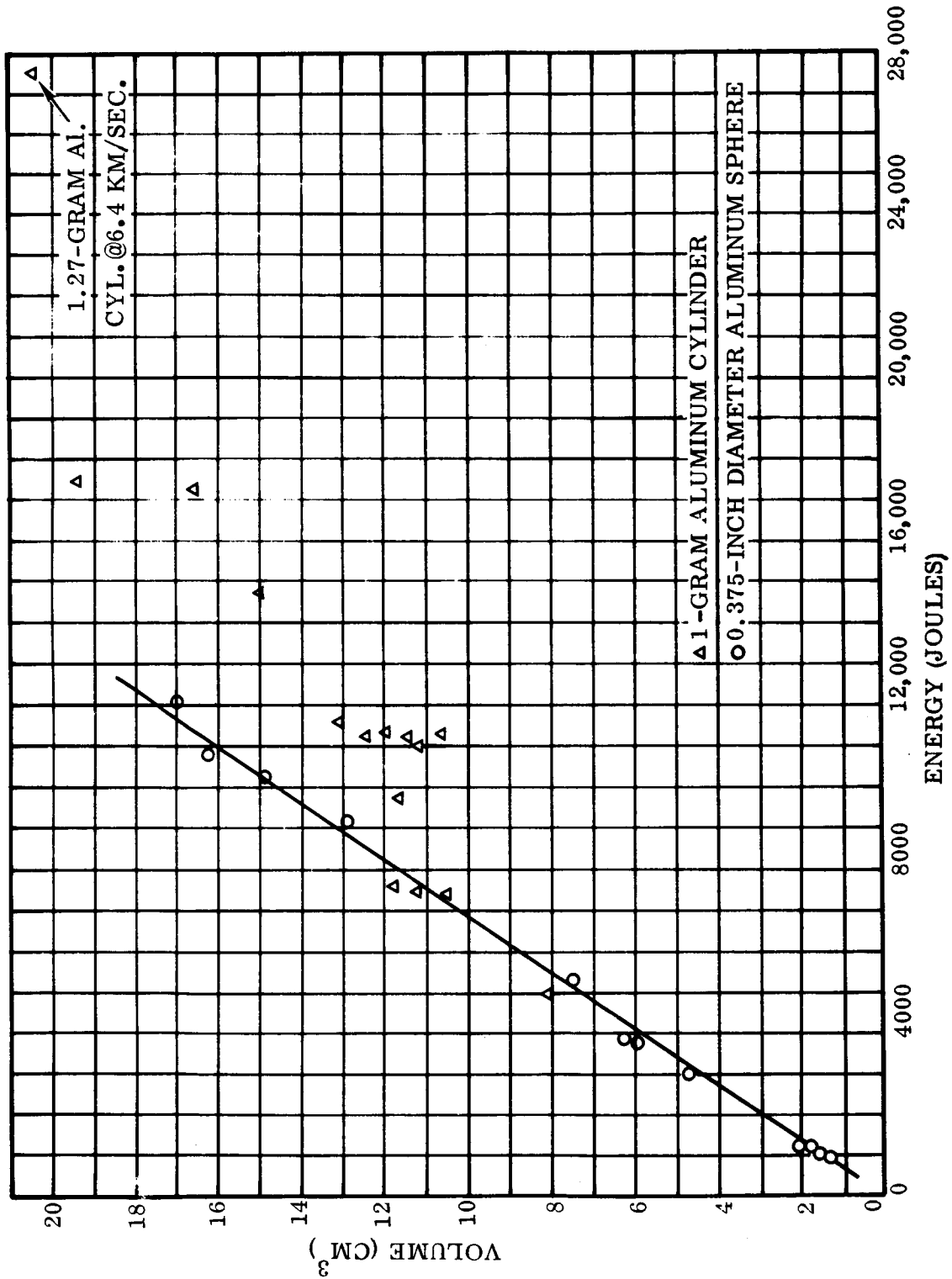


Figure 22. Crater Volume Versus Impact Energy for Aluminum Spheres and Cylinders into 1100F Aluminum [Ref 53]

April 1962

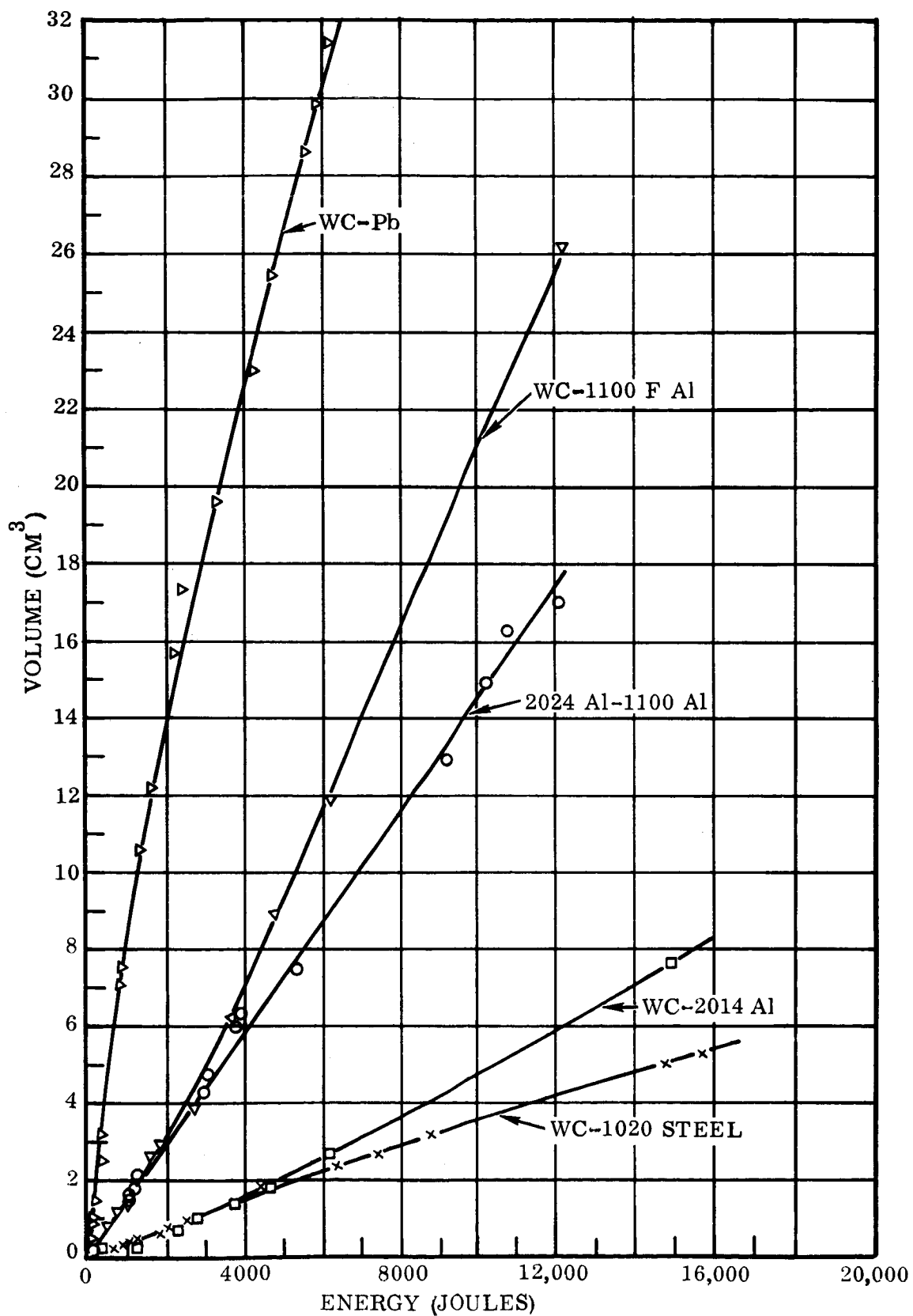


Figure A-23. Crater Volume Versus Projectile Energy for Several Projectile-Target Systems [Ref 53]

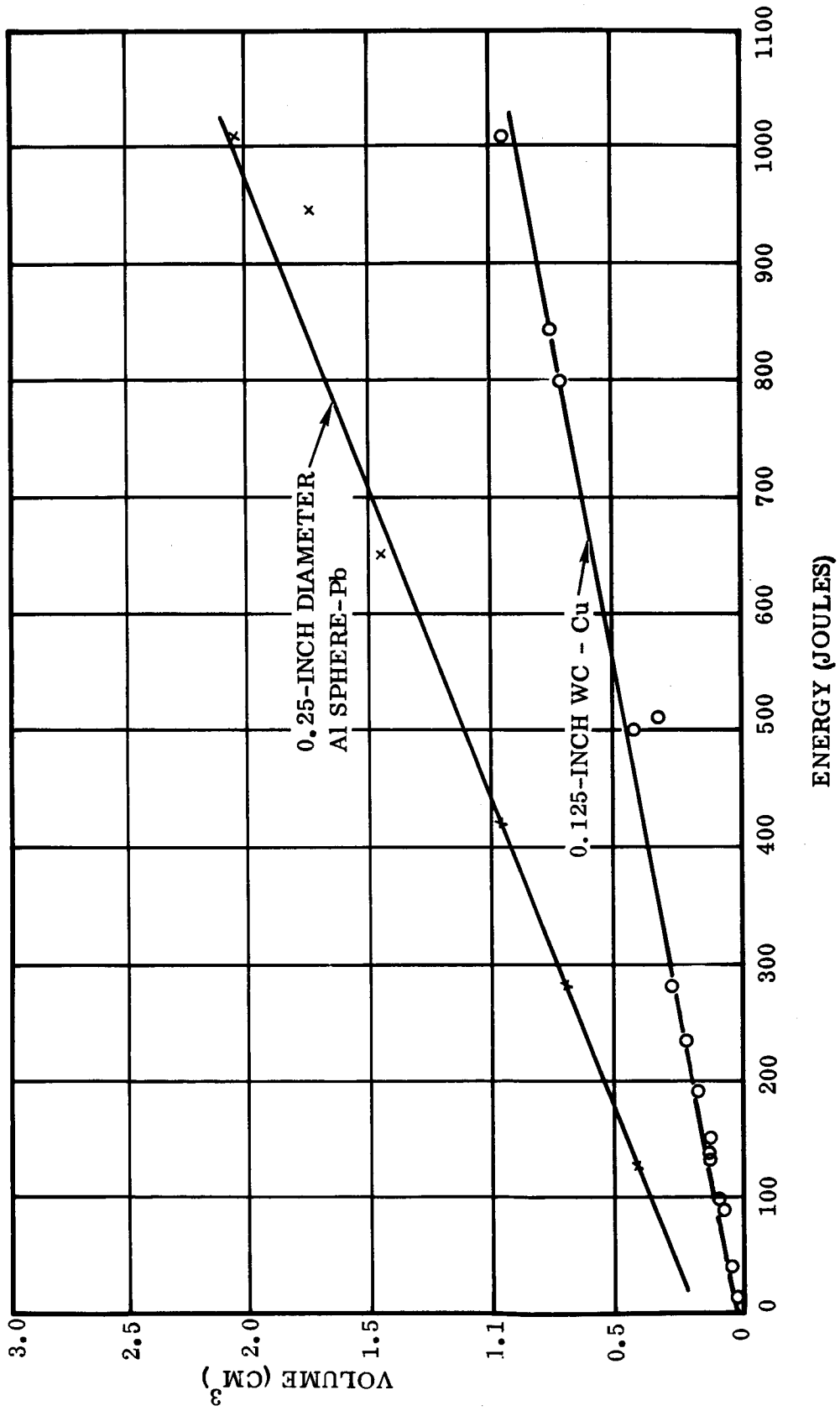


Figure A-24. Volume-Energy for Al into Pb and WC into Cu [Ref 53]

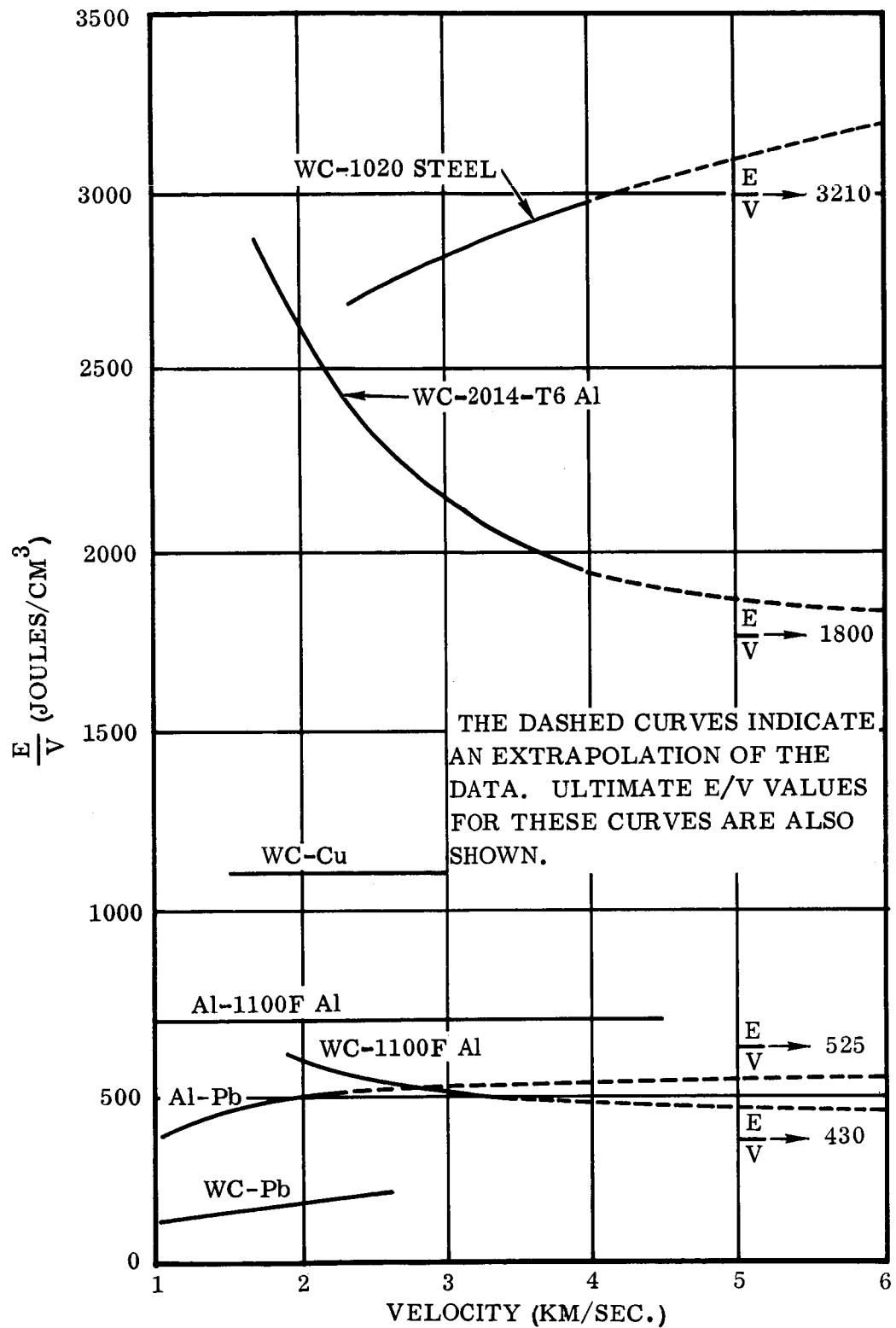


Figure A-25. Striking Energy/Cavity Volume as a Function of Velocity [Ref 53]

April 1962

Table A-1. Summary of Penetration Data

PENETRATION DATA			PENETRATION, CM.	
PROJECTILE-TARGET	K_1 JOULES/CM ³	VELOCITY, KM/SEC	MEASURED	CALCULATED
Al-Al	690	5	2.38	2.22
Al-Al	690	10	----	3.52
WC-Cu	1100	3	0.95	0.79
WC-Cu	1100	10	----	1.76
WC-Pb	200	2.6	2.86	2.53

It can be seen that the more nearly the cavity is hemispherical, the better the concordance between the measured and calculated penetration values. The previous equation is empirical and can be used to calculate the approximate depth of penetration as a function of impact velocity, if the impact occurs in the hypervelocity region on infinitely thick plates.

Turner, et al. [71], observed that the crater volume-projectile energy (velocities up to 7800 ft/sec) equation was linear for each projectile material. The form of this equation is:

$$V = i_1 + k_1 E$$

where

V = crater volume

E = kinetic energy of the projectile

i_1 = crater volume intercept

k_1 = slope of the line.

The constant, k_1 , indicates the amount by which the volume of a crater is increased per-unit-increase in projectile energy. In addition, k_1 varies over a wide range for the projectile materials considered. Consequently, the crater volume-per-unit of projectile energy is dependent upon the projectile material. Pertinent data are summarized in the following table.

Table A-2. Projectile Materials and the Constants for the Equations, $V = i_1 + k_1 E$, and $A = i_2 + k_2 M$

PROJECTILE			i ₁ (m ³)	k ₁ (m ³ /joule)	i ₂ (m ²)	k ₂ (m-sec/kg)
MATERIAL	MASS (gm)	DENSITY (gm/cc)				
Nylon	0.066	1.16	0.006 × 10 ⁻⁶	0.87 × 10 ⁻⁹	0.101 × 10 ⁻⁴	4.14
Magnesium	0.098-0.109	1.74	0.031 × 10 ⁻⁶	1.40 × 10 ⁻⁹	0.034 × 10 ⁻⁴	5.50
Pyrex Glass	0.149	2.64	0.007 × 10 ⁻⁶	3.63 × 10 ⁻⁹	-0.107 × 10 ⁻⁴	6.08
Aluminum	0.159	2.80	0.047 × 10 ⁻⁶	1.81 × 10 ⁻⁹	-0.012 × 10 ⁻⁴	5.10
Diamond	0.147-0.182	3.30	0.065 × 10 ⁻⁶	2.96 × 10 ⁻⁹	-0.043 × 10 ⁻⁴	5.51
Stainless Steel Type 440	0.431	7.63	0.217 × 10 ⁻⁶	3.65 × 10 ⁻⁹	-0.744 × 10 ⁻⁴	5.97
High Carbon Chrome Steel	0.440	7.85	0.170 × 10 ⁻⁶	4.25 × 10 ⁻⁹	-0.788 × 10 ⁻⁴	5.93
Stainless Steel Type 302	0.446	7.90	0.272 × 10 ⁻⁶	3.21 × 10 ⁻⁹	-0.720 × 10 ⁻⁴	5.76
Naval Brass	0.477	8.45	0.252 × 10 ⁻⁶	3.76 × 10 ⁻⁹	-0.616 × 10 ⁻⁴	5.59
K-Monel Metal	0.479	8.48	0.221 × 10 ⁻⁶	3.71 × 10 ⁻⁹	-0.719 × 10 ⁻⁴	5.22
Copper	0.500	8.90	0.598 × 10 ⁻⁶	3.30 × 10 ⁻⁹	-0.575 × 10 ⁻⁴	5.60
Lead	0.675-0.712	11.34	0.057 × 10 ⁻⁶	4.70 × 10 ⁻⁹	-0.622 × 10 ⁻⁴	4.92
Tungsten	1.234-1.332	19.20	0.584 × 10 ⁻⁶	5.89 × 10 ⁻⁹	-2.070 × 10 ⁻⁴	4.44

April 1962

A-13 MOMENTUM. Penetration into semi-infinite aluminum (2024-T3) targets is dependent upon the momentum of the projectile, as seen in Figure A-26. However, the previous discussion of the $\rho_p v L$ parameter indicates that penetration should be independent of the total mass. This independency [61] would indicate that a sphere and a cylinder with the same diameter and length-to-diameter ratio would have one-third greater mass. The experimental results given in Figure A-27 substantiate the conclusion that penetration should not be correlated with the total momentum of the impacting projectile, but to the momentum per-unit-area.

Turner, et al. [71], observed that the crater area-projectile momentum (velocities up to 7800 ft/sec) equation was linear for each projectile material. The form of this equation is:

$$A = i_2 + k_2 M$$

where

A = crater area

M = projectile momentum at impact

i_2 = crater area intercept

k_2 = the slope of the line

The values for the constants i_2 and k_2 are given in Table A-2.

A-14 PENETRATION RELATED TO THE VOLUME AND AREA OF THE CRATER. The crater depth, versus the ratio of crater volume to crater area, is shown [71] in Figure A-28 for nylon, copper, and tungsten projectiles. Each projectile material gives a group of points which falls on a line expressed by the equation $p = 1.7 V/A$. The relative position of each group on the line apparently is a function of the projectile material density. Only three projectile materials are shown in Figure A-28, but all of the other projectile materials give a similar group of points, and they fall on the same line.

Combination of the three equations,

$$V = i_1 + k_1 E$$

$$E = i_2 + k_2 M$$

$$P = 1.7 V/A$$

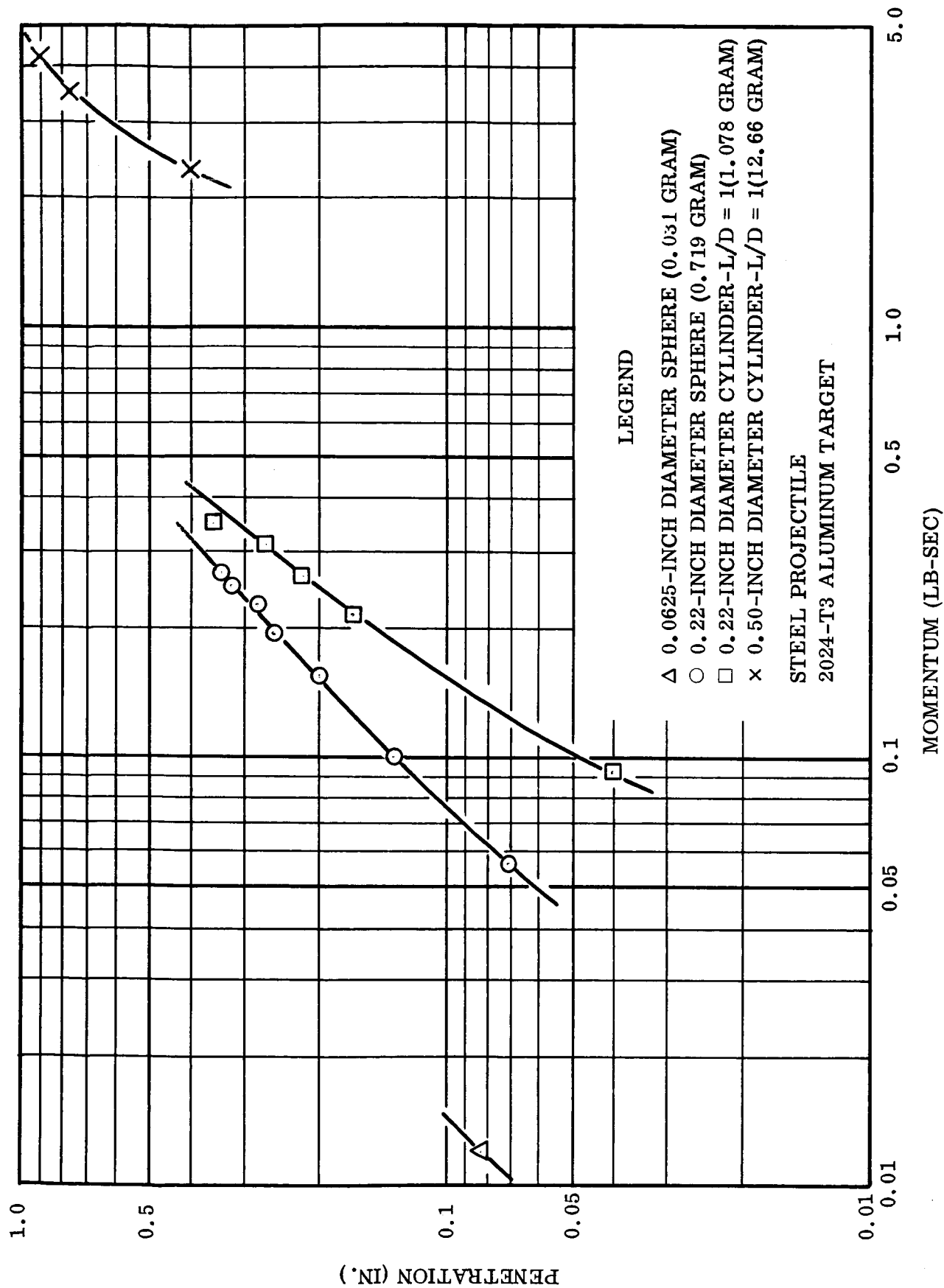


Figure A-26. Penetration Dependence on Momentum [Ref 61]

April 1962

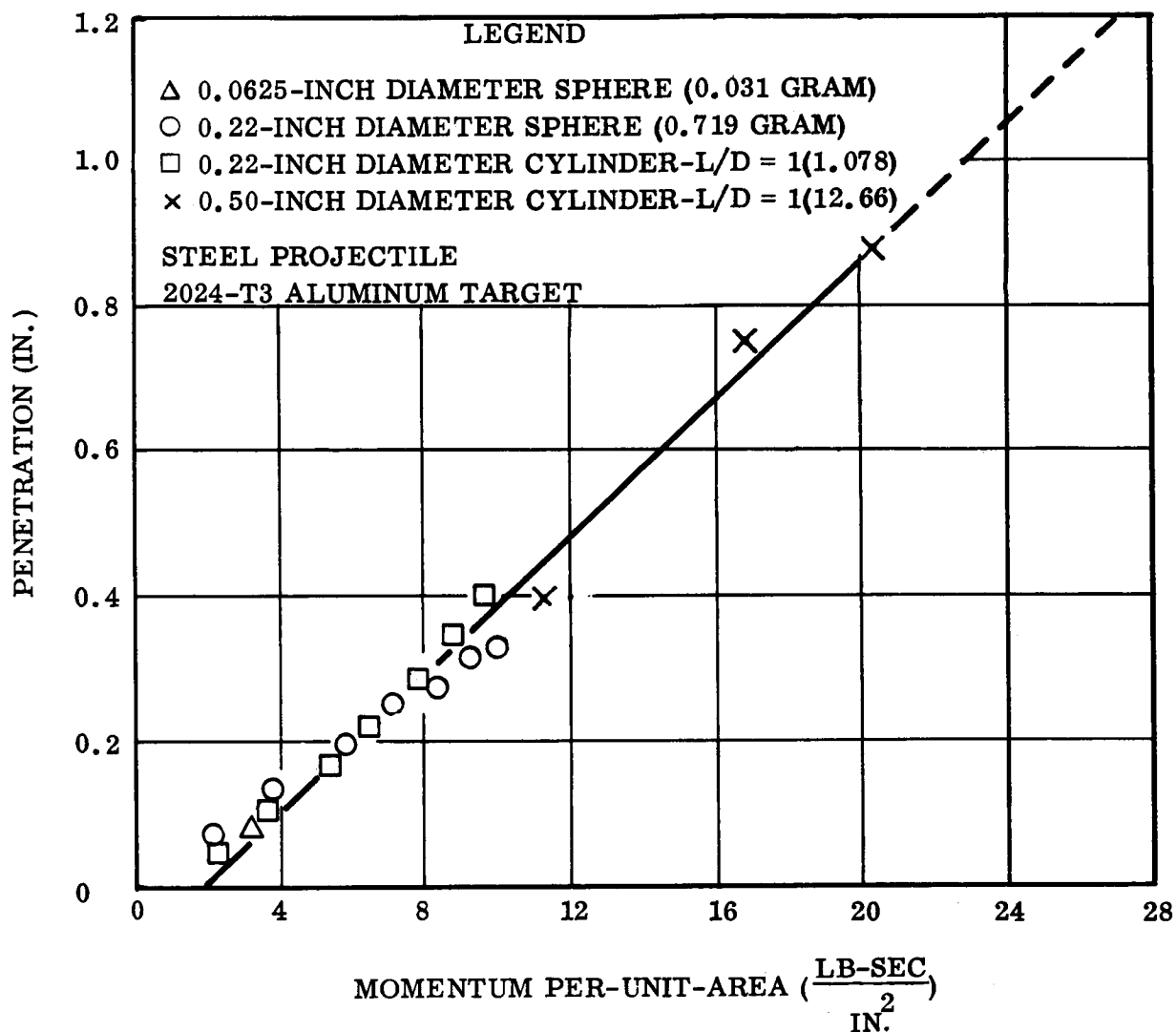
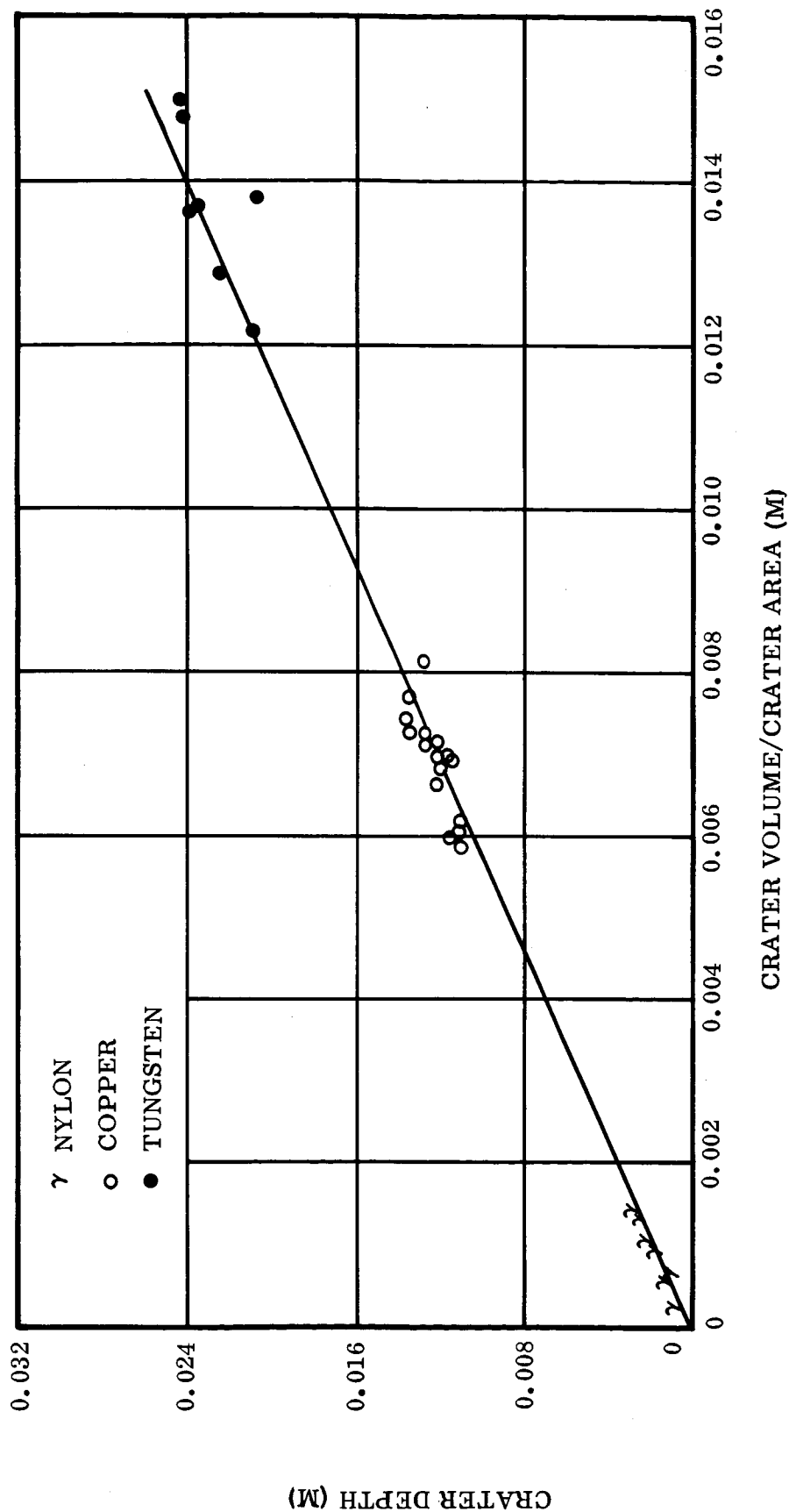


Figure A-27. Penetration Dependence on Momentum Per-Unit-Area [Ref 61]



April 1962

results in the equation,

$$p = 1.7 \left(\frac{i_1 + k_1 E}{i_2 + k_2 M} \right)$$

A-15 SINGLE BUMPERS. Humes, et al. [72], measured the total penetration in a bumper protected-vehicle wall combination at varying impact velocities (Figure A-29). The total penetration (bumper thickness plus penetration in the vehicle wall) is plotted on the ordinate with the impact velocity on the abscissa. Shown for comparison are the penetrations achieved at identical impact velocities in quasi-infinite aluminum (2024-T4) targets with no bumper shields. The thickness of the aluminum (2024-T3) bumper shields were all one-half the diameter of the impacting projectiles. The copper spherical projectile was 0.0625 inch in diameter.

Penetration into the unprotected quasi-infinite targets increased with increasing impact velocities for the entire velocity range observed. In the low velocity range, penetration into the bumper protected targets also increased with increasing impact velocities up to a velocity of about 6000 ft/sec. At this velocity, the penetration appears to reach a maximum value, and as the impact velocities are further increased, the penetration decreases.

The low velocity range shows that at these impact velocities, the bumper shields were ineffective in reducing the penetration. Deeper penetration was observed in bumper protected targets than in the unprotected targets. This was attributed to the fact that less projectile momentum or energy was required to penetrate the bumper shield, than was required to penetrate an equal depth in the quasi-infinite targets.

Impact velocities at values of 9000 ft/sec or greater indicates that the bumpers were effective in reducing the total penetration below that obtained in the unprotected targets. The copper projectiles were observed to start fragmenting during the penetration of the bumpers at impact velocities above 9000 ft/sec, which is almost twice the velocity required to fragment larger aluminum projectiles.

A-16 MULTIPLE BUMPERS. Halperson and Fuller [64] studied the impact damage of 0.0625-inch aluminum (2024-T3) plates spaced four inches apart, from 0.25 inch diameter spherical steel projectiles (Rockwell hardness of 60 to 65C) with a mass of 1.04 grams and velocities from 1100 to 8300 ft/sec. The damage dependence on the number of plates and velocity is given in Figure A-30. No damage indicates that the last aluminum plate in the series was not penetrated, while major damage implies that the perforation diameter in the last plate was equal to or greater than the 0.250-inch diameter of the projectile.

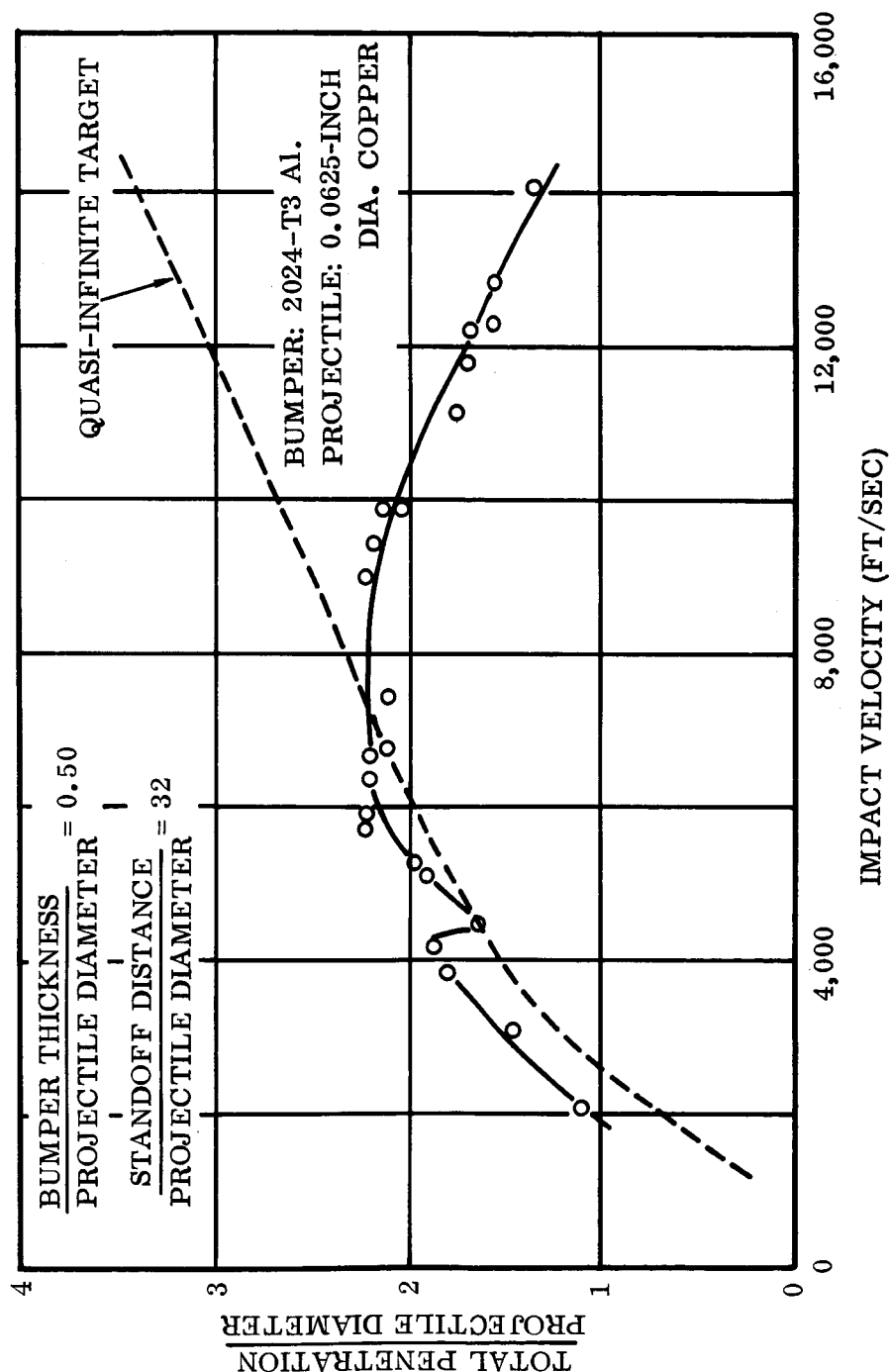


Figure A-29. Variation of Total Penetration With Impact Velocity in a Bumper Protected Target [Ref 72]

April 1962

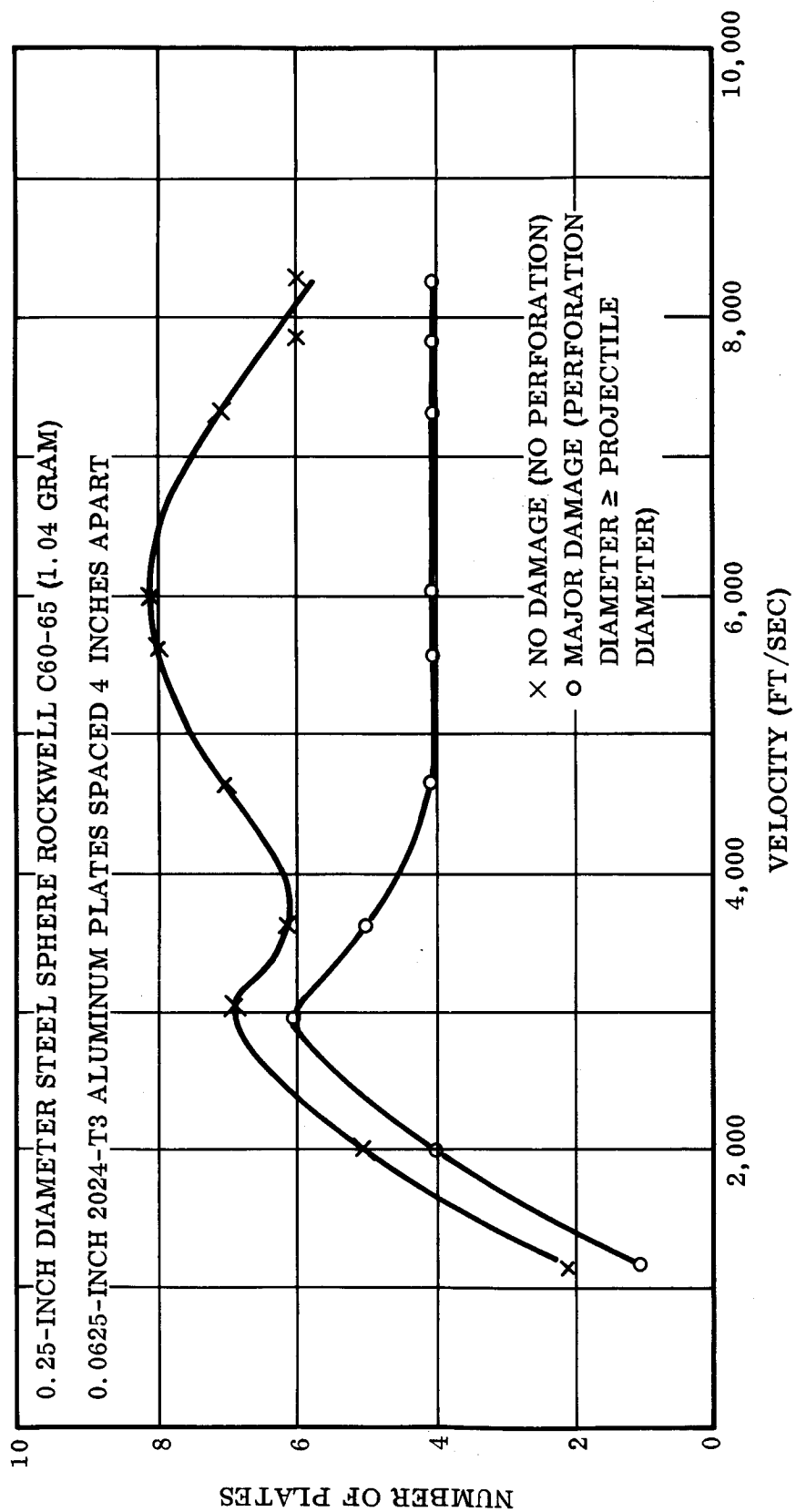


Figure A-30. Penetration of Varying Number of Plates With Increasing Velocity [Ref 64]

The data from a number of plates with a constant 4-inch spacing, given in Figure A-8, can be explained from a comparison with Charters' [52] data which are given in Figure A-2. Penetration increases (or the number of plates that can be penetrated increases) by increasing the velocity from 1100 to 3000 ft/sec, since the projectile maintains its integrity. However, at 3000 ft/sec the first transition for the experimental system (Figure A-30) is attained, and due to the increased kinetic energy (available from the higher velocity) the projectile will begin to fragment. Beyond the first transition range, penetration will increase with increasing velocity until the projectile break-up-to-fluid impact transition is attained. With a further increase in velocity, penetration will decrease, and the total number of plates required to defeat the pellet will decrease, since pellet fragmentation will be more complete on contact with the first plate. The total initial energy is divided over the large number of projectile fragments and the momentum per-unit-impact-area is significantly reduced.

Olshaker [59] observed that an 0.054-inch lead bumper was effective (Figure A-4) in protecting (0.50-inch spacing) a lead target from a lead projectile (0.124-inch diameter, 0.188 gram, 8366 ft/sec). The original 0.054-inch lead bumper was compared to two lead bumpers (each 0.027 inch thick) spaced 0.250 inch and 0.50 inch from the target, and it was observed that target penetration was twice as great as that behind the single 0.054-inch bumper.